# Effectiveness of roof overhang on mid-rise buildings: field measurements and improved assessment based on ISO Standard

Firouzeh Souri

A Thesis
in
The Department
of
Building, Civil and Environmental Engineering

Presented in Partial Fulfillment of the Requirements
for the Degree of
Master of Applied Science (Building Engineering) at
Concordia University
Montreal, Quebec, Canada

September 2018

**CONCORDIA UNIVERSITY**

**School of Graduate Studies**

This is to certify that the thesis prepared

By: Firouzeh Souri

Entitled: Effectiveness of roof overhang on mid-rise buildings: field measurements and improved assessment based on ISO standard

and submitted in partial fulfillment of the requirements for the degree of

**Master of Applied Science (Building Engineering)**

Complies with the regulations of the University and meets the accepted standards with respect to originality and quality.

Signed by the final Examining Committee:

| | |
|---|---|
| *Dr. Radu Zmeureanu* | Chair |
| *Dr. Biao Li* | Examiner |
| *Dr. Lyes Kadem* | Examiner |
| *Dr. H. Ge* | Co-supervisor |
| *Dr. T. Stathopoulos* | Co-supervisor |

Approved by *Dr. F. Haghighat*

GPD, Department of Civil and Environmental Engineering

*Dr. A. Asif*

Dean, Faculty of Engineering and Computer Science

4th of September 2018

## ABSTRACT

**Effectiveness of roof overhang on mid-rise buildings: field measurements and improved assessment based on ISO standard**

Firouzeh Souri

Wind-driven rain (WDR), as one of the most important boundary conditions, not only influences hydrothermal performance and material durability of the building enclosures but also its penetration through building's assemblies may lead to different types of moisture related failures. In recently completed studies, a unique set of high resolution data through field measurements under real life conditions is provided by monitoring three mid-rise buildings in three Canadian cities (Vancouver, Montreal and Fredericton). All test buildings are instrumented with weather stations and driving rain gauges for wind driven-rain measurements on building's façade. In addition, Vancouver building is equipped with a retractable overhang extendable to 1.2 m, partially covering east and north facades. The previous studies have shown that estimation of wind driven-rain by applying semi-empirical methods, is generally subjected to overestimation in comparison with measured wind driven-rain. The accuracy of ISO method can be improved significantly by using more accurate wall factors calculated based on onsite measurements. Moreover, the effectiveness of roof overhang in reduction of wind driven-rain deposition on a mid-rise building have been studied and quantified for 0.6 m and 1.2 m overhang.

As a follow-up, this thesis conducted further analysis and tests with the purpose of improving wind-driven rain assessment based on ISO standard by achieving three main objectives: first, to develop a correlation between overhang width and amount of wind driven-rain load reduction on the facade under it, with respect to wind characteristics; second, to develop a methodology to generalize the proposed reduction coefficient for similar mid-rise building geometry being protected by roof overhang; and finally, to carry out further investigation of error sources for the discrepancy between measurements and calculated wall indices, therefore, improving the accuracy of ISO semi-empirical model.

To fulfill these objectives, established methodology in previous studies such as the similarity and symmetry approach is followed by analyzing additional available data. Proposed wind driven-rain reduction coefficient is calculated based on the weighted-effectiveness methodology.

Validation of generalizing proposed reduction coefficients for similar mid-rise building geometry is conducted by comparison of wind velocity near the upstream façade of study buildings model, with and without overhang, in Concordia's atmospheric boundary layer wind tunnel.

In addition, more detailed analysis regarding the effect of time resolution and data conversion on the accuracy of ISO model is provided. The detailed study of meteorological wind data, registered onsite and reported by the weather station, confirms that wind characteristic changes from point to point could be stated as other sources of discrepancies.

## ACKNOWLEDGEMENTS

*Foremost, I would like to express my sincere gratitude to my fabulous supervisors Dr. Hua Ge and Dr. Theodore Stathopoulos for their continuous support of my study and research, for their patience, motivation, enthusiasm, and immense knowledge. I had this chance not only extend my knowledge under their supervision but learn lessons for life.*

*A special thanks to Vincent Chiu for his support and always being available throughout this research, Hatem Alrawashdeh for his help in wind tunnel experiment and all my friends who have supported.*

*It was a great pleasure for me to have this chance working with all the amazing people in Department of Building, Civil and Environmental Engineering in Concordia University, Montreal, Quebec.*

*I would also like to express appreciation to the financial supports received from NSERC Discovery Grant, BC Housing, and the Faculty of Engineering and Computer Science of Concordia University.*

*Finally, I must express my very profound gratitude to my spouse and best friend Agha Allahyar Khan for all the joy and happiness he has brought to my life and my parents for their endless support.*

Contents

# List of Figures

# List of Tables

# List of Symbols

Roman Symbols

| | | |
|---|---|---|
| $A_d$ | Equivalent frontal area of a raindrop | $m^2$ |
| $C_D$ | Drag coefficient | - |
| $C_R$ | Terrain roughness coefficient | - |
| $C_T$ | Topography coefficient | - |
| D | Hourly mean wind direction from north | degree |
| $E_{AW}$ | Adhesion-water-evaporation error | mm |
| $E_{EVAP}$ | Evaporation error from the tipping bucket and collection plate | mm |
| EHF | Exposure and height factor | - |
| $E_{RW}$ | Rest-water error | gram |
| $E_{TIP}$ | collection loss during every tip | gram |
| ETOT | Total error in the wind-driven rain measurement | mm |
| $e_{TOT}$ | Relative error associated with the wind-driven rain measurement | % |
| $E_{UC}$ | Condensation error | mm |
| $F_D$ | Rain deposition factor | - |
| $F_E$ | Rain exposure factor | - |
| $I_{WS}$ | Wall indices | mm |
| $K_R$ | Terrain factor | - |
| O | Obstruction factor | - |
| $R_{Airfield}$ | Airfield index | mm |
| RDF | Rain deposition factor | - |
| $R_h$ | Horizontal rainfall intensity | mm/hr |
| $R_{wdr}$ | Wind-driven rain intensity | mm/hr |
| $S_h$ | Total accumulated horizontal rain | mm |
| $S_{wdr}$ | Total accumulated wind-driven rain | mm |
| TOF | Topography factor | - |
| U | Wind speed | m/s |
| $U_{10}$ | Hourly average wind speed at the height of 10 m | m/s |
| $U_g$ | Wind speeds at gradient height | m/s |
| $U_z$ | Wind speeds at height z | m/s |
| $V_{Bowl}$ | Content of the bowls | gram |

| | | |
|---|---|---|
| $V_t$ | Raindrop terminal velocity | m/s |
| W | Wall factor | - |
| WDR | Wind-driven rain | - |
| Zg | Gradient height | m |
| $Z_0$ | Roughness length | - |
| $Z_{min}$ | minimum height | - |

Greek Symbols

| | | |
|---|---|---|
| α | Mean speed exponent | - |
| $\mu$ | Catch ratio | - |
| θ | wind direction relative to north | degree |
| φ | Equivalent spherical raindrop diameter | mm |
| $\delta$ | effectiveness | - |

# 1. Introduction

## 1.1. Problem Statement

Buildings must provide their inhabitants and users a comfortable and healthy environment, suited to their needs. This ought to be achieved in an economically and ecologically sound way, imposing demands on the building's durability and performance. The durability and performance of building facades is governed to a large extent by moisture conditions (Blocken & Carmeliet 2002). The presence, accumulation and the periodic variations of moisture in the mass and on the surface of building components affects its hydrothermal performance, causes various building materials' deterioration (Kontoleon & Giarma 2016) and may affect occupancy health.

Wind-driven rain (WDR) is known as one of the most important moisture sources and boundary conditions of building envelope. WDR is the type of rain that has a horizontal velocity vector due to the effect of wind flow occurring at the same time (Kubilay et al. 2015) and resulting in rain water impinging on building facade. In turn, the simultaneous wind pressure on this supply of water (WDR pressure) may result in the penetration of water into the materials, even in new enclosures without significant surface defects (Domínguez-Hernández et al. 2016).

Moisture accumulation in porous materials can lead to several undesired phenomena in building physics such as frost damage at exterior wall surfaces, erosion of building materials, moisture induced salt migration discoloration by efflorescence, surface soiling on curtain walls, structural damage (Zhou et al. 2016) and mold growth at interior wall surfaces (Abuku et al. 2009a). In addition to the economic cost associated with repairs and maintenance, presence of moisture decreases thermal resistance of building materials (Zhou et al. 2016) especially insulation layers and consequently hydrothermal performance of the enclosure. Also, the increase of building materials moisture content leads to a parallel increase of their ability to store energy within their thermal mass (Kontoleon & Giarma 2016). Unsatisfactory hydrothermal performance of the building increases the amount of energy consumption of the building and the emission of air pollutants associated with generating this energy. In addition, the health of inhabitants may be affected due to illnesses, allergies and unhealthy conditions associated with biological growths and indoor air quality (Domínguez-Hernández et al. 2016) due to the presence of moisture within building envelope assemblies.

As the result, accurate assessment of WDR load acting on building enclosures is crucial for accurate simulation of building energy performance and enclosure detail design. Moreover, providing solutions and detailing that reduce WDR load on building facades improve building energy performance, ensure materials long-term service life and reduce construction environmental impacts due to building retrofitting associated with moisture penetration failures and damages.

## 1.2. Objectives of the Current Study

The main objective of this study is to improve the assessment of WDR using ISO method for mid-rise buildings and provide engineers and designers with recommendations on overhang design with respect to site meteorological data, more specifically to:

**(a)** Establish a correlation between overhang width and percentage of WDR load reduction on different portions of the facade with respect to wind characteristics

**(b)** Introduce WDR reduction coefficient in estimation the amount of WDR load on mid-rise building façade protected by roof overhang based on ISO formula; with respect to overhang width, wind speed and wind direction

**(c)** Develop a methodology to generalize the calculated WDR reduction coefficient for similar mid-rise building geometries being protected by roof overhang

**(d)** Investigate other possible contributing sources leading to discrepancy between wall index calculated using ISO model and onsite measurement.

## 1.3. Outline of the Thesis

This study is presented in seven chapters starting in Chapter 1 with the importance of WDR studies and objectives of the current research work.

Chapter 2 includes detailed review of previous studies and methodology used in the estimation of WDR and continues with experimental studies that have investigated the overhang effectiveness and the accuracy of ISO Standard. This chapter is concluded existed knowledge gape.

Chapter 3 presents the measurement setups of test buildings and wind tunnel experiment followed by the validation of onsite data and wind tunnel measurements. This chapter also includes the introduction of methodology used in quantifying overhang effectiveness, defining WDR reduction coefficient, the procedure in generalizing results for mid-rise buildings with similar geometries and investigating sources leading to discrepancy between the wall indices calculated based on ISO model and measured values.

Chapter 4 introduces WDR Reduction Coefficient calculated based on overhang effectiveness with respect to overhang size and wind characteristics.

Chapter 5 discusses the possibility of generalizing results for mid-rise buildings with similar geometries through wind tunnel experimentation.

Chapter 6 investigates the effect of applied data time-resolution and averaging on the calculation of wall factors. Moreover, the discrepancy between wind characteristics measured onsite and the data reported by Environment Canada for the same period of time and its effect on the calculation of wall index is discussed.

Finally, in Chapter 7, conclusions of this study, recommendations and suggestions for further work are provided.

The references cited in this thesis are listed in the References section.

# 2. Literature Review

## 2.1. Wind-driven Rain

The movement of a raindrop as the result of its own weight (gravity) and wind flow (drag force) simultaneously leading to oblige rain drop trajectories. According to Blocken & Carmieliet (2004), the term "driving rain intensity" means the component of rain vectors that causes rain flux through a vertical surface of the building. As it is shown in Figure 2.1, the other component of the rain intensity vector, that causes rain flux through a horizontal plane, is termed (horizontal) rainfall intensity.

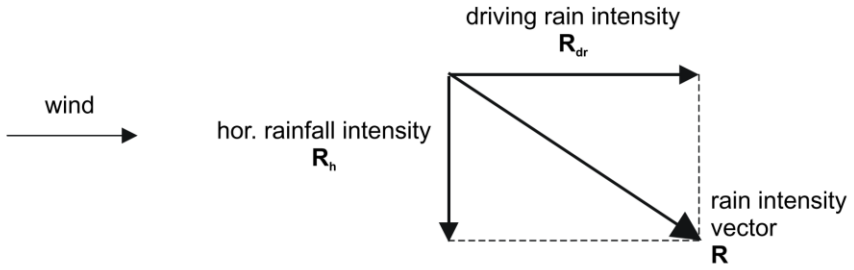


Figure 2.1 - Rain intensity vector R and its components: driving rain intensity $R_{dr}$ and horizontal rainfall intensity $R_h$ (Blocken & Carmeliet 2002)

The amount of impinged WDR and its spatial distribution on building façade is governed by a wide range of parameters including wind speed, wind direction, rainfall characteristics (drop size distribution and intensity), and the duration and frequency of the rain event. In addition, building characteristics such as: building geometry, facade orientation and location on the façade and surrounding topology further affect the WDR load (Blocken & Carmeliet 2004; Choi, 1994).

When the building is placed in the wind field, its presence significantly modifies the flow of approaching wind, also known as blockage effect. As it is shown in Figure 2.2, there is a slow-down of the wind upstream of the building and a speed-up of the wind sweeping sideways around the corners of the front face and upwards around the top of the building (Choi, 1999), thus, the wind-building interaction is directly related to the spatial distribution of WDR on the building facade(s) (Chiu, 2016).

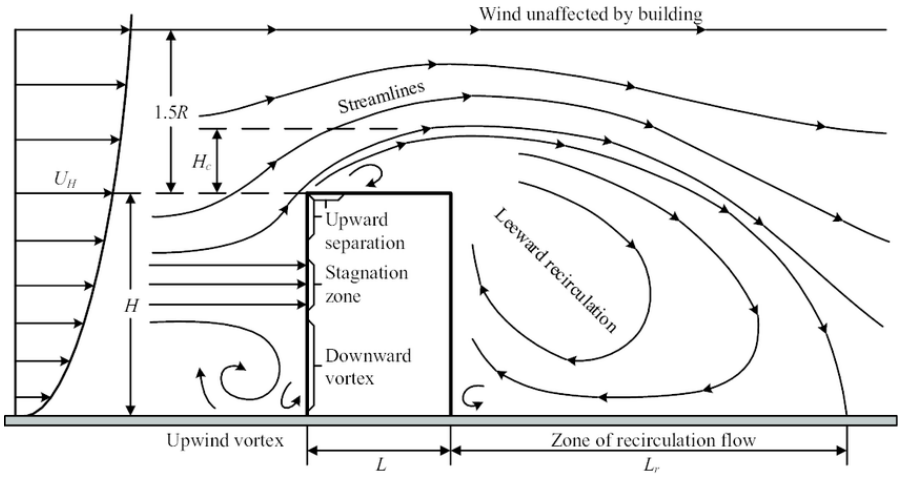


Figure 2.2 - Schematic representation of wind flow around a high-rise building (Mao & Gao 2015)

When rain is added to the flow field, it will be driven against the windward facade of the building. As a result of the specific flow features, the course of the raindrop trajectories is changed, which results in a non-uniform wetting of the façade (Blocken et al. 2004). Since the drag coefficient is a function of the drop size, the trajectories for raindrops of different sizes will be different. The trajectories of the smaller raindrops are more slanting and more effected by the local flow close to the building (Choi, 1999).

The accurate estimation of WDR is essential to design building envelopes with satisfactory hydrothermal performance. Also quantifying the amount of WDR received by building façade is required as boundary condition for heat-air-moisture (HAM) transfer analysis. The amount of WDR can be estimated by (a) experimental methods, (b) semi-empirical methods and (c) numerical methods.

## 2.2. Estimation of WDR

### 2.2.1. Experimental Method

**Field Measurements**

The experimental approach consists of measuring WDR with wind-driven rain gauges (a) in the free field where the flow is not influenced by the presence of the building using free standing WDR gauges, and (b) on the building facades by wall-mounted WDR gauges. Although, this approach, provided valuable information for understanding WDR under real-life conditions and spatial distribution of WDR on building façade, it is not widely used due to numerous associated

drawbacks including the time and costs. Furthermore, limited spatial and temporal information and the fact that measurements at one site have a limited application to another site, limits the application of experimental methods. Also, studies have shown that WDR measurements applying WDR gauges can suffer from large errors (Blocken et al. 2004). The design of WDR gauges are not standardized and they are usually customized by different laboratories for research purpose. However, all WDR gauges consist of collection area, drainage channel and a reserve or tipping bucket, Figure 2.3.

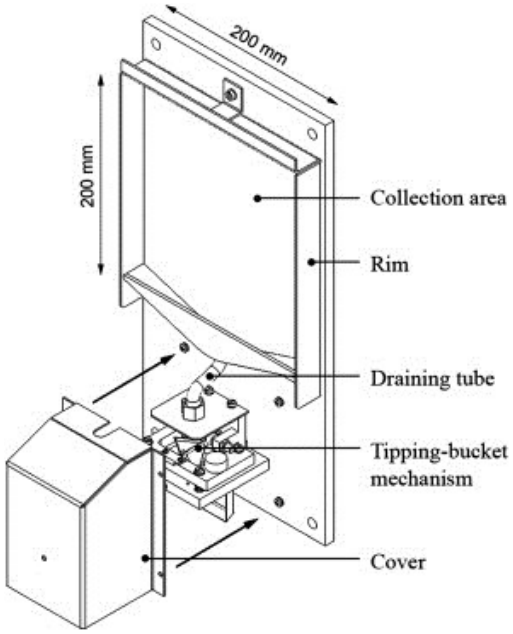


Figure 2.3 – Wind-driven rain gauge, designed and manufactured at Eindhoven University of Technology (Briggen et al. 2009).

Several studies have been conducted to investigate WDR gauges performance and possible sources of errors. The study conducted by Högberg (1999), investigated the effect of applying wiper and coating on collector surface on the amount of WDR measured by four different WDR gauges. The results show that smooth, hydrophobic collector surface is not totally sufficient and WDR gauges with vapour measured two times of WDR (Högberg et al. 1999). In 2004, Blocken categorized errors associated with WDR measurements into five main categories, namely (a) evaporation of adhesion water from the collection area, (b) evaporative losses from the reservoir, (c) splashing of drops from the collection area, (d) condensation on the collection area and (e) wind errors (Blocken & Carmeliet 2006a). Evaporation loss of adhesion water from the collection area is the most important source of error. The presence of this error depends on the type of WDR

gauges as well as the type of rain event. Estimation of condensation errors can be simulated with HAM transfer model. Information about splashing and wind error is limited, however, wind errors can be studied though CFD modeling. In the study conducted by Nath it was shown that splashing errors are negligible given the low wind speed and horizontal rainfall intensity values at the experiment location. The wind errors are insignificant for the times wind direction is approximately perpendicular to building façade and condensation on the gauge during the rain event is negligible (Nath 2015).

However, field measurements provide a basic understanding of WDR spatial distribution on building façade. Several studies have used the experimental results to develop and assess the accuracy of semi-empirical methods and to validate the numerical methods. Moreover, this approach has been used to investigate the influence of complex building geometries and design details such as the roof overhang on the amount of WDR received on building façade (Chiu 2016).

**Wind Tunnel Experiment**

The simulation of WDR in a wind tunnel setup consists of generating wind flow in a boundary layer wind tunnel and rainfall by nozzles. This method has been used only a limited number of times due to several drawbacks associated with it.

The first wind tunnel test with the intention of quantification of WDR on a building model was conducted by Surry in a boundary layer wind tunnel at the University of Western Ontario (Inculet & Surry 1995). A 1:64 scaled of building model was used and the wind speed and rain drop sizes were scaled down. The water-sensitive-paper was placed on the building model to study the WDR spatial distribution and quantify impinged WDR on façade. Classical wetting was observed on the building façade; however, the variation of calculated catch ratio was not consistent with respect to distance from façade boundaries. Very limited time of the rain shower, 5-10 seconds, providing homogenous distribution of rain from nozzles and the labour-intensive of quantitative analysis were mentioned as the main difficulties of WDR studies in wind tunnel (Surry et al. 1994). Difficulties of proper simulation of rain and WDR measurement on the model façade make this approach less practical.

Another experiment was conducted by Baheru on the study of WDR distribution on a three low-rise building geometries with flat, gable and hip roof (Baheru et al. 2015) in Florida International University (FIU). All model surfaces were designed with grid-format of openings

used to mount WDR collection buckets. The FIU's 12-fan Wall of wind was used for the experiment to simulate the wind flow and the WDR was generated by four vertical lines of spray nozzles in front of the fans, Figure 2.4. The study quantifies the distribution of direct impinging rain drops and surface rainwater over the building surface in simulated tropical and hurricane weather conditions (Baheru et al. 2014).

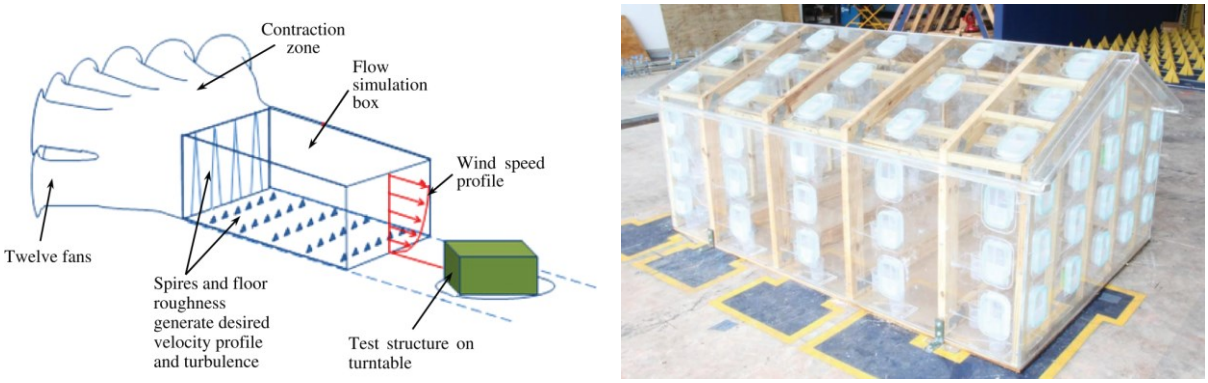


(a) (b)

Figure 2.4 – (a) Schematic diagram of 12-fan wall of wind, (b) Large-scale building model (1:4) with WDR collecting buckets, (Baheru et al. 2015)

### 2.2.2. Semi-empirical Methods

Semi-empirical relations were established to correlate the amount of WDR with respect to influencing climate parameters wind speed, wind direction and horizontal rain fall intensity. The development of these relationships was guided by the experimental observations; however, formulas have theoretical basis and free parameters have been chosen to fit experimental data. Semi-empirical methods are practical for design applications due to their simplicity (Blocken & Carmeliet 2004). Two semi-empirical methods can be divided into two categories: (1) the WDR index and (2) the WDR relation.

The "WDR index" is the product of wind speed and horizontal rainfall intensity and indicates the wetness of geographic location not the actual amount of WDR received by the building facade. Calculating WDR index for a variety of places leads to generation of WDR maps of countries. This approach indicates the WDR and does not account for local phenomena introduced by the topography and by the building itself.

The "WDR relation" is the method that relates WDR intensity received by building vertical façades considering wind speed, wind direction, horizontal rainfall intensity and WDR coefficient accountant for local phenomena induced by the topography and the building itself:

$$R_{wdr} \approx \alpha.\ \mathrm{U}.R_h.\ \cos\theta \tag{2.1}$$

where α is WDR coefficient, U is wind speed, $R_h$ is the amount of rain fall intensity and θ is the angle between normal of façade and wind direction (Blocken & Carmeliet 2010). There are several models for the semi-empirical method. The ISO model 15927 (Bureau voor Normalisatie 2009), the ASHRAE 160 model (Anon 2009) and the SB model (Straube & Burnett 2000) are the three commonly used methods for the calculation of WDR. The main difference of these methods can be found in the prescribed approach of calculating the WDR coefficient, which transfer the calculated free field (or airfield) WDR to the amount received by a building with respect to building geometry and exposure type.

**ISO Model**

In the ISO model 15927, a detailed procedure is provided to assess the actual wind-driven rain impinged on building surfaces based on meteorological data reported by weather stations. The amount of WDR in free field condition, named air field index ($R_{Airfield}$) is calculated by equation 2.2.

$$R_{Airfeild} = \frac{2}{9} \sum U\ .\ R_h^{\frac{8}{9}}\ .\cos(D - \theta) \tag{2.2}$$

where, U is the hourly mean wind speed in m/s, $R_h$ is the hourly rainfall total in mm, D is hourly mean wind direction from north and θ is the wall orientation relative to north; where cos(D-θ) is positive, i.e., all those occasions when the wind is causing flux through the imaginary wall of interest. Different correction coefficients are introduced by ISO model to convert the airfield indices calculated at the place of weather station ($R_{Airfield}$) to wall indices ($I_{WS}$), which is the amount of WDR impinged on the building. These correction coefficients include terrain roughness coefficient ($C_R$), topography coefficient ($C_T$), obstruction factor (O), and wall factor (W). The actual amounts of rain that would impinged on a real wall (wall indices) can be quantified as per equation 2.3.

$$I_{WS} = R_{Airfield}.\ C_R.\ C_T.\ O.\ W \tag{2.3}$$

**Roughness coefficient**

The roughness coefficient accounts for the variability of mean wind velocity due to the height above ground and the upstream roughness of the terrain. Using the procedure outlined in ISO 15927 (2009), the roughness coefficient at height $z$ is given by equations 2.4 and 2.5. The required parameters for each type of terrain category is presented in Table 2.1

$$C_R(z) = K_R \ln\left(\frac{Z}{Z_0}\right) \qquad \text{for } Z \geq Z_{min} \tag{2.4}$$

$$C_R(z) = C_R(Z_{min}) \qquad \text{for } Z < Z_{min} \tag{2.5}$$

Table 2.1 - Terrain categories and related parameters Description (Bureau voor Normalisatie 2009)

| Terrain Category | Terrain description | $K_R$ | $Z_0$ | $Z_{min}$ |
|---|---|---|---|---|
| 1 | Rough open sea; lake shore with at least 5 km open water upwind and smooth flat country without obstacles | 0.17 | 0.01 | 2 |
| 2 | Farm land with boundary hedges, occasional small farm structures, houses or trees | 0.19 | 0.05 | 4 |
| 3 | Suburban or industrial areas and permanent forests | 0.22 | 0.3 | 8 |
| 4 | Urban areas in which at least 15 % of the surface is covered with | 0.24 | 1 | 16 |

**Topography Coefficient ($C_T$)**

The topography coefficient ($C_T$) accounts for the increase of mean wind speed over isolated hills and escarpments. The procedure outlined in the ISO 15927-3, 2009 suggests including $C_T$ for locations (1) more than half-way up the slope of the hill and (2) within 1.5 times the height of the cliff from the base of a cliff. It is defined as follows:

$$C_T = 1 \qquad \text{for} \quad \varphi < 0.5$$

$$C_T = 1 + 2s\varphi \qquad \text{for} \quad 0.5 \leq \varphi \leq 0.3$$

$$C_T = 1 + 0.6s \qquad \text{for} \quad 0.3 < \varphi$$

Where $S$ is a factor obtained from Figure 2 and 3 in the ISO 15927-3, 2009 and $\varphi$ is the upwind slope ($H/L_u$).

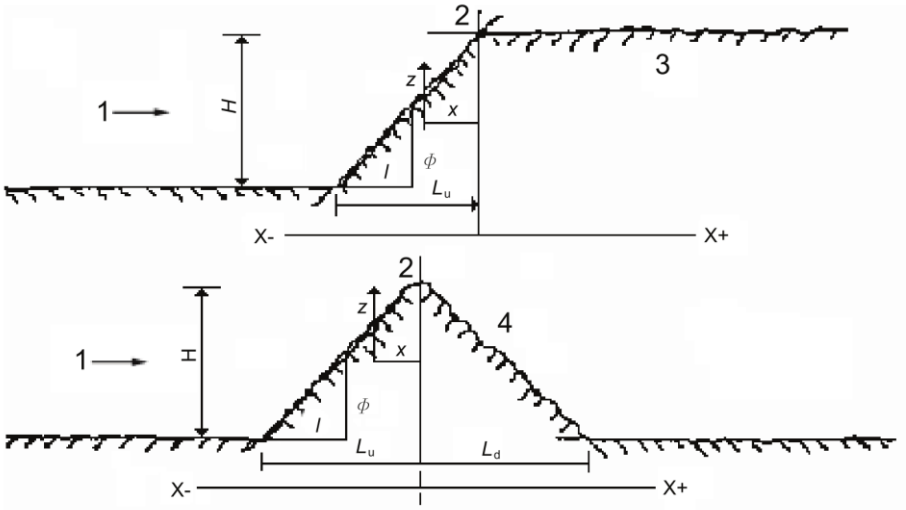


Key
1 wind
2 crest
3 downwind slope < 0.05
4 downwind slope > 0.05
$L_u$ is the actual length of the upwind slope in the wind direction
$L_d$ is the actual length of the downwind slope
Le is the effective length of the upwind slope defined in Table 2
H is the effective height of the feature
X is the horizontal distance of the site from the top of the crest
Z is the vertical distance from the ground level of the site

Figure 2.5 - Definition of factor determining topography coefficient (Bureau voor Normalisatie 2009)

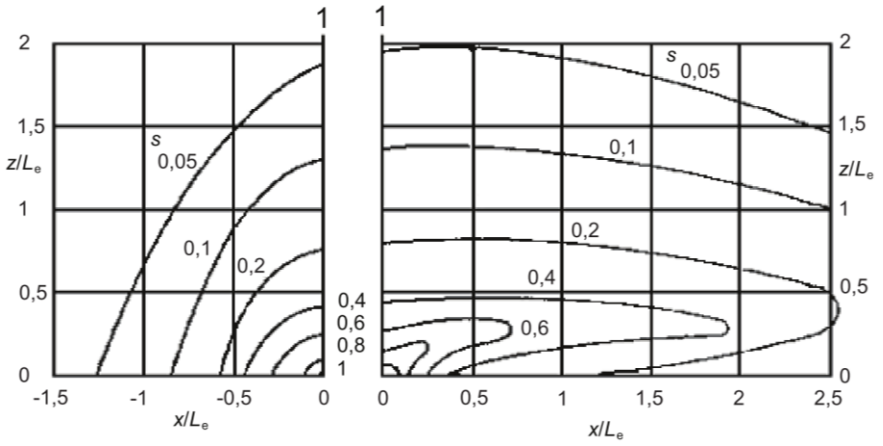


a) Upwind b) Downwind

Figure 2.6 - Factor for cliffs and escarpments (Bureau voor Normalisatie 2009)

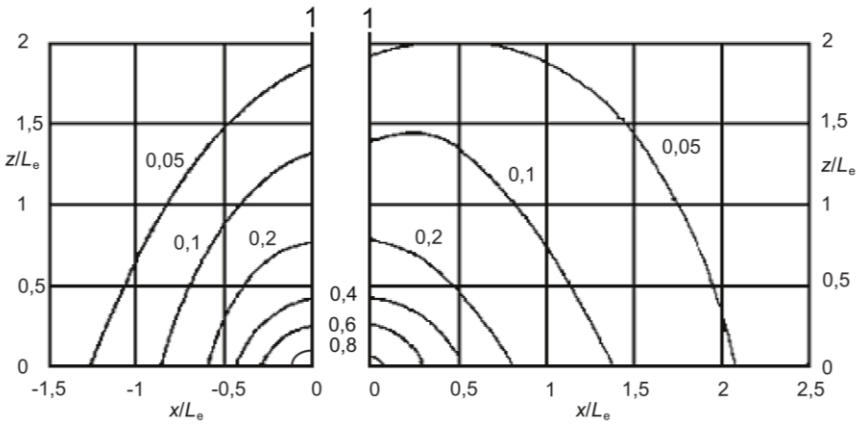


a) Upwind b) Downwind

Figure 2.7 - Factor for hills and ridges (Bureau voor Normalisatie 2009)

**Obstruction Factor (*O*)**

The obstruction factor (*O*) accounts for nearby obstacles that are of equal or greater height to the building. Table 2.2 presents suggested obstruction factors

Table 2.2 – Obstruction factor prescribed by ISO (Bureau voor Normalisatie 2009)

| Distance of obstruction form wall (m) | Obstruction factor (O) |
|---|---|
| From 4 to 8 | 0.2 |
| Over 8 to 15 | 0.3 |
| Over 15 to 25 | 0.4 |
| Over 25 to 40 | 0.5 |
| Over 40 to 60 | 0.6 |
| Over 60 to 80 | 0.7 |
| Over 80 to100 | 0.8 |
| Over 100 to 120 | 0.9 |
| Over 120 | 1.0 |

**The Wall Factor (*W*)**

The amount of rain incident on a wall depends on the type of wall, its height and other factors such as overhangs or the orientation of bricks, etc., within the structure. In addition, the amount of incident rain varies significantly over the surface of a wall due to the flow of air around corners, over the roof, etc. The prescribed wall factor (W) accounts for interaction of WDR with respect to building geometry and the location on the façade.

Table 2.3 – ISO prescribed wall factors (W) for different building geometries (Bureau voor Normalisatie 2009).

| Description of wall | Average value | Distribution |
|---|---|---|
| Two-storey gable | 0,4 | 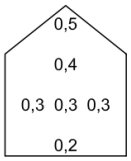 |
| Three-storey gable | 0,3 |  |
| Multi-storey building with flat roof (pitch < 20°) | 0,2 for a ten-storey building, for example, but with a higher intensity at top | 0,5 for top 2,5 m<br>0,2 for remainder |
| Two-storey wall with eaves | 0,3 | 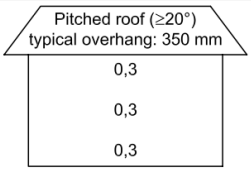 |
| Three-storey wall with eaves | 0,4 | 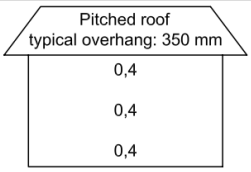 |
| Two-storey building with flat roof (pitch < 20°) | 0,4 | 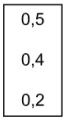 |

**ASHRAE 160 Model**

In this model, the amount of WDR received by vertical facades of building is calculated using equation 2.6.

$$R_{wdr} = 0.2.F_E.F_D.U_{10}.\cos\theta\,.R_h \tag{2.6}$$

where, $F_E$ is the rain exposure factor and $F_D$ is the rain deposition factor. ASHRAE 160 model provides recommended values for these parameters. $R_h$ is the horizontal rainfall intensity in mm/hr, $U_{10}$ is the hourly average wind speed at 10 m in m/s and θ is the angle between wind direction and normal to the wall. Rain exposure factor is influenced by the surrounding topography and building height, Table 2.4. While rain deposition factor represents the vulnerability of wall in receiving WDR or rain runoff, Table 2.5.

Table 2.4 – Prescribed Exposure factor ($E_F$) by ASHRAE in calculation of WDR (ASHRAE 160, 2009)

| Building Height, m (ft) | Type of Terrain | | |
|---|---|---|---|
| | Sever | Medium | Sheltered |
| <10 (<33) | 1.3 | 1 | 0.7 |
| 10-15 (33-49) | 1.3 | 1.1 | 0.8 |
| 15-20 (49-66) | 1.4 | 1.2 | 0.9 |
| 20-30 (66-98) | 1.5 | 1.3 | 1.1 |
| 30-40 (98-131) | 1.5 | 1.4 | 1.2 |
| 40-50 (131-164) | 1.5 | 1.5 | 1.3 |
| >50 (>164) | 1.5 | 1.5 | 1.5 |

Table 2.5 - Prescribed Deposition factor ($D_F$) by ASHRAE in calculation of WDR (ASHRAE 160, 2009)

| Wall Type | Deposition Factor (FD) |
|---|---|
| Walls below a steep-slope roof | 0.35 |
| Walls below a low-slope roof | 0.5 |
| Walls subject to rain runoff | 1 |

**SB Model**

The SB method (Straube & Burnett 2001) use equation 2.7 to calculate the amount of WDR in a free field based on wind direction, wind velocity, rainfall intensity, and driven rain factor (*DRF*), which is defined as the inverse the raindrop terminal velocity of fall ($V_t$), as per equation 2.8.

$$R_{wdr} = DRF.U.R_h.\cos\theta \tag{2.7}$$

$$DRF = {}^{1}/_{V_t} \tag{2.8}$$

The terminal velocity, equation 2.9, of the fall is calculated considering equivalent spherical raindrop diameter ($\varphi$) defined based on horizontal rain fall intensity, equation 2.10.

$$V_{t(\varphi)} = -0.166033 + 4.1984\,\varphi - 0.888016\varphi^2 + 0.054888\varphi^3 \leq 9.20 \tag{2.9}$$

$$\varphi = 1.1042\,.R_h^{0.232} \tag{2.10}$$

Where φ is the equivalent spherical raindrop diameter (mm), $R_h$ is the horizontal rainfall intensity. To transform the amount of WDR from a free field to a particular building some correction factors introduced reflecting building geometry (*RDF*), exposure and height factor (*EHF*) and topography factor (*TOF*), equation 2.11.

$$R_{WDR} = RDF.\ DRF.\ U.\ R_H.\ Cos\ \theta.\ EHF.\ TOF \quad (2.11)$$

The prescribed values for RDF for different building geometries and EHF for different exposure type are presented in Figure 2.8 and Figure 2.9 respectively.

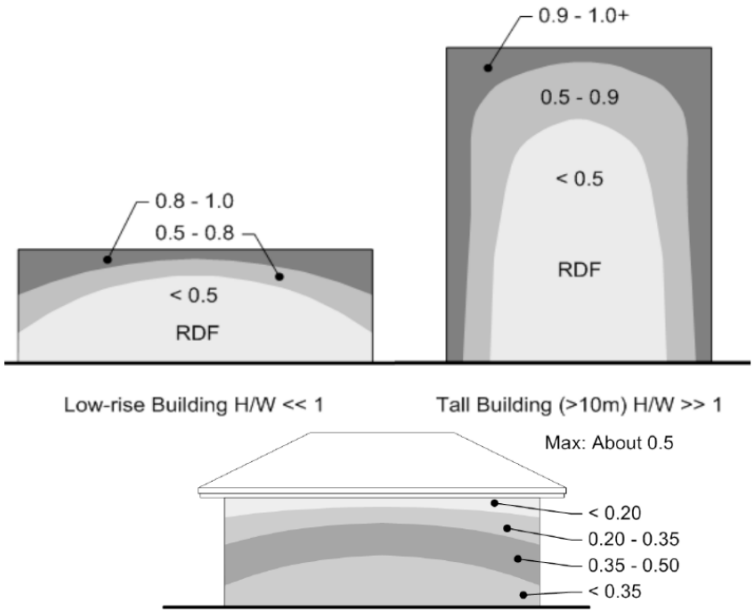


Figure 2.8 – Recommended values for RDF (Straube & Burnett 2001)

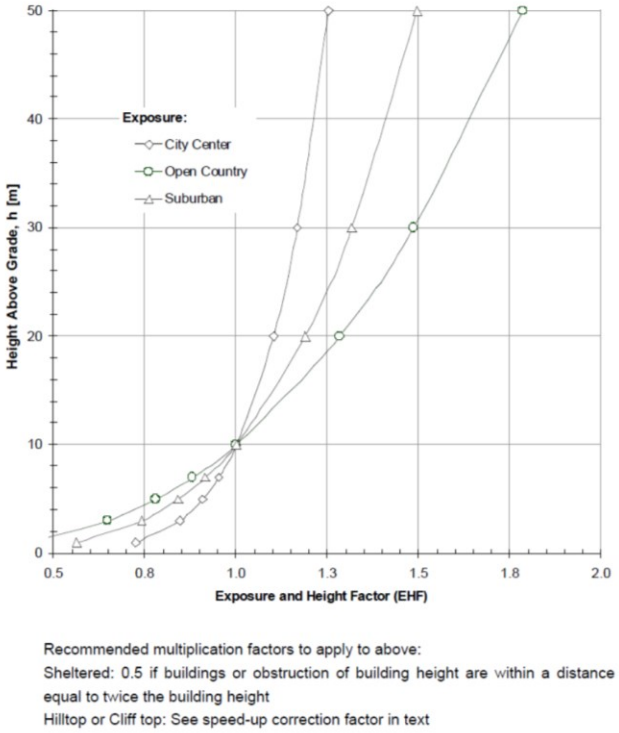


Figure 2.9 - Recommended values for EHF (Straube & Burnett 2001)

Studies shows that discrepancies in calculation of WDR applying different methods is mainly due to the coefficients represent the interaction of building and WDR.

### 2.2.3. Numerical Method

A numerical method for the prediction of WDR intensity on building façade using a computational fluid dynamic techniques (CFD) was proposed by Choi (Choi, 1993). In this method WDR is calculated as the function of the upstream unobstructed rain fall intensity, the rain drop size distribution of the rainfall, the upstream wind speed and the extreme statistics of the co-occurrence of wind and rain(Choi, 1994). The method can be divided into three steps: (a) calculation of the flow pattern around the building, (b) calculation of raindrop trajectories for raindrops of different size and (c) calculation of WDR intensity. Blocken and Carmeliet advanced this simulation method to determine spatial and temporal distribution of WDR on building façade by (1) introducing temporal component and (2) by developing a new weighted data averaging technique (Blocken & Carmeliet 2002).

The results of Numerical method have been validated through experimental measurements in different studies. Blocken, B. calculated the catch ratios on four critical points of three building geometries representing low-rise cubic building, mid-rise wide building slab, high-rise building slab and tower building. The catch ratio is calculated as the function of wind velocity and horizontal rainfall intensity (Blocken 2004) for normal wind direction, Figure 2.10. The CFD modeling is capable of providing accurate spatial distribution of WDR for complex geometries including standalone building or within an array of buildings, investigating the effect of influential factors such as wind speed, wind direction and rainfall intensity on the amount of impinged WDR, studying the effect of building's cornice or overhang in reduction of WDR deposited on areas beneath them.

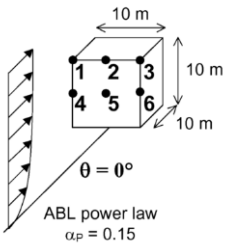


(a)

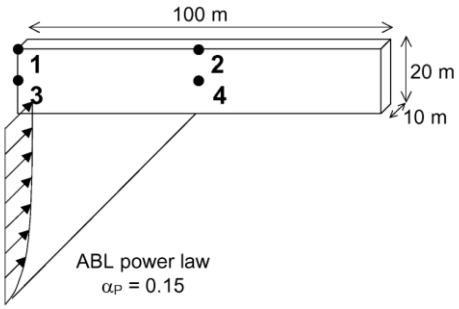


(b)

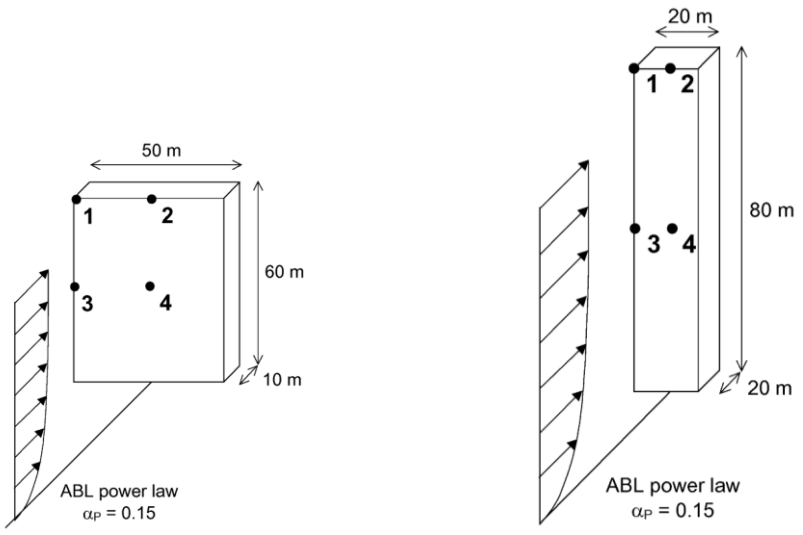


(c) (d)

Figure 2.10 – Catch ratio measuring point on wind-ward façade of (a) low-rise cubic building model, (b) mid-rise wide building slab, (c) high-rise building slab and (d) tower building for normal wind direction (Blocken 2004)

## 2.3. Review of Previous Studies

As mentioned in Chapter 1, the objective of this study is to quantify overhang effectiveness in reduction of impinged WDR on mid-rise buildings and improve the assessment of WDR on building façade using the ISO model. Field measurements and calculations using the ISO semi-empirical model are the two procedures applied in the current study to fulfill the research objectives. This section focuses mainly on reviewing existing studies to identify the knowledge gaps related to the two outlined objectives. Previous studies are presented in three categories, namely: (a) field measurements and WDR spatial distribution, (b) accuracy of ISO semi-empirical model and (c) roof overhang effectiveness in reduction of WDR impinged on building's windward façade.

**Field Measurements and WDR Spatial Distribution**

In the field studies of WDR, WDR gauges were installed on building facades with respect to prevailing wind direction of the study area, surrounding conditions, building geometry and vulnerability of different parts of the façade in receiving WDR. Also, on-site meteorological data

typically including wind speed, wind direction and rainfall intensity, was monitored during the study period.

The results from field measurements have yielded and validated the classic wetting pattern, whereby: (1) the windward facade receives the majority of wetting, (2) on the windward facade, wetting increases from the bottom of the facade to the top and from the middle of the facade to the sides; the top corners are the most wetted, followed by the top and side edges, (3) for tall and wide buildings, the windward facade receives relatively little rain, except for the top corners and top and side edges due to building's blocking effect, (4) The WDR intensity at a specific location increases proportionally with wind speed and horizontal rainfall intensity (Blocken et al. 2004).

In the experiment conducted by Blocken & Carmeliet (Blocken & Carmeliet 2004), the amount of WDR on windward facade of a low-rise building located in Belgium was measured. A comprehensive guideline was provided concerning the design of WDR gauges and guidelines for the selection of accurate and reliable WDR measurement data from WDR databases (Blocken et al. 2005; Blocken & Carmeliet 2006c). Nore quantifies the errors of a wall mounted WDR gauge with tipping bowls and their frequency of occurrence based on rain spell and climate characteristics (Nore et al. 2007). Ge (2007) studied the WDR spatial distribution on a low-rise building. A more comprehensive study by Ge and Krpan carried out field measurements of WDR on eight buildings with different geometries in the coastal climate of British Columbia, Canada. Field measurements showed that roof overhangs can significantly reduce the amount of received WDR and the provided protection can be extended up to the half of the low-rise building and 2.5 m below the roof line of the mid-rise buildings (Ge & Krpan 2009).

Briggen (2009) carried out field WDR measurements on a monumental tower and the field data was used for validation of the CFD modeling. The discrepancy in catch ratio between field measurements and CFD simulations was acceptable for upper parts of the tower, however, the difference was considerable for lower positions. The difference is mainly attributed to not considering turbulence on the dispersion of the rain drops in CFD modeling. In 2009, Abuku investigate the reliability of simplified implementation of WDR in traditionally approach of HAM analysis through an experimental set up. The "splashing/bouncing error" and "averaging error" was introduced as the main reason of discrepancy between experimental results and numerical analysis (Abuku et al. 2009b).

Kubilay investigated the WDR intensity distribution in a multi-building configuration including an array of nine low-rise cubic buildings. WDR was measured on the wind-ward façade of two buildings to investigate the sheltering effect of nearby buildings on the amount of WDR received. Significant discrepancies were observed between measurements and estimations using semi-empirical ISO model (Kubilay et al. 2014).

Juras and Jakubcik studied the hydrothermal performance of a traditional brick wall, facing prevailing wind direction, by applying WDR measured onsite in comparison with applying WDR values estimated based on ISO Standard, WUFI WDR estimation, and CFD simulations. While the moisture content of brick wall by applying WUFI WDR model and CFD simulation shows a good agreement with measured data, the ISO model overestimated the moisture content of brick wall (Juras & Jakubcik, 2016).

Ge, H. et al. (2017a) generates high resolution and high-quality field measurements of WDR on mid and high-rise buildings located in two Canadian regions. The spatial distribution of WDR is discussed in term of catch ratio and wall factor with respect to wind speed, wind direction, rain fall intensity and building geometry. Wind tunnel test conducted by Chiu (2016) investigated wind velocity near windward façade of the scaled down model of Vancouver test building. The results show that there is a good agreement between WDR distribution on the façade under real life condition and normalized wind velocity near the façade measured on the wind tunnel. The highest normalized wind velocity can be observed on top corners followed by top and side edges. Both values reduce with respect to distance from the roof and side edges towards the central part of the façade (Ge et al. 2018).

**Accuracy of ISO model**

Semi-empirical models have been widely used by building engineers and designers due to their simplicity. However, these methods are based on WDR measurements, for which no error estimation were provided (Baheru et al. 2014). As a result, the assessment of the accuracy of these models is necessary. For the ISO model, the validity of the cosine projection, which takes into account the effect of varying wind direction on the WDR intensity received by building facade and prescribed wall factor for different building geometries have been studied.

The validity of cosine projection is investigated based on 3D CFD numerical simulations of WDR by Blocken and Carmeliet (2006 b) for a simple cubic building. It is shown that the cosine

projection, although generally accepted, is not valid and it can give rise to significant errors. For more complex building models, the complexity of wind flow around the buildings increase the complexity of WDR distribution pattern. In such cases, the failure of the cosine projection is likely to be even more pronounced (Blocken & Carmeliet 2006b), however, no alternative is available.

Blocken use WDR measurement of two study buildings to assess the accuracy of semi-empirical methods, i.e. ISO and SB model, in the calculation of WDR. The main contributing factors in discrepancy between measurements and calculations by the empirical methods are the lack of variation in wall factor along building width, limited building geometries, and not considering the effect of roof overhang (Blocken et al. 2011).

Carbonez et al discussed the impact of spell definition on the rain deposition on the building façade in comparison with 5-minute data that contains important information on the peak loads discarded by the spell definitions (Carbonez et al. 2015). The effect of time resolution and averaging techniques was studied by Ge, H. on the estimation of wind-driven rain load on building facades. 5-minute data was converted to hourly data using arithmetic and weighted averaging. The analyses show that when semi-empirical WDR models are used, the arithmetic averaging gives a better estimation while the weighted averaging tends to overestimate the WDR amount (Ge 2015).

The accuracy of prescribed wall factor by ISO model for mid-rise buildings was studied by Nath (2015). The field study included measurement of onsite meteorological data and impinged WDR on wind-ward façades of three test buildings, located in three Canadian cities, with high resolution in time and space, which provides a unique set of data to calculate the wall factor based on onsite measurements. The results show that wall factor varies with respect to the distance from roof top and side edge of the building. Building geometry and meteorological data are other factors which lead to discrepancy in wall factor (Nath et al. 2015). It also has been shown that although applying wall factor calculated based on onsite measurement instead of ISO prescribed wall factor improves the estimation of WDR using meteorological data from weather stations, the discrepancy cannot be completely eliminated (Ge et al. 2017).

**Roof Overhang Effectiveness**

Roof overhangs have been traditionally used for several purposes including protection against rain. Field observations have shown that the shape of roofs and overhangs have a significant impact on WDR wetting of building facades under certain climatic conditions (Ge et al. 2017).

Field observations have shown that overhangs are effective in reducing WDR wetting of building facades under certain climatic conditions, there has not been any systematic study on quantifying the effect of overhangs on WDR loads, especially through field measurements. In many previous studies, overhangs are part of the buildings on which data is collected. The existence of the overhang is, thus, merely reported rather than being studied as a parameter.

Surry and Inculet (1994) studied the influence of building geometry and architectural details such as balconies, cornices, pitched roofs, and inset corners on the wetting pattern of scaled down building models placed in a boundary layer wind tunnel. Water-sensitive paper has been used to investigate the effect of each of factors in spatial distribution of WDR on facades. The results indicated that cornices may be successful in protecting the top of the building facade just below the cornice. In a survey published by CMHC investigating building envelope failures in lower mainland of British Columbia, lack of water management principles in wall assemblies design and construction was the main contributing factor in water penetration. Also, it has been observed that roof overhangs have reduced the wall WDR exposure and related damages proportional to overhang width (Hazleden & Rousseau 1996).

Blocken and Carmeliet (2006a) performed WDR measurements on a low-rise building with a combination of a flat-roof and a sloped-roof with different overhang widths. Their study found that the flat roof with a smaller overhang width received significantly more rain than the sloped roof with a slightly larger overhang. Overhangs protect the walls below them by shadowing and redirecting airflow (Blocken & Carmeliet 2006a). Field measurements of WDR carried out by Ge and Krpan (Ge et al. 2009) in Southern British Columbia showed that by having typical overhangs (0.3-0.6 m width) on low-rise buildings and a 0.9 m overhang on a 12-story high-rise building, the deposition of WDR on the building can be significantly reduced, especially at the upper portion of the façade. By reducing the amount of WDR impinged on the top of the façade, the rainwater runoff that will add to moisture load to the lower portion of the façade, will also be reduced.

Quantifying roof overhang was conducted using CFD modeling by Blocken (2004, 2007) and more comprehensively by Foroushani (2013, 2014) with respect to wind speed, wind direction and rainfall intensity for various overhang sizes for a cubic building geometry (Mohaddes Foroushani 2013; Mohaddes Foroushani et al. 2014). A similar study was conducted for a mid-rise building by Khalilzadeh (2017). Both studies shows that the sensitivity of the overhang effectiveness under a variety of rainfall intensities is not large enough to make a significant difference in the effectiveness

(Khalilzadeh 2017). In a more recent study, Kublilay investigated the effect of façade detailing such as roof overhang and balconies on the deposition of WDR on a mid-rise building (Kubilay et al. 2017) by CFD modeling. In general, WDR spatial distribution agree with field measurement results observed by Chiu (2016) for mid-rise building. Also, it has been indicated that higher wind velocities reduce overhang and cornice performance in reduction of WDR received by the facade.

The only systematic study on quantifying the effect of overhangs on WDR loads, through field measurements, has been conducted by Ge (2017) for a mid-rise building located in Vancouver, BC. In this study, the amount of WDR deposited on different portions of the façade is studied as a function of overhang width. The percentage of protection provided by different overhang size is calculated based on area-weighted catch ratios. Also overhang effectiveness is discussed with respect to wind speed and wind characteristics. The results show an exponential relation between overhang size and percent of protection provided for the entire façade (Chiu 2016; Ge et al. 2017; Ge et al. 2017).

## 2.4. Knowledge Gap

A comprehensive research program is designed to quantify wind-driven rain loads on mid-rise buildings and the effectiveness of overhang in reducing WDR wetting of building façade. Within this research program, field measurements of WDR on four mid-rise buildings in three Canadian regions were carried out. A six-story building in Vancouver is fitted with retractable overhang to quantify the effectiveness of overhang. Findings from these research work have been reported in Nath (2015) and Chiu (2016). Current study is a continuation of the previous studies by Nath and Chiu and focuses on further analysis of field measurements of WDR to quantify the effectiveness of overhang with more complete data and further investigation of the accuracy of ISO WDR model in WDR estimation as a semi-empirical method.

# 3. Experimental Setup and Methodology

The research work presented in this thesis is a follow-up of research work carried out within a comprehensive research program in quantifying wind-driven rain loads on mid-rise buildings and overhang effectiveness and is a continuation of the previous studies by Nath (2015) and Chiu (2016). Therefore, the methods and procedures established in previous studies are followed and presented here.

Nath (2015) reported the field measurements and analysis of WDR on three buildings in Montreal and Fredericton. Chiu (2016) reported the methodology developed in quantifying the effectiveness of overhang based on field measurements and validation of onsite WDR measurements using wind tunnel experiment. Based on data available, Chiu's study established the correlation between WDR loads on facade with overhang size and investigated the effect of wind speed and wind direction on the overhang effectiveness for the six-story mid-rise building in Vancouver. In this thesis, the following work have been carried out:

1) Further data analysis on the effectiveness of overhang on the six-story mid-rise building in Vancouver; with more data available, following the established procedure, the current study is able to establish more detailed correlation between overhang size and WDR loads on facade considering wind speed and wind direction. Results of the further analysis reported in this thesis validate the methodology developed in Chiu's work. This work is reported in Ch. 4.

2) Development of a method to generalize the WDR reduction coefficients for different overhang widths provided through field measurements for mid-rise buildings with similar geometry; wind tunnel measurements are carried out to confirm the similarity of wind flow around the six-story building in Vancouver and the seven-story building in Fredericton. A procedure is developed to apply the WDR reduction coefficients by overhangs established based on measurements on Vancouver building to Fredericton building. Considering the wind speed and wind direction characteristics of the specific site of Fredericton building, the effectiveness of overhang on WDR loads on facade of the Fredericton building is quantified. This work is reported in Ch. 5.

3) Improvement of accuracy of ISO model to assess the WDR loads on façade; previous studies show that estimation of WDR based on ISO standard is generally subjected to overestimation. The

ISO prescribed wall factor was considered as the main contributing factor for the over-estimation. Applying wall factor calculated based on measurements instead of ISO prescribed wall factor improves the results, however, a significant amount of discrepancy can still be observed between measured WDR and calculated wall indices. Further investigation of main contributing factors is carried out. Parameters investigated include: 1) time resolution, 2) difference in wind speed and wind direction between site and nearby weather station; and 3) type of precipitation. This work is reported in Ch. 6.

The procedures and methods reported in section 3.1-3.6 have been established in previous studies by Nath and Chiu, while methods reported in section 3.7 and 3.8 are developed within this thesis.

## 3.1. Measurement Setup

WDR load on building façade has been studied under real life condition by monitoring four test buildings located in three Canadian regions as shown in Figure 3.1. The field measurements were set up and carried out by Nath (2015) and Chiu (2016) and the preliminary data analysis and findings were reported in IBPC 2015 (Nath et al. 2015; Chiu et al. 2015), Building and Environment (Ge et al. 2017), CCBAT 2017 (Ge et al. 2017), and Journal of Wind Engineering & Industrial Aerodynamics (Ge et al. 2018). For the purpose of completeness, description of test buildings, field measurement setup, instrumentation and sensor locations are included in this thesis. All test buildings are equipped with a roof top weather station and WDR gauges on the facades.


Figure 3.1 - Location of test buildings for wind-driven rain studies across Canada (Google Maps)

### 3.1.1. Test Buildings

All test buildings are multi-storey mid-rise building with low slopped (flat) roof equipped with weather station for simultaneous record of meteorological data. Sufficient number of WDR gauges has been installed on each building's facades specifically on facades facing prevailing wind direction. Detail of these buildings, terrain type and number of installed WDR gauges are shown in Table 3.1. Moreover, Vancouver building is equipped with a retractable roof overhang to study the effect of overhang in reduction of WDR load on building façade.

Table 3.1 - Test building`s specifications and site type

| ***Test Building Location*** | ***Exposure*** | ***Construction type*** | ***Roof type*** | ***Buildings` Façade Orientation From N*** | ***No. WDR Gauges*** |
|---|---|---|---|---|---|
| Cassiar Building, Vancouver, BC | Suburban | Six- Storey Residential Building | Flat roof without overhang | 0° (North)<br>90° (East)<br>180° (South)<br>270° (West) | 11 (North)<br>18 (East)<br>1 (South)<br>1 (West) |
| McLeod house, Fredericton, NB | Suburban | Seven- storey, Residential Building | Flat roof without overhang | 33° (North-east)<br>123° (South- east)<br>213° (South- west)<br>303° (North- west) | 2 (North-east)<br>6 (South- east)<br>7 (South- west)<br>1 (North- west) |
| Concordia University, FB Building, Montreal, QC | Urban | Thirteen-storey, Office Building | Flat roof without overhang | 42° (North-east)<br>132° (South- east)<br>222° (South- west)<br>312° (North- west) | 10 (North-east)<br>6 (South- east)<br>7 (South- west)<br>1 (North- west) |

The satellite image of test buildings and their surrounding area are presented in Figure 3.2. Vancouver building is a six-storey residential building located in fairly open site within suburban setting (Figure 3.2a). The building sits atop an escarpment surrounded by three-storey residential buildings to its north and west and a highway to its east and south. The building has a simple cubic geometry with dimension of 39.2 m long, 15.2 m wide, and 19.8 m high with facades facing the cardinal directions. This building's main axis is north-south causing the main building façade facing towards the east, which is the prevailing wind direction.

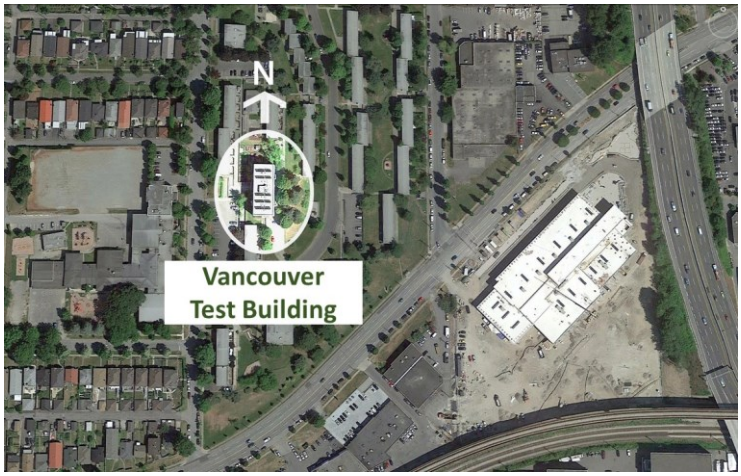


(a)


(b)


(c)

Figure 3.2 - Aerial view of the test buildings' site, (a) Vancouver, (b) Fredericton (c) Montreal (Google Maps)

McLeod House is a seven-storey student residence located at University of New Brunswick, Fredericton (Figure 3.2 b). On the west to south-west side is a parking lot with a long field of trees. These trees are about 40 m away from the building. There are a couple of low-rise houses on the south-east side, located over 100 m away from the building. On the north-east side is an open grass field with some low-rise constructions across the road, over 130 m away from the building. The height of the building is 22 m and the building's footprint consists of two overlapping rectangles. The building's main axis is rotated by around 60 degrees from cardinal directions.

Concordia FB Building is a thirteen-storey office building located in downtown Montreal (Figure 3.2 c). On the south-west direction there is a five-storey wing attached to the building. On the north-west side there is a five-storey building located about 25 m away. Farther, there exists a fifteen-storey building located about 60 m away. On the south-east side there is a four-storey building located about 22 m away. On the north-east side the nearby building is three storeys high with 23 m distance. The building is 45.6 m high with the main axis of north-west to south-east rotation angle of 48 degrees from the cardinal direction.

### 3.1.2. Instrumentation and Sensor Location

The equipment installed consists of a wind anemometer, a temperature and relative humidity probe, a horizontal rain gauge, and a number of customized driving rain gauges. The wind anemometer measures the wind speed and wind direction and is mounted on top of a tripod cross-arm that is 4.6 m above the mechanical room located on top of the main roof for both the office building in Montreal and the residential building in Vancouver, while the tripod is located at the centre of the main roof of the student residence in Fredericton (Ge et al. 2017). The specifications of used measuring equipment are provided in APPENDIX A. WDR gauge installed has a dual tipping bucket and a square collection area customized to minimize the wind error. More detailed information for each measuring instrument can be found in Chiu, 2016.

Locations of driving rain gauges on building façades are selected strategically based on the prevailing wind direction, building geometry and surroundings. Prevailing wind direction during rain hours is identified for each test building based on the analysis of historical meteorological data provided by Environment Canada. A greater number of WDR gauges are installed on façade facing prevailing wind direction.

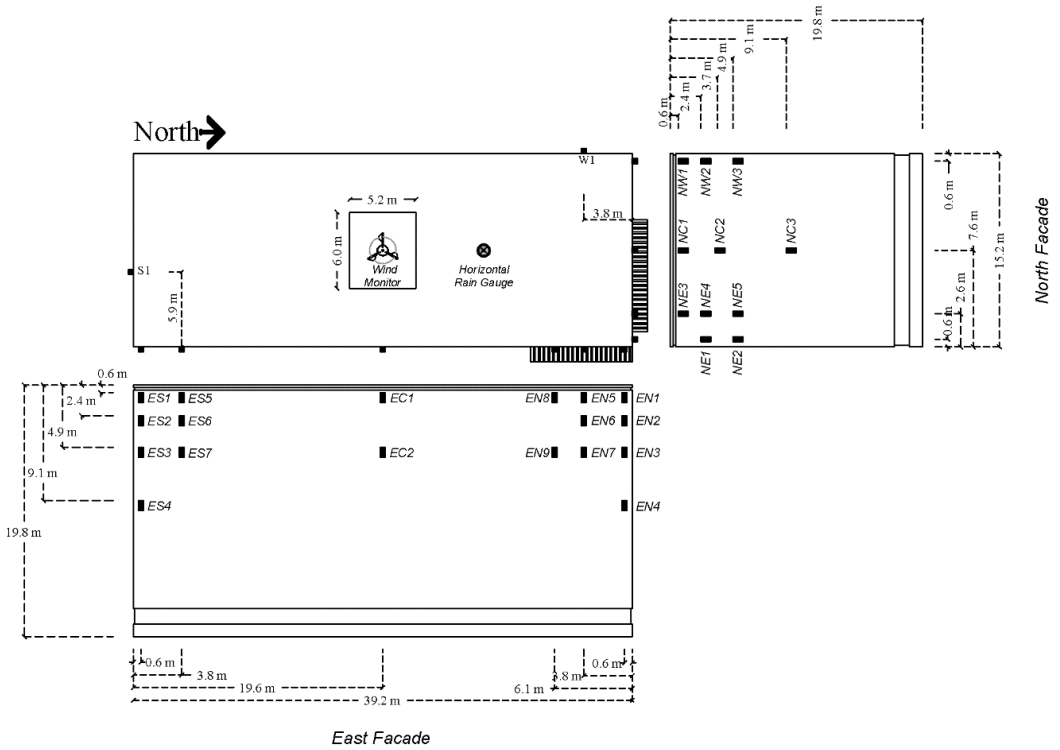
North
W1
5.2 m
3.8 m
6.0 m
Wind Monitor
Horizontal Rain Gauge
S1
5.9 m
0.6 m
2.4 m
4.9 m
9.1 m
19.8 m
ES1 ES5 EC1 EN8 EN5 EN1
ES2 ES6 EN6 EN2
ES3 ES7 EC2 EN9 EN7 EN3
ES4 EN4
0.6 m
3.8 m
19.6 m
6.1 m
39.2 m
East Facade
NW1 NW2 NW3
NC1 NC2 NC3
NE3 NE4 NE5
NE1 NE2
0.6 m
7.6 m
15.2 m
2.6 m
North Facade

(a)

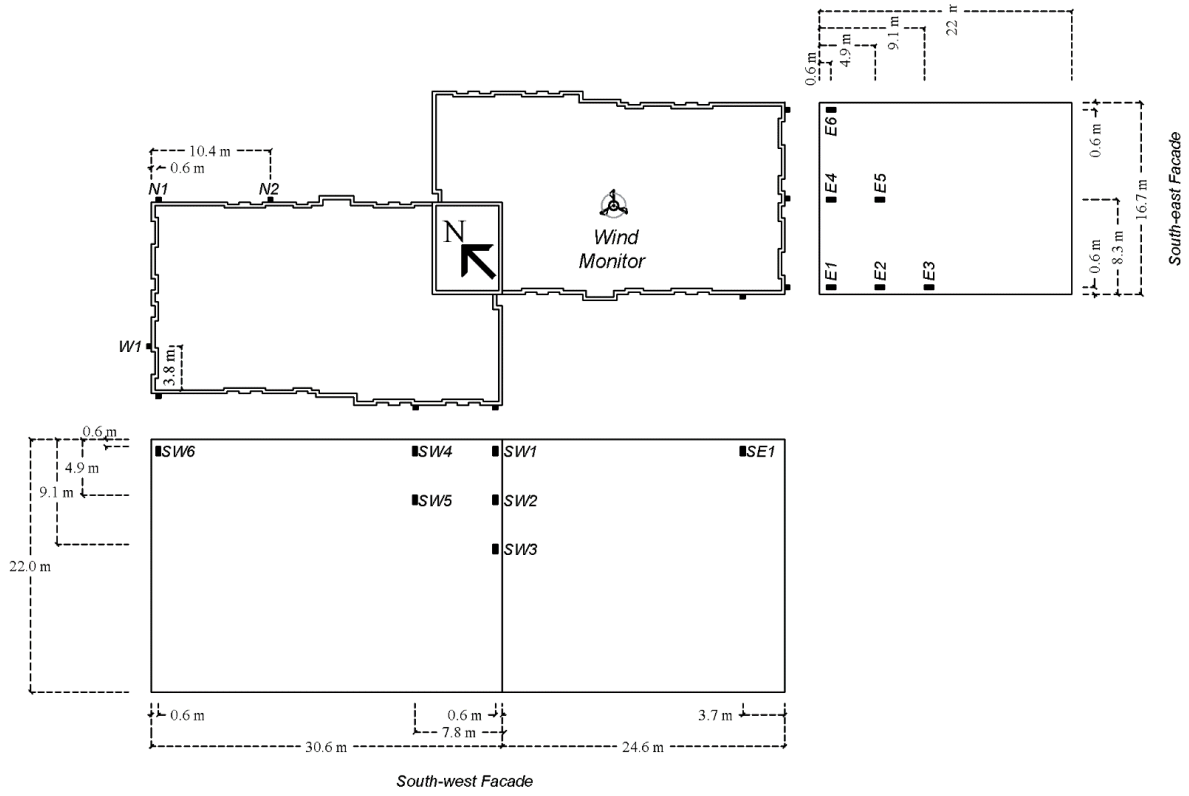
10.4 m
0.6 m
N1
N2
N
Wind Monitor
W1
3.8 m
0.6 m
4.9 m
9.1 m
22.0 m
SW6 SW4 SW1 SE1
SW5 SW2
SW3
0.6 m
7.8 m
3.7 m
30.6 m
24.6 m
South-west Facade
0.6 m
4.9 m
9.1 m
22 m
E6
E4 E5
E1 E2 E3
0.6 m
16.7 m
8.3 m
South-east Facade

(b)

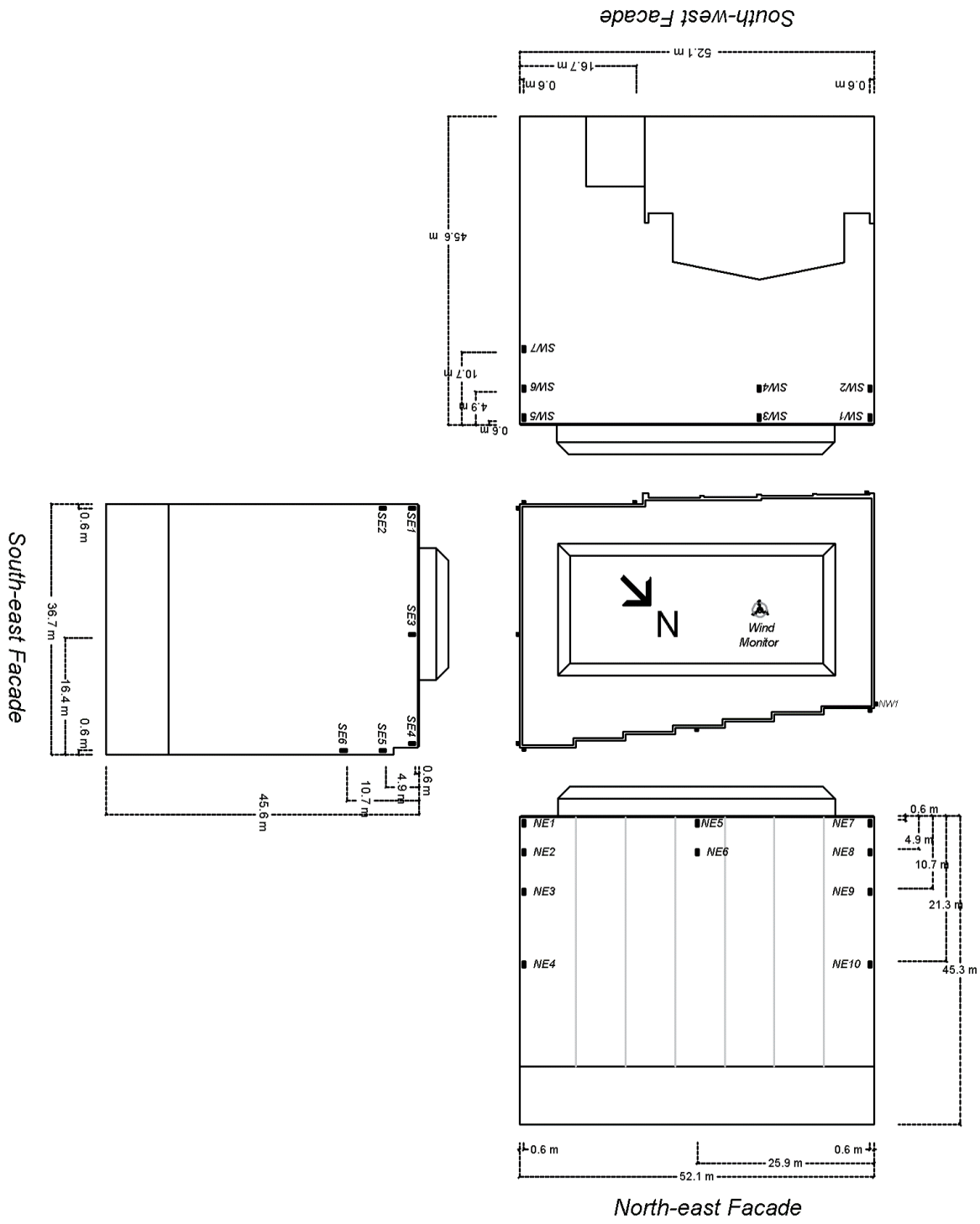


(c)

Figure 3.3 - Driving rain gauge locations on main façade of (a) residential building in Vancouver (b) student residence in Fredericton; and (c) office building in Montreal.

To capture the distribution of WDR on façade, the driving rain gauges are placed at various locations both horizontally and vertically with a focus at the top, sides and corners to create a grid representing a typical wetting pattern on façades. These gauges are typically installed vertically along the corner of the façade at varying heights i.e. 0.61 m (2′), 2.44 m (8′), 4.88 m (16′) below the roofline and at a half height of the building. Figure 3.3 shows the location of anemometer on roof and the location of installed WDR gauges on the main facades of these three buildings.

### 3.1.3. Data Collection and Processing

All equipment is connected to a data logger that collects and saves the data every 5 min. Arithmetic-averaging technique is used to obtain hourly data. Vancouver building data collection started in August 2013 to February 2018 and can be divided into 5 sub-periods regarding overhang size including:

1) No Overhang: 16 August 2013 to 1 December 2014 (456 days)
2) 4 feet OH (1.2 m): 2 December 2014 to 1 March 2015 and 3 December 2015 to 21 April 2016 (263 days)
3) 2 feet OH (0.6 m): 2 March 2015 to 2 December 2015 (275 days)
4) 3 feet OH (0.9 m): 22 April 2016 to 14 September 2017 (510 days)
5) 1 feet OH (0.3 m): 15 September 2017 to 20 February 2018 (158 days)

For Fredericton data measured during the period of 21$^{th}$ of June 2015 to 7$^{th}$ of November 2016 (505 days) are used for analysis. The data collection in Montreal consists of two study periods, first, 25$^{th}$ of July 2014 to 16$^{th}$ of June 2015 and second, 13$^{th}$ of October 2016 to 13$^{th}$ of July 2017; in total 595 days. Monitoring test buildings for long period of time provided this opportunity to study WDR during different annual climate condition.

For all study periods, onsite wind and rain conditions have been analyzed and compared with data collected from nearby meteorological weather station. Similar procedures developed in the previous studies are followed to carry out error analysis, calculate catch ratio, driven rain airfield index and wall factors. These parameters are used for further calculations regarding quantification of overhang effectiveness and the assessment of ISO model accuracy.

## 3.2. Wind Tunnel Setup

First, given that overhang effectiveness is calculated and quantified based on field measurement on Vancouver Building, results should be generalized for similar mid-rise building geometries located in similar terrain. To fulfill this objective wind velocity near the Vancouver building east facade and Fredericton south-west façade that have almost similar geometry has been measured and normalized velocities has been compared. Later, the effect of overhang on wind flow deflection and wind velocity reduction near the mentioned facades has been studied by adding 0.6 cm (1.2 m) overhang on the rooftop of 1:200 scale model of both test buildings.

In Fredericton test building, the weather station is installed on the main roof with enough distance from the mechanical room. The height of the anemometer is 4.5m above the main roof, which is comparable to the height of the mechanical room. The second objective is to confirm whether the presence of the mechanical roof has an influence on the wind flow at the anemometer location. The wind velocity has been measured at the place of anemometer of Fredericton down scaled model with and without presence of mechanical room on the model. Prior to the studies, a suburban exposure has been created using roughness elements and a suburban exposure of south-west facades of Fredericton building has been verified.

### 3.2.1. Concordia Atmospheric Boundary Wind Tunnel

Concordia University's atmospheric boundary-layer wind tunnel is located in the Building Aerodynamics lab of the Engineering, Computer Science and Visual Arts Integrated Complex at the Sir George Williams campus. It is an open-circuit blow down wind tunnel with a centrifugal blower and a rectangular cross-section. The tunnel has a test section 12.20 m long, 1.80 m wide and has an adjustable suspended roof with a minimum and maximum height of 1.40 m and 1.80 m, respectively. The wind tunnel is equipped with a 1.21 m diameter turntable downstream of the test section (Chiu 2016).

A MARK HOT double inlet centrifugal blower with a capacity of 40 $m^3/s$ at a static pressure of 4 cm of water is capable of producing a maximum wind velocity of 14 m/s. The velocity distribution in an empty tunnel is approximately symmetric with respect to the vertical axis passing through the center of the turntable. Measurements show that there is a ±4% deviation from the

mean velocity below 250 mm height (Stathopoulos 1984). A schematic of the wind tunnel is shown in APPENDIX A.

### 3.2.2. Exposure and Model

The model of two study buildings (Vancouver and Fredericton) have been tested in the wind tunnel. As both buildings are located in a suburban environment, a suburban exposure is simulated in the wind tunnel. Similar to the experiment conducted by Chiu (Chiu 2016), a mixture of roughness elements have been placed along the length of the test section of the tunnel to obtain a similar exposure with the right mean speed exponent for suburban terrain. The roof of the wind tunnel was adjusted along the length of the test section to satisfy the condition of zero longitudinal pressure gradient for a suburban exposure. The blower was set to the maximum speed.

Figure 3.4 - Wind tunnel exposure simulation, Suburban terrain

### 3.2.3. Test Buildings Model

For the first objective, a 1:200 scale of stand-alone models of Vancouver and Fredericton building was placed in ABL wind tunnel. Due to high wind velocity in wind tunnel, the effect of 1.2 m overhang was not evident at the measurement points of 1:400 model.

Each model was fabricated of plywood and placed in the middle of turning table. The wind velocity was measured at the distance of 14 mm from the façade due to the profile of Cobra probe and size of the overhang added to the models, 6 mm, making sure the velocity is measured at the similar points with and without overhang. The measurement grids over the facades are mainly defined based on the location of WDR gauges on the Vancouver building. For comparison purposes an almost similar grid is defined for Fredericton model. In total the wind velocity is measured at 29 points and 52 points near Vancouver and Fredericton model respectively. Dimensions of 1:200 scale models and location of measuring points of each test building is shown in Figure 3.5 and Figure 3.6.

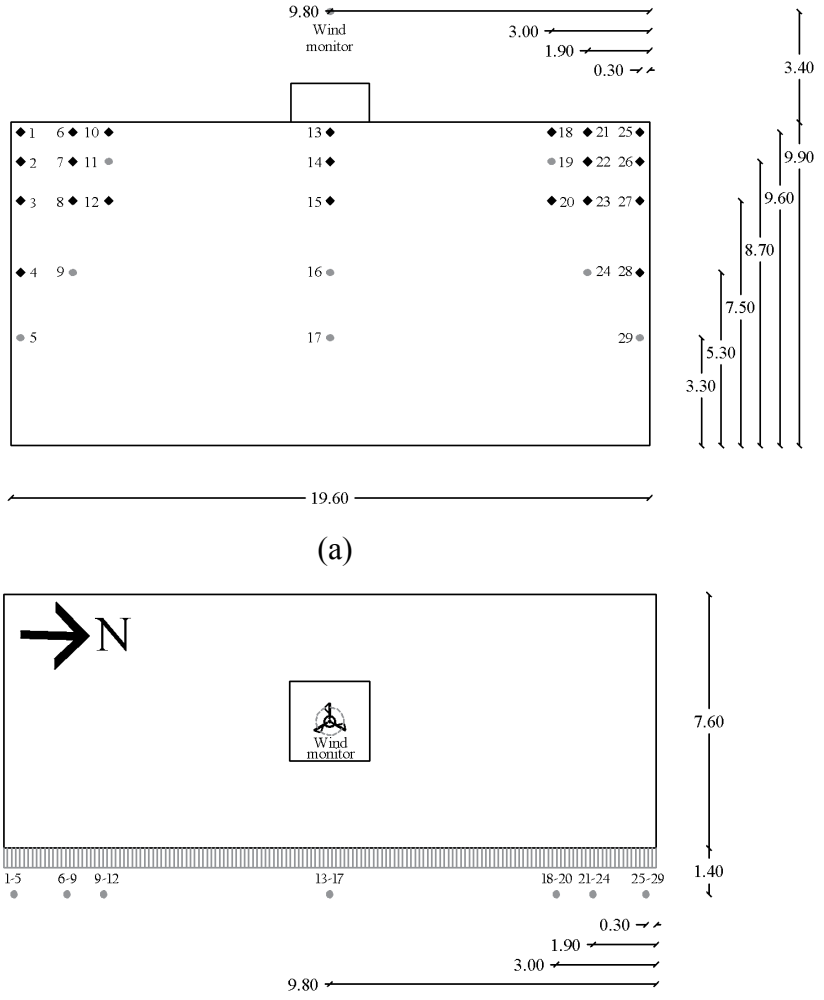


Figure 3.5 - East elevation (a) and top view (b) of the Cassiar building model with 1.2 m overhang (scale 1:200). The measurement points near the east facade are shown in addition to the wind monitor location. All values are in cm.

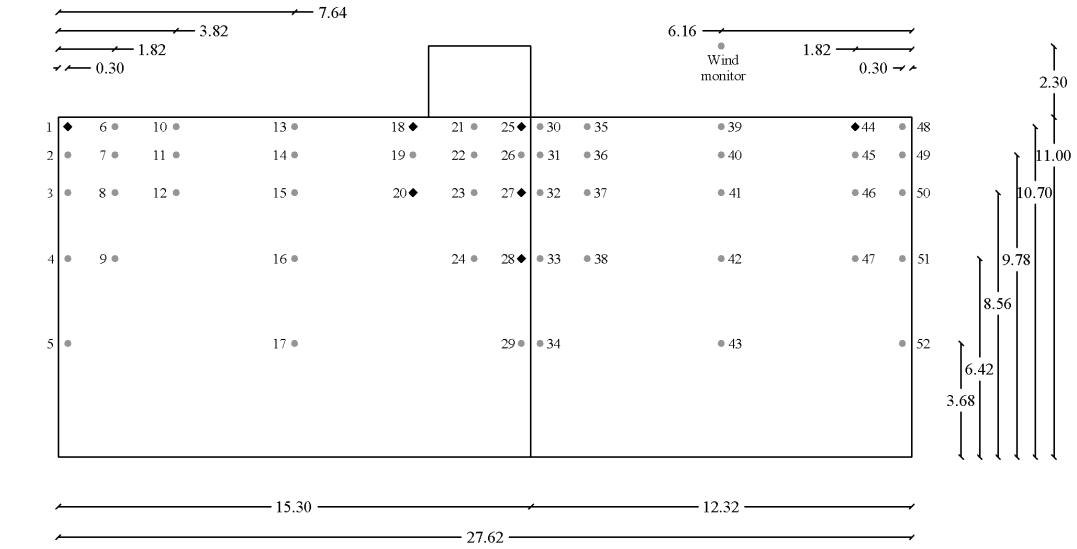


(a)

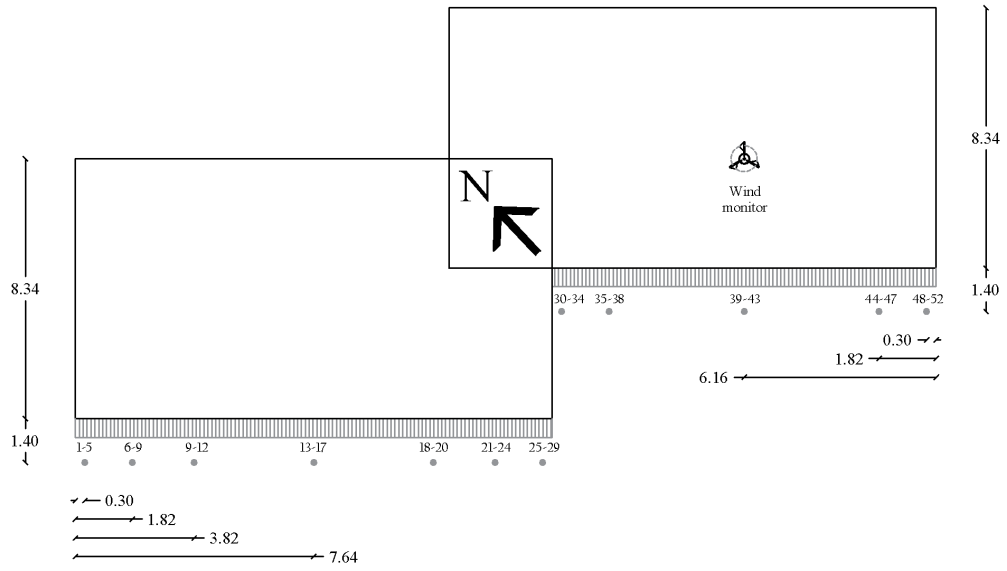


(b)

Figure 3.6 - South-west elevation (a) and top view (b) of the McLeod House building model with 1.2 m overhang (scale 1:200). The measurement points near the south-west facade are shown in addition to the wind monitor location. All values are in cm.

For the second objective, a 1:400 scale model of the Fredericton building and its surroundings within a 200 m radius have been fabricated and placed in an ABL wind tunnel. The 1:400 scale was selected based on the surroundings and successful simulations at this scale of the most important variables of the atmospheric boundary layer under strong wind conditions, carried out in this wind tunnel (Stathopoulos, 1984). The wind velocity was measured at the place of anemometer

for eight wind directions with 45 degrees interval with and without the mechanical room, as shown in Figure 3.7. The same experiment was repeated for the 1:400 and 1:200 standalone models of Fredericton building for comparison purposes.

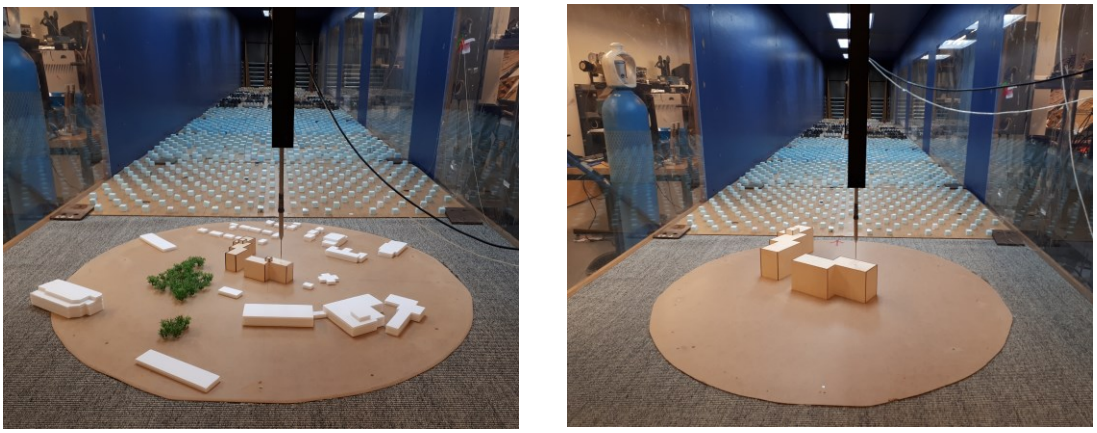

(a) (b)

Figure 3.7 - McLeod House model for wind tunnel experiment, (a) 1:400 model with surroundings, (b) 1:200 model without surroundings

### 3.2.4. Wind Velocity Measurement

To measure the velocities in the wind tunnel, a Series 100 Cobra Probe was used. The Cobra Probe is a multi-hole pressure probe that provides dynamic, 3-component velocity and local static pressure measurements in real-time. The Probe is capable of a linear frequency response from 0 Hz to more than 2 kHz and is available in various ranges for use between 2 m/s and 100 m/s (Turbulent Flow Instrumentation, 2011). Also, the angles between velocity vectors is provided which is used to determine the flow direction near the façade. Yaw angle can be defined as the azimuth and the pitch is the angle between the flow velocity vector and the XY plane, Figure 3.8.

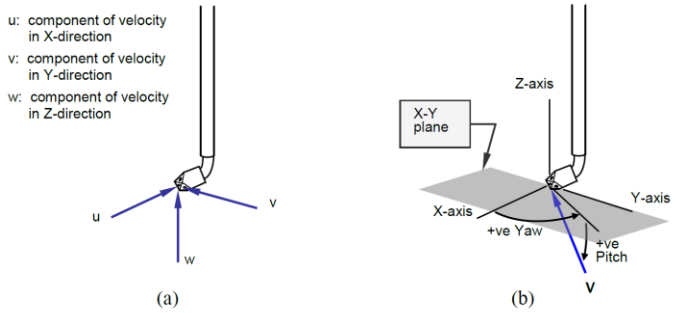


Figure 3.8 - (a) Flow axis system with respect to the Probe head, (b) Positive flow pitch and yaw angels {Formatting Citation}

## 3.3. Onsite Data Validation

### 3.3.1. Measured Onsite Data

To ensure that the on-site measurements are reliable, a comparison of the meteorological data measured onsite was made with meteorological data reported by Environment Canada from a nearby weather station for the same period of time. The procedure involves the comparison of wind characteristics considering both all hours and rain hours. Wind direction is categorised based on 22.5° intervals and the frequency is presented by use of wind rose. Wind speed is categorised to five main categories and the frequency has been calculated for each category considering all hours and rain hours. The cumulative frequency shows that for all test buildings, 90% of times the speed is less than 4 m/s. Vancouver Sea Island, Fredericton and Montreal International Airport weather stations are the nearby weather stations identified for the comparison for Vancouver, Fredericton and Montreal study building, respectively. Considering the results, presented in APPENDIX A, there is good agreement between onsite and weather station data. However, some differences can be observed between onsite wind characteristics in comparison with weather station due to the local topography and obstruction.

### 3.3.2. Site Exposure

The wind speed and direction are of particular importance to WDR studies; therefore, more accurate comparison of the onsite measured wind data is conducted following the same procedure as previous studies. The comparison consist of converting consecutive hours of high wind speeds with similar wind directions, from one station to another, using the power law (Chiu 2016) and roughness and elevation correction. For each façade facing prevailing wind direction, consecutive hours of high wind speeds measured at the test building ($U_{ref} > 5$ m/s) and the wind direction within a narrow range almost perpendicular to the façade for both site and reference weather station have been considered. As it is shown in Figure 3.9, the corrected wind speed at the Vancouver test building location is in general agreement with the wind speed measured at Sea Island weather station for the same period. The results confirm the considered suburban exposure for Vancouver and Fredericton building and urban exposure for Montreal building for the areas upstream of each studied facade. The related graphs are presented in APPENDIX A.

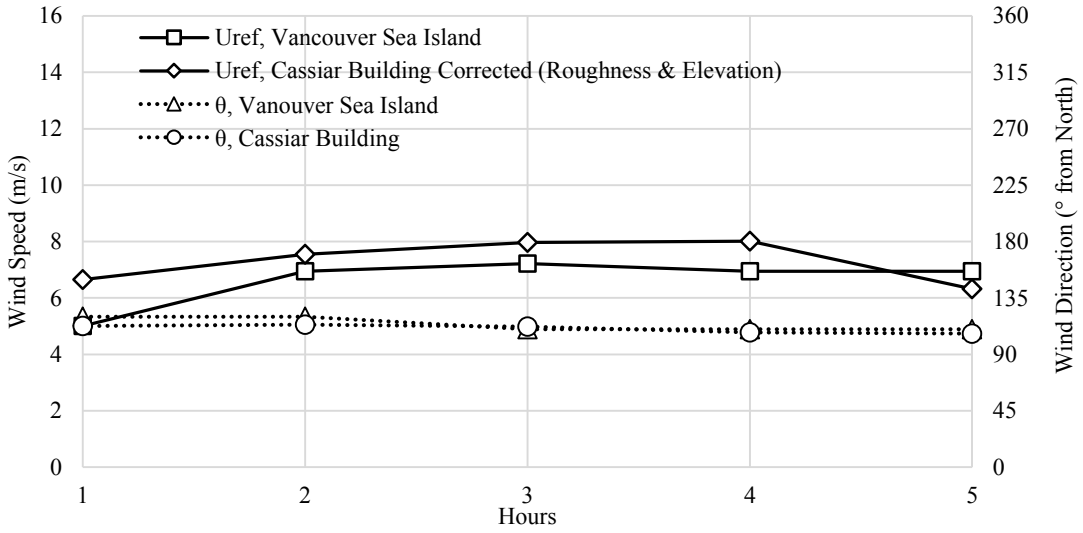


East façade, February 5th, 2014 from 14:00 to 18:00

Figure 3.9 - Wind speed at the Cassiar building corrected to Vancouver Sea Island, Average onsite WD 110° from the North(Chiu 2016)

## 3.4. Wind Tunnel Validation

Prior to the wind tunnel experiments, the agreement of new wind tunnel setting has been verified with previous experiment and onsite measured data.

### 3.4.1. Suburban Exposure Wind Profile

Wind velocity have been measured along the vertical axis at the center of wind tunnel round table with no model presents. The velocities were normalized by simply dividing the mean velocities measured ($\bar{U}$) by the mean gradient velocity ($\bar{U}g$) measured, as per equation 3.1. The relation between normalized heights of each measuring point is shown in Figure 3.10 as a function of normalized velocity.

$$\text{Normalized velocity} = \frac{\bar{U}}{\bar{U}_g} \tag{3.1}$$

The mean speed exponent of 0.24 obtained in the wind tunnel is very close to the 0.25 value assigned to suburban terrain. The normalized mean velocities and turbulence intensities measured in the wind tunnel for the suburban configuration are shown in Figure 3.11. There is a good agreement between current and previous experiment conducted by Chiu (2016).

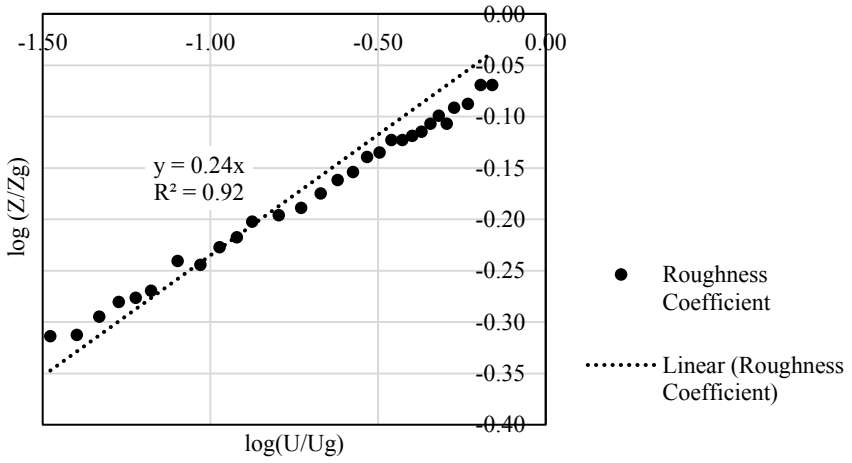


Figure 3.10 – Roughness coefficient for suburban exposure in the boundary layer wind tunnel

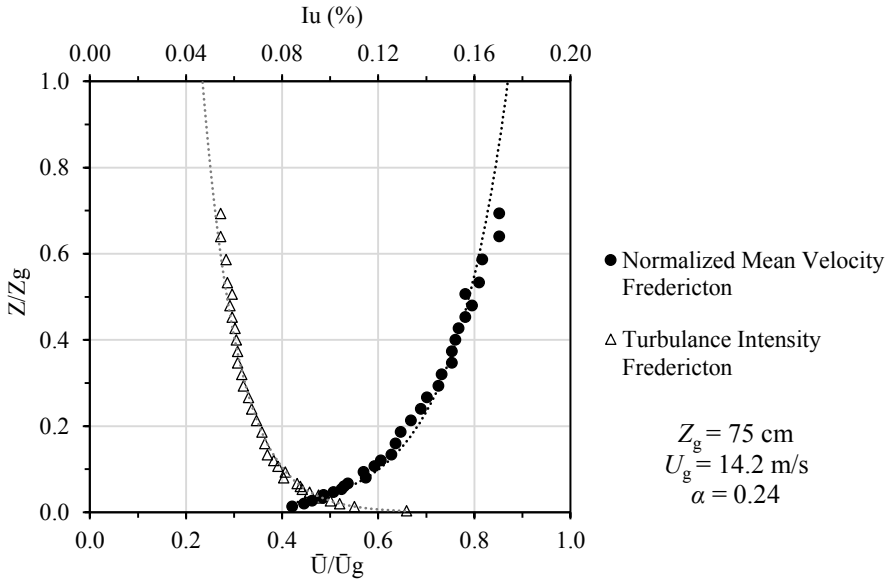


Figure 3.11 - Normalized mean velocity and turbulence intensity for a suburban exposure measured in the boundary layer wind tunnel

### 3.4.2. Wind Monitor

Once a suburban exposure was successfully modeled in the wind tunnel, the building model(s) were placed in the wind tunnel and tested. To verify the wind profile and the terrain roughness for Fredericton building, similar procedure applied by Chiu (2016) for Vancouver wind tunnel test, is followed. To compare wind tunnel measurement to the field measurements, the normalized velocities measured by the wind monitor in the field were compared to the normalized velocities

measured at the wind monitor location in the wind tunnel. The validation is performed for the 1:400 building model with and without surroundings and the 1:200 stand-alone model.

For onsite measurements, hourly records with wind speed higher than 5 m/s and the most similar wind directions between the test building and the weather station were selected. Moreover, wind direction is limited to winds approaching from 135° (normal to south-east façade), 180° and 225° (normal to south-west façade) considering prevailing wind directions. The hourly data meeting mentioned criteria were verified to have relatively stable wind with small fluctuations of wind speed and direction within the hour by analyzing the five-minute data. Figure 3.12 shows the results for 225°. It can be observed that both 5-min wind speed and direction measured are fairly stable. The mean wind velocity for the observed hour is 5.92 m/s with a standard deviation of 0.8 m/s. The wind direction is almost identical.

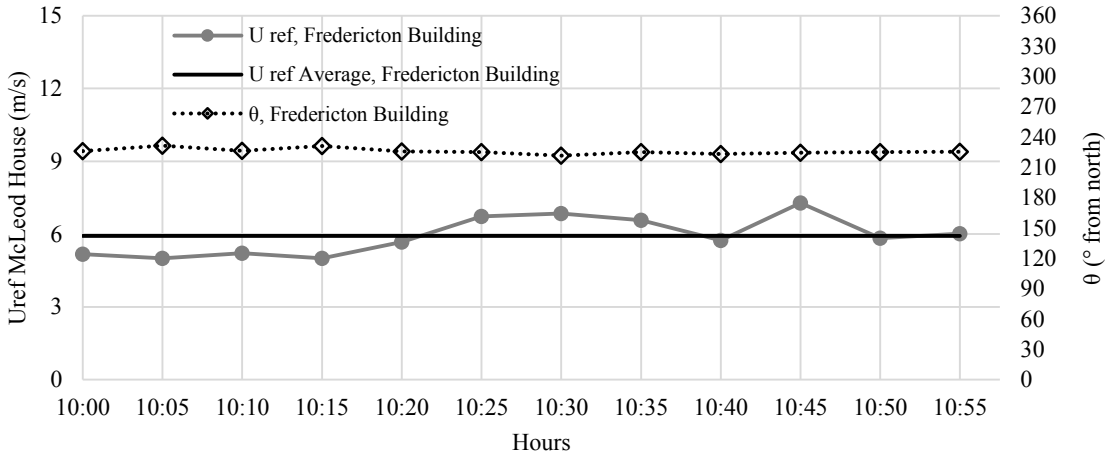


Figure 3.12 - Five-minute data record for 1-hour, McLeod House Fredericton, September 29th t 2015, 10 AM, WD south (225°)

In order to perform a direct comparison between the field data and the wind tunnel data, the wind tunnel model(s) was subjected to wind blowing from similar direction and wind velocity was measured at the place of anemometer. Figure 3.13 compares the normalized velocities at the wind monitor location between the wind tunnel and the field for wind direction approaching from south-west (225°). There is a good agreement between the wind tunnel and field measurements, however, better agreement can be observed for 1:400 scale model. Also, wind speed approaching from south-west is not affected by surroundings given the similar results between stand-alone and surroundings. Good agreement can be observed for south and south-east wind direction as well, the results are presented in APPENDIX A.

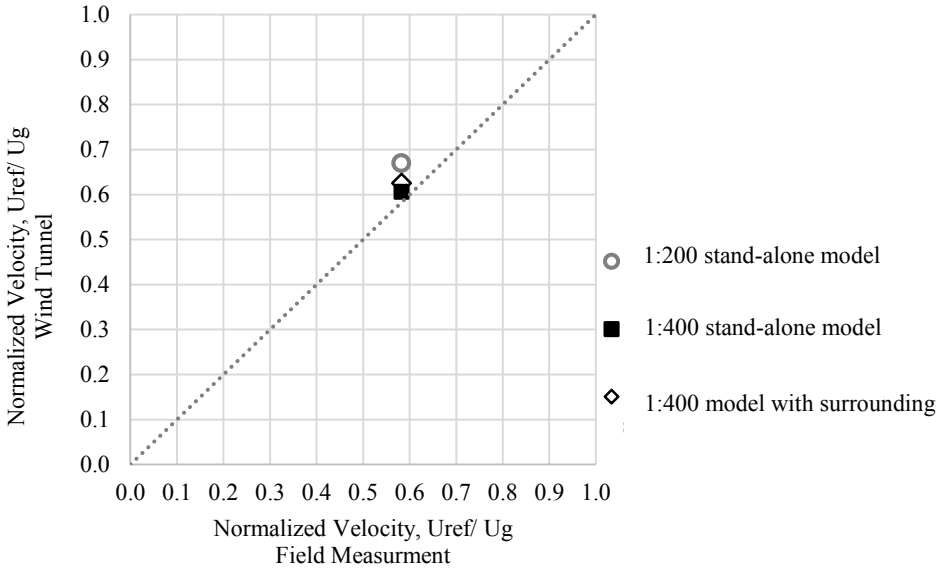


Figure 3.13 - Comparison of the normalized velocity at the wind monitor location in the wind tunnel vs. in the field (Stand-alone test building, 1:400 scale and 1:200 scale test building with surrounding, scale 1:400); for the direction θ=225° (south- west)

## 3.5. Wind-driven Rain Analysis

In current study WDR analysis includes spatial distribution of WDR on facade, wall index using ISO model, and calculation of wall factor for all three test buildings. As field measurements are subjected to various sources of errors, error analysis has been conducted for collected data.

### 3.5.1. Spatial Distribution of Wind-Driven Rain on the Building Façade

The spatial distribution of WDR is reported for all monitoring periods of Vancouver, Fredericton and Montreal buildings. Moreover, spatial distribution of WDR has been calculated for each individual rain events during all five study periods of Vancouver for overhang effectiveness analysis. In current study rain events will be separated if there is a continuous period of no rain lasting more than 96 hours (Chiu 2016).

The associated errors with WDR experiments using WDR gauges are discussed in Section 3.5.1.1. The spatial distribution of WDR on the building facades is determined as catch ratios and wall factors. The catch ratio is discussed in Section 3.5.1.2, while the wall factor is discussed in Section 3.5.3.1. Wall index, which is the amount of rain that would impact a real wall, obtained by

multiplying the airfield driving rain index, considering meteorological data from weather station, by several correction factors is discussed in Section 3.5.3.

#### 3.5.1.1. Error Analysis

As mentioned in literature review WDR measurements are subjected to different sources of errors and an adequate measurement of WDR should be accompanied by their associated error estimation including:

(1) Adhesion water evaporation; for applied type of WDR gauges associated error is 0.05 mm for each rain event during the study period

(2) Evaporative losses from the reservoir; this error is deemed to be negligible.

(3) Splashing of drops from the collection area; this error is considered negligible.

(4) Condensation on the collection area; condensation errors are deemed negligible

(5) Wind error; this error is considered negligible.

(6) Rest Water Evaporation (ERW); the average value of rest water (ERW) in the tipping bucket was 5.5 g, which is equivalent to 0.060 mm. In current study the worst-case scenario is considered and 0.06mm error is considered for each interruption during a rain event.

(7) Loss of Incoming Water during a Tip (ETIP); this error deemed negligible due to the WDR gauge's two bucket design

**Total error**

A conservative estimate of the total absolute errors in the WDR measurement at the end of a rain event is made by combining all errors (Nore et al. 2007); (Osoria, 2013) so that:

$$E_{Total} = E_{AW} . \sum E_{EVAP} . \sum E_{EU} . S_{WDR} \left(\frac{E_{RW} + nE_{TIP}}{nV_{BOWL}}\right) \quad (3.2)$$

where, $E_{AW}$ is the adhesion water evaporation error during and at the end of the rain event (mm) assuming the worst case scenario (complete evaporation of adhesion water after every break or dry period in the rain event), $E_{EVAP}$ is the hourly evaporation error from the tipping bucket at every hour in the rain event (mm), $E_{UC}$ is the hourly condensation error at every hour in the rain event (mm), $E_{RW}$ is the rest water error (g), $E_{TIP}$ is the collection loss during every tip (g), n is the amount of tips during the rain event, $V_{BOWL}$ is the content of the bowls (g) and $S_{wdr}$ is the total accumulated WDR for the rain event (mm).

Adhesion water evaporation ($E_{AW}$) is determined by multiplying the adhesion water for a single occurrence by the number of interruptions of the rainfall by dry periods, so that:

$$E_{AW} = \text{AW} \times \text{Number of interruptions} \tag{3.3}$$

Based on the conclusions made by Osorio, M., $E_{EVAP}$, $E_{UC}$, and $E_{TIP}$ are considered negligible and are omitted, simplifying equation 3.2 to:

$$E_{TOT} = E_{AW} + E_{RW} \tag{3.4}$$

Finally, the relative error associated with the WDR measurement with a wall mounted WDR gauge can be expressed as

$$e_{TOT} = \frac{E_{TOT}}{S_{wdr}} \tag{3.5}$$

#### 3.5.1.2. Catch Ratio

The catch ratio (η) is the total amount of WDR collected on a wall surface divided by the total amount of horizontal rainfall over the same period, so that:

$$\text{Catch Ratio } (\eta) = \frac{S_{wdr}}{S_h} \tag{3.6}$$

Where $S_{wdr}$ is the total accumulated WDR amount (mm) and $S_h$ is the total accumulated horizontal rainfall amount (mm).

The analysis includes:

1) Catch ratios plotted on the east and north façade of Vancouver building for all five monitoring periods to show the spatial distribution of WDR across the building façade and quantified the overhang effectiveness in reduction of impinged WDR over the façade

2) The catch ratio has been also calculated based singled out data with respect to different wind speeds and wind direction to investigate the effect of wind characteristics on overhang effectiveness

3) Catch ratio is also calculated on south-east and south-west façade of Fredericton and north-east, south-east and south-west façade of Montreal Building to study WDR spatial distribution under different climate condition and terrain

### 3.5.2. Airfield Driving Rain Index

The airfield driven rain index ($R_{airfield}$) which expresses the amount of rain incident on an imaginary unobstructed wall surface and is a relative indicator of the severity of a specific wall orientation to the wind-driven rain exposure. In current study $R_{airfield}$ is calculated based on meteorological onsite data and data reported by weather station. For each façade orientation $R_{airfield}$ during the study period is the summation of data when Cos (D-θ) is positive (periods when the wind is causing flux through the imaginary wall of interest).

At the place of study buildings, $R_{airfield}$ is calculated at the height of WDR gauges to estimate wall factors on different locations of the façade. As the wind speed is different with respect to height, power Law is used to convert measured wind speed at the place of anemometer to desired heights, height of WDR gauges, as per equation 3.7:

$$\frac{U_z}{U_g} = \left[\frac{Z}{Z_g}\right]^{\propto} \tag{3.7}$$

where $U_z$ is the wind speed at the desired height above grade, $U_g$ and $Z_g$ is gradient speed and height respectively defined by ISO based on exposure type, and α is mean speed exponent, Table 3.2. The airfield driving rain indices ($R_{airfield}$) have also been calculated using equation 2.3 and applying meteorological (i.e. wind speed and wind direction) data from Vancouver Sea Island station, Fredericton International Airport and Montreal International airport for Cassiar building, McLeod House and FB building respectively. Since, hourly rainfall is not recorded at typical weather stations, the hourly rainfall measured at the test building is used.

Table 3.2 - Typical values of parameters in wind profile (Aynsley et al, 1977)

| Terrain Category | Terrain description | Gradient Height, Zg (m) | Roughness length, $Z_0$ (m) | Mean speed exponent α | Gust speed exponent β |
|---|---|---|---|---|---|
| 1 | Open sea, ice, tundra, desert | 250 | 0.001 | 0.11 | 0.07 |
| 2 | Open country with low scrub or scattered trees | 300 | 0.03 | 0.15 | 0.09 |
| 3 | Suburban area, small towns, well wooded areas | 400 | 0.3 | 0.25 | 0.14 |
| 4 | Numerus tall buildings, city centers, well developed industrial areas | 500 | 3 | 0.36 | 0.20 |

### 3.5.3. Wall Index

As discussed in literature review, the wall index ($I_{WS}$) is the amount of rain that would impact a real wall by multiplying the airfield driving rain indices ($R_{airfield}$) by a number of correction factors, as per equation 2.3, Chapter 2.

Meteorological data is typically not available at the building site, therefore, data from the closest weather station is normally used. The terrain roughness coefficient ($C_R$) and the topography coefficient ($C_T$) are used to convert the mean wind speed measured at the weather station to the building site at the building height of interest. For Vancouver and Fredericton buildings the terrain roughness coefficient is estimated based on suburban exposure, while for Montreal Building urban exposure is considered. The topography coefficient is considered as 1.0 with respect to site characteristics. The obstruction factor (O) takes into account the sheltering effect provided by the obstacles nearby, while wall factors (W) describes the spatial distribution of WDR on the building facade(s) as a result of the complex interaction between the wind flow and the building. The obstruction factor is equal as 1.0 for all test buildings due to sufficient distance of adjusted buildings. All three buildings are multi-story buildings with flat roof. For this type of building, a wall factor of 0.5 is assigned to the top 2.5 m of the facade, while the remainder of the facade is assigned with a wall factor of 0.2. It is noted that these are general and conservative values of wall factors for this particular type of building since there is no variation across the building facade nor does it take into consideration the orientation of the building, assuming all the facades of the building have the same wall factor values assigned.

The wall index analysis includes:

1) Wall indices are calculated for east and north façade of Vancouver for the period without overhang, south-east and south-west façade of Fredericton and north-east, south-east and south-west façade of Montreal for all monitoring period.

2) The actual measured WDR at each gauge location compared to: (1) the wall indices using the measured wall factors with different time resolution and (2) the wall indices using the ISO suggested wall factors.

3) The effect of wind speed and wind direction changes from weather station to the site and its effect on the wall indices has been investigated

The wall indices are presented and discussed in Section 6.5

#### 3.5.3.1. Wall Factor

The actual WDR rain received on a building surface at a specific location is influenced by the airflow along the building surface(s), which is a product of the wind and building interaction. The amount of WDR varies significantly over the surface of a wall due to the flow of air around edges, corners, over the roof, etc. Wall factor is accountant for the effect the building geometry and building details have on the WDR load. ISO 15927-3 (2009) suggests several wall factors for different building configurations (i.e. height, type of roof, roof overhang) as shown in Chapter 2. These wall factors are based on long-term field measurements and do not take in account the specific wind and rain conditions. Collection of high resolution data through field measurements provides a unique opportunity to assess the accuracy of prescribed wall factors.

Since the on-site meteorological data (i.e. wind speed, wind direction, horizontal rainfall, WDR) are available at the test buildings, the roughness factor ($C_R$), topography factor ($C_T$), and obstruction factor (O) can be set equal to 1. Thus, the wall factor becomes the quantity of measured WDR divided by the airfield driving rain index. Equation 3.7 then becomes:

$$W = \frac{S_{wdr}}{R_{airfiled}} = \frac{S_{wdr}}{\frac{2}{9}.U.R_h^{\frac{8}{9}}.cos(\theta - \Theta)} \tag{3.7}$$

where $S_{wdr}$ is the total accumulated WDR amount (mm) and $R_{airfield}$ is the amount of rain incident on an imaginary unobstructed wall surface calculated from equation 2.2. The analysis includes:

1) Wall factors plotted on test buildings facades' facing prevailing wind direction for monitoring period to show the spatial distribution of WDR and the influence of building geometry on the WDR load.

2) Comparison of measured wall factors to the wall factors suggested by the ISO standard.

3) Investigation of the effect of applied data time resolution and averaging method on calculated wall factor

The results for wall factor analysis are presented in Section 6.4.

## 3.6. Overhang Effectiveness

Overhang studies are conducted on Vancouver test building which is equipped with retractable overhang. The effectiveness in reduction of WDR is calculated based on two different approaches:

(a) WDR reduction at the place of WDR gauges; namely local overhang effectiveness and (b) the overhang area-weighted effectiveness which is defined as the percentage reduction of received WDR on the façade that is calculated based on local overhang effectiveness and area-weighted average catch ratio. Both procedures are established by Chiu and Ge (Chiu 2016; Ge et al. 2017; Ge et al. 2017).

### 3.6.1. Local Overhang Effectiveness

The effectiveness of overhang at the place of WDR gauges, δ, is defined as the percentage reduction in catch ratios with and without the overhang. The overhang effectiveness is assessed by two approaches: 1) similarity, which compares two similar rain events during the periods with and without overhang; 2) symmetry, which uses a symmetrical distribution of WDR across the building facade during a rain event. In both approaches overhang effectiveness is calculated based on equation 3.8 at the place of WDR gauges sheltered by the overhang.

$$\delta = \frac{\mu - \mu_{OH}}{\mu} \times 100 \tag{3.8}$$

Where $\mu$ is the catch ratio without overhang, $\mu_{OH}$ is the catch ratio with overhang. In previous studies by Chiu (2016), the effectiveness of 0.6m and 1.2m overhang size have been presented (Chiu 2016). In current study additional provided data is used to investigate 0.3m and 0.9m overhang effectiveness. Table 3.3, indicates the total amount of precipitation and number of considered rain events for each study period. In total 73 rain events has been analyzed during the whole study periods and the events with acceptable meteorological characteristics are used in evaluations. This assure that for all study periods sufficient data under different climate conditions has been collected and considered in estimations.

Table 3.3 – Number of rain events during each study period and total amount of precipitation

| Study Period | Number of Considered Rain events | Total Precipitation (mm) |
|---|---|---|
| No OH | 15 | 1948 |
| 1’ OH (0.3 m) | 9 | 1214 |
| 2’ OH (0.6 m) | 7 | 729 |
| 3’ OH (0.9 m) | 19 | 1030 |
| 4’ OH (1.2 m) | 8 | 1996 |

**Similarity**

The overhang effectiveness can be assessed by comparing the catch ratios at the gauge locations that are directly under the overhang (gauges EN1 to EN9) in one rain event with the catch ratios at the same gauge locations in a similar rain event without overhang, Figure 3.14 .

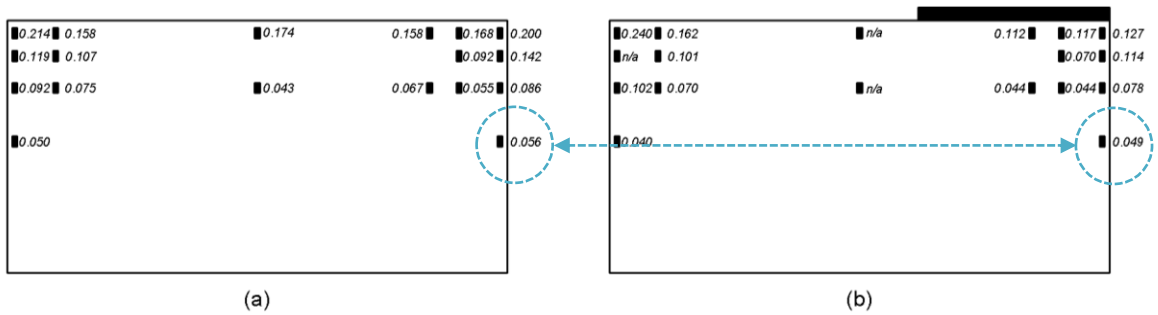


Figure 3.14 – Comparison of catch ratio on similar measurement points, (a) without overhang as the reference and (b) with overhang, for calculation of overhang effectiveness; namely similarity approach

To establish similarity, both rain events should have similar meteorological characteristics, i.e. wind speed, wind direction and rainfall intensity, ultimately leading to similar catch ratios at the gauge locations that are not influenced by the overhang. Once this similarity has been established, the catch ratios at gauge locations EN1 to EN9 (under the overhang) during rain events without overhang can be compared to the catch ratios during rain events with overhang. An example of similarity procedure is provided in APPENDIX A.

**Symmetry**

The symmetry is established by similar catch ratios observed during the period without overhang. Calculated catch ratios are more or less symmetrical on the east façade given that the predominant wind direction is from the east during rain hours, which is normal to the façade. Therefore, a symmetrical distribution of WDR can be assumed to evaluate the effectiveness of overhang by directly comparing the catch ratios at gauge locations underneath the overhang on the north side of the façade (EN1 to EN7) to those on the south side of the façade (ES1 to ES7), which do not have an overhang above them. Rain events with the prevailing wind direction coming from the east are selected and the percentage reduction in catch ratios for all four overhang sizes are calculated.

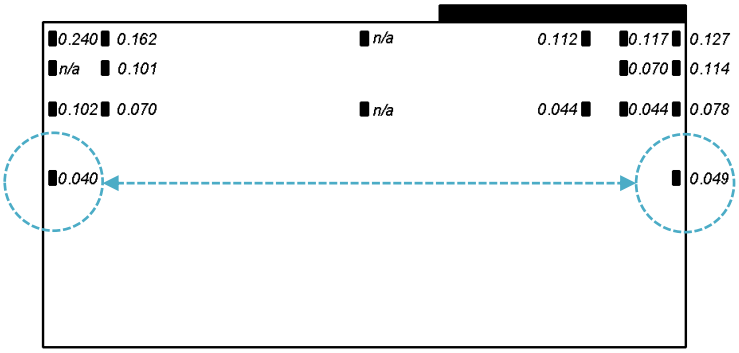


Figure 3.15 – Comparison of catch ratio on symmetrical measurement points for calculation of overhang effectiveness; namely symmetry approach

Overhang effectiveness calculated based on similarity and symmetry approach is the average of overhang effectiveness for rain events during each study period.

**Overhang effectiveness with respect to wind characteristics**

To evaluate the effect of wind characteristics on overhang effectiveness measured data are singled out with respect to wind speed and wind direction. Catch ratio at measurement points are calculated for defined data sets and the effectiveness is evaluated based on percentage reduction of catch ratio at the place of WDR gauges for the period with overhang in comparison with no overhang situation as reference.

### 3.6.2. Overhang Area-Weighted Effectiveness

To quantify the effect of overhang on the reduction of WDR impinged on the façade, an area-weighted average catch ratio ($\bar{\mu}$) is introduced (equation 3.14). Overhang area-weighted effectiveness is calculated for four areas shown in Figure 3.16 (a), namely A1, A2, A3 and A4 representing 15%, 30%, 60% and 100% of the façade area, respectively. This evaluation is carried out for the case that the entire east façade width is fitted with overhang (i.e. full overhang)(Ge et al. 2017).

$$\bar{\mu} = \frac{1}{\sum_{i=1}^{n} A_i} \sum_{i=1}^{n} \mu_i A_i \qquad (3.14)$$

Where, the summation index i is the cell number, Ai is the area of the $i_{th}$ cell and n is the total number of the cells over which the average is calculated. The façade is divided into cells in such a

way that rain gauges are located in the centre of a cell. There are twenty-five cells, five columns and five rows on the east façade. For the cells with rain gauge, a constant catch ratio is assigned with value measured by the gauge located in its centre. For the remaining nine cells located at the lower and centre parts of the façade, a constant catch ratio interpolated from the adjacent cells is assigned. For these areas, the catch ratios are quite small Figure 3.16 (b).

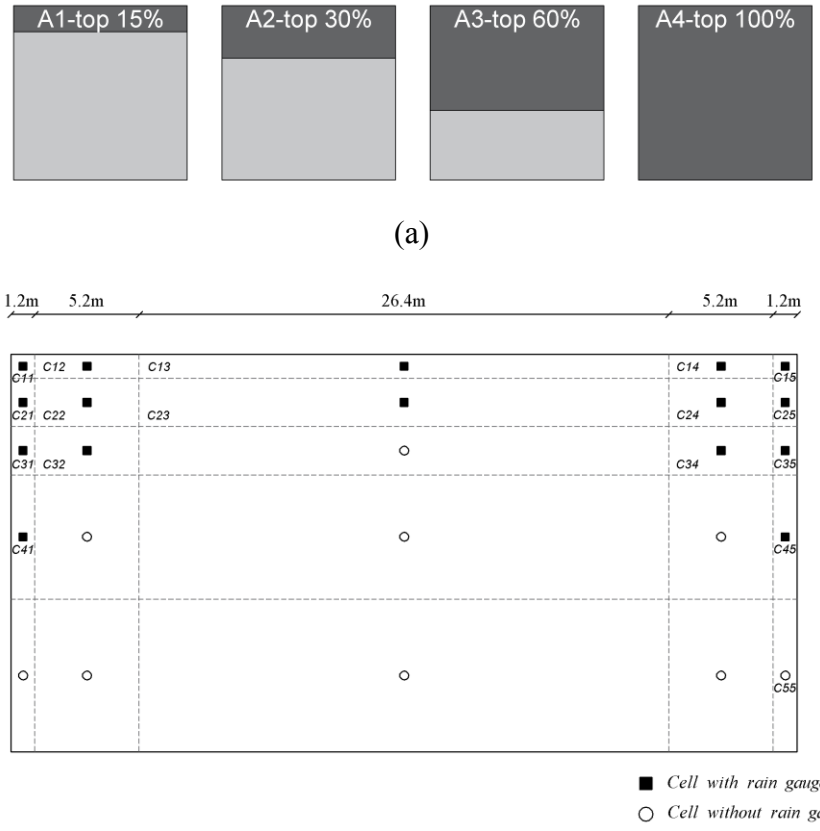


Figure 3.16 – Areas (a) and cells (b) on the east façade for the calculation of area- weighted overhang effectiveness(Ge et al. 2017)

Given that the Vancouver prevailing wind direction is almost perpendicular to the east façade, calculated local overhang effectiveness are assigned symmetrically on both sides of the east façade. The amount of received WDR on different portions of the façade is calculated considering area-weighted average catch ratio for the period without overhang along with local overhang effectiveness at measurement points based on similarity approach; due great agreement between the results of similarity and symmetry approach (Ge et al. 2017). Overhang area-weighted

effectiveness for different portions of the façade is calculated as percentage of reduction in area-weighted catch ratios with and without the overhang. The effect of wind characteristics on overhang area-weighted effectiveness is evaluated based on local effectiveness with respect to defined categories of wind speed and wind direction.

Moreover, WDR reduction coefficient is introduced in calculation of WDR amount based on ISO model. This value is defined as percentage reduction of WDR load received on different portions of the façade and is defined as per equation 3.9. The amount of received WDR on different portions of the façade can be estimated applying equation 3.10.

*WDR reduction coefficient = 1-WDR with overhang/WDR without overhang* (3.9)

*WDR received on facade = WDR amount based on ISO x (1 – WDR reduction coefficient)* (3.10)

Different Overhang size effectiveness and calculated overhang area-weighted effectiveness is discussed on chapter four.

## 3.7. Generalizing Results for Similar Mid-Rise Buildings

Field measurements on Vancouver building establish the correlation between overhang size and its effectiveness in reducing WDR for mid-rise buildings. This correlation may be applied to other mid-rise buildings with similar building geometry and wind flow characteristics. To test this hypothesis, wind tunnel measurements were carried out on Fredericton building to confirm the wind flow. Upstream wind flow is disturbed by the presence of the building, which is also known as the building wind blocking effect and is related to building scaling length BSL:

$$\text{BSL}= (B_L B_S^2)^{1/3} \quad (3.10)$$

where the $B_L$ is the larger and the $B_S$ the smaller dimension of the windward façade. The BSL was defined by Wilson (1989) for estimating the dimensions of flow recirculation regions on building roofs. Previous studies related the wind-blocking effect to BSL and showed that the larger the wind-blocking effect the lower the WDR exposure of the façade (Blocken et al. 2010) .

Vancouver building has a rectangular footprint with dimension of 39.2m x 15.2m. While the Fredericton Building's footprint consists of two overlapping rectangles each with the dimension of

30.6m x 16.7m that lead to non-leveled elevations on all direction. The south-west façade of the building has the total length of 55.2m in 22m height, while the right wing is offset by 9.45m behind the left wing. However, South-west façade of Fredericton and east façade of Vancouver have similar BSL; 29.4 and 24.7 respectively. As a result, it is predicted that wind velocity near the facades, as one of the main contributing factors in affecting the amount of WDR, will be similar. The wind velocity near both facades are measured for situations with and without overhang at 52 points near Fredericton 1:200 model and 29 points near Vancouver 1:200 model. Normalized wind velocities are then compared to evaluate the effect of overhang in reduction of wind velocity near the façade. The wind tunnel results are presented and discussed in Chapter 5.

## 3.8. Accuracy of ISO Model

Previous studies show that applying wall factor calculated based on onsite measurements instead of ISO prescribed wall factor improves estimation of WDR using weather station meteorological data. Given that the onsite data is collected at 5-min interval, the effect of time resolution, converting 5-min data to hourly data and averaging method is investigated and discussed in calculation of airfield driven rain index and calculated wall factors. Moreover, the comparison of meteorological measured onsite data with the data reported by Environment Canada for same period of time shows different wind characteristic which can affect the calculation of WDR. The result of this comparison and its effect on WDR estimations are discussed in Chapter 6.

# 4. Overhang effectiveness

## 4.1. Introduction

Roof overhang reduces the amount of WDR deposition on the building façade, however, its effect is not considered in WDR load estimation based on semi-empirical models. The purpose of this chapter is to quantify different overhang widths effectiveness in reduction of WDR load on a mid-rise building façade and introduce WDR reduction coefficient which can be used by designers and engineers for accurate assessment of WDR.

The data measured at Vancouver building is considered in this part of study. First the overhang effectiveness in reduction of received WDR at the place of WDR gauges is calculated; namely local overhang effectiveness. This is calculated based on (1) similarity and symmetry approach and (2) with respect to wind characteristics. To evaluate and quantify the overhang effectiveness on reduction of impinged WDR on different portions of façade area, calculated local overhang effectiveness are applied in area-weighted methodology; namely overhang area-weighted effectiveness. The results are used to establish an accurate correlation between overhang size and the amount of WDR reduction on different portions of the façade with respect to wind characteristics. WDR reduction coefficient is defined as percentage reduced in amount of received WDR on façade area. Also, the percentage of received WDR on entire façade is discussed for each overhang size considering all available data and with respect to wind characteristics.

## 4.2. Onsite Weather Condition

Prior to the main discussion of this chapter, a brief comparison among meteorological characteristics of all study periods are presented. The onsite measurements on Vancouver test building began on August 16, 2013 and continued up to February 20, 2018. A sufficiently long period of measurements has been collected to obtain reliable and accurate data. The field study can be separated into five monitoring periods: (1) No overhang, (2) with a 0.6 m overhang, (3) with a 1.2 m, (4) 0.9 m overhang and (5) 0.3 m overhang. A summary and comparison of the onsite weather conditions including wind speed, wind direction and rainfall intensity for the different monitoring periods is presented in Figure 4.1 to Figure 4.3.

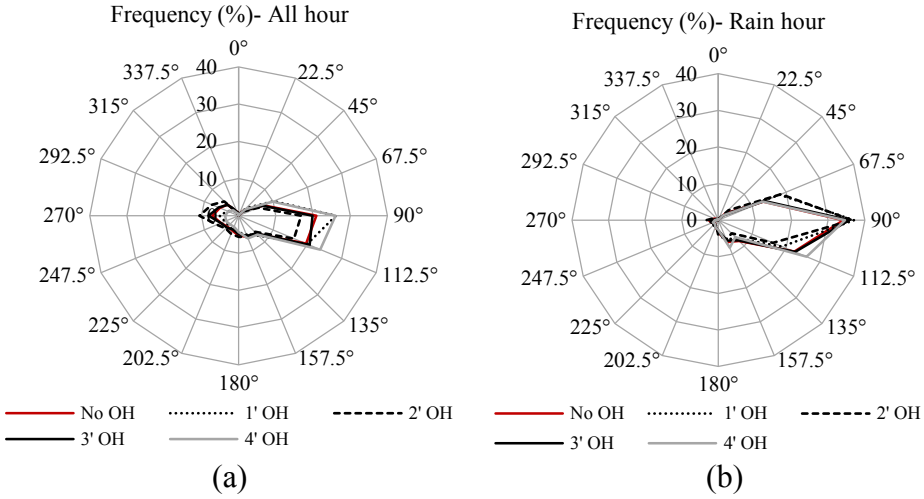


Figure 4.1- Frequency distribution of wind direction (a) all hours and (b) rain hours for all five sub-periods of study, Cassiar building, Vancouver

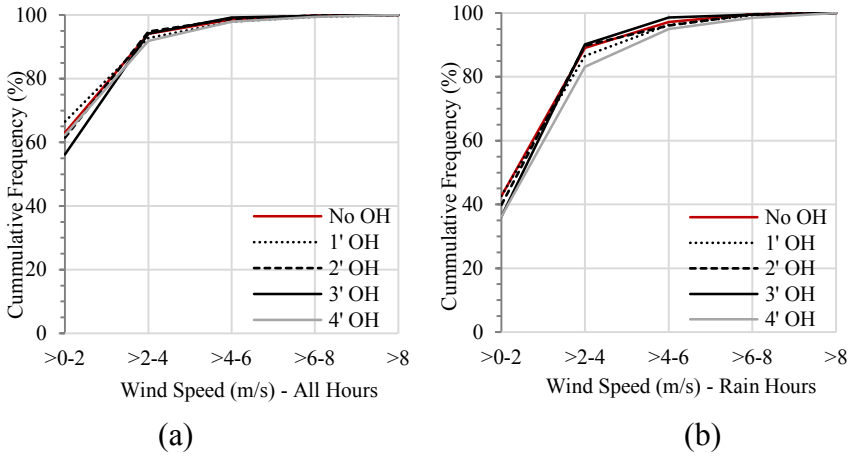


Figure 4.2- Cumulative frequency of wind speed for all hours (a) and rain hours (b) all five sub-periods of study, Cassiar building, Vancouver

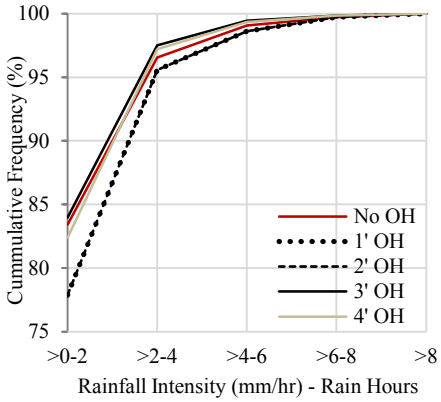


Figure 4.3 - Cumulative frequency of rainfall intensity for all five sub-periods of study, Cassiar building, Vancouver

Onsite weather data analysis shows similar wind and rain conditions during the five monitoring periods, which allows the comparison of catch ratios at WDR gauge locations for periods with and without overhang to calculate overhang effectiveness using the similarity approach. Based on the analysis prevailing wind direction is mostly frequent within a narrow band between east-south-east to east-north-east directions with the highest frequency from the east. The majority of wind speeds are in the range of 2 to 4 m/s during rain hours. Rainfall intensity is mostly light to moderate with less than 2 mm/hr for the majority of the time.

## 4.3. Catch Ratios

Calculated catch ratios, at the place of each WDR gauge, show the spatial distribution of WDR across the building facades which are also used to evaluate overhang effectiveness in the reduction of WDR load on facade. Figure 4.4 shows calculated catch ratios on the Vancouver east façade for all study periods. Due to normal prevailing wind direction, a symmetrical distribution of WDR and classical wetting pattern can be observed across the east façade during the period without overhang Figure 4.4(a). Top corners of the building receive the highest amount of WDR load followed by the top and side edges. The wetting decreases from top to bottom and from sides to middle of the façade. The symmetrical distribution allows the use of "*symmetry*" approach to calculate the overhang effectiveness.

Similar wind and rain characteristics during all study periods lead to approximately similar catch ratios on the south side of the east façade, where no overhang is added. Partially covering east façade reduces catch ratio of WDR gauges below it in comparison with catch ratios at symmetrical measuring points on the south side of the façade. The similarity of wind and rain conditions and WDR deposition on the south side without overhang during all study periods allows the use of "*similarity*" approach to calculate the overhang effectiveness. As shown in Figure 4.4, regardless of overhang width the gauges right below it is almost entirely protected (EN1, EN5, and EN8). The remaining locations beneath the overhang are protected to various degrees depending on the overhang size. Wider overhangs provide protection that can be extended to areas further down from the roofline (Ge et al. 2017). The results for north façade in presented in APPENDIX B.

.

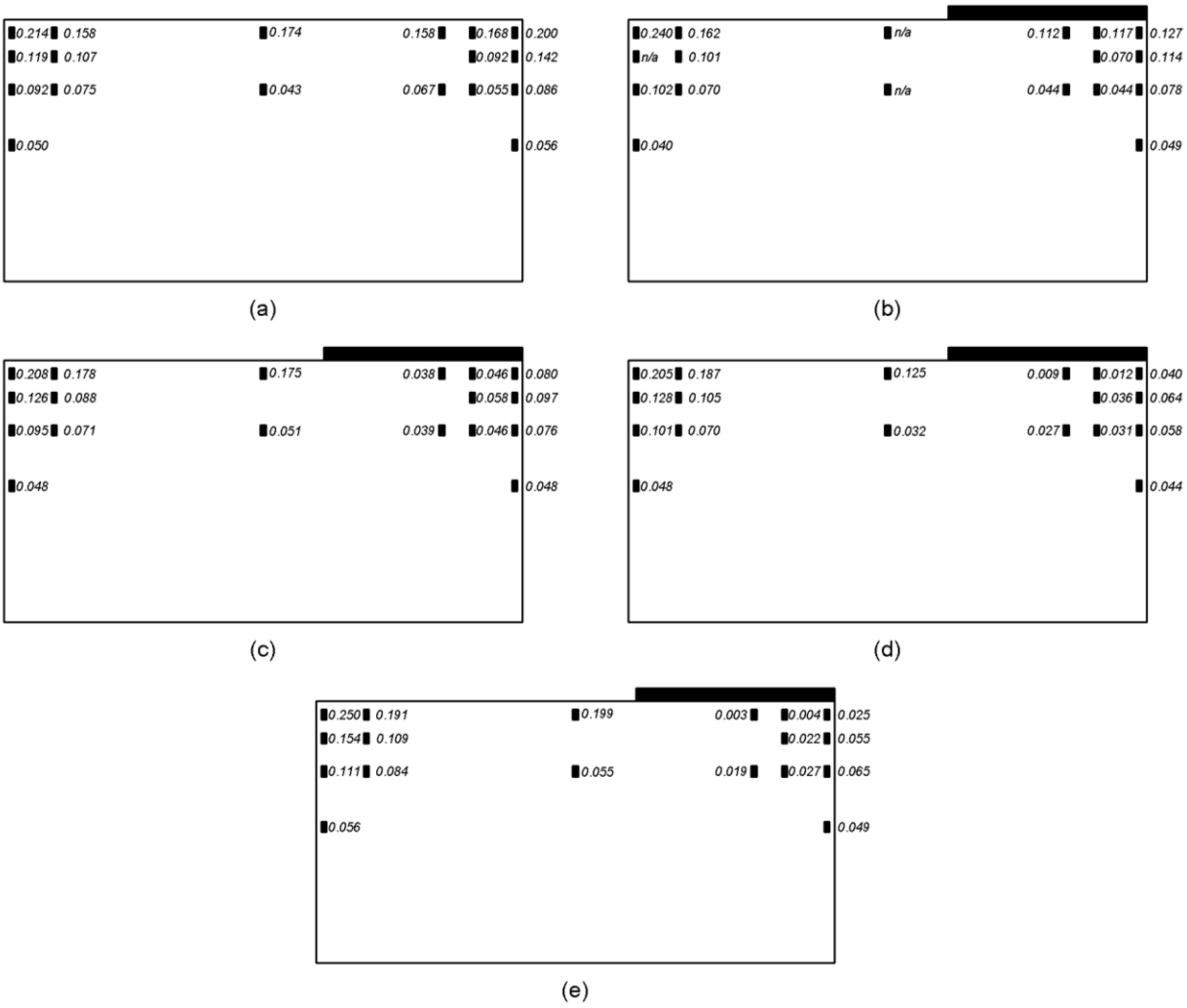


Figure 4.4 - Catch ratios on the east façade: (a) no overhang; (b) 0.3 m overhang, (c) 0.6 m overhang, (d) 0.9 m overhang and (e) 1.2 m overhang, Cassiar Building, Vancouver

## 4.4. Overhang Effectiveness

### 4.4.1. Local Overhang Effectiveness

Local overhang effectiveness is defined as the percentage reduction of WDR at the location of WDR gauges when being protected by the overhang based on both similarity and symmetry approach. The data sets collected up to February 2018 is used for analysis, which extended the work by Chiu with longer period of measurements. The results confirmed the previous findings on longer period of data for new tested overhang widths. The comparison of overhang effectiveness

calculated based on both procedures shows a great agreement for all tested overhang widths for east façade; mainly due to normal prevailing wind direction (Ge et al. 2017). There for, in the following discussions only results for similarity approach is presented and used in further analysis.

Overhang effectiveness in reduction of impinged WDR is shown on Figure 4.5 for Vancouver east facade. In general, more protection is provided at the measuring point with increase of overhang width. The effectiveness of the overhang decreases when moving from the upper edge towards the ground and from the center towards the side edge of the façade. Overhang reduced the WDR deposition on the façade especially area beneath it, however, the provided protection varied on average between 40% up to almost 100% for 0.3 m to 1.2 m overhang width.

The overhang effectiveness is also plotted in relation to the normalized building height, as shown in Figure 4.6 for the east façade. With the increase of distance from the roofline, the overhang effectiveness decreases, which exhibits a quasi-linear relationship. At a distance 0.3 m below the roofline (i.e. 3% of the building height), provided protection ranges between 70% to 99% for overhang size between 0.6 m to 1.2 m with respect to distance from building side edge. However, decrease of overhang size to 0.3 m significantly reduces the protection to the range between 30% up to 40% for areas right below the overhang. The results for north façade is presented in APPENDIX B.

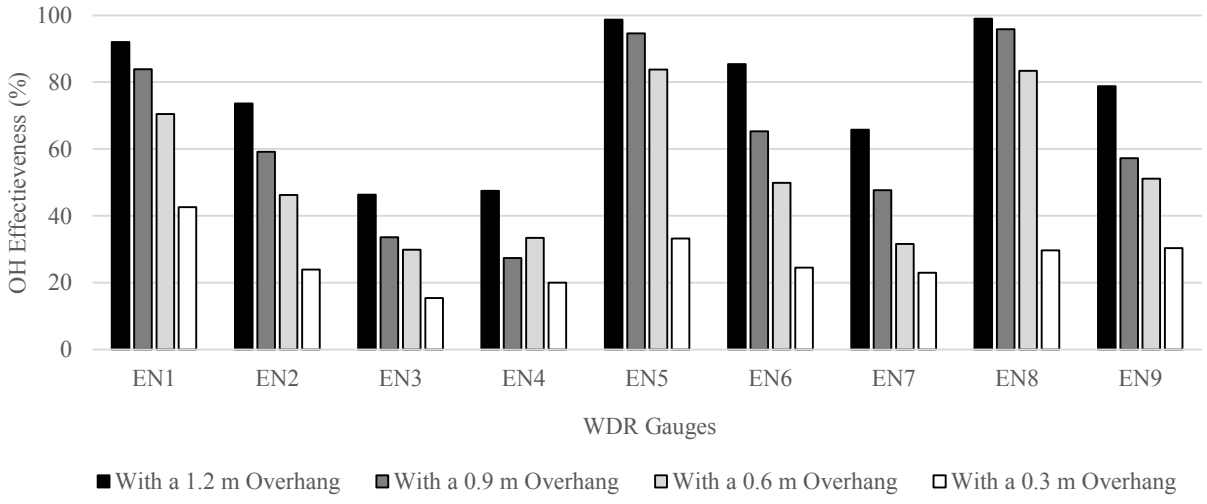


Figure 4.5 - Effectiveness of overhangs on the east façade of Cassiar Building, Vancouver

Effectiveness reduces almost linearly up to 4.9 m below the roofline (i.e. 25% of the building height, EN3, EN7, EN9) ranging between 15% up to 80% and remains almost stable up to 9.1 m distance (i.e. about 45% of the building height, EN4) which is almost half of the building height.

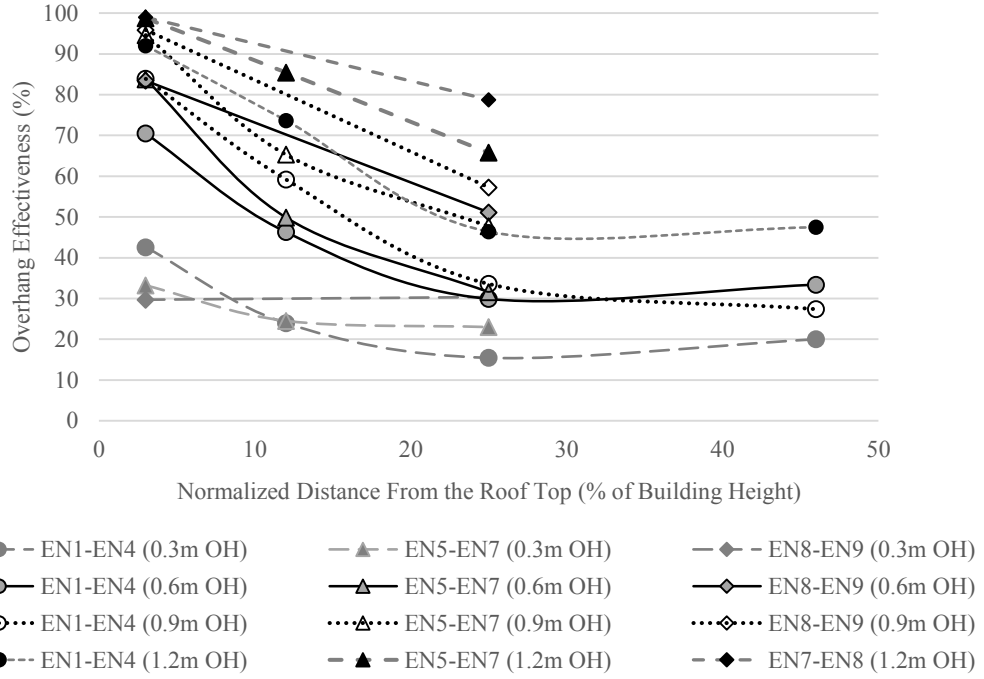


Figure 4.6 – Overhang effectiveness on the east façade with respect to normalized distance from the roofline, Cassiar Building, Vancouver

### 4.4.2. Overhang Area-Weighted Effectiveness

Area- weighted average catch ratio is calculated on four defined areas of A1, A2, A3 and A4, represents the amount of received WDR by each portion. As it is indicated in Table 3.2, the top 15% and 30% of the façade area received 56% and 70% of the total WDR deposited on the entire façade. With a 0.3 m overhang added, 27% of protection is provided over the top 30% of the façade area. Provided protection significantly increases for the 0.6 m overhang and 70% of WDR deposited on the top 30% of façade area can be reduced by 60%, which is about a 42% reduction in the total amount of impinged WDR. This reduction can be increased to about 50% and 60% when a 0.9 and 1.2m overhang is added respectively, as indicated in Table 4.1.

These results show that the addition of an overhang is effective significantly in reducing WDR amount on the top area. The total amount of WDR impinged on the façade can be reduced by 21%

with a 0.3 m overhang, 45% with a 0.6 m overhang, 55% with a 0.9 m overhang and by 63% with a 1.2 m overhang respectively.

Table 4.1 - Effect of full overhang on WDR reduction on the east façade

| Façade area | No overhang | | 0.3m overhang | | 0.6 m overhang | | 0.9 m overhang | | 1.2 m overhang | |
|---|---|---|---|---|---|---|---|---|---|---|
| | $\sum_{i=1}^{n} \eta_i A_i$ | WDR distribution on façade (%) | $\sum_{i=1}^{n} \eta_i A_i$ | Area-weighted effectiveness (%) | $\sum_{i=1}^{n} \eta_i A_i$ | Area-weighted effectiveness (%) | $\sum_{i=1}^{n} \eta_i A_i$ | Area-weighted effectiveness (%) | $\sum_{i=1}^{n} \eta_i A_i$ | Area-weighted effectiveness (%) |
| A1 (15%) | 15.04 | 56 | 10.73 | 29 | 5.01 | 67 | 3.36 | 78 | 1.58 | 90 |
| A2 (30%) | 18.61 | 70 | 13.50 | 27 | 7.45 | 60 | 5.26 | 72 | 2.85 | 85 |
| A3 (60%) | 23.61 | 89 | 18.12 | 23 | 11.71 | 50 | 8.90 | 62 | 6.69 | 72 |
| A4 (100%) | 26.66 | 100 | 21.16 | 21 | 14.75 | 45 | 11.94 | 55 | 9.74 | 63 |
| **Total WDR reduction (%)** | | | 21 | | 45 | | 55 | | 63 | |

To improve the accuracy of ISO method in calculation of WDR over building façade, overhang reduction coefficient is proposed. Due to test building geometry specifications, results can only be used for mid-rise buildings with similar aspect ratios. Generalizing results for similar building geometry have been validated through wind tunnel testing and will be discussed in Chapter 5. Overhang WDR reduction coefficient for different portions of façade is evaluated for tested overhang widths.

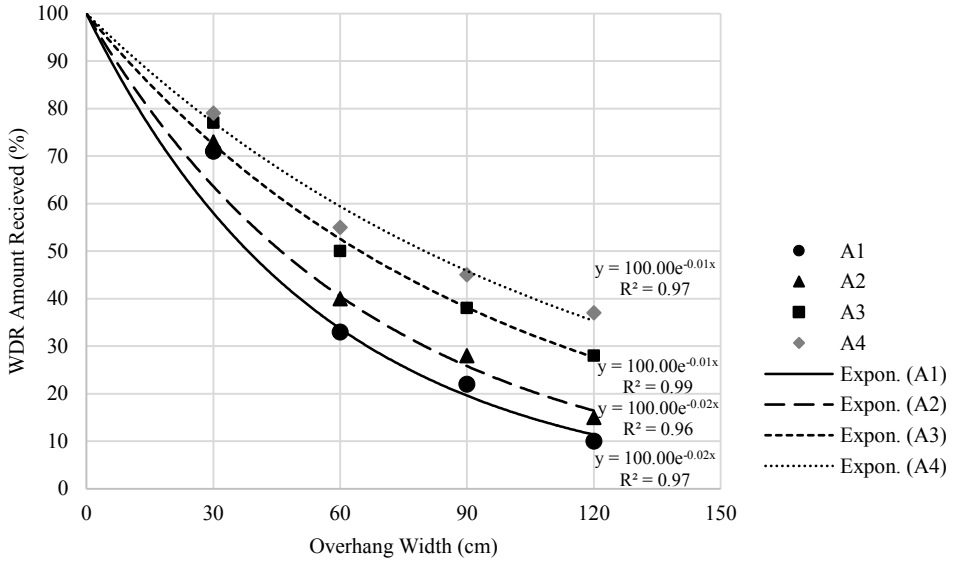


Figure 4.7 - Relationship between overhang width and the amount of WDR deposited on east façade for four different areas

Figure 4.7 shows the relation between WDR received on different portions of the façade with respect to overhang width. The trend line plotted considering the data points available, indicates an exponential relationship with good correlation between amounts of WDR impinged on the façade and overhang width. Received WDR on entire façade is reduced from 80% to around 40% by increasing overhang width form 0.3m to 1.2m. It is anticipated that increase of overhang wide would not reduce the impinged WDR significantly due to observed exponential trend line especially on top 15% of the façade.

## 4.5. Overhang Effectiveness with Respect to Wind Characteristics

Previous studies show that wind speed and wind direction influence the wetting pattern on the façade and overhang effectiveness. Considering onsite wind data frequency and variability, the effect of wind speed and wind direction on overhang effectiveness has been studied.

### 4.5.1. Wind Speed

Higher wind velocities lead to more oblique rain trajectories in almost similar rain fall intensities. To assess the effect of wind speed on provided protection, measured data during the each period of studies is categorized based on wind speed. Given the onsite wind speed frequency, three categories are defined as $0<U<2$ m/s, $2<U<4$ m/s and winds speed higher than 4 m/s. To eliminate the more complex wetting patterns caused by oblique wind directions, only perpendicular wind direction ±15 degrees to east façade have been considered.

Prior to the estimation of overhang effectiveness, the number of available data, total amount of precipitation, rain fall intensity, average and standard deviation of wind speed and wind angles for different categories of each study periods is presented in Table 4.2. The good agreement between characteristics of defined data set for each overhang width with data for situation without overhang proves the reliability of further analysis. However, wind speeds higher than 4 m/s are less frequent in comparison with the other two categories. The average of wind speed is 1.5 m/s, 2.7 m/s and 4.7 m/s for the first, second and third category respectively.

Table 4.2 - Data set specification for wind speed categories and different overhang size

| Rain Hours | | Rainfall Intensity (mm) | | Wind Speed (m/s) | | Wind Direction | |
|---|---|---|---|---|---|---|---|
| | NO. Data | Total | Average | Average | S Dev. | Average | S Dev. |
| **0<U<2** | | | | | | | |
| No OH | 393 | 308.1 | 0.78 | 1.45 | 0.39 | 92.92 | 8.03 |
| 1' OH | 242 | 258 | 1.07 | 1.46 | 0.36 | 92.19 | 8.43 |
| 2' OH | 143 | 143.7 | 1.00 | 1.50 | 0.35 | 91.45 | 8.45 |
| 3' OH | 324 | 303.3 | 0.94 | 1.51 | 0.35 | 92.39 | 8.20 |
| 4' OH | 234 | 219.7 | 0.94 | 1.44 | 0.37 | 93.12 | 7.98 |
| **2<U<4** | | | | | | | |
| No OH | 412 | 532.8 | 1.29 | 2.73 | 0.51 | 93.23 | 9.02 |
| 1' OH | 247 | 336.9 | 1.36 | 2.67 | 0.48 | 91.86 | 9.21 |
| 2' OH | 198 | 299.4 | 1.52 | 2.73 | 0.48 | 89.99 | 9.03 |
| 3' OH | 590 | 687.8 | 1.17 | 2.72 | 0.50 | 92.91 | 8.88 |
| 4' OH | 353 | 464.7 | 1.32 | 2.80 | 0.52 | 93.18 | 8.93 |
| **4<U** | | | | | | | |
| No OH | 39 | 63.3 | 1.62 | 4.57 | 0.59 | 90.28 | 9.11 |
| 1' OH | 23 | 51.8 | 2.25 | 4.77 | 0.69 | 88.85 | 10.60 |
| 2' OH | 5 | 6.6 | 1.32 | 4.59 | 0.58 | 92.00 | 7.65 |
| 3' OH | 48 | 64.9 | 1.35 | 4.48 | 0.45 | 89.23 | 8.82 |
| 4' OH | 68 | 100.4 | 1.48 | 4.94 | 0.65 | 91.26 | 9.07 |

#### 4.5.1.1. Overhang Effectiveness With Respect to Wind Direction

Catch ratios at the measurement points are calculated using defined data sets and overhang effectiveness is calculated based on similarity approach. Regarding different wind speed categories, with the increase of wind speed, the effectiveness of the overhang decreases. For wind speed lower than 2 m/s, 1.2 m overhang provides 78% up to full protection within the distance of 9.1 m below the roof top, while this rate is limited to the range of 14- 37% for 0.3m overhang. For higher wind speed between 2-4 m/s, although the protection area for 1.2m and 0.9 m overhang is still extended up to 45% of the building height, the lower threshold decreased to 30% at the place of EN4 and EN3. Smaller size overhangs provide protection for places within the distance of 2.4 m from the roof top with the range of 11-33% and 20-72% for 0.3 m and 0.6 m overhang, respectively. Higher wind speeds, greater that 4 m/s, reduce both overhang effectiveness and protected area beneath it. While 1.2 m and 0.9m overhang are still effective in reducing the impinging WDR within the distance of 4.9m below the overhang, the maximum protection provided by the 0.3 m overhang is limited to 24% for locations just below the overhang, Figure 4.8.

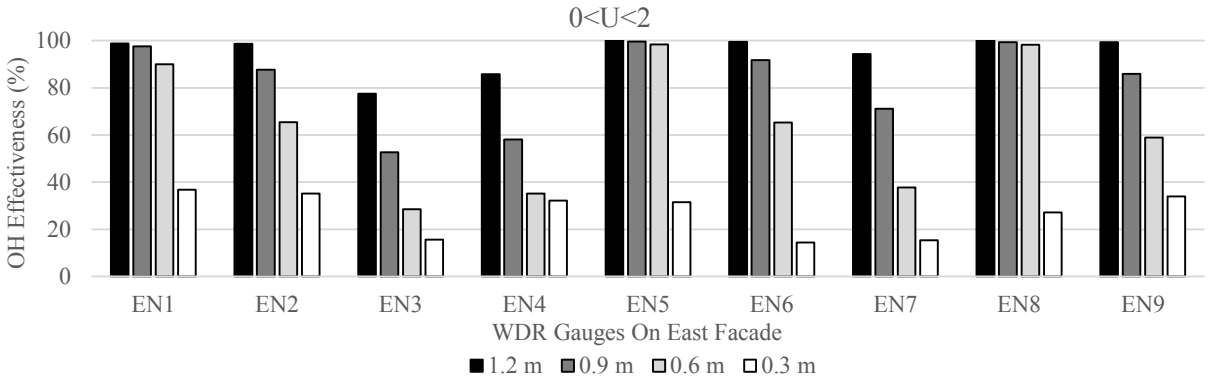


(a)

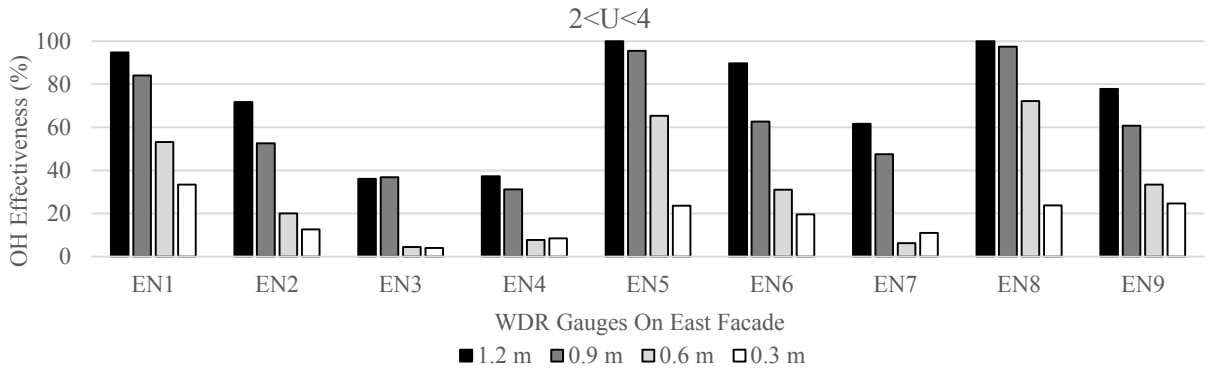


(b)

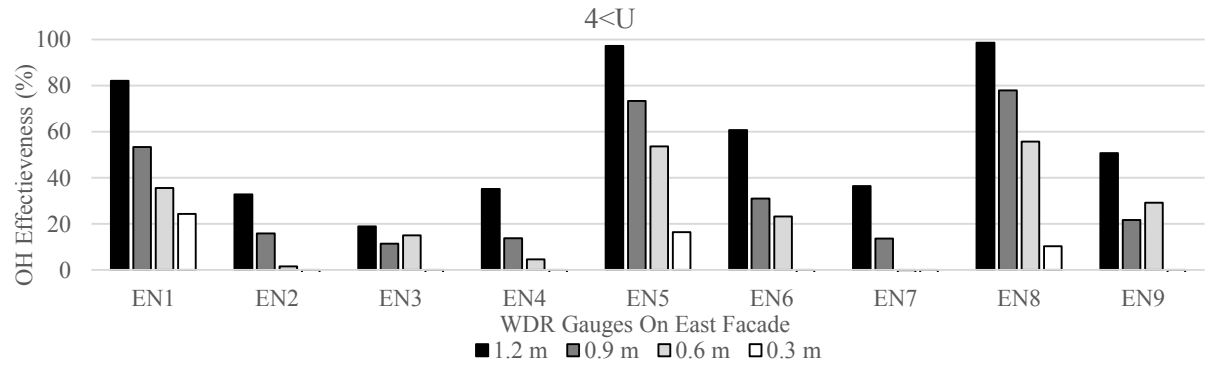


(c)

Figure 4.8 - Overhang effectiveness at the place of protected gauges for different overhang size and wind speed categories, (a) 0<U<2 m/s, (b) 2<U<4 m/s and (c) 4<U m/s

#### 4.5.1.2. Overhang Area-Weighted Effectiveness With Respect to Wind Direction

To quantify the effect of wind speed on provided protection by the overhang on different portions of facade area, the overhang area-weighted effectiveness for different wind speed categories are calculated. The results for each wind speed category are shown in the Table 4.3.

Table 4.3 - Overhang area-weighted effectiveness for (a) 0<U<2 m/s, (b) 2<U<4 m/s and 4<U m/s

(a) 0<U<2m/s

| Façade area | No overhang | | 0.3m overhang | | 0.6 m overhang | | 0.9 m overhang | | 1.2 m overhang | |
|---|---|---|---|---|---|---|---|---|---|---|
| | $\sum_{i=1}^{n} \eta_i A_i$ | WDR distribution on façade (%) | $\sum_{i=1}^{n} \eta_i A_i$ | Area-weighted effectiveness (%) | $\sum_{i=1}^{n} \eta_i A_i$ | Area-weighted effectiveness (%) | $\sum_{i=1}^{n} \eta_i A_i$ | Area-weighted effectiveness (%) | $\sum_{i=1}^{n} \eta_i A_i$ | Area-weighted effectiveness (%) |
| A1 (15%) | 9.23 | 58 | 6.96 | 25 | 1.87 | 80 | 0.59 | 94 | 0.04 | 100 |
| A2 (30%) | 11.36 | 71 | 8.85 | 22 | 3.22 | 72 | 1.25 | 89 | 0.20 | 98 |
| A3 (60%) | 14.24 | 89 | 11.50 | 19 | 5.68 | 60 | 3.37 | 76 | 1.96 | 86 |
| A4 (100%) | 15.99 | 100 | 13.25 | 17 | 7.44 | 53 | 5.13 | 68 | 3.72 | 77 |
| Total WDR reduction (%) | | | 17 | | 53 | | 68 | | 77 | |

(b) 2<U<4 m/s

| Façade area | No overhang | | 0.3m overhang | | 0.6 m overhang | | 0.9 m overhang | | 1.2 m overhang | |
|---|---|---|---|---|---|---|---|---|---|---|
| | $\sum_{i=1}^{n} \eta_i A_i$ | WDR distribution on façade (%) | $\sum_{i=1}^{n} \eta_i A_i$ | Area-weighted effectiveness (%) | $\sum_{i=1}^{n} \eta_i A_i$ | Area-weighted effectiveness (%) | $\sum_{i=1}^{n} \eta_i A_i$ | Area-weighted effectiveness (%) | $\sum_{i=1}^{n} \eta_i A_i$ | Area-weighted effectiveness (%) |
| A1 (15%) | 19.78 | 55 | 15.60 | 21 | 9.77 | 51 | 4.22 | 79 | 1.87 | 91 |
| A2 (30%) | 24.73 | 69 | 20.06 | 19 | 13.99 | 43 | 6.89 | 72 | 3.95 | 84 |
| A3 (60%) | 31.58 | 88 | 26.78 | 15 | 20.69 | 34 | 11.61 | 63 | 9.56 | 70 |
| A4 (100%) | 35.85 | 100 | 31.05 | 13 | 24.96 | 30 | 15.89 | 56 | 13.84 | 61 |
| Total WDR reduction (%) | | | 13 | | 30 | | 56 | | 61 | |

(c) U>4m/s

| Façade area | No overhang | | 0.3m overhang | | 0.6 m overhang | | 0.9 m overhang | | 1.2 m overhang | |
|---|---|---|---|---|---|---|---|---|---|---|
| | $\sum_{i=1}^{n} \eta_i A_i$ | WDR distribution on façade (%) | $\sum_{i=1}^{n} \eta_i A_i$ | Area-weighted effectiveness (%) | $\sum_{i=1}^{n} \eta_i A_i$ | Area-weighted effectiveness (%) | $\sum_{i=1}^{n} \eta_i A_i$ | Area-weighted effectiveness (%) | $\sum_{i=1}^{n} \eta_i A_i$ | Area-weighted effectiveness (%) |
| A1 (15%) | 33.81 | 52 | 29.05 | 14 | 19.83 | 41 | 16.16 | 52 | 7.78 | 77 |
| A2 (30%) | 42.84 | 66 | 37.35 | 13 | 27.59 | 36 | 23.99 | 44 | 13.78 | 68 |
| A3 (60%) | 56.49 | 86 | 50.52 | 11 | 40.60 | 28 | 36.85 | 35 | 26.14 | 54 |
| A4 (100%) | 65.36 | 100 | 59.39 | 9 | 49.47 | 24 | 45.72 | 31 | 35.00 | 46 |
| Total WDR reduction (%) | | | 9 | | 24 | | 31 | | 46 | |

The comparison of the amount of WDR received by different areas of the façade shows that higher wind velocities lead to more deposition on greater distances from the roof top; however, more than 50% of total WDR impinged on top 15% of the façade regardless of the wind velocity.

For the times wind speed is lower than 2m/s, 0.6 m overhang provides 53% of protection over top 15% of façade, which reduces the total amount of impinged wind driven rain by 46%. This percentage increases up to 54% and 58% for 0.9 m and 1.2 m overhang respectively, while 0.3 m overhang provides less than 15% of protection. For wind speed between 2 to 4 m/s, increasing the overhang size from 0.3m up to 0.9 m, almost doubled the provided protection on entire façade for each 0.3 m increase in overhang size and reaches to 56% for 0.9 m overhang. However, the effect of increasing the width from 0.9 m to 1.2 m in reducing WDR is almost negligible. In higher wind velocities, above 4 m/s, smaller overhang sizes become less productive. Impinged WDR on entire façade is reduced by only 9% for 0.3 m overhang and can be improved to 46% by applying 1.2 m overhang.

#### 4.5.1.3. WDR Reduction Coefficient with Respect to Wind Speed

Figure 4.9, indicates the relation between WDR reduction coefficient for entire façade as the function of wind velocity. Considering the available data, the relation is generated for wind speeds within the range of 1.5 m/s to 4.7 m/s. These values represent the average of wind velocity for defined wind speed categories of each overhang widths. As shown in Figure 4.9 , an exponential relation exist between the overhang width and the evaluated WDR reduction coefficient.

Based on the evaluations, WDR reduction coefficient for 0.3m overhang is less sensetive to wind speed changes and even in the low wind speeds, the façade still recives more than 80% of WDR. For 1.5m/s wind speed the amount of received WDR on the façade can be reduced by 50%, 70% and 80% for 0.6m, 0.9m and 1.2m overhnag width respectively; however with increase of wind speed to 4.7m/s the WDR reduction coefficient reduces by around 50% for all meantioned overhnagd widths. Also *WDR reduction coefficient with respect to wind speed* is compared with *WDR reduction coefficient* presented in Section 4.4.2; *WDR reduction coefficient* is calculated considerin all availabe data. The average of wind speed during each study period is considered for this comparison. There is a good agreement for 0.9 m and 1.2 m overhang while there is a slight difference for smaller overhang sizes.

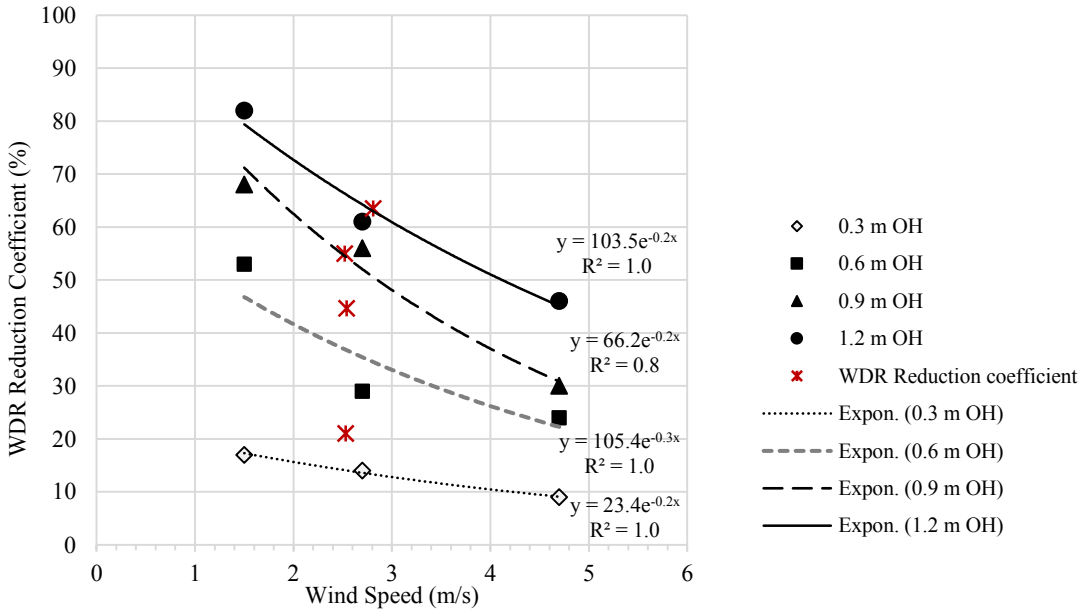


Figure 4.9 – WDR reduction coefficient for entire facade area as a function of wind speed for different overhang widths and in comparison with *WDR reduction coefficient based on all data

### 4.5.2. Wind Direction

To see the effect of wind direction on the amount of provided protection, measured data of each study period is categorised with respect to wind direction. Five wind direction categories with 30° intervals are defined. For each given category, the wind direction of considered data are within the range of ±15 degree from the assigned principle direction, as shown Figure 3.14.

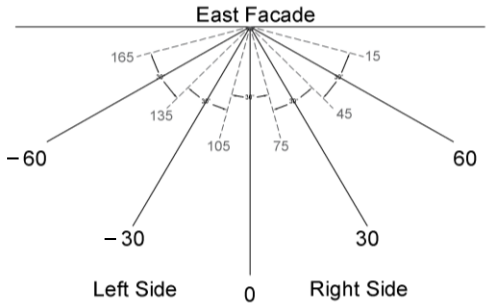


Figure 4.10 - Wind direction categories considering 30° intervals

Prior to the analysis, agreement of meteorological data of each data sets are investigated to validate the comparison of calculated catch ratios for periods with overhang with those for the

period without overhang. Table 4.4 shows the number of data and other critical information for each data set. Wind speed at 30° from the north, equal to 60° from the right, is not frequent and number of provided data is not sufficient to assess overhang effectiveness for this direction.

Table 4.4 - Data set specification for different wind directions

| Rain Hours | | Rainfall Intensity (mm) | | Wind Speed (m/s) | | Wind Direction | |
|---|---|---|---|---|---|---|---|
| | NO. Data | Total | Average | Average | S Dev. | Average | S Dev. |
| θ=60±15° (Left) | | | | | | | |
| No OH | 169 | 201.4 | 1.19 | 3.66 | 2.13 | 149.98 | 8.64 |
| 1' OH | 92 | 88.4 | 0.96 | 3.96 | 2.39 | 150.26 | 9.31 |
| 2' OH | 59 | 90.3 | 1.53 | 4.39 | 2.43 | 151.46 | 9.33 |
| 3' OH | 177 | 184.4 | 1.04 | 3.47 | 2.19 | 149.53 | 8.38 |
| 4' OH | 142 | 135.6 | 0.95 | 4.50 | 2.73 | 151.04 | 8.03 |
| θ=30±15° (Left) | | | | | | | |
| No OH | 343 | 435.2 | 1.27 | 2.56 | 1.23 | 116.34 | 8.64 |
| 1' OH | 149 | 175.8 | 1.18 | 2.75 | 1.59 | 115.97 | 9.13 |
| 2' OH | 90 | 140.1 | 1.56 | 2.51 | 1.06 | 115.43 | 8.39 |
| 3' OH | 369 | 370.1 | 1.00 | 2.53 | 1.14 | 116.02 | 8.87 |
| 4' OH | 279 | 335.3 | 1.20 | 2.69 | 1.30 | 114.05 | 8.29 |
| θ=0±15° | | | | | | | |
| No OH | 844 | 904.2 | 1.07 | 2.22 | 0.93 | 92.95 | 8.60 |
| 1' OH | 512 | 646.7 | 1.26 | 2.19 | 0.93 | 91.88 | 8.95 |
| 2' OH | 271 | 420.7 | 1.58 | 2.30 | 0.92 | 98.82 | 14.73 |
| 3' OH | 962 | 1056 | 1.10 | 2.40 | 0.87 | 92.55 | 8.69 |
| 4' OH | 655 | 784.8 | 1.20 | 2.54 | 1.14 | 92.96 | 8.64 |
| θ=30±15° (Right) | | | | | | | |
| No OH | 209 | 243.4 | 1.16 | 2.34 | 0.90 | 65.13 | 7.89 |
| 1' OH | 140 | 178 | 2.41 | 2.41 | 7.53 | 66.99 | 7.53 |
| 2' OH | 116 | 145.8 | 1.26 | 2.33 | 0.87 | 65.49 | 7.51 |
| 3' OH | 226 | 235.5 | 1.04 | 2.46 | 1.02 | 66.53 | 7.28 |
| 4' OH | 144 | 151.9 | 1.05 | 2.56 | 1.26 | 66.13 | 7.82 |
| θ=60±15° (Right) | | | | | | | |
| No OH | 18 | 13.9 | 0.77 | 1.66 | 0.59 | 37.38 | 5.86 |
| 1' OH | 13 | 9 | 0.69 | 2.70 | 1.92 | 33.12 | 8.57 |
| 2' OH | 18 | 9.4 | 0.85 | 2.02 | 0.83 | 39.08 | 5.60 |
| 3' OH | 11 | 25 | 1.39 | 1.67 | 0.70 | 34.46 | 7.33 |
| 4' OH | 6 | 6.4 | 1.07 | 1.95 | 0.50 | 37.80 | 4.39 |

There is a good agreement between average and standard deviation of wind speeds during different periods of study for each given wind direction categories. It can be observed that wind blowing from south-east are slightly stronger and more frequent than the wind coming from north-

east. The average of wind speed coming from south-east (60° Left) is almost 4 m/s while this amount is around 2.5 m/s for other data sets.

#### 4.5.2.1. Overhang Effectiveness With Respect to Wind Direction

Similar trend is followed in the calculation of catch ratio at measurement points for each wind direction. As it was mentioned earlier for normal wind direction, for period without overhang, the calculated catch ratios are almost symmetrical on both sides of the façade. For inclined wind direction although classical wetting pattern can be observed, there is a slight difference between catch ratios of both sides. The reason can be explained by wind flow around the building. Considering wind tunnel experiment the normalized wind velocity increases from the windward edge of the building towards the leeward edge. However, as shown in Figure 4.11, the incident angle increases gradually across the façade and wind flow becomes more parallel to the facade. As a result, windward areas of the façade (B) receive more WDR and have higher catch ratios in comparison with leeward parts (A).

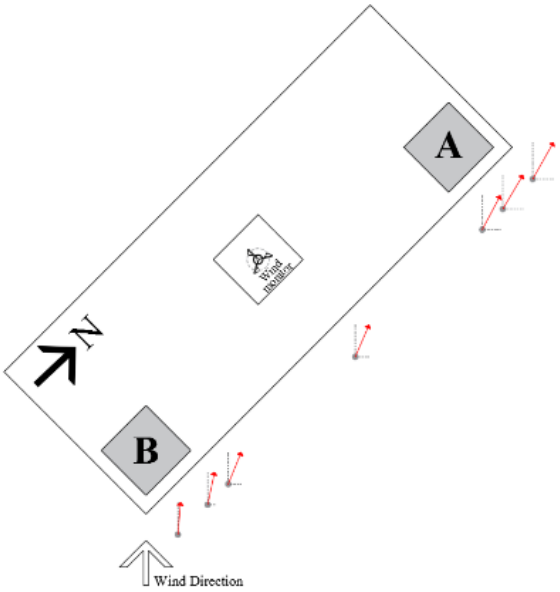


Figure 4.11. Wind velocity vectors near the façade at the 0.6 m distance from the roof top, Cassier Building stand-alone model, scale 1/200

Considering wind directions within the range of normal to the 60° from the left, overhang effectiveness increases for more oblique wind angles blowing from south-east towards the east façade and reached to its maximum at 60°. The decrease of incident wind angle from 60° to 30°

slightly influences the effectiveness, while this change is more significant for decrease of incident angle from 30° to normal. The overhang is less effective for north-east wind directions and lower protection is provided specifically for points located close to building edge.

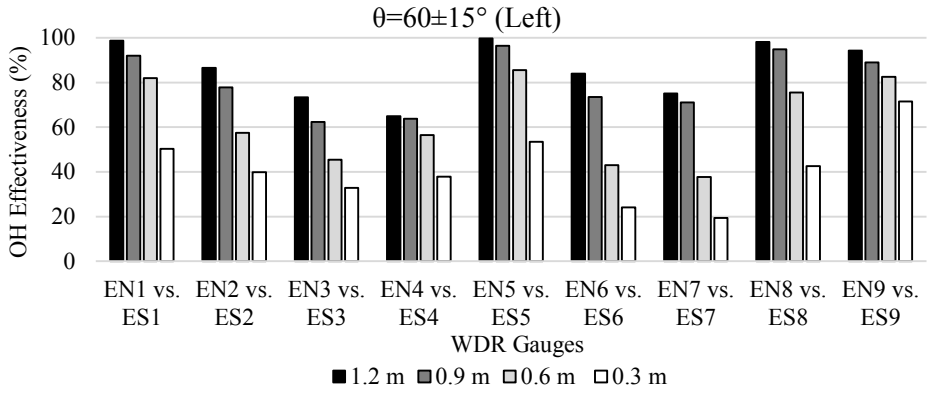


(a)

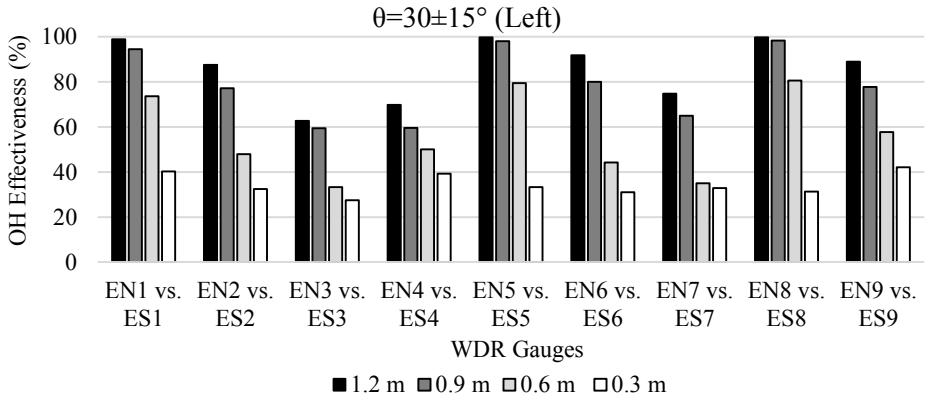


(b)

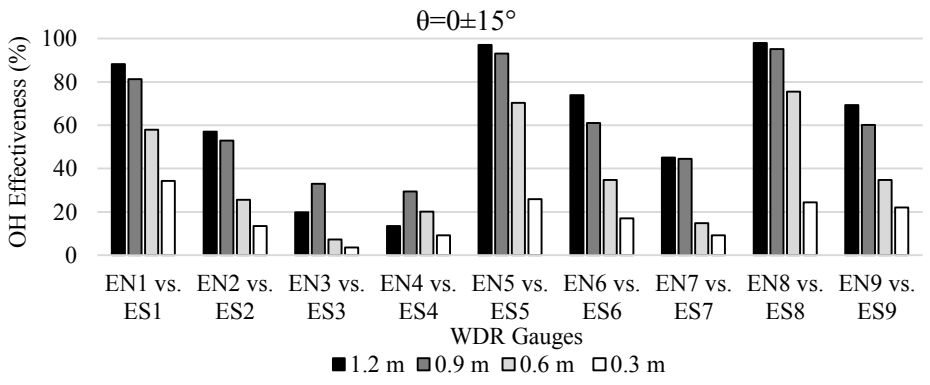


(c)

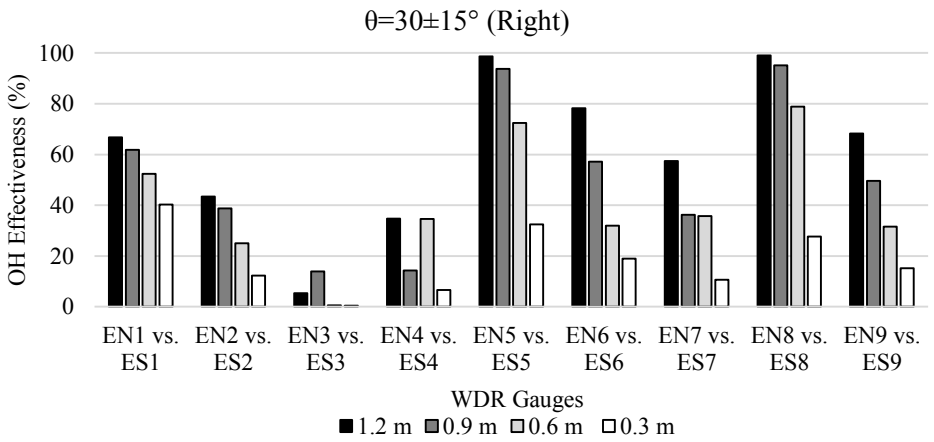


(d)

Figure 4.12- Overhang effectiveness at the place of protected gauges for different overhang size and wind direction categories, (a) θ=60±15° (Left), (b) θ=30±15° (Left), (c) θ=0±15°and (d) θ=30±15° (Right)

It can be observed that the overhang effectiveness is not the same for wind approaching the façade from 30° form right and left. As shown in Figure 4.13, the area protected by the overhang is a leeward area for wind approaching from south-east while it is the windward area for wind coming from north-east. The leeward areas of the buildings receive less WDR and more protection is provided by the overhang. In contrast, more WDR is deposited on windward areas and overhang is less effective in the reduction of WDR impinged on the façade.

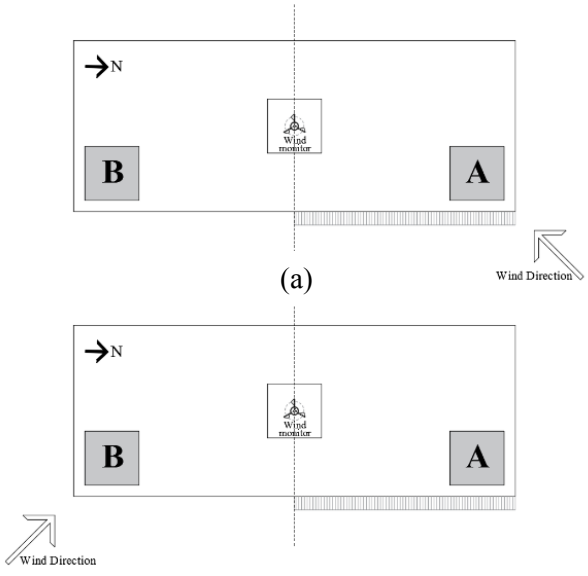


Figure 4.13 – The position of the overhang and its protected area (A) with respect to approaching wind direction, (a) windward corner, (b) leeward corner

#### 4.5.2.2. Overhang Area-Weighted Effectiveness with Respect to Wind Direction

To study the effect of wind direction on overhang area-weighted effectiveness accurately, calculations are conducted for half of the building façade. The protected area acts as leeward and windward area for south-east and north-east respectively. In general, by increasing wind angle from normal of the façade less wind driven rain is deposited over the façade. Table 4.5 presents the percentage of wind driven rain reduction over the half of the façade area protected by different overhang widths. The provided protection ranges between 14% - 33% for 0.3 m, 62-83% for 1.2m overhang and in between for other overhang widths when the incident wind angle changes from normal to 60° from the south-east (left side). The area-weighted effectiveness for wind angle 30° from the right, windward areas, remains almost similar to the normal condition.

Table 4.5 - Overhang area-weighted effectiveness for different overhang sizes under different wind directions for entire facade

**Overhang area weighted effectiveness for entire façade; A4 (100%)**

| | θ From North | 1' (0.3 m) | 2' (0.6 m) | 3' (0.9 m) | 4' (1.2 m) |
|---|---|---|---|---|---|
| θ=60±15° (Left) | -60 | 33 | 53 | 69 | 82 |
| θ=30±15° (Left) | -30 | 24 | 47 | 66 | 73 |
| θ=0±15° | 0 | 14 | 32 | 52 | 62 |
| θ=30±15° (Right) | 30 | 16 | 34 | 46 | 60 |
| θ=60±15° (Right) | 60 | n/a | n/a | n/a | n/a |

#### 4.5.2.3. WDR Reduction Coefficient with Respect to Wind Direction

Figure 4.14 shows the *WDR reduction coefficient with respect to wind direction* for each overhang size with respect to wind incident angel. In general, the lowest value of WDR reduction coefficient can be observed for wind directions normal to the façade and the building façade received less rain for inclined wind directions. Considering wind directions approaching from the south-east, increase of wind incident angle from normal to 60°, increase WDR reduction coefficient by around 20% for all overhang widths.

WDR reduction coefficient can be used as the more conservative approach by designers in estimation of WDR load received by the façade. However, for inclined wind directions, it should be noticed that overhang effectiveness is not uniform, and its effectiveness decreases gradually from windward areas towards leeward areas of the facade. Considering building geometries similar

to the study building, for inclined wind directions, half of the façade can be considering as leeward and the other half as windward area. For Vancouver building, for 30° wind direction, related catch ratios and effectiveness is assigned to windward and leeward areas to calculate amount of WDR received by the façade protected by roof overhang. Calculations shows that the total provided protection is almost similar to the condition wind blows normal to the facade, although one side receives more WDR and the other side is less exposed to rain precipitation.

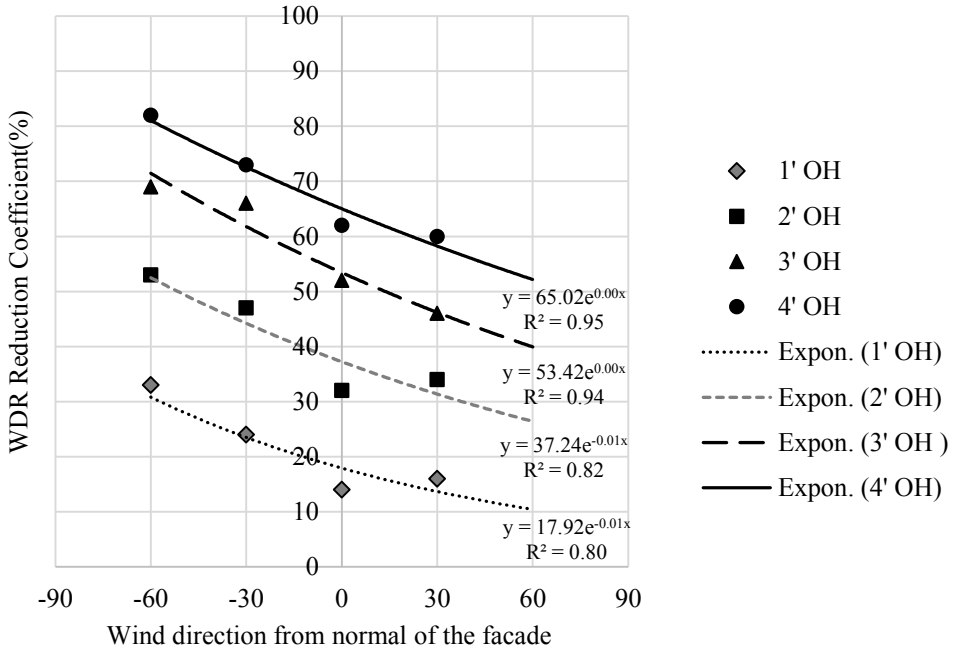


Figure 4.14 – WDR reduction coefficient for entire facade with respect to wind direction for different overhang widths

### 4.5.3. Wind Speed and Direction

To assess the simultaneous effect of wind direction and wind speed on overhang effectiveness, the measured data is categorised first based on the wind speed and later regarding different wind direction within each wind speed categories. In total fifteen data sets are defined for each overhang widths.

Similar procedure is followed in calculation of catch ratio and consequently overhang effectiveness for each measurement point. Overhang area-weighted effectiveness is calculated based on local overhang effectiveness for three wind categories each divided to five wind direction subcategories. The general trend in overhang area-weighted effectiveness, considering combined

effect of wind speed and wind direction follows the observed principles discussed in Section 4.5.2 and Section 4.5.3; the overhang effectiveness decrease with the increase of wind speed and improves with the increase of wind incident angle. WDR reduction coefficient with respect to wind speed and direction is presented in Figure 4.15. More detailed analysis shows that, for leeward protected areas, overhang WDR reduction coefficient is more sensitive to wind direction changes in higher speeds. As an example, for 1.2 m overhang, wind direction changes from normal to 30° from the left, increase WDR reduction coefficient by 5% for wind speeds less than 2 m/s, while this rate is 20% for speeds higher than 4 m/s. Also overhang WDR reduction coefficient experience less improvement by increase of wind incident angles more than 30°.

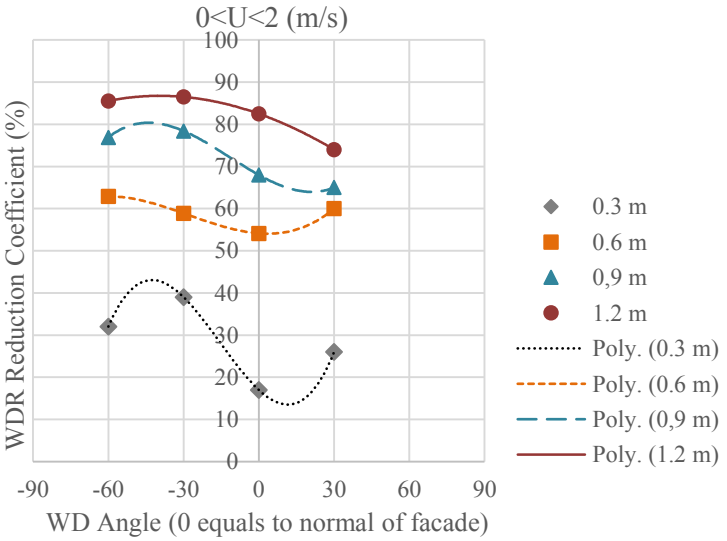


(a)

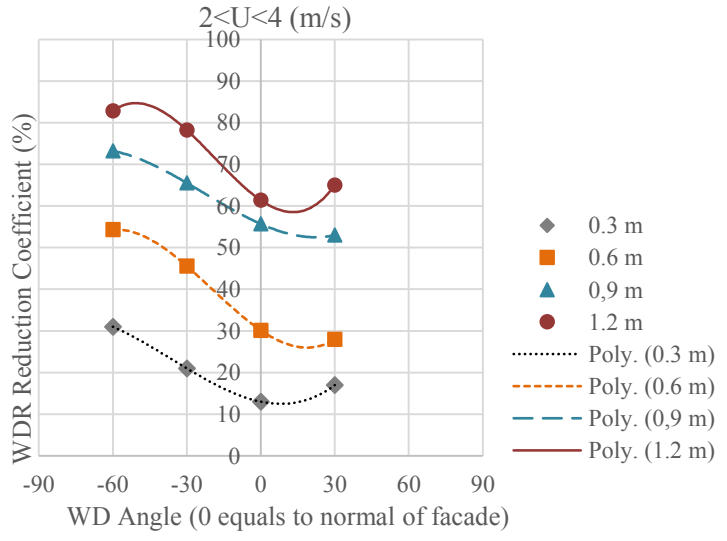


(b)

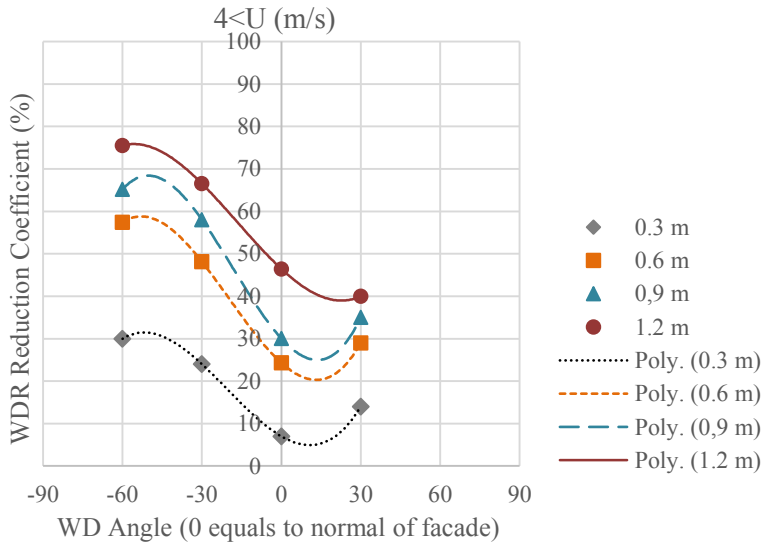


(c)

Figure 4.15 - Comparison of WDR reduction coefficient with respect to wind directions for wind speed categories of (a) 0<U<2, (b) 2<U<4 and (C) 4<U

## 4.6. WDR reduction coefficient validation for north facade

To evaluate the estimated WDR reduction coefficient, the amount of WDR deposited over north façade is evaluated by applying obtained results in estimation of received WDR. As it is shown on the Figure 4.16, the north façade is divided into 25 cells centred by WDR gauges. For comparison purposes, the total amount of received WDR by north façade is estimated for each period of study applying two approaches. First, the amount of WDR is estimated by area-weighted methodology. The measured amount of WDR at the measurement points is assigned to the related cell. The amount of WDR for cells without gauge is interpolated considering adjusted cells. The total amount of WDR received by the façade is the sum of area-weighted WDR of all cells. This amount is calculated for period without overhang as the reference and for the periods façade was protected by different overhang widths. In the Second approach, the amount of received WDR is calculated based on the amount WDR received by the façade during the period without overhang multiplied by WDR reduction coefficients.

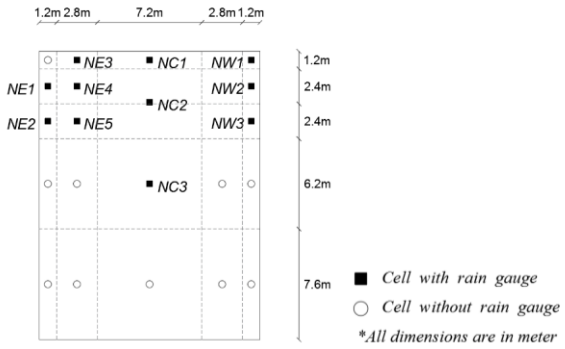


Figure 4.16 – North façade cell pattern and location of WDR gauges, Cassiar Building, Vancouver

The average wind speed ranges between 2.01m/s up to 2.51 m/s for different study periods of north façade. The prevailing wind direction towards the north façade approaches from the north-east with average incident angle of 75°. As the data for 60° wind direction is not available for both leeward and windward areas, WDR reduction coefficient, presented in Table 4.1, and WDR reduction coefficient with respect to wind speed, presented in Table 4.3 (b), are used.

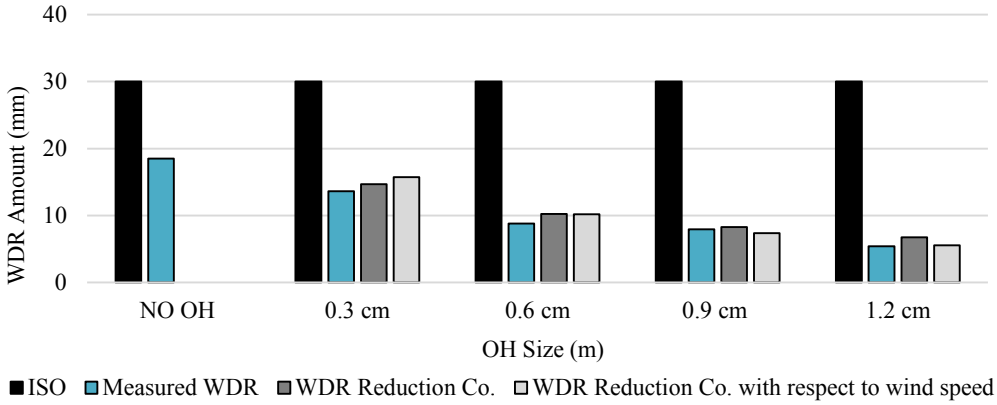


Figure 4.17 – Validation of WDR reduction coefficient for Vancouver north façade in comparison with WDR based on ISO and WDR measured onsite

As indicated in Figure 4.17, there is a good agreement between measured WDR and estimated amount applying WDR reduction coefficients. Also, the results show that estimation of WDR based on ISO equation is subjected to over estimation especially for facades protected by roof overhang. Regarding study surfaces' geometry, the BSL is 24 and 18 for east and north façade of Vancouver building respectively. The close BSL of these two facades might be the reason of good agreement between measured amounts of WDR on the north façade with the values estimated by applying WDR reduction coefficient calculated based on east façade measurements.

## 4.7. Summary and Conclusion

Catch ratio has been calculated at the place of WDR gauges for all five periods of study including: no overhang, 0.3m, 0.6m, 0.9m and 1.2m. The primary results show that roof overhangs significantly reduce the amount of WDR at locations close to rooftop and away from edges of the building.

Overhang effectiveness at the place of WDR gauges is calculated based on similarity and symmetry approach and for defined data sets with respect to wind characteristics. Calculated effectiveness, indicates that for all overhang sizes, the protection increases from the side edge to the center and from the bottom to the top of the façade. More protection is provided by the wider overhangs and the protected area can be expanded to half of the building height for 1.2 m overhang.

Results for area-weighted catch ratios for period without overhang shows that more than 70% of the total amount of impinged WDR is received by the top 30% of the façade. As the result overhangs that can protect this part of the façade can effectively reduce facade wetting. Assessed overhang area-weighted effectiveness shows that 0.3m, 0.6m, 0.9m and 1.2 m overhang can reduce WDR load on this part of the façade by 27%, 60%, 72% and 85% respectively. To apply the effect of overhang in semi-empirical methods such as ISO model, WDR reduction coefficient is introduced as the percentage reduction in amount of WDR load received by the building façade.

The analysis shows WDR reduction coefficient decreases with the increase of wind speed, while increases with the increase of wind incident angle. However, the effect of overhang in reduction of WDR is not uniform across the façade for inclined wind directions. As the result proper WDR reduction coefficient should be assigned to windward and leeward areas; windward areas receive more WDR in comparison with leeward areas.

# 5. Generalizing WDR Reduction Coefficient for Mid-Rise Buildings

## 5.1. Introduction

Field measurements on Vancouver building establish the correlation between overhang size and its effectiveness in reducing WDR wetting for mid-rise buildings. This correlation may be applied to other mid-rise buildings with similar building geometry and wind flow characteristics. To test this hypothesis, wind tunnel measurements were carried out on Fredericton building to confirm the wind flow on windward façade. The south-east façade of Fredericton building has similar geometry as the east façade of Vancouver building. Measurement of wind speed in front of the south-east façade of Fredericton building are taken. The obtained results are compared with the experimental test results conducted by Chiu (2016). The effect of adding overhang on wind velocity near the windward façade of both models has been tested and discussed for normal and inclined wind directions.

## 5.2. Comparison of Cassier Building and MacLeod House

Prior to the wind tunnel test, onsite wind characteristics, measured catch ratio and geometrical characteristics of east façade of Vancouver building and south-west façade of Fredericton building have been compared. The agreement of received WDR in term of catch ratio with respect to wind speed confirms the similarity of wind flow in interaction of buildings in real life condition due to geometrical similarities.

To compare the wind velocity blowing towards the study facades, wind direction of considered data is limited within the range of normal ±15 degrees. The average of wind velocity during rain hours at the height of 10 m above the ground is 1.73 m/s for Vancouver building, while it is slightly higher at Fredericton, 3.21m/s. The average of rain fall intensity during rain hours is 1.07 and 1.30 mm/hr for Vancouver and Fredericton respectively. Also, calculated catch ratios at the measurement points of Frdericton building is higher than corresponding points on Vancouver building due to higher wind velocity and rain fall intensity. For instance, the catch ratio at the place of ES1 (Vancouver) is 0.254 while it is 0.323 at the place of SW6 (Fredericton), both located on top left corner of the facades. The predicted catch ratio for top corner of the mid-rise building as a

function of wind speed $U_{10}$ and horizontal rain fall intensity, estimated by Blocken (2004), is almost 0.272 and 0.396 for Vancouver and Fredericton respectively. The slight difference can be attributed to difference of current test buildings' geometry and mid-rise building geometry assumed by Blocken. A good agreement between meteorological data, calculated catch ratios and building geometry of these two buildings, allows further analysis for study of wind flow in wind tunnel.

## 5.3. Wind Tunnel Experiment

### 5.3.1. Normalized Wind Velocity

Wind flow is one of the main contributing factors on rain drop trajectories. Thus, it is expected that wind flow patterns be similar around similar building geometries. Normalized wind velocity near south-west façade of 1:400 stand-alone model of Fredericton is shown in Figure 5.1. As it is indicated the normalized velocity increases from the center to the sides of the façade. There is a symmetrical distribution of velocity near the edges of the façade, however, it is not symmetrical on the center parts due to the building geometry; the right wing of the building is offset by 9.45m. The lowest velocities are encountered in the center of the south-west façade.

The comparison of normalized wind velocities measured in the similar experiment conducted by Chiu (2016) on Vancouver building shows a good agreement in normalized wind velocities near the windward façades between these two models, as shown in Figure 5.2. This experiment verifies that similar wind flow around these two buildings with similar geometry for normal wind direction.

The similar procedure is applied to study normalized wind velocity with approaching angle of 45° from right and left sides. The results are presented in Figure 5.3. In general, the velocities are lower at the windward edge and increase gradually towards the leeward edge. In comparison with Vancouver experiment for inclined wind direction (shown in Figure 5.4), for wind approaching at 45° from the right, the normalized wind velocity is lower near the windward areas of Fredericton model. While wind approaching form 45° from right, leads to higher normalized wind velocity on windward areas of the façade and creates a protected area on rear area of south-west faced. Non-leveled south-west façade of Fredericton can be considered as the main contributing factor.

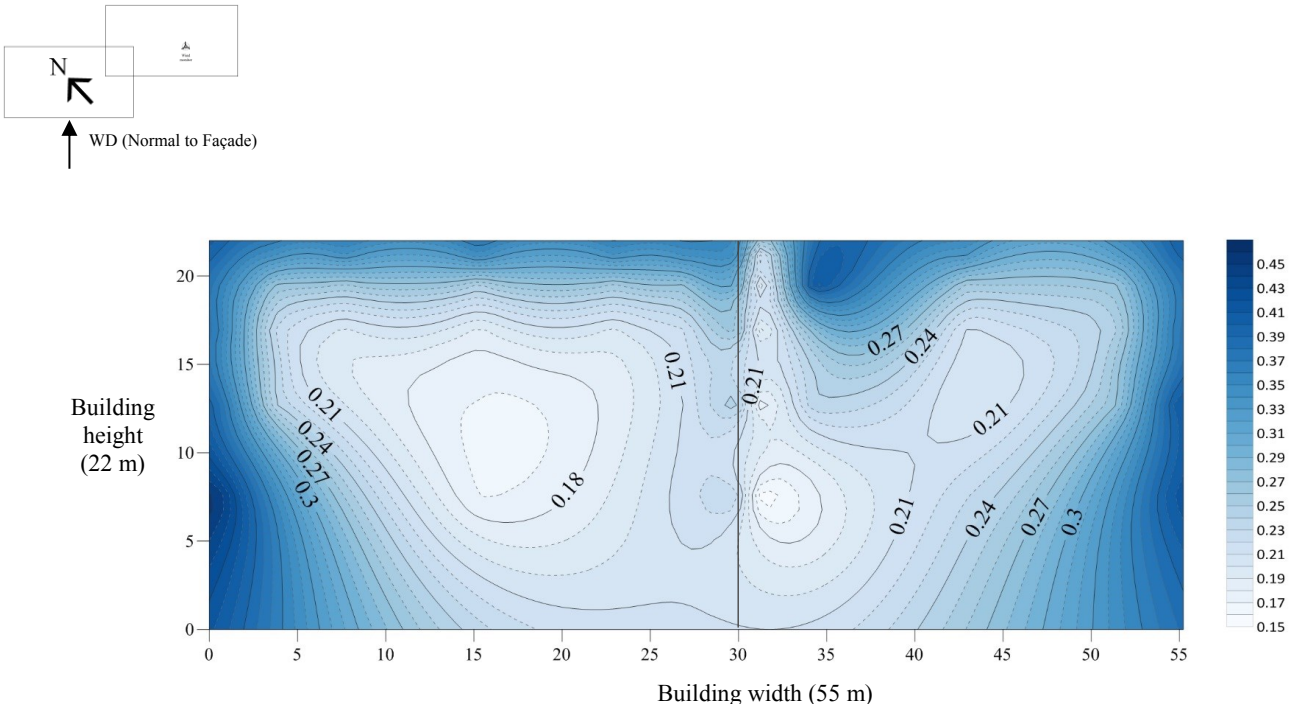


Figure 5.1- Normalized Wind Velocities on south-east façade of Macleod House, 1:400 stand-alone model, θ = 0° (from south-west)

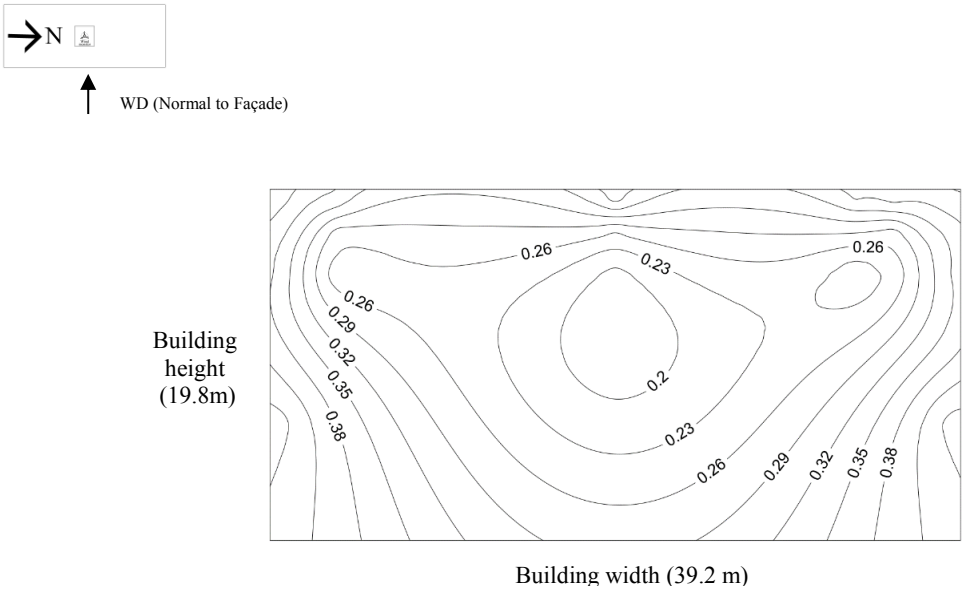


Figure 5.2 - Normalized Wind Velocities on south-east façade of Cassiar Building, 1:400 stand-alone model, θ = 0° (from east)(Chiu, 2016)

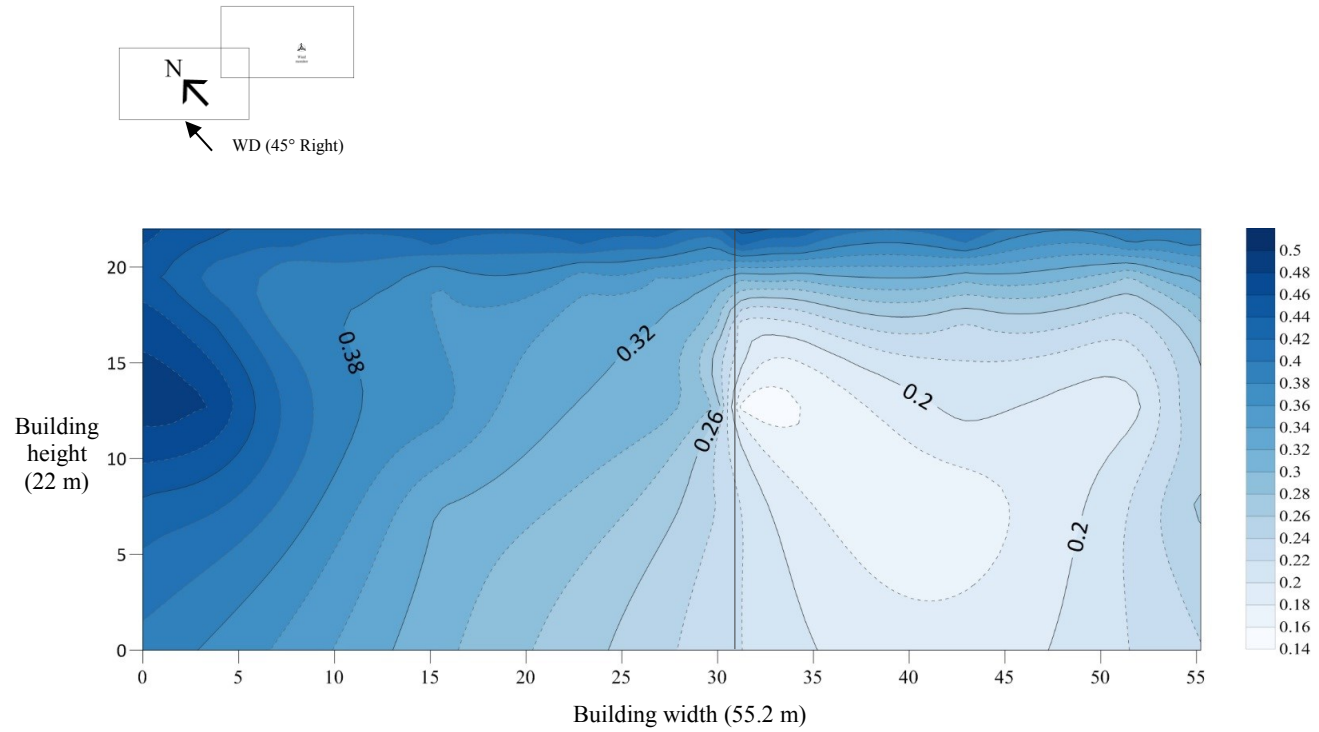


(a)

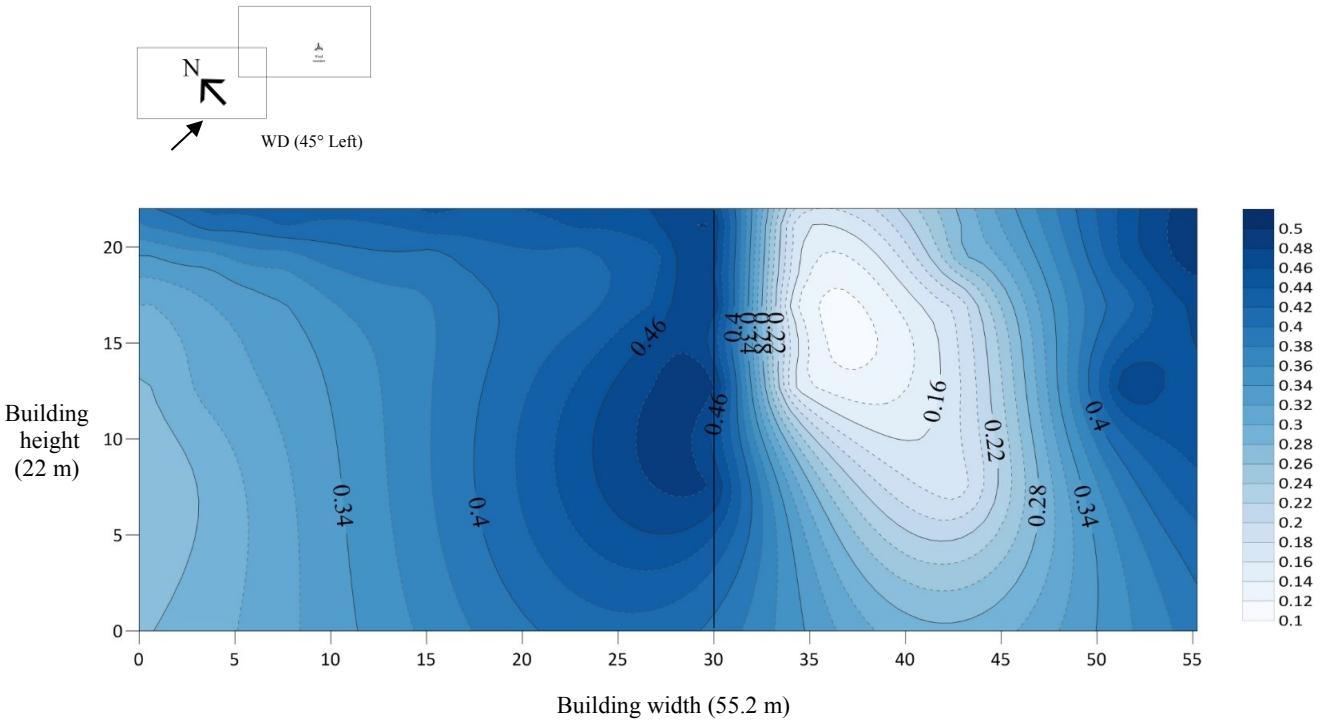


(b)

Figure 5.3 - Normalized Wind Velocities on south-east façade of Macleod House, 1:400 stand-alone model, (a) θ = 45° Right and (b) θ = 45° Left

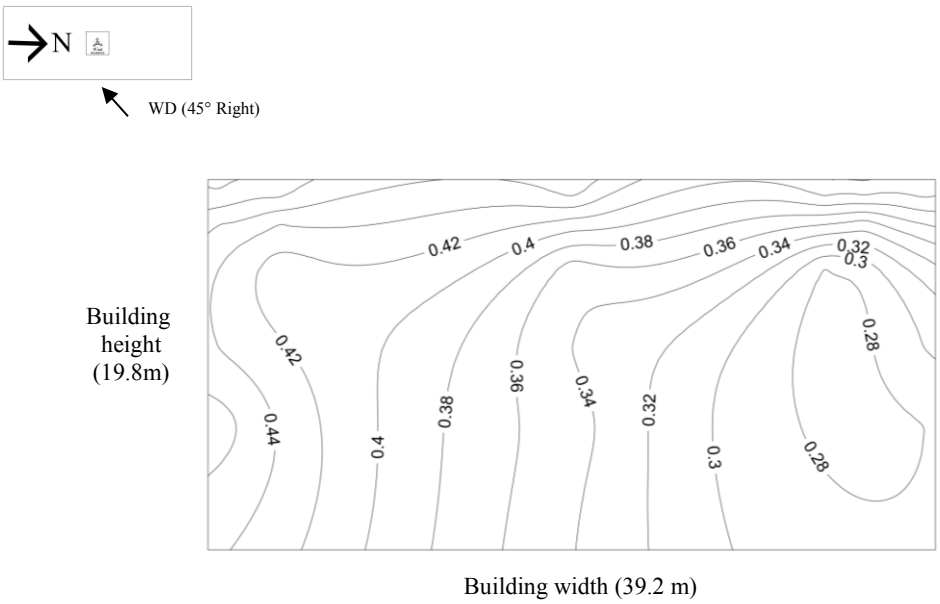


Figure 5.4 - Normalized Wind Velocities on south-east façade of Cassiar Building, 1:400 stand-alone model, θ = 45° (from north-east)(Chiu, 2016)

### 5.3.2. Effect of Overhang on Wind Velocity for Prevailing Wind Direction

**Normal wind direction**

Adding overhang on buildings' roof top deflects upstream wind flow and consequently rain fall trajectories. To evaluate the effect of overhang on reduction of normalized wind velocity, a 1:200 stand-alone model with a 6 mm (1.2m) overhang is used in the experiment. The normalized wind velocity near south-west façade of the Fredericton model and east façade of Vancouver model are presented in form of contour lines for situations (a) with and (b) without overhang in APPENDIX C, for normal wind direction. The gradient of normalized wind velocity reduction near the area below the overhang is presented in Figure 5.5 and Figure 5.6 for south-west façade of Fredericton and east façade of Vancouver model respectively. As it is indicated the effect of overhang in reduction of wind velocity increases from the side edges towards the center of the facade and from the center towards the roof line. Wind velocity is less affected at the side edges. The maximum reduction can be observed at the locations right beneath the overhang with enough distance from the edge. Similar trend can be observed in reduction of wind velocity on both wings of Fredericton model, however, more consistent reduction can be seen across left wing façade which is wider. In general, there is a good agreement between the observed results for east façade of Vancouver and south-west faced of Fredericton.

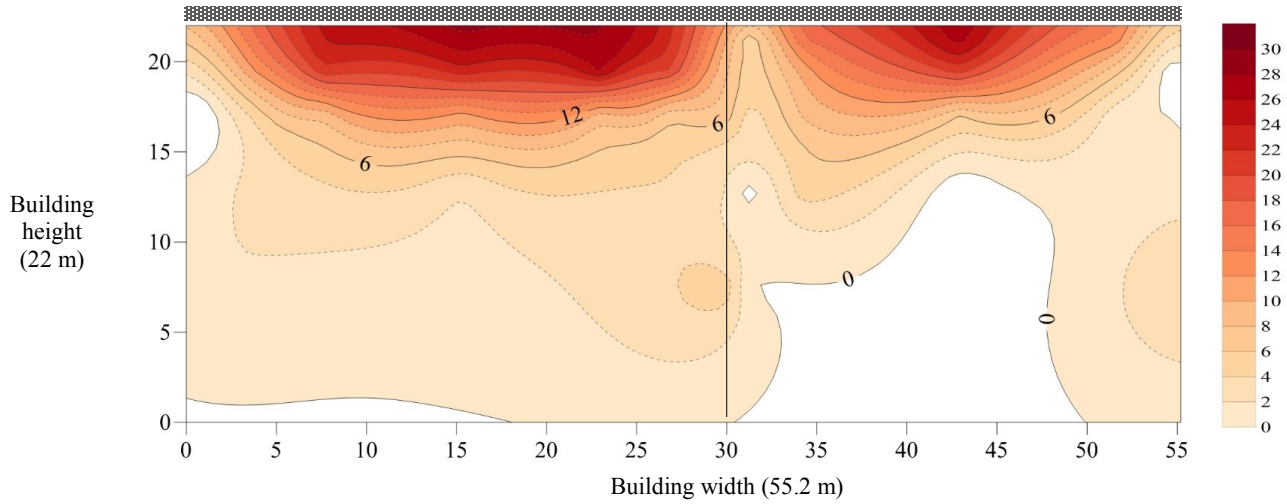


Figure 5.5 – Wind velocity reduction near south-west façade of Fredericton 1:200 stand-alone model, θ = 45°

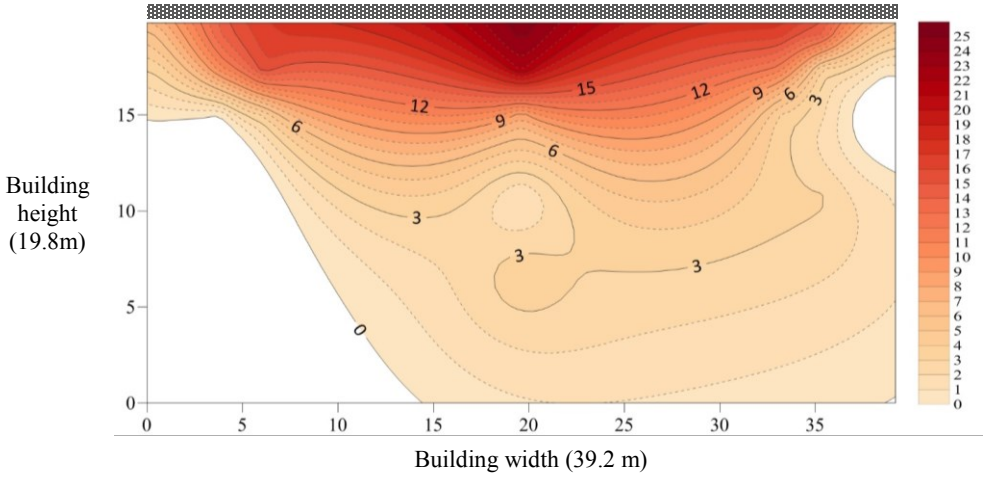


Figure 5.6 – Wind velocity reduction near east façade of Vancouver 1:200 stand-alone, θ = 45°

Figure 5.7 and Figure 5.8 show percentage reductions of wind velocity as a result of adding overhang for south-west and east façade of Fredericton and Vancouver model respectively. Fredericton façade is slightly wider, as a result location of measurement points is indicated based on their distance from the roof top and normalized distance across the façade. The effect of adding overhang in reduction of wind velocity is extended up to quarter of the model's height. Higher protection is provided for areas right beneath the overhang and reduces with increase of distance from the roof top. Similar trend can be observed in reduction of impinged WDR on the façade by applying roof top overhang based on field measurements experiment conducted on Vancouver building. This confirms that part of provided protection is due to airflow and rain trajectories deflection caused by adding overhang on building's roof top.

For points 0.6 m below the roof line, the minimum amount of wind velocity reduction is around 5% at the top corners. This amount increases gradually toward the middle of the façade and reaches to 28% for Fredericton and 24% for Vancouver. For distance of 4.88 m, the percent reduction of wind velocity is between almost 0% at the corners and reaches to 10% at the middle of each surfaced.

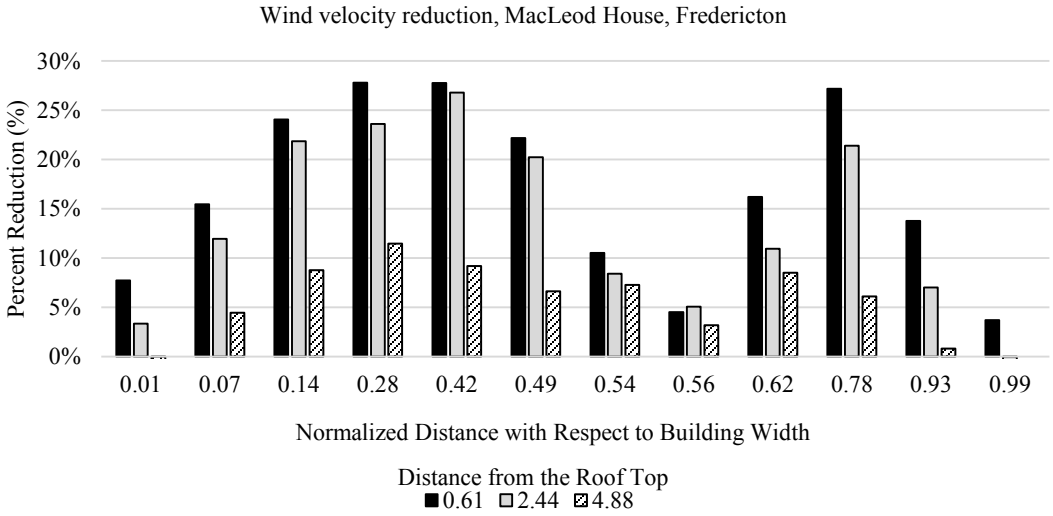


Figure 5.7 – Overhang effect on reduction of wind velocities on south-west façade of Fredericton building with respect to building width and distance from roof the top, Model scale: 1/200, standalone building, θ = 0°

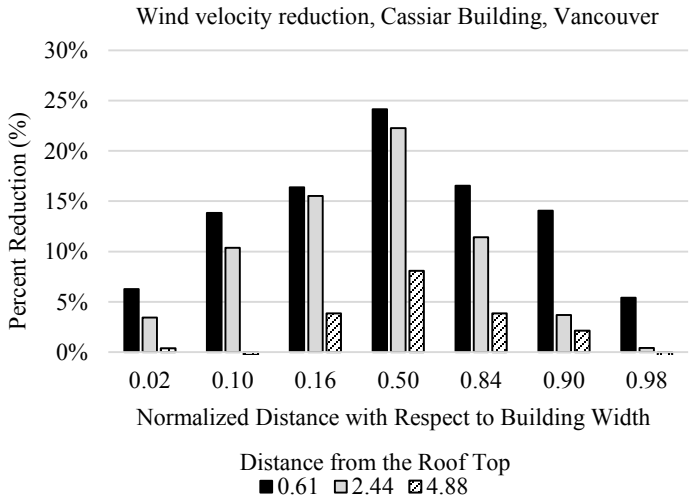


Figure 5.8 - Overhang effect on reduction of wind velocities on east façade of Vancouver building with respect to building width and distance from the roof top, Model scale: 1/200, standalone building with overhang, θ = 0°

Considering façades aspect ratios, BSL is 24.56 for left wing of the Fredericton building south-west façade, this amount is 22.83 for right wing and 24.7 for east façade of the Vancouver building. Close BSL of three tested facades, can be considered as the main reason of similar impact of overhang on reduction of wind velocities near the façade.

Also testing two scales of the Fredericton House model, 1/400 and 1/200, under the same conditions, provides an opportunity to study normalized wind velocity changes at the place of corresponding measurement points. The comparison shows that for most points, located on top half of the model, wind velocity is higher for larger model in comparison with similar points on the smaller model. The higher differences are observed on top and edges of the models and could be as large as 11%. However measured wind velocity for points which are closer to the ground are higher in 1/400 model. This could be as the result of higher wind turbulence in lower heights closer to the ground.

**Oblique wind direction**

To study the effect of overhang for oblique wind directions, the 1/200 model of Vancouver building is tested with and without overhang for wind direction 45°from the left. The normalized wind velocity near the façade is presented in APPENDIX C. The percent reduction of wind velocity contours indicates that the provided protection is within the range of 7% up to 14% for points with distance of 0.6 m from the roof top, as presented in Figure 5.9. The provided protection is extended up to quarter of building height and gradually reduces towards the leeward edge of the model.

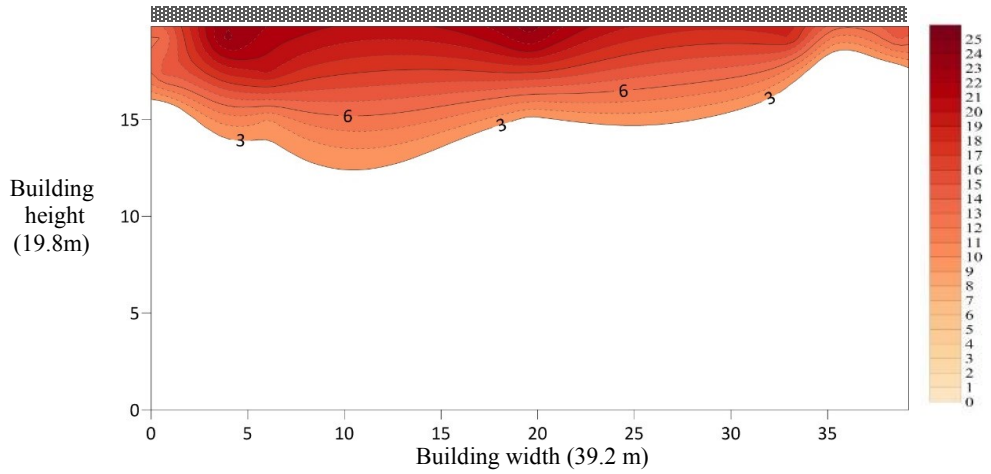


Figure 5.9 – Wind velocity reduction (%) on east façade of Cassiar Building, Model scale: 1/200, standalone, θ = 45° (from south-east)

In comparison with normal wind direction, adding overhang is less effective in reduction of wind velocity near the façade. Based on WDR field measurements and overhang effectiveness analysis more protection is provided for leeward areas, while wind tunnel experiment shows that adding overhang is less effective in reduction of wind velocity on leeward parts of the facade. Air flow and raindrops trajectory can be considered as the main contributing factors; however, this contrast should be investigated through more detailed wind tunnel or CFD simulation.

## 5.4. WDR on Fredericton Building

Geometrical analysis of both buildings has validated the similarity of these two buildings. Moreover, comparison of meteorological onsite data shows that rainfall intensity is almost similar in both sites. Given that there is a good agreement between the wind flow pattern around both buildings with or without overhang, based on the wind tunnel experiment, the correlation established on Vancouver building between overhang size and reduction of WDR can be applied to the Fredericton building.

As the majority of WDR gauges are installed on left wing of south-west façade and observations show that adding overhang has similar effect in reduction of wind velocity on both wings of south-west façade, the effect of adding different overhang sizes in reduction of received WDR is discussed.

First, the amount of received WDR is estimated on this part based on the field measurements. As it is shown in Figure 5.10, left wing of south-west façade of Fredericton is divided to 20 cells with WDR gauges at their center. The amount of WDR received by the wing façade is estimated by assigning the measured WDR at the location of gauge to the whole cell area. For cells without WDR gauge, the amount of received WDR is interpolated considering adjusted cells or considering similar value as the symmetrical cells on the other side of the façade. The total amount of WDR received by the façade wing is the sum of area-weighted WDR of each cell.

The amount of impinged WDR on the whole façade of left wing is calculated based on onsite measurements and ISO model considering weather station meteorological data. The amount of WDR received by the façade when being protected by roof overhang is estimated by applying (a) WDR reduction coefficient, Table 4.1, and (b) WDR reduction coefficient with respect to wind characteristics, Figure 4.15, as presented in chapter 4, on the primary calculated WDR amount. The

average of wind direction on south-west façade is 202° which makes a 10° angle with the normal of the façade. Also, the average of wind speed is 3.6 m/s converted to the weather station condition. As it can be observed in Table 5.1, there is a good agreement between both procedures in estimation of the amount of WDR received by the facade.

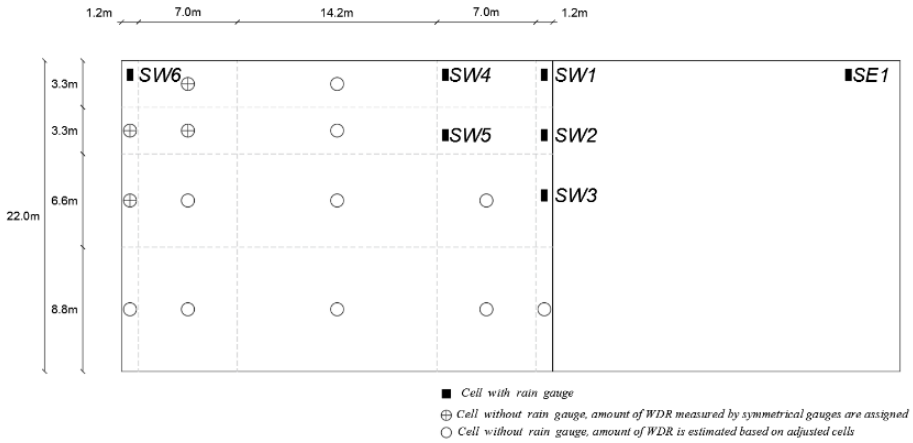


Figure 5.10 - Cells on the left wing of south-west façade of Fredericton Building for calculation of area-weighted WDR

Table 5.1– Amount of received WDR by the whole façade of left wing being protected by different overhang size for (a) overall OH reduction coefficient and (b) OH reduction coefficient with respect to wind characteristics.

(a) WDR Reduction Coefficient

**Based on all data**

| OH Size | Reduction Coefficient (%) | Measured WDR | ISO WDR |
|---|---|---|---|
| No OH | - | 149 | 178 |
| 0.3 m | 80 | 119 | 142 |
| 0.6 m | 60 | 89 | 107 |
| 0.9 m | 45 | 67 | 80 |
| 1.2 m | 35 | 52 | 62 |

(b) WDR Reduction Coefficient with respect to wind characteristics

**D: 10°, 2<U<4 m/s**

| OH Size | Reduction Coefficient (%) | Measured WDR | ISO WDR |
|---|---|---|---|
| No OH | - | 149 | 178 |
| 0.3 m | 85 | 127 | 151 |
| 0.6 m | 65 | 97 | 116 |
| 0.9 m | 45 | 67 | 80 |
| 1.2 m | 35 | 52 | 62 |

## 5.5. Summary and Conclusion

An accurate correlation between overhang width and WDR reduction coefficient has been established based on analysis of field measurements. This correlation may be applied to other mid-rise buildings with similar building geometry and wind flow characteristics. To test this hypothesis, wind tunnel measurements were carried out on Fredericton building to confirm the wind flow on windward façade.

The results of wind tunnel experiment on the east façade of Vancouver building and south-west facade of Fredericton building show the similarity of wind flow near mentioned façades for normal wind direction. This similarity observed for both situations with and without roof overhang can be attributed to similarity of facades geometrical characteristics.

Given the similarity of meteorological data for rain hours, for both study buildings, the WDR reduction coefficient for different overhang sizes can be applied on WDR estimation on Fredericton south-west façade. To have a more accurate estimation of WDR load proper WDR reduction coefficient can be chosen base on wind speed and wind direction. However, the possibility of application of presented WDR reduction coefficient for mid-rise buildings located in different climate conditions needs more investigations.

# 6. Accuracy of ISO Model

## 6.1. Introduction

WDR received by buildings' facades can be estimated by applying semi-empirical methods including ISO model 15927 (Bureau voor Normalisatie, 2009). The accuracy of ISO model has been investigated by Ge et al. three test buildings located in three Canadian cities, Fredericton, Montreal and Vancouver, have been monitored and high-resolution sets of WDR data has been collected. Previous studies show that estimation of WDR based on ISO standard is generally subjected to overestimation. The ISO prescribed wall factor was considered as the main contributing factor for the over-estimation. Applying wall factors calculated based on field measurements instead of ISO prescribed wall factor improves the results, however, a significant amount of discrepancy can still be observed between measured WDR and calculated wall indices. Further investigation of other influential factors is necessary.

The objective of this part of study is to identify major contributing factors to improve the accuracy of ISO model in estimating WDR on façade. The availability of high-resolution WDR field data collected in three Canadian cities over a long period of time makes a detailed analysis possible. The main parameters studied include 1) time resolution; in previous WDR analysis 5-minute data is converted to hourly wind and rain data for the calculations including wall factors and airfield WDR indices. WDR estimation using 5-minute data and hourly data is compared. 2) Difference in wind speed and wind direction between site and nearby weather station; Semi-empirical methods apply established correlation in wind engineering to convert wind speed measured at weather station to the specific site with assumed terrain and topography. This converted wind speed may differ from actual wind speed profile at site. In addition, the onsite wind direction is assumed to be the same as at the weather station, however, the terrain, local surroundings and obstacles may alter the wind direction on site. Given wind speed and wind direction are the main two parameters in calculating the WDR wall indices, the difference in wind characteristics between the weather station and site may contribute to the discrepancy. And 3) type of precipitation; ISO model is used to estimate amount of received WDR based on horizontal rainfall intensity. In onsite measurements, accumulated snow on horizontal rain gauge gradually melted and added to the amount of measured rainfall intensity. While, snow accumulation rarely

occurred on collection area of WDR gauges due to different trajectories of snow grains in comparison with rain drops. The effect of snow precipitation on the estimation of driven airfield indices and WDR analysis is investigated by comparison of the results based on all registered data with the data sets in which all registered data during snowy days have been removed.

## 6.2. Catch Ratio and Spatial Distribution of WDR

Meteorological data and the amount of impinged WDR on the windward facades of study buildings has been collected during sufficient period. Catch ratio values is calculated for the entire monitoring period with all approaching wind angles at rain gauge locations on windward façades. The results for south-east and south-west of Fredericton, east and north façade of Vancouver Building and north-east, south-east and west-east façade of Montreal, are presented in APPENDIX D. The catch ratio values are typically higher on the façade facing the prevailing WDR direction compared to other façades. The catch ratio values and hence the amounts of rain deposited on the building surface vary with locations. Over all study facades, catch ratios are higher at the top of the facade and decrease towards the bottom and the corners and edges receive higher amount of rain, which is consistent with the classical wetting pattern on building façades.

## 6.3. Accuracy ISO Standard Wall Factor

To investigate the accuracy of ISO standard and prescribed coefficients, the amount of WDR at the place of WDR gauges on buildings' façades are estimated using the ISO model (ISO, 2009) and are compared to measurements. Similar procedure applied in previous studies in calculation of catch ratio, wall index and wall factor (Ge et al. 2017) is followed considering additional sets of data. Hourly wind speed and wind direction data obtained from the nearby meteorological stations operated by Environment Canada for the monitoring period are used for the analysis. As hourly rainfall data for the monitoring period is not available at the meteorological station, hourly rainfall intensity measured onsite is used instead. Figure 6.1 shows the comparison between measured WDR and estimated WDR using ISO model with prescribed wall factors. As shown in Figure 6.1, in general estimation of WDR based on ISO method is subjected to overestimation for 80% of locations.

Considering results for the Fredericton Building (a), the ISO model underestimates the WDR amount for 9 monitored locations out of total of 13. For three remaining locations, the percent of difference is less than 5%. There is a better agreement between measured and estimated amount of WDR on south-west façade. The percent of discrepancies is higher for south-east façade and can be as high as 40% for locations with the distance of 4.9 m from the roof top. For Vancouver Building (b), the ISO model overestimates the WDR amount at 93% of the monitored locations (26 out of 28) and slightly underestimates for the remaining two locations. The overestimation can be as high as more than two times for locations typically at 2.4 m below the roofline. For the Montreal Building (c), the ISO model overestimates the WDR amount at 83% of the monitored locations (19 out of 23) and underestimates for the remaining four locations. The discrepancy between measurements and predictions is less than 10% for 6 locations, greater than 25% for 11 locations, and twice as high for the remaining 6 locations. The highest discrepancies are found at bottom locations on the north-east façade, which are located at 10.7 m and 21.3 m below the roofline.

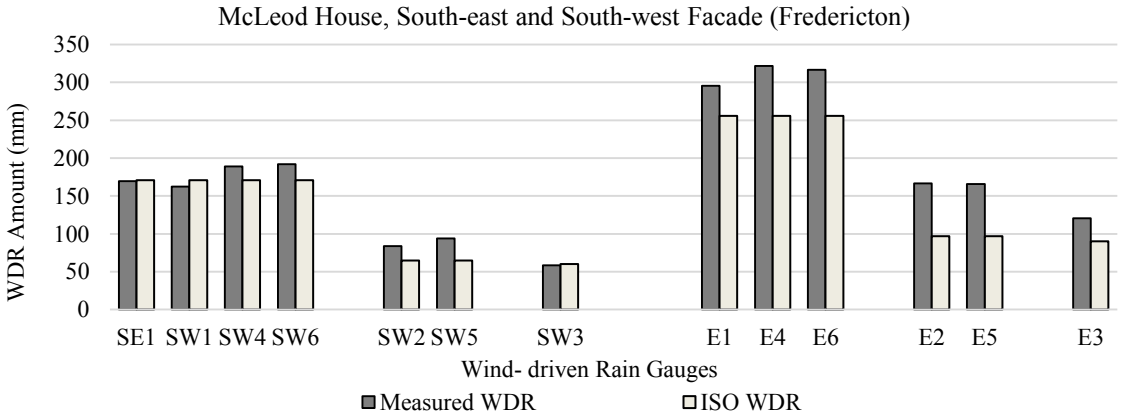


(a)

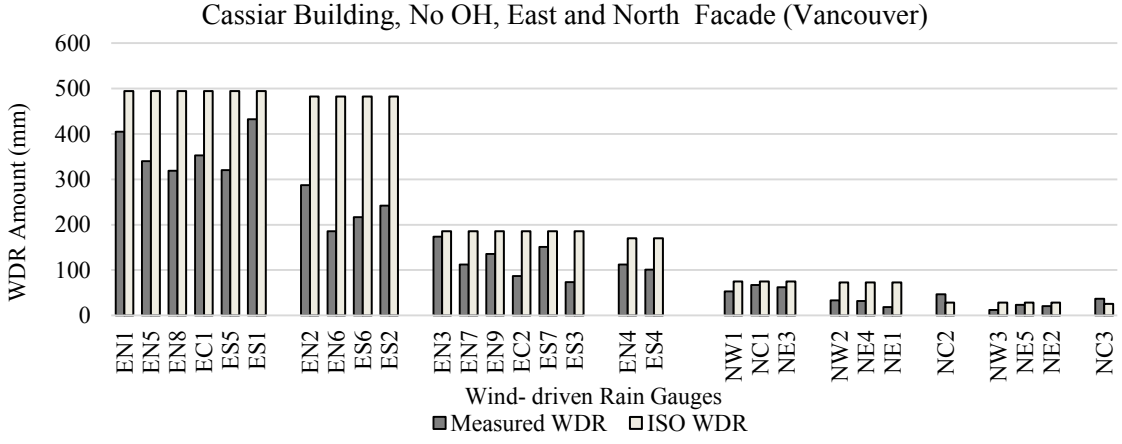


(b)

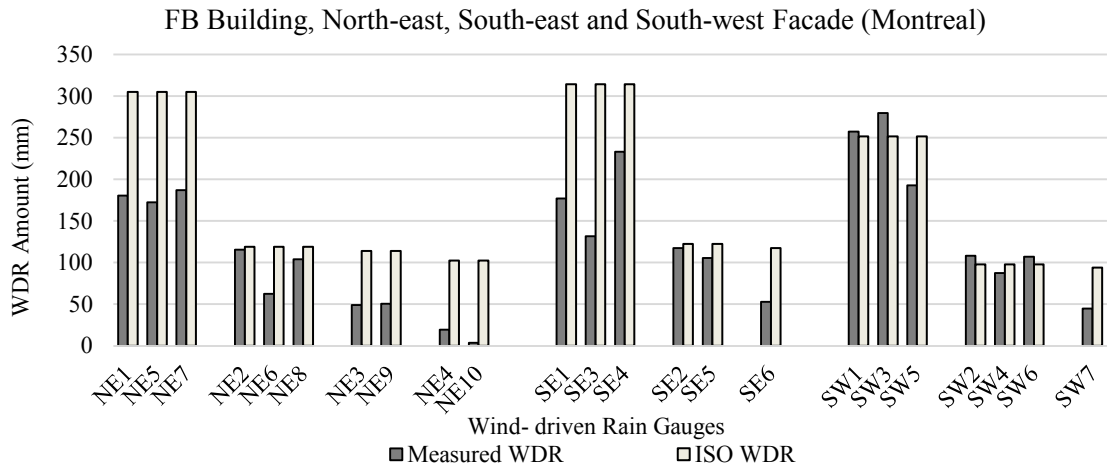


(c)

Figure 6.1– Comparison of measured WDR at the place of WDR gauges with ISO standard wall indices for all test buildings, (a) Vancouver, (b) Fredericton and (c) Montreal

## 6.4. Sources of Discrepancy

### 6.4.1. Wall Factor

Wall factor is a correction factor accounting for complex interaction between wind, rain and building geometry. Wall factor at the place of WDR gauges on the facades of interest is calculated considering measured amount of WDR divided by calculated airfield index. Measured wind speed, wind direction and rainfall intensity during study periods is used to estimate amount of airfield index at the height of measuring points. Figure 6.2-4, shows the comparison between the calculated wall factors in comparison with the wall factor prescribed by ISO for multi-storey buildings with flat roof. Wall factors calculated based on field measurements vary depending on its location on façade, decreasing from the top of the façade to the bottom and from the side to the center. However, there are only two values suggested by ISO, which are constant across the building façade.

Figure 6.2 shows the calculated wall factors on the south-west (a) and south-east (b) façade of Fredericton Building. Measured wall factors at the top and bottom row of the gauges (0.6 m and 4.9 from the roof top) are smaller than recommended wall factors, while there is a good agreement for the second row.

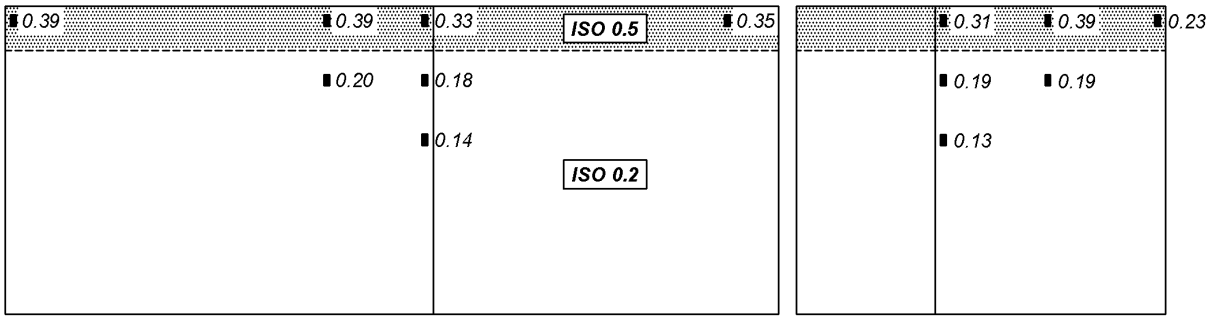


(a) (b)

Figure 6.2 - Calculated wall factors at the location of rain gauges on the (a) south-west and (b) south-east façade of McLeod House, Fredericton

Considering calculated wall factors for Vancouver building (Figure 6.3) for the period without overhang, symmetrical distribution of wall factor can be observed due to almost normal prevailing wind direction during rain hours. The highest wall factors encountered on the East facade are at the corner gauges ES1 and EN1, with values of 0.53 and 0.49, respectively; which is close to 0.5 suggested by ISO at these locations. In general, the ISO suggested wall factors are an overestimation across the East facade; although they provide a good estimation at the top corners and at the third row of gauges, except for the center area. The prevailing wind direction is inclined for north façade, which leads to unsymmetrical distribution of WDR across the façade. Calculated wall factors are higher in comparison with ISO, which results in an underestimation of WDR on the north façade estimated by ISO model.

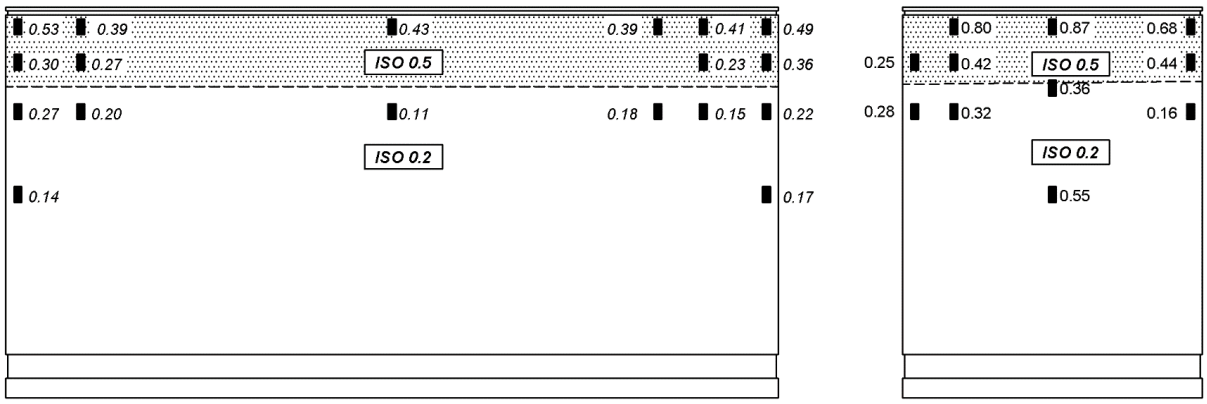


(a) (b)

Figure 6.3 - Calculated wall factors at the location of rain gauges on the (a) east and (b) north façade of Cassiar Building for the period of NO OH, Vancouver

For Montreal Building, although the calculated wall factors are slightly higher at corners, there is a good agreement between calculated and prescribed wall factor in the top row of the measurement points on the north-east façade, as shown in Figure 6.4 (a). The measured wall factor of the second row is higher than ISO suggested wall factor of 0.2 at this height. Measured wall factors on points with greater distance from the roof top have lower values in comparison with ISO and reduces to one third of ISO at the mid-height of the façade. The results for south-west façade is shown in Figure 6.4 (c). As it can be observed there is a good agreement between calculated and ISO prescribed wall factor for the points with distances greater than 4.9 m from the roof top, while there are significant underestimations for top rows of WDR gauges.

The wall indices at the measurement points are calculated using calculated wall factors instead of ISO prescribed values, while the other three correction factors used are the same. Figure 6.5 to Figure 6.7shows the comparison of wall indices calculated applying ISO-prescribed and calculated hourly wall factors with measured WDR. It can be observed that the results are not consistent, the application of calculated wall factors improves the estimations on 65% of measuring points (42 points out of 65), while increases the discrepancy for the rest of locations.

For the south-east façade of Fredericton building, applying calculated wall factors reduces the discrepancy, however the calculated amount is overestimated in comparison with measured amount. The inverse trend can be observed for the south-west façade. The application of calculated wall factors increases the discrepancy specifically for points at a distance of 0.6 m from the roof top. For Vancouver Building, the discrepancy on east façade is reduced to 20%, while the use of calculated wall factors increases the discrepancy at most locations on north façade. The effect of applying calculated wall factor for Montreal building is not consistent. For the north-east and south-east façade, the use of calculated wall factors leads to an overestimation of WDR by about 80%, while this amount is around 14% for the south-west façade.

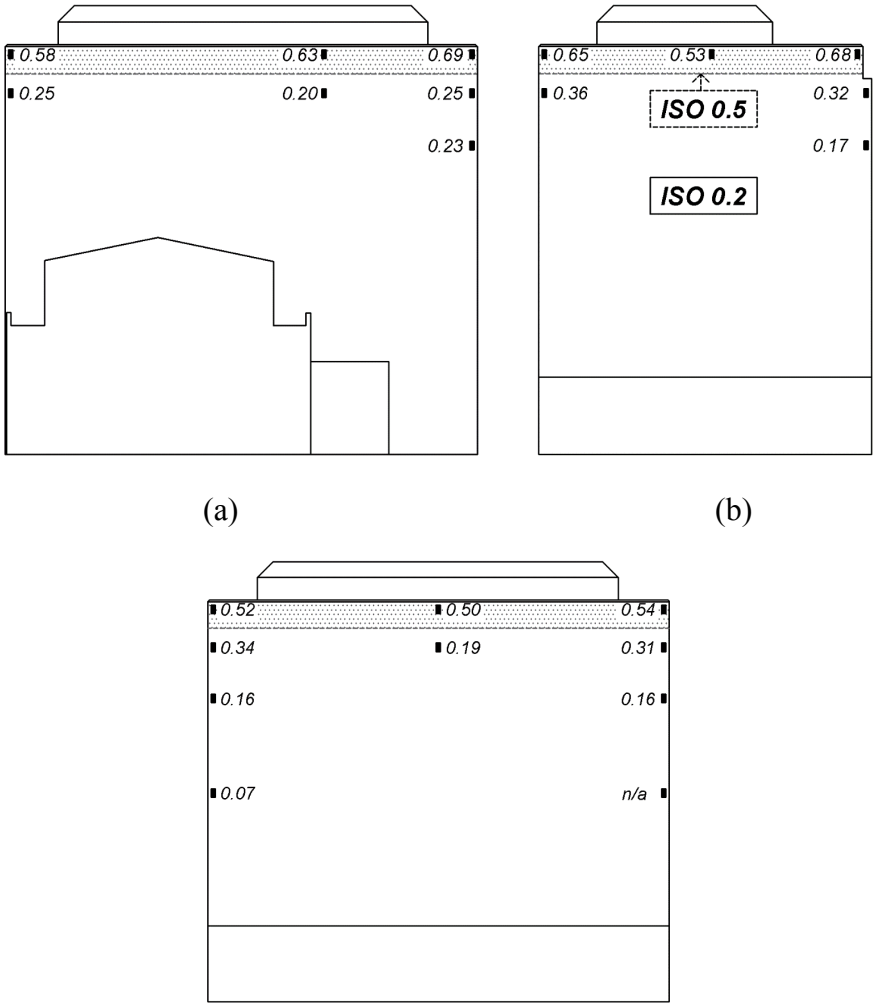


Figure 6.4 - Calculated wall factors at the location of rain gauges on the (a) north-east, (b) south-east and (c) south-west façade of FB Building, Montreal

#### 6.4.1.1. Time Resolution

The wind, rain and WDR measurements were taken at 5-minute intervals. In the calculation using ISO model, 5-minute data is converted to hourly data for the calculation of wall factors and WDR indices. To investigate the effect of time resolution in calculation of wall factor, measured 5-min data is used in the estimation of airfield index and wall factor at the location of WDR gauges. Applying 5-min data leads to greater amount of airfield index at the measuring heights and consequently lower wall factors. The calculated values of wall factors and related wall indices using 5-minute data and hourly data is presented in APPENDIX D.

Figure 6.5-7, also shows the comparison between measured amount of WDR and wall indices calculated applying ISO prescribed wall factor, calculated hourly and calculated 5-min wall factors. Applying wall factors calculated based on 5-minute data leads to more accurate estimation of WDR in most cases. The comparison of hourly and 5-min results shows that for Vancouver building the rate of discrepancy is reduced from 20% to 1% for the east façade and from 93% to 1% for the north façade, respectively.

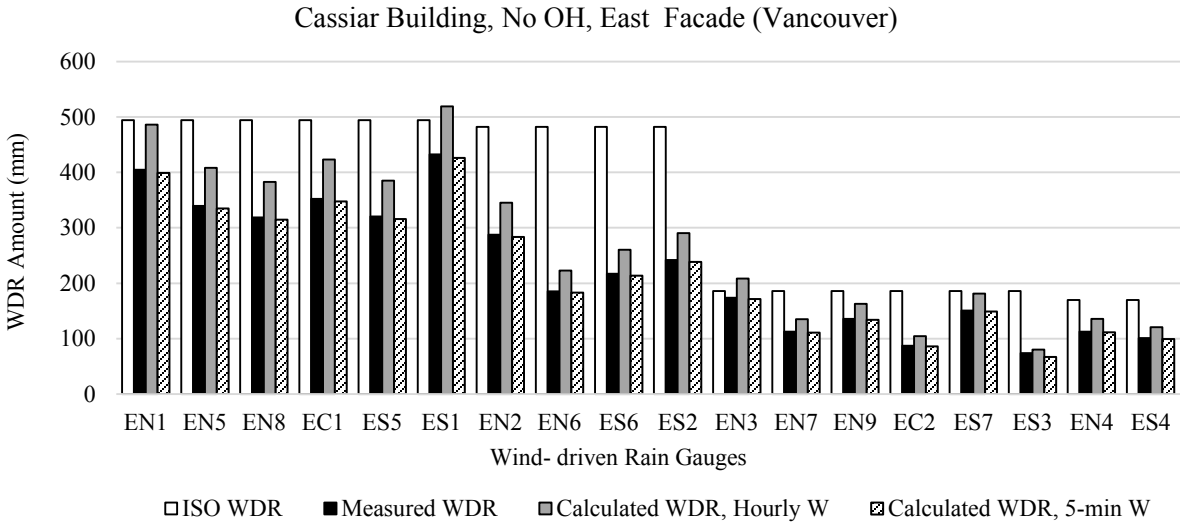


(a)

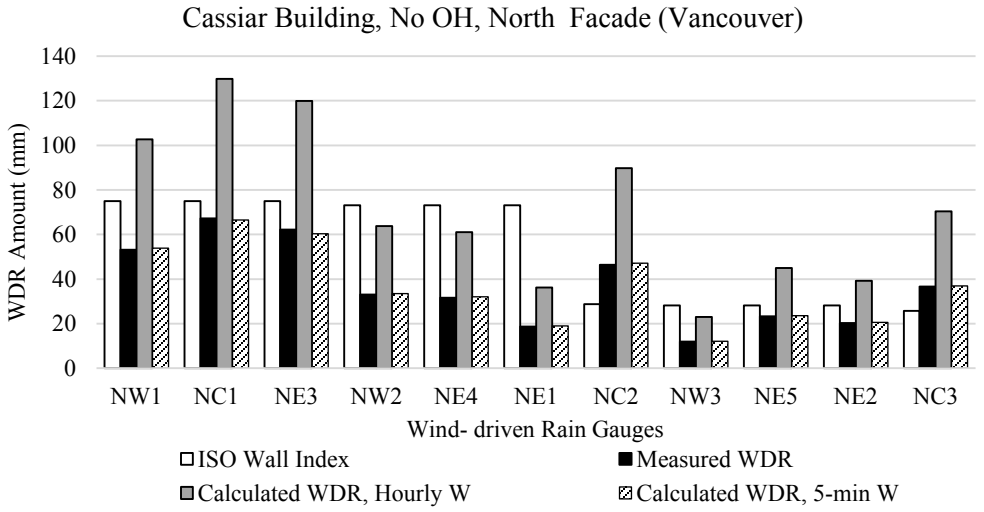


(b)

Figure 6.5 - Comparison of measured WDR with estimated WDR using ISO prescribed W, and wall factors calculated based on 5-minute and hourly data: (a) east façade and (b) north façade, Cassiar Building, No OH period, Vancouver

As shown in Figure 6.6, the application of wall factors calculated based on 5-minute data reduces the discrepancy between measurements and estimation for north-east and south-east of the Montreal Building by 52 % and 36% respectively. For the south-west façade, applying 5-min wall factor will cause underestimation of WDR and the average percent of discrepancy changes from -14% to 15%.

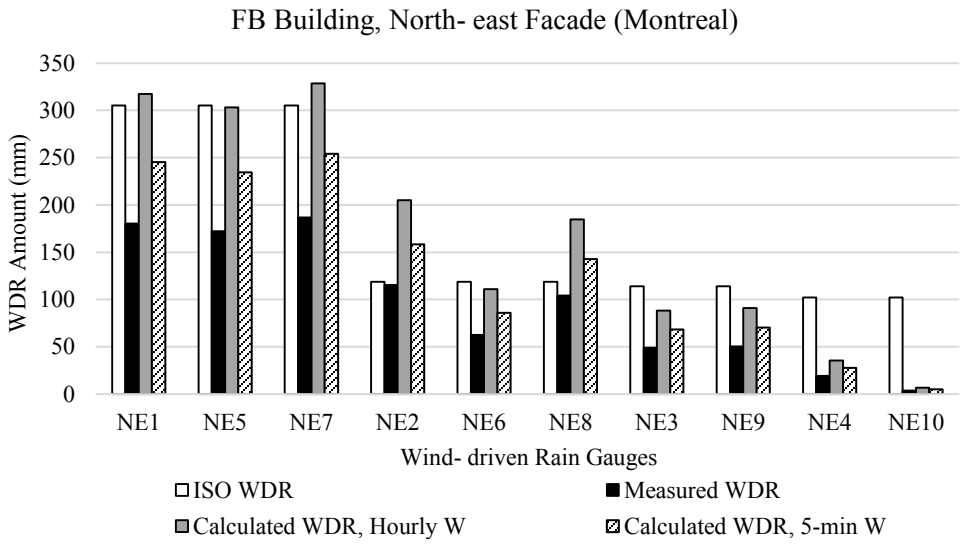


(a)

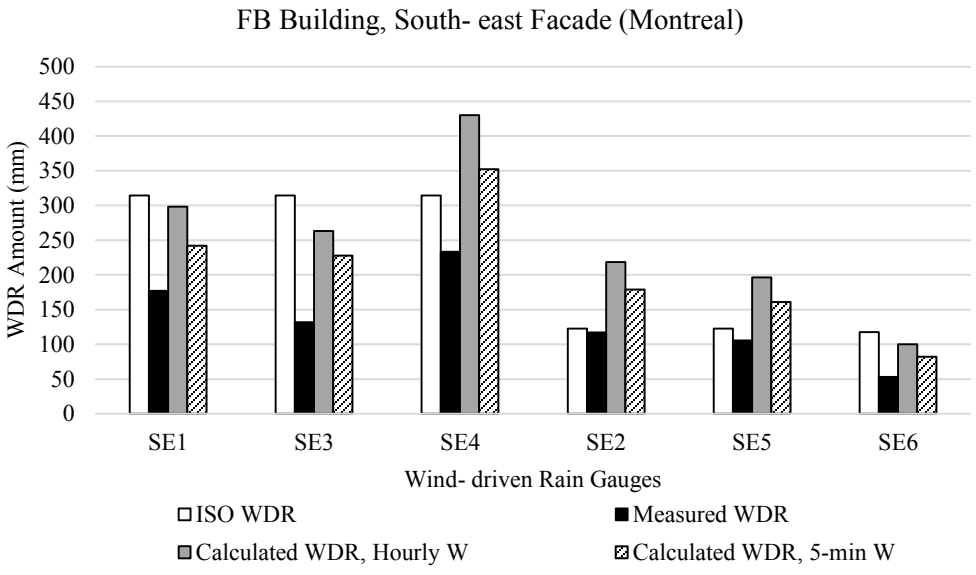


(b)

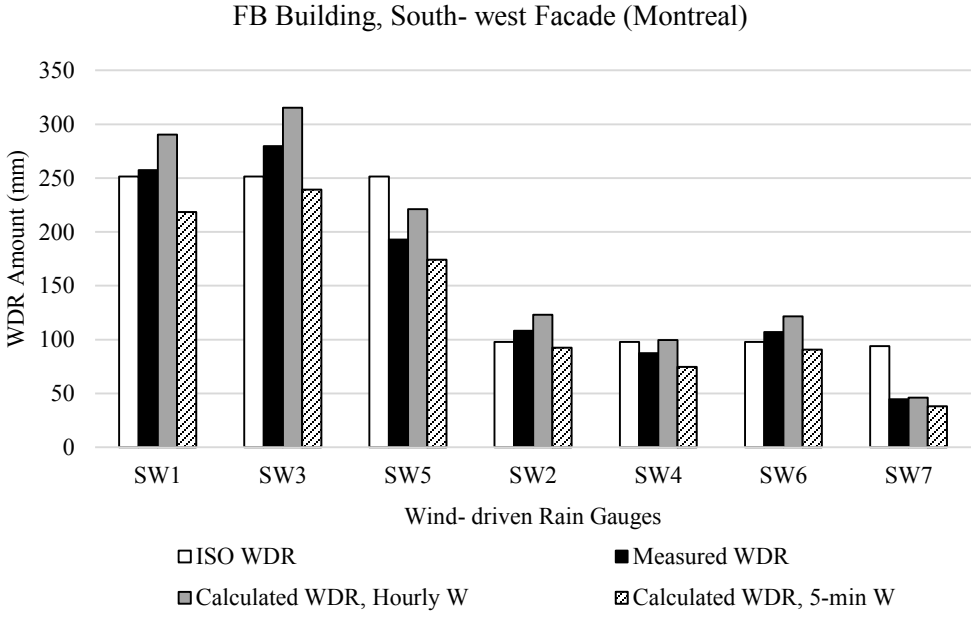


(c)

Figure 6.6 - Comparison of measured WDR with estimated WDR using ISO prescribed W and wall factors calculated based on 5-minute and hourly data, (a) north-east façade , (b) south- east façade and south-west façade FB Building, Montreal

For the Fredericton building, the use of wall factors calculated based on 5-minute data results in the increase in discrepancy between measurements and estimation for south-west façade from 30% to 43%, while decrease in discrepancy for the south-east from 12% to 7%.

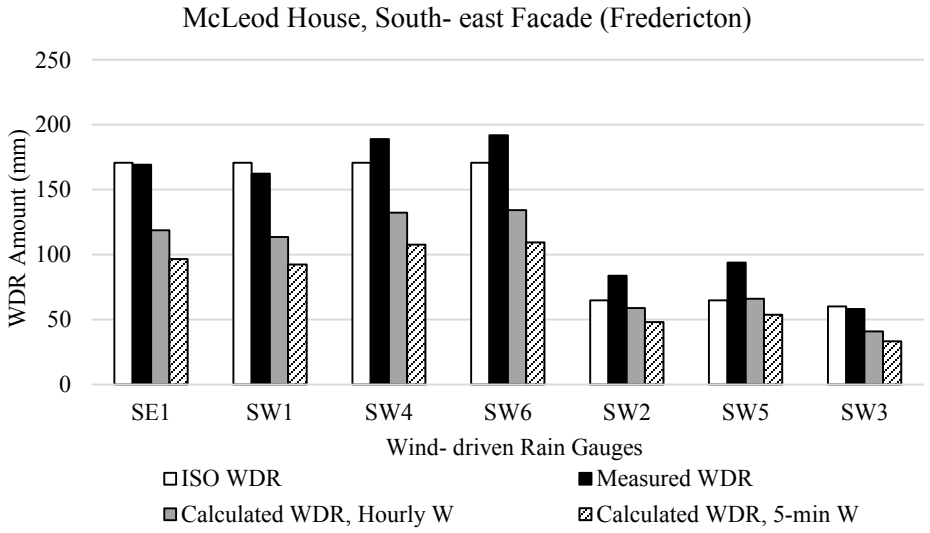


(a)

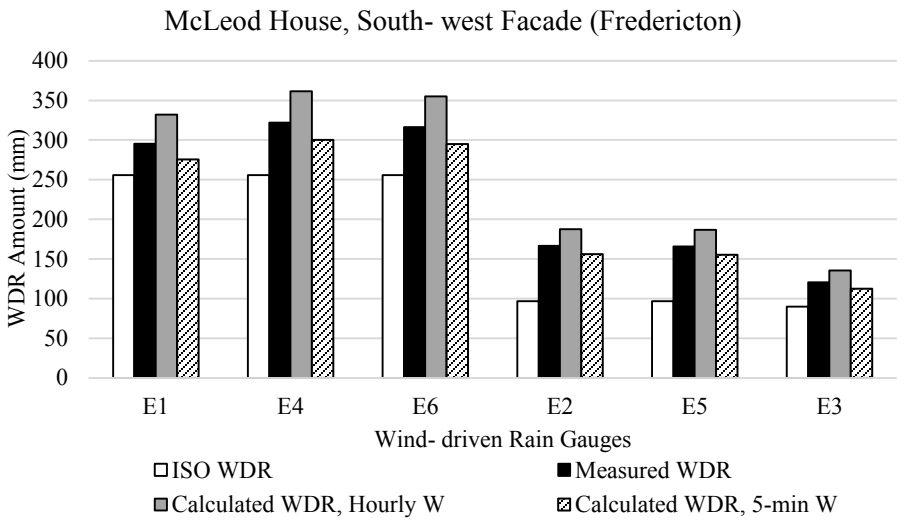


(b)

Figure 6.7 - Comparison of measured WDR with estimated WDR using ISO prescribed W and wall factorscalculated based on 5-minute and hourly data(a) south- west façade and (b) south- west façade, McLeod House, Fredericton

The parameter contributing to the difference in wall factors calculated based on the 5-minute and hourly data is mainly the rainfall intensity. In calculation of airfield index using hourly data, the sum of measured 5-min rainfall data over an hour, hourly average of wind speed and wind direction is used. In the ISO model, hourly rainfall intensity has an exponent of 8⁄9, which contributes to the difference in wall indices calculated using 5-minute data and hourly data. As illustrated below, assuming one hour of data, the following two equations results in different values and equation (6.2) gives a greater amount.

$$\text{Hourly Data: } (a + b + c + \cdots + z)^{8/9} \tag{6.1}$$

$$\text{5-min Data: } (a^{8/9}) + (b^{8/9}) + (c^{8/9}) + \cdots + (z^{8/9}) \tag{6.2}$$

The amount of difference depends on the number of registered data within an hour and their values. Higher rainfall intensity or more number of registered data during one hour result in greater discrepancy in calculated airfield index. Figure 6.8 shows the comparison of calculated airfield index for one rainy day for Vancouver building at all four measurement heights. In general, 5-minute data results in higher airfield indices, therefore, smaller wall factors compared to hourly data.

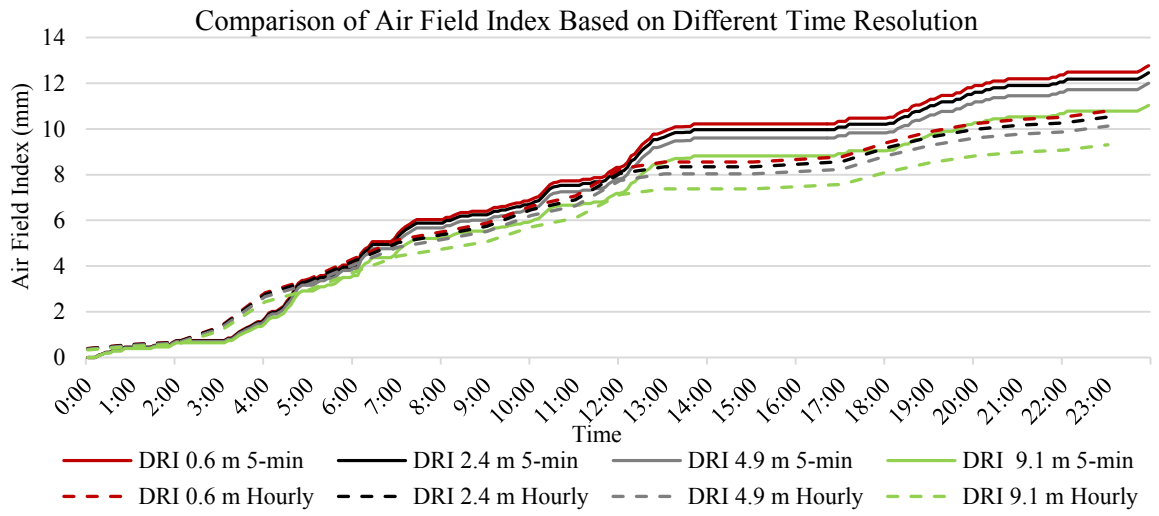


Figure 6.8 – Comparison of accumulated wall indices at the height of WDR gauges using 5-minute data and hourly average for a single rainy day, October 28th 2014, Cassiar Building, Vancouver

### 6.4.1.2. Data Conversion (5-min to hourly data)

Conversion of 5-min measured data to hourly data by applying arithmetic averaging can also influence the results. Frequency distribution, mean value and standard deviation of wind speed and wind direction is studied for all three test buildings with respect to time resolution. Considering all registered data during the study period of each test building, the results shows a very slight difference between 5-minute data and hourly average in these statistics, which cannot lead to the significant discrepancy in WDR analysis. The results analyzed for Vancouver Building during the period without overhang is shown in APPENDIX D. As an example, Figure 6.9 shows the comparison between 5-minute and hourly average data for one random rainy week (a), i.e. the last week of October 2014 and one rainy day (b), i.e. 28th October 2014.

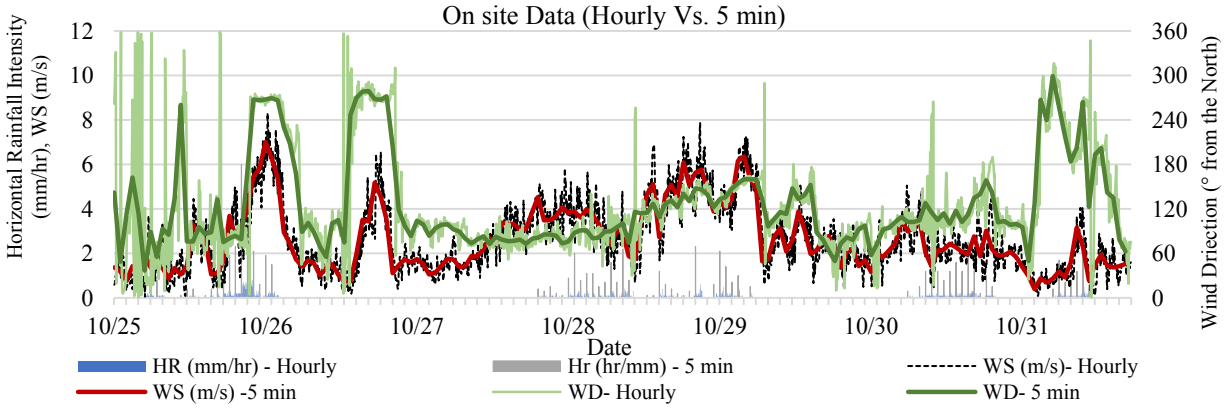


(a)

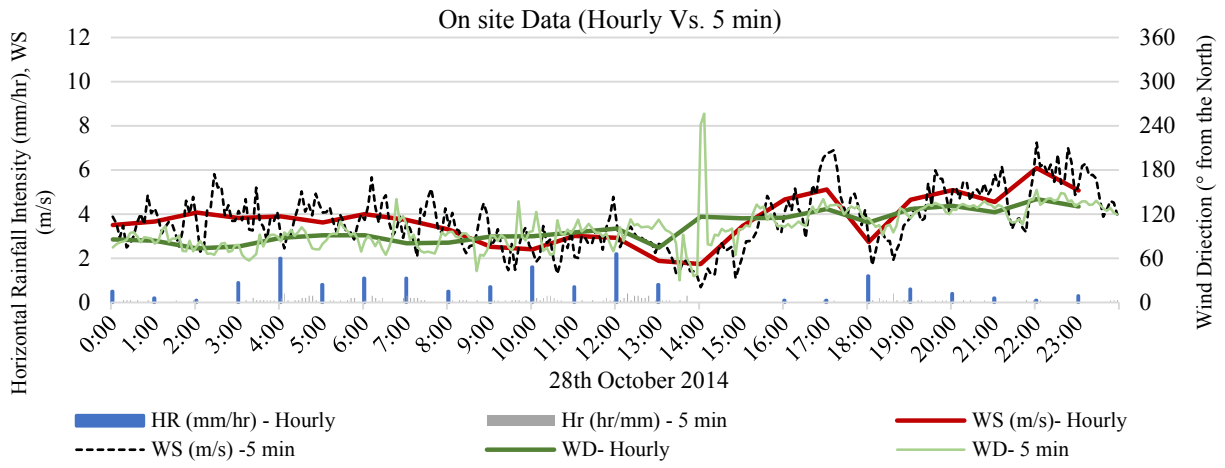


(b)

Figure 6.9 - Comparison of wind speed, wind direction and rainfall intensity for a studied period of one week (a) and one day (b) based on 5-minute-interval data and hourly data, October 2014, Cassiar Building Vancouver

In general, there is a good agreement between hourly and 5-min results, the main differences can be observed for the times when wind direction experiences sudden changes. These sudden changes are eliminated in the hourly data as the result of averaging.

In the ISO equation, the effect of wind direction is defined as the term of cosine of wind incident angle. Figure 6.10 shows the comparison of values of $\cos(D-\Theta)$ calculated based on 5-minute data and hourly average.

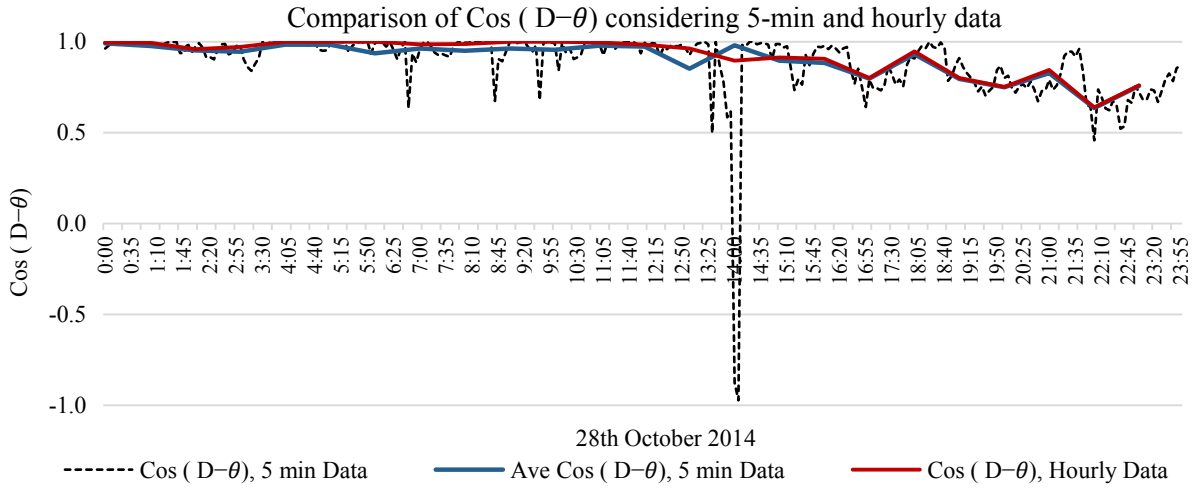


Figure 6.10 - Comparison of Cosine equation using registered 5-minute-interval data and the hourly average data, October 28th 2014, Cassiar Building, Vancouver

The other comparison can be made between cosines terms calculated based on hourly data with the average of 5-min cosine term during each hour. These two plots are almost the same. The slight difference between the plots based on 5-minute data and hourly average could be considered as the result of wind direction changes, which are not captured by hourly average. High deviation in wind direction cause more differences between these two plots.

To evaluate the effect of averaging wind speed and wind direction, airfield index is calculated based on two time-resolution with an assumption of Rh exponent as 1.0 to eliminate its effect. Therefore, the remaining difference could be considered as the result of converting 5-minute wind speed and direction data to the hourly data. Table 6.1, shows the results for all facades of study buildings. Considering percentage of discrepancies and prevailing wind directions approaching towards each façade, it can be concluded that facades with inclined prevailing wind directions are more sensitive to the applied time resolution. The difference listed in Table 6.1 is calculated using 5-min results as the reference.

Table 6.1- Comparison of airfield indices at the place of anemometer of each test building for windward façade, considering different time resolution and Rh power

| *Test Building* | *Façade Orientation* | *Air Field Index(mm), Rh Power 8/9* | | | *Air Field Index(mm), Rh Power 1* | | |
|---|---|---|---|---|---|---|---|
| | | 5-min Data | Hourly Data | Difference (%) | 5-min Data | Hourly Data | Difference (%) |
| Cassiar Building, Vancouver | East | 1091 | 895 | 18% | 927 | 964 | -4% |
| | North | 161 | 84 | 48% | 137 | 90 | 34% |
| McLeod House, Fredericton | South- east | 579 | 481 | 17% | 529 | 555 | -5% |
| | South- west | 632 | 514 | 19% | 578 | 583 | -1% |
| FB Building, Montreal | North- east | 480 | 371 | 23% | 415 | 401 | 3% |
| | South- east | 445 | 364 | 18% | 383 | 401 | -5% |
| | South- west | 594 | 526 | 11% | 477 | 512 | -7% |

### 6.4.1.3. Data Averaging

In WDR studies two approaches can be applied to obtain hourly data from 5-min data including arithmetic-averaging and weighted averaging. As the data is registered with high resolution over the time, in general there is a good agreement between hourly data calculated applying arithmetic averaging in comparison with weighted averages. Both procedures have been applied for calculation of hourly wind speed considering sufficient period of time. As shown in Figure 6.11,

the averaging techniques do not result in any significant difference in the hourly averaged wind speed. The same for wind direction.

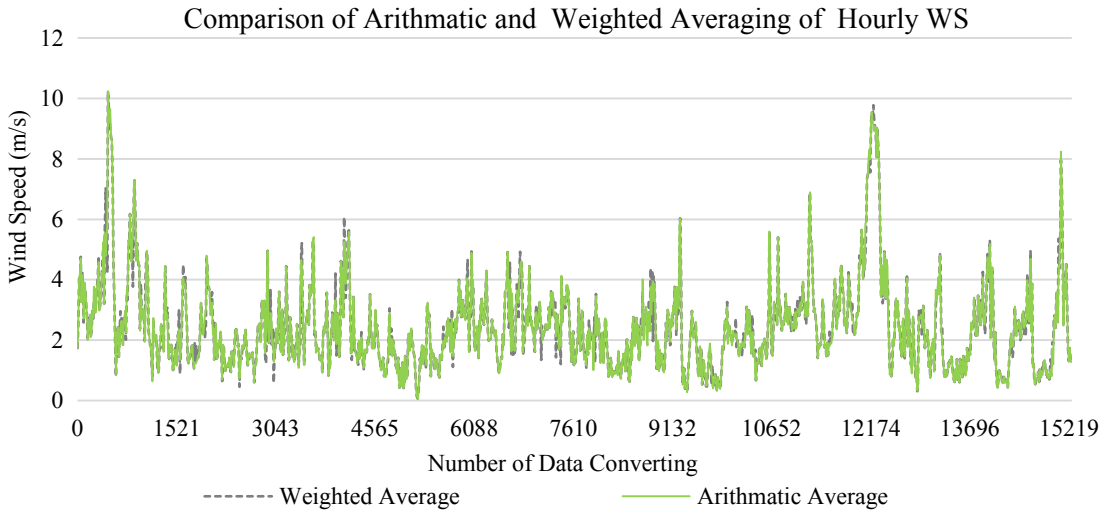


Figure 6.11 – Comparison of arithmetic and weighted method in calculation of wind speed based on measured 5-minute onsite data, October 13th 2016 – December 4th 2016, Cassiar Building, Vancouver

## 6.5. Improvement of Hourly Assessments

Estimation of wall index based on ISO model involves the airfield driven rain index and correction factors. Given that the calculated wall factors are based on site measurements the influence of local topography and obstruction factor has been taken into account. The terrain category and applied roughness coefficient has been verified through field measurements as discussed in the Chapter 3. As the result, the remaining discrepancy most likely comes from the difference in wind and rain data between the site and the weather station. Similar rainfall intensity is used in the calculation of airfield index, so the remaining discrepancy can be attributed to the difference in wind speed and wind direction between site and weather station.

In general, wind speed and direction measured onsite agree well with the meteorological data reported by nearby Environment Canada weather station for the same period, however slight differences can be observed. The contributing factors can be divided into two major categories. First, local topography and obstructions. This is investigated through detailed comparison of data registered onsite with reported data by the weather station. The comparison of onsite and weather station wind direction frequency for each facade is presented in APPENDIX D. Second, the effect

of obstacles near onsite weather station on the wind speed and wind direction measurements, which is studied through wind tunnel measurements.

### 6.5.1. Local Wind Speed Conversion

The assumption of a constant mean wind speed exponent in the power law correlation converting wind speed from the airport to the building site is valid for stable atmospheric condition, while it is highly influenced by atmospheric stability, wind speed and land features (Gualtieri & Secci, 2011).

Comparison between measured and converted wind speed is carried out for three study sites with respect to prevailing wind directions. Wind speed reported by nearby station is converted to the site situation considering height and terrain features. In general, the converted wind speed at anemometer height is higher than the measured values. A wind speed correction factor, for each façade orientation, is defined based on the average of wind speed discrepancies over the monitoring period. Only rain hours during which wind approaches towards the façade is considered in the calculation of correction factors, which are listed in Table 6.2. To compensate the existing difference, the estimated correction factor is applied to the airport wind speed for the calculation of airfield driving rain index.

As shown in Table 6.4-5, this adjustment improves the estimation of impinged WDR on measuring point for all facades except the south-west façade of Fredericton building.

Table 6.2 – Wind speed correction factors from site to weather station for test buildings

| Test Building | Windward Facade | WS Correction Factor |
|---|---|---|
| Cassiar building, Vancouver | East | 0.81 |
| | North | 0.72 |
| McLeod House, Fredericton | South-east | 0.91 |
| | South- West | 0.94 |
| FB Building, Montreal | North-east | 0.94 |
| | South-east | 0.91 |
| | South- West | 0.92 |

The discrepancy is reduced from 21% to 2% and from 93% to about 40% for east and north façade of Vancouver. The improvement is from 12% to 2% for the south-east façade of Fredericton.

Considering Montreal Building, the discrepancy decreases from 80% to 54% for the north-east facade, from 14% to 2% for the south-east façade, and from 85% to 63% for the south-west façade, respectively. The reported errors are the average of discrepancy for all rain gauges on each façade.

### 6.5.2. Local Wind Direction Change

In the calculation of airfield driven rain index for specific façade orientation, only the data during which the wind is approaching to the façade is considered. Since the analysis is conducted based on two sets of data, onsite and weather station data, it is important to eliminate the wind direction that are not consistent in both sets.

In some instances, the airport data shows that wind is approaching the study façade, while onsite data shows that the actual wind is not approaching that façade, as shown in Figure 6.12. This will result in the overestimation of driving rain on the building façade based on the airport wind direction. These data should be eliminated from weather station defined data set.

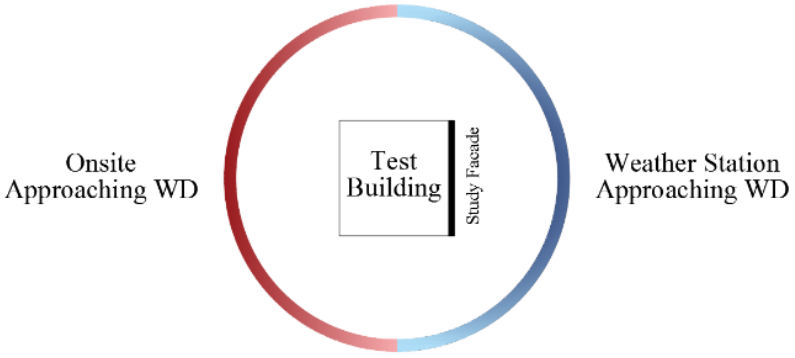


Figure 6.12 – Wind direction discrepancy based on onsite and weather station data.

Therefore, to eliminate the error from the difference in wind direction between airport and site, the measured data was filtered to include only the period during which the wind approaches the façade and this period is applied to filter airport data as well. As shown in Table 6.4-5, the discrepancy is reduced in most cases. The difference is almost eliminated for north facade of Vancouver and south-east façade of Fredericton. The result for other facades shows improvement between a 2% for the east façade of Vancouver building up to 14% for the north-east façade of Montreal building. No improvement observed for the south-west façade of Fredericton.

Considering Montreal and Vancouver analysis, the comparison of wind direction standard deviation for onsite data and weather station data, indicates that wind direction modification is

mainly effective for higher differences between calculated standard deviations. However, for Fredericton building calculated standard deviation is almost similar for both data sets of each façade.

Table 6.3 – The comparison of wind direction standard deviation for different wind direction based on onsite and weather station data

| Building | Facade | Onsite | Weather Station |
|---|---|---|---|
| Cassiar building (Vancouver) | East | 30 | 34 |
| | North | 60 | 80 |
| FB Building (Montreal) | North-east | 76 | 109 |
| | South-east | 56 | 56 |
| | South-west | 45 | 51 |
| McLeod House (Fredericton) | South-east | 57 | 56 |
| | South-west | 48 | 47 |

### 6.5.3. Combined Local Modified Wind Speed and Direction

The combination of these two adjustments will improve accuracy of WDR estimation impinged on the façade based on hourly data and reduce the discrepancy with measured amount of WDR. Table 6.4-5 shows the hourly results based on the adjustment of wind speed and wind direction in comparison with results based on 5-min measured data. The errors listed in the tables for each category; measured WDR is used as the reference. The discrepancy for Vancouver building is reduced from -21% to 4% with modification of hourly data, this amount is 1% based on 5-minute data, for east façade. However, for north façade there is a significant difference between modified hourly (28%) and 5-min data (1%) estimation. For Fredericton south-east façade both approaches lead to the same results equal to 7% difference, while for the south-west façade the best result can be obtained based on 5-min wall factor. For Montreal building south-east and north-east façade, 5-minute data leads to a better estimation of WDR with discrepancy of -38% and -58%, while these amounts are -54% and -64% based on hourly modified data respectively. For the south-west façade applying hourly modified data almost eliminates the discrepancy between estimated and measured WDR, while 5-minute data leads to 15% of difference. The comparison between measured WDR with the amount calculated based on hourly, modified hourly and 5-min data is presented in Table 6.4 -Table 6.6; the graphical presentation is provided in APPENDIX D for all three test buildings.

Other possible sources of discrepancy include: (a) averaging wind speed correction factor, (b) wind direction and frequency discrepancy between onsite and weather station considering same set of data; although general agreement can be observed, (c) simplification of cosine projection for the incident wind angle and (d) the constant value of WDR coefficient of 2/9 used in ISO equation can be mentioned as other possible sources of discrepancy.

Cassiar Building, Vancouver

Table 6.4 - Comparison between measured WDR and calculated WDR on the (a) East façade and (b) North facade with wind speed and wind direction corrections and wall factors calculated using 5-min measured data, Cassiar building, Vancouver

**(a) East Facade**

| Site Data | | | Calculated Wall Index (mm), Hourly *W* | | | | | | | | Calculated wall index (mm), 5-min *W* | | |
|---|---|---|---|---|---|---|---|---|---|---|---|---|---|
| WDR Gauges | Measured WDR (mm) | Calculated Wall factor (Hourly) | ISO-Calculated wall factor | Error | WD correction | Error | WS Correction | Error | Combined WD and WS correction | Error | Calculated Wall factor (5 min) | ISO, Calculated wall factor | Error |
| EN1 | 402 | 0.492 | 486 | -21% | 478 | -19% | 394 | 2% | 388 | 4% | 0.404 | 399 | 1% |
| EN5 | 338 | 0.413 | 408 | -21% | 401 | -19% | 331 | 2% | 325 | 4% | 0.339 | 335 | 1% |
| EN8 | 317 | 0.387 | 383 | -21% | 377 | -19% | 310 | 2% | 305 | 4% | 0.318 | 314 | 1% |
| EC1 | 350 | 0.428 | 423 | -21% | 416 | -19% | 343 | 2% | 337 | 4% | 0.351 | 347 | 1% |
| ES5 | 319 | 0.389 | 385 | -21% | 379 | -19% | 312 | 2% | 307 | 4% | 0.320 | 316 | 1% |
| ES1 | 430 | 0.525 | 520 | -21% | 511 | -19% | 421 | 2% | 414 | 4% | 0.431 | 426 | 1% |
| EN2 | 285 | 0.358 | 345 | -21% | 340 | -19% | 280 | 2% | 275 | 4% | 0.294 | 284 | 1% |
| EN6 | 184 | 0.231 | 223 | -21% | 219 | -19% | 180 | 2% | 178 | 4% | 0.189 | 183 | 1% |
| ES6 | 216 | 0.270 | 261 | -21% | 256 | -19% | 211 | 2% | 208 | 4% | 0.222 | 214 | 1% |
| ES2 | 240 | 0.301 | 291 | -21% | 286 | -19% | 235 | 2% | 232 | 4% | 0.247 | 239 | 1% |
| EN3 | 172 | 0.225 | 209 | -21% | 205 | -19% | 169 | 2% | 166 | 4% | 0.184 | 171 | 1% |
| EN7 | 112 | 0.145 | 135 | -21% | 133 | -19% | 109 | 2% | 108 | 4% | 0.119 | 111 | 1% |
| EN9 | 135 | 0.175 | 163 | -21% | 160 | -19% | 132 | 2% | 130 | 4% | 0.144 | 134 | 1% |
| EC2 | 86 | 0.112 | 104 | -21% | 103 | -19% | 85 | 2% | 83 | 4% | 0.092 | 86 | 1% |
| ES7 | 150 | 0.195 | 181 | -21% | 178 | -19% | 147 | 2% | 145 | 4% | 0.160 | 149 | 1% |
| ES3 | 73 | 0.269 | 80 | -9% | 78 | -6% | 65 | 12% | 63 | 14% | 0.225 | 67 | 9% |
| EN4 | 112 | 0.171 | 136 | -22% | 134 | -20% | 110 | 1% | 108 | 3% | 0.140 | 112 | 0% |
| ES4 | 100 | 0.142 | 121 | -20% | 119 | -18% | 98 | 3% | 96 | 4% | 0.117 | 99 | 1% |
| Weather Station Airfield Index (mm) | | | 1081 | | 1063 | | 875 | | 861 | | | 1081 | |

(b) North Façade

| Site Data | | | Calculated Wall Index (mm), Hourly *W* | | | | | | | | Calculated wall index (mm), 5-min *W* | | |
|---|---|---|---|---|---|---|---|---|---|---|---|---|---|
| WDR Gauges | Measured WDR (mm) | Calculated Wall factor (Hourly) | ISO-Calculated wall factor | Error | WD correction | Error | WS Correction | Error | Combined WD and WS correction | Error | Calculated Wall factor (5 min) | ISO, Calculated wall factor | Error |
| NW1 | 53 | 0.685 | 103 | -93% | 53 | 0% | 74 | -39% | 38 | 28% | 0.359 | 54 | -1% |
| NC1 | 67 | 0.866 | 130 | -93% | 68 | 0% | 94 | -39% | 49 | 28% | 0.455 | 67 | 1% |
| NE3 | 62 | 0.800 | 120 | -93% | 62 | 0% | 86 | -39% | 45 | 28% | 0.420 | 60 | 3% |
| NW2 | 33 | 0.436 | 64 | -93% | 33 | 0% | 46 | -39% | 24 | 28% | 0.229 | 33 | -1% |
| NE4 | 32 | 0.417 | 61 | -93% | 32 | 0% | 44 | -39% | 23 | 28% | 0.219 | 32 | -1% |
| NE1 | 19 | 0.248 | 36 | -93% | 19 | 0% | 26 | -39% | 14 | 28% | 0.130 | 19 | -1% |
| NC2 | 46 | 0.625 | 90 | -93% | 47 | 0% | 65 | -39% | 34 | 28% | 0.328 | 47 | -1% |
| NW3 | 12 | 0.164 | 23 | -93% | 12 | 0% | 17 | -39% | 9 | 28% | 0.086 | 12 | -1% |
| NE5 | 23 | 0.320 | 45 | -93% | 23 | 0% | 32 | -39% | 17 | 28% | 0.168 | 24 | -1% |
| NE2 | 20 | 0.278 | 39 | -93% | 20 | 0% | 28 | -39% | 15 | 28% | 0.146 | 21 | -1% |
| NC3 | 37 | 0.546 | 70 | -92% | 37 | 0% | 51 | -38% | 26 | 28% | 0.287 | 37 | -1% |
| Weather Station Airfield Index (mm) | | | 164 | | 85 | | 118 | | 61 | | | 164 | |

Fredericton

Table 6.5- Comparison between measured WDR and calculated WDR on the (a) South-west and (b) South-east façade with wind speed and wind direction corrections and wall factors calculated using 5-min measured data, McLeod house, Fredericton

(a) South- west Façade

| Site Data | | | Calculated Wall Index (mm), Hourly *W* | | | | | | | | Calculated wall index (mm), 5-min *W* | | |
|---|---|---|---|---|---|---|---|---|---|---|---|---|---|
| WDR Gauges | Measured WDR (mm) | Calculated Wall factor (Hourly) | ISO-Calculated wall factor | Error | WD correction | Rate of Error | WS Correction | Rate of Error | Combined WD and WS correction | Error | Calculated Wall factor (5 min) | ISO, Calculated wall factor | Error |
| SE1 | 169 | 0.348 | 119 | 30% | 117 | 31% | 112 | 34% | 110 | 35% | 0.283 | 97 | 43% |
| SW1 | 162 | 0.333 | 114 | 30% | 112 | 31% | 107 | 34% | 105 | 35% | 0.271 | 93 | 43% |
| SW4 | 189 | 0.387 | 132 | 30% | 130 | 31% | 124 | 34% | 122 | 35% | 0.315 | 108 | 43% |
| SW6 | 192 | 0.393 | 134 | 30% | 132 | 31% | 126 | 34% | 124 | 35% | 0.320 | 109 | 43% |
| SW2 | 84 | 0.182 | 59 | 30% | 58 | 31% | 55 | 34% | 54 | 35% | 0.148 | 48 | 43% |
| SW5 | 94 | 0.204 | 66 | 30% | 65 | 31% | 62 | 34% | 61 | 35% | 0.166 | 54 | 43% |
| SW3 | 58 | 0.136 | 41 | 30% | 40 | 31% | 38 | 34% | 38 | 35% | 0.111 | 33 | 43% |
| Weather Station Airfield Index (mm) | | | 364 | | 358 | | 342 | | 333 | | | 364 | |

(b) South- east Façade

| Site Data | | | Calculated Wall Index (mm), Hourly *W* | | | | | | | | Calculated wall index (mm), 5-min *W* | | |
|---|---|---|---|---|---|---|---|---|---|---|---|---|---|
| WDR Gauges | Measured WDR (mm) | Calculated Wall factor (Hourly) | ISO-Calculated wall factor | Error | WD correction | Rate of Error | WS Correction | Rate of Error | Combined WD and WS correction | Error | Calculated Wall factor (5 min) | ISO, Calculated wall factor | Error |
| E1 | 295 | 0.649 | 332 | -12% | 297 | -1% | 302 | -2% | 270 | 8% | 0.539 | 276 | 7% |
| E4 | 322 | 0.707 | 362 | -12% | 324 | -1% | 329 | -2% | 294 | 9% | 0.587 | 300 | 7% |
| E6 | 316 | 0.695 | 355 | -12% | 318 | 0% | 323 | -2% | 289 | 9% | 0.577 | 295 | 7% |
| E2 | 167 | 0.387 | 188 | -13% | 168 | -1% | 171 | -2% | 153 | 8% | 0.322 | 156 | 6% |
| E5 | 166 | 0.386 | 187 | -13% | 167 | -1% | 170 | -3% | 152 | 8% | 0.320 | 155 | 6% |
| E3 | 121 | 0.301 | 135 | -12% | 121 | -1% | 123 | -2% | 110 | 8% | 0.250 | 112 | 7% |
| Weather Station Airfield Index (mm) | | | 545 | | 487 | | 496 | | 443 | | | 545 | |

Montreal

Table 6.6- Comparison between measured WDR and calculated WDR on the (a) North-east, (b) South-west and (c) South-east façade with wind speed and wind direction corrections and wall factors calculated using 5-min measured data, FB Building, Montreal

(a) North-East Façade

| Site Data | | | Calculated Wall Index (mm), Hourly *W* | | | | | | | | Calculated wall index (mm), 5-min *W* | | |
|---|---|---|---|---|---|---|---|---|---|---|---|---|---|
| WDR Gauges | Measured WDR (mm) | Calculated Wall factor (Hourly) | ISO-Calculated wall factor | Error | WD correction | Error | WS Correction | Error | Combined WD and WS correction | Error | Calculated Wall factor (5 min) | ISO, Calculated wall factor | Error |
| NE1 | 180 | 0.520 | 317 | -76% | 292 | -62% | 273 | -51% | 274 | -52% | 0.402 | 245 | -36% |
| NE5 | 172 | 0.497 | 303 | -76% | 279 | -62% | 260 | -51% | 262 | -52% | 0.384 | 234 | -36% |
| NE7 | 187 | 0.539 | 329 | -76% | 302 | -62% | 282 | -51% | 284 | -52% | 0.416 | 254 | -36% |
| NE2 | 115 | 0.345 | 205 | -78% | 188 | -63% | 176 | -53% | 177 | -53% | 0.267 | 158 | -37% |
| NE6 | 63 | 0.187 | 111 | -78% | 102 | -63% | 95 | -53% | 96 | -53% | 0.144 | 86 | -37% |
| NE8 | 104 | 0.311 | 185 | -78% | 170 | -63% | 159 | -53% | 160 | -53% | 0.240 | 143 | -37% |
| NE3 | 49 | 0.155 | 88 | -80% | 81 | -65% | 76 | -55% | 76 | -55% | 0.120 | 68 | -39% |
| NE9 | 50 | 0.159 | 91 | -80% | 83 | -65% | 78 | -55% | 78 | -55% | 0.123 | 70 | -39% |
| NE4 | 19 | 0.070 | 36 | -84% | 33 | -69% | 31 | -58% | 31 | -59% | 0.054 | 28 | -42% |
| NE10 | 4 | 0.013 | 7 | -84% | 6 | -69% | 6 | -58% | 6 | -59% | 0.010 | 5 | -42% |
| Weather Station Airfield Index (mm) | | | 668 | | 614 | | 574 | | 577 | | | 509 | |

(b) South-West Façade

| Site Data | | | Calculated Wall Index (mm), Hourly *W* | | | | | | | | Calculated wall index (mm), 5-min *W* | | |
|---|---|---|---|---|---|---|---|---|---|---|---|---|---|
| WDR Gauges | Measured WDR (mm) | Calculated Wall factor (Hourly) | ISO-Calculated wall factor | Error | WD correction | Error | WS Correction | Error | Combined WD and WS correction | Error | Calculated Wall factor (5 min) | ISO, Calculated wall factor | Error |
| SW1 | 257 | 0.577 | 290 | -13% | 283 | -10% | 260 | -1% | 260 | -1% | 0.434 | 218 | 15% |
| SW3 | 280 | 0.627 | 315 | -13% | 307 | -10% | 282 | -1% | 283 | -1% | 0.476 | 239 | 14% |
| SW5 | 193 | 0.690 | 221 | -15% | 216 | -12% | 198 | -3% | 198 | -3% | 0.543 | 174 | 10% |
| SW2 | 108 | 0.251 | 123 | -14% | 120 | -11% | 110 | -2% | 110 | -2% | 0.189 | 92 | 15% |
| SW4 | 87 | 0.203 | 100 | -14% | 97 | -11% | 89 | -2% | 89 | -2% | 0.152 | 75 | 15% |
| SW6 | 107 | 0.249 | 122 | -14% | 119 | -11% | 109 | -2% | 109 | -2% | 0.186 | 91 | 15% |
| SW7 | 45 | 0.228 | 46 | -3% | 45 | -1% | 41 | 8% | 41 | 8% | 0.188 | 38 | 15% |
| Weather Station Airfield Index (mm) | | | 551 | | 536 | | 492 | | 493 | | | 313 | |

(c) South-East Façade

| Site Data | | | Calculated Wall Index (mm), Hourly *W* | | | | | | | | Calculated wall index (mm), 5-min *W* | | |
|---|---|---|---|---|---|---|---|---|---|---|---|---|---|
| WDR Gauges | Measured WDR (mm) | Calculated Wall factor (Hourly) | ISO-Calculated wall factor | Error | WD correction | Error | WS Correction | Error | Combined WD and WS correction | Error | Calculated Wall factor (5 min) | ISO, Calculated wall factor | Error |
| SE1 | 177 | 0.648 | 298 | -68% | 285 | -61% | 258 | -46% | 261 | -48% | 0.526 | 242 | -37% |
| SE3 | 132 | 0.527 | 263 | -100% | 256 | -94% | 232 | -76% | 233 | -76% | 0.456 | 228 | -73% |
| SE4 | 233 | 0.685 | 430 | -85% | 417 | -79% | 378 | -62% | 379 | -63% | 0.561 | 352 | -51% |
| SE2 | 117 | 0.357 | 218 | -86% | 212 | -80% | 192 | -64% | 192 | -64% | 0.292 | 179 | -53% |
| SE5 | 106 | 0.321 | 197 | -86% | 190 | -80% | 173 | -64% | 173 | -64% | 0.263 | 161 | -53% |
| SE6 | 53 | 0.170 | 100 | -89% | 97 | -83% | 88 | -66% | 88 | -66% | 0.139 | 82 | -55% |
| Weather Station Airfield Index (mm) | | | 688 | | 666 | | 604 | | 606 | | | 369 | |

### 6.5.4. Effect Of Nearby Obstacle on Measured Wind Speed and Direction

The effect of nearby obstacle on measured wind speed and wind direction is studied through wind tunnel experiment on MacLeod house, Fredericton. As explained in Chapter 3, the anemometer is installed 4.6 m above the main roof, which is at comparable height of a nearby mechanical room located on the south-east side of the anemometer. The presence of this mechanical room may have an influence on the wind flow around the building where the anemometer measuring wind speed and wind direction. To investigate the potential impact of this mechanical room, wind tunnel measurements were carried out. Two models, one 1:400 the other 1:200 were carried out with and without the mechanical room. Using the 1:200 scale of the building is to check the reliability of the results for 1:400 model.

Wind velocity is measured at the place of anemometer for (1) 1:400 model with surrounding, (b) 1:400 stand-alone mode and (c) for 1:200 stand-alone model for eight wind angles with 45° intervals. The wind velocity is first measured for the situation without mechanical room on models and then with the mechanical room. The measured values are used as the reference due the velocity is not affected by any nearby obstacle. The velocity measured by the probe presents the size of three-dimensional velocity vector (3D), however the applied onsite anemometer measures the wind velocity on the XY plane (2D). As the result the wind velocity changes is compared in term of both 3D and 2D.

The results of wind velocity changes at the place of anemometer are shown in Figure 6.13 for different models. The comparison is calculated for measured wind velocity and projected wind velocity, on XY plane, at the place of anemometer with and without mechanical room. Presence of mechanical room affect both wind velocity and wind direction very slightly.

In general, the measured wind speed at the place of anemometer in 1:400 models are lower in comparison with 1:200 model. Measuring the wind velocity at the lower distance from the wind tunnel ground and existence of surrounding buildings and vegetation in 1:400 model with surrounding could be considered as the contributing factors. The highest observed difference in measured wind velocities at the place of anemometer for 1:400 model with and without surrounding is 10% for wind approaching from the west, for the models without mechanical room; this is due to the building located on left side of the building in 1:400 model with surroundings.

Considering projected wind velocity, for 1:400 model with surrounding wind velocity decreases due to presence of the mechanical room for wind approaching from east to north-west. The maximum difference is 3.34% for wind approaching from the east. This amount is 5.49% for 1:400 stand-alone model. For 1:200 the wind approached from south-east increase by around 4% while for wind approaching from north-west the wind velocity reduced by around 7%. For wind coming from south-west, wind velocity experiences slight differences due to presence of the mechanical room; around 1% for 1:200 stand-alone model, 2% for 1:400 stand-alone model and 3% for 1:200 scale with surroundings.

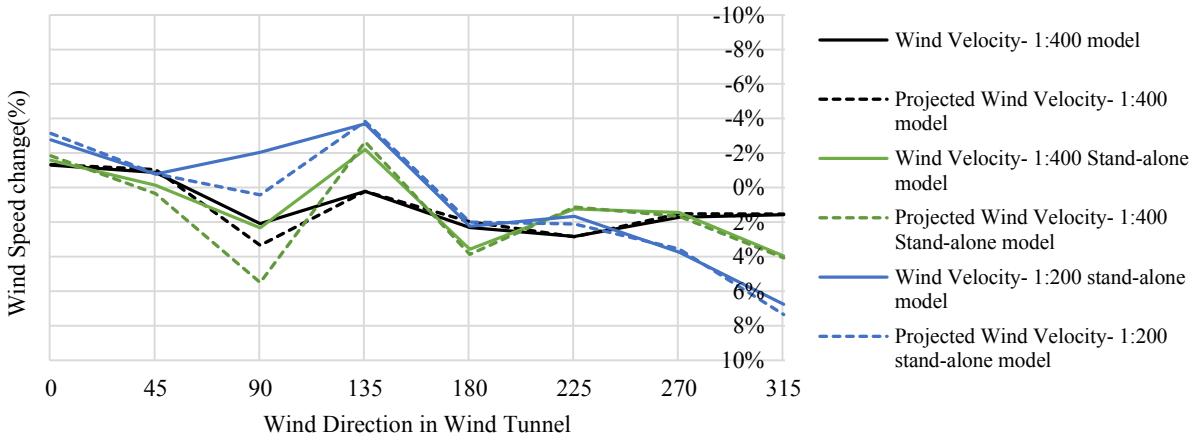


Figure 6.13 - Trend and rate of wind speed fluctuation at different wind incidence angles (%), for two model scales and surroundings

The other important factor which might also be affected by the presence of mechanical room is wind direction. In order to investigate how the wind direction is affected the "Yaw Angle" provided by the Cobra Probe is compared in different situations for both scales. In general, there is good agreement between all conducted experiments, Figure 6.14. The maximum wind direction change is 4.8, 4.95 and 5.8 degree for 1:400 model with surrounding, 1:400 stand-alone model and 1:200 stand-alone model respectively for the time wind is blowing from east (90°). For normal wind direction on south-west façade (225°), wind direction experienced less than 2 degrees of difference. So, it can be concluded that WDR analysis on the south-west façade is not affected due wind direction changes, however slight changes might be observed on south-east façade estimations.

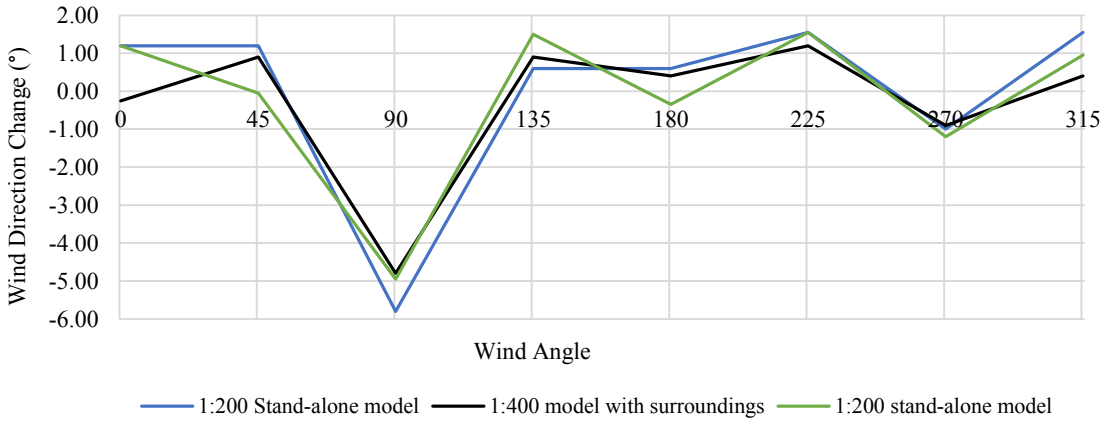


Figure 6.14 – Wind Direction change due to the presence of mechanical room in 1:400 stand-alone and with surrounding model and 1:200 stand-alone model

Based on wind tunnel experiment results, both wind speed and wind direction experience some changes when the mechanical room was added to the building`s model. To see the effect of these changes on the calculated wall factor and onsite airfield indices, onsite wind data is modified based on the wind tunnel experiment results for 1:400 model with surrounding; the model with surrounding is more realistic simulation of real life condition and the accuracy of this scale in wind tunnel experiments has been verified by Stathopoulos (Stathopoulos, 1984). As it is shown in Table 6.7, adding mechanical room change wind velocity by around 1% in average.

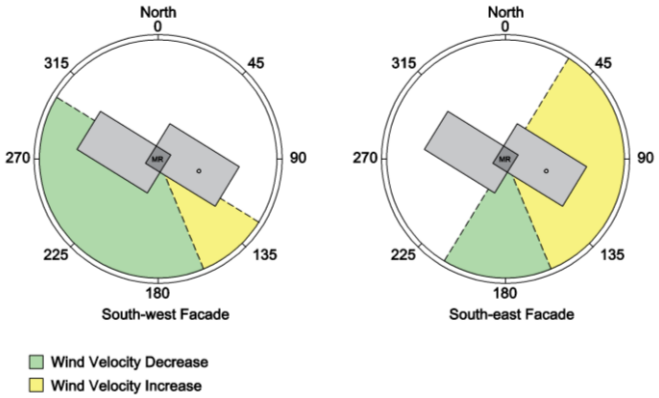


Figure 6.15 - Wind speed change with adding the mechanical room to the model.

To modify the onsite wind speed data, two coefficients are introduced. For the times adding mechanical room decrease the speed, the introduced coefficient is greater than 1 to eliminate the effect of mechanical room is estimated based on the average of wind speed change in different directions. The coefficient calculated for the time when wind speed increases as the result of

mechanical room, is less than 1. The estimated coefficients and associated angles are presented in Table 6.7 for both building facades.

Table 6.7 - Introduced wind speed coefficient for each windward façade regarding different wind direction range

| | Façade orientation | | Decrease | | Increase | |
|---|---|---|---|---|---|---|
| | Normal angle from North | Onsite Wind Range | WD Range | Coefficient | WD Range | Coefficient |
| South-east | 123 | 33<θ≤213 | 33<θ≤157.5 | 0.99 | 157.5<θ≤213 | 1.02 |
| South-west | 213 | 123<θ≤303 | 123<θ≤157.5 | 0.98 | 157.5<θ≤303 | 1.03 |

Incident wind angle blowing within the range of 67.5° up to 112.5 ° is increased by 4.5 degree on average when the mechanical room is added, as shown in Figure 6.16.

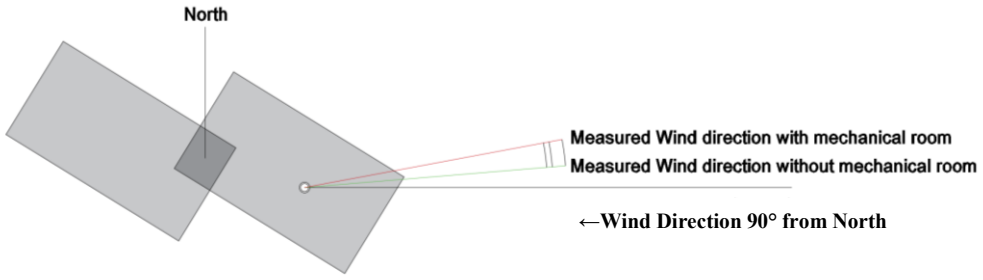


Figure 6.16 - Wind direction change at the place of anemometer when wind blowing from the east

The calculations show that correction of wind characteristics based on wind tunnel experiment change the estimation of airfield index by 1%. The calculated wall factor remains the same, Table E.5-6. It can be concluded that the presence of mechanical room does not affect the measurements at the anemometer height given that the weather station is installed far enough from the mechanical room. Therefore, the WDR analysis carried out using the on-site wind measurements at the anemometer height is valid.

### 6.5.5. Precipitation Type

The precipitation type was another factor that might affect WDR estimations. Snow precipitation rarely occurs in Vancouver due to its moderate oceanic climate condition, as the result there is no need for data filtration. However, other two test buildings are located in humid continental climate with significant amount of snow precipitation during cold seasons. The snow precipitation and uncertain data are removed from both onsite and weather station data sets.

Data filtration with respect to precipitation type reduces the calculated air field index around 10%, 5% and 13% on average for north-east, south-east and south-west facade of Montreal building, respectively using data sets listed in Table 6.8. The highest difference is 6% for Fredericton building that can be observed for hourly estimation based on airport data.

Table 6.8 – Comparison of Airfield DRI (mm) for windward façades of test buildings at the height of wind-driven rain gauges considering all and filtered data with hourly and 5-min time resolution

| Test Building | Windward Façade Orientation | Distance from the Roof Top | Onsite Airfield DRI (mm), Hourly Data | | Difference (%) | Onsite Airfield DRI (mm), 5-min Data | | Difference (%) | Weather station Airfield DRI (mm), Hourly Data | | Difference (%) |
|---|---|---|---|---|---|---|---|---|---|---|---|
| | | | All Data | Filtered Data | | All Data | Filtered Data | | All Data | Filtered Data | |
| Cassier Building, Vancouver | East | 0.6 m | 824 | without filtering | | 1003 | without filtering | | 989 | without filtering | |
| | | 2.4 m | 803 | | | 978 | | | 965 | | |
| | | 4.9 m | 773 | | | 942 | | | 929 | | |
| | | 9.1 m | 711 | | | 866 | | | 849 | | |
| | North | 0.6 m | 148 | | | 78 | | | 150 | | |
| | | 2.4 m | 144 | | | 76 | | | 146 | | |
| | | 3.7 m | 142 | | | 74 | | | 144 | | |
| | | 4.9 m | 139 | | | 73 | | | 141 | | |
| | | 9.1 m | 128 | | | 67 | | | 129 | | |
| McLeod House, Fredericton | South-east | 0.6 m | 455 | 441 | 3% | 548 | 533 | 3% | 511 | 502 | 2% |
| | | 4.9 m | 431 | 417 | 3% | 519 | 504 | 3% | 485 | 475 | 2% |
| | | 9.1 m | 401 | 388 | 3% | 483 | 470 | 3% | 450 | 442 | 2% |
| | South-west | 0.6 m | 487 | 473 | 3% | 598 | 585 | 2% | 341 | 322 | 6% |
| | | 4.9 m | 461 | 448 | 3% | 566 | 553 | 2% | 324 | 305 | 6% |
| | | 9.1 m | 429 | 417 | 3% | 527 | 515 | 2% | 301 | 283 | 6% |
| FB Building, Montreal | North-east | 0.6 m | 347 | 314 | 10% | 449 | 407 | 9% | 610 | 555 | 9% |
| | | 4.9 m | 335 | 303 | 10% | 433 | 392 | 9% | 594 | 541 | 9% |
| | | 10.7 | 317 | 286 | 10% | 410 | 371 | 9% | 570 | 518 | 9% |
| | | 21.3 | 278 | 251 | 10% | 359 | 326 | 9% | 511 | 465 | 9% |
| | South-east | 0.6 m | 341 | 326 | 4% | 416 | 399 | 4% | 629 | 588 | 6% |
| | | 4.9 m | 329 | 314 | 4% | 401 | 385 | 4% | 612 | 572 | 6% |
| | | 10.7 | 311 | 297 | 4% | 380 | 364 | 4% | 587 | 549 | 6% |
| | South-west | 0.6 m | 446 | 395 | 12% | 556 | 495 | 11% | 503 | 429 | 15% |
| | | 4.9 m | 430 | 381 | 12% | 536 | 478 | 11% | 490 | 418 | 15% |
| | | 10.7 | 407 | 360 | 12% | 507 | 452 | 11% | 469 | 400 | 15% |

For all facades of Montreal building and south-west façade of Fredericton building data filtration does not affect the calculated wall factor and wall indices considering data sets with different time resolutions (Table E.7-8). However, this procedure increase the discrepancy of calculated WDR considering hourly wall factor and measured WDR on Fredericton south-east façade by two times while improve the estimations applying 5-min data.

## 6.6. Summary and Conclusion

Previous studies have shown that estimation of impinged WDR on building façade based on meteorological data reported by weather stations and ISO model is encountered to significant overestimation or underestimation in general. Lack of variation in prescribed wall factor by ISO is identified as one of the main contributing factors that lead to inaccuracy of WDR estimations. Applying wall factors calculated based on onsite measurements reduce the discrepancy between measured and estimated WDR. However, remaining discrepancy indicates that there may exist other contributing sources.

Although good agreement can be observed between wind characteristics measured onsite with the data reported by Environment Canada for same period of time, more detailed investigations show that the differences in wind conditions (wind speed and wind direction) between airport and the site is the main contributor to the discrepancy that still exists. This difference can be reduced by applying high resolution data; 5-min data instead of hourly data or by adjusting the hourly wind speed and filtering the hourly wind direction. Conversion of 5-min data to hourly data might eliminate or reduce the effect of influential data as the result of averaging specifically in term of wind direction. Considering there might be significant changes of wind direction from weather station to site data filtering may be necessary. The measured wind speed at the place of anemometer is generally lower than what it is expected based on weather station data with power law conversion for stable conditions. As the result applying proper correction factor based on onsite data will improve the estimations significantly.

In general, semi-empirical ISO model can be used to estimate WDR façade with accuracy if proper procedures measuring on-site wind conditions and calculating spatial distribution correction factors using high- resolution measurements are followed.

# 7. Conclusion and Future Work

## 7.1. Conclusion

Wind driven-rain is considered as one of the main boundary conditions and moisture sources, which affect hydrothermal performances of the building enclosure. As the result accurate estimation of wind drive-rain load on the façade is critical. A comprehensive research program is designed to quantify wind-driven rain loads on mid-rise buildings and the effectiveness of overhang in reducing WDR wetting of building façade. Within this research program, field measurements of WDR on four mid-rise buildings in three Canadian regions were carried out. A six-story building in Vancouver is fitted with retractable overhang to quantify the effectiveness of overhang. Findings from these research work have been reported in Nath (2015) and Chiu (2016). Current study is a continuation of these two previous studies and focuses on further analysis of field measurements of WDR to quantify the effectiveness of overhang with more complete data and further investigate the accuracy of ISO WDR model in WDR estimation as a semi-empirical method. Findings include:

**1) Further data analysis of the overhang effectiveness on the six-story building in Vancouver;**

- There is a great consistency with what have been concluded in the previous study;
    - Overhangs provide the highest protection for areas right beneath them. Overhang effectiveness decreases from roofline towards the bottom of the façade and is extended to almost half of the building height for 1.2m overhang. Provided protection is not uniform across the overhang length; more protection is provided for locations away from the edges.
    - The results show that 70% of WDR load is deposited on the top 30% of the façade area, therefore, overhangs that can shelter the top 30% of the façade can effectively protect the façade from WDR wetting.
    - Good exponential relation is observed between overhang widths and percentage of WDR load impinged on different portions of the facade. The application of 0.3 m, 0.6

m, 0.9 m and 1.2 m overhang on building roof top reduces the amount of received WDR on entire façade by 21%, 45%, 55% and 63% respectively. It is anticipated that by applying wider overhangs, above 1.2m, the percentage of WDR load reduction will not significantly change especially for the top portions of the façade.

- The increase of wind speed significantly reduce the WDR reduction coefficient. The increase of wind speed from 1.5m/s to 4.7m/s reduces the WDR reduction coefficient almost by 50% for 0.6m, 0.9m and 1.2m overhang and by less than 10% for the 0.3m overhang.
- Overhangs have the minimum efficiency in reduction of WDR for normal wind directions; in general, with the increase of wind incident angle the WDR reduction coefficient increases. Therefore applying WDR reduction coefficient for normal wind direction can be considered as a more conservative approach in estimation of received WDR by mid-rise building façade.
- Overhang effectiveness is not uniform across its length for inclined wind direction. Windward areas of the façade are more exposed to WDR in comparison with leeward areas.

**2) Generalization of the WDR reduction coefficients for mid-rise buildings with similar geometry**

- Same wind flow pattern is observed around the south-west façade of Fredericton Building and east façade of Vancouver building for normal wind direction due to geometrical characteristics of facades.
- Adding 6mm (1.2 m) overhang on the models' rooftop has the similar impact on reduction of normalized wind velocity near the facades for normal wind direction; the effect is extended up to quarter of model height.
- The percentage reduction of wind velocity decreases from roofline towards the bottom of the model façade and increases for locations away from the edges; similar pattern has been observed in overhang effectiveness in reduction of impinged WDR based on field measurements.

- For points with distance of 3 mm (0.6 m) from the rooftop, the lowest percentage of normalized wind velocity reduction is around 5% for locations near the edges and reaches around 25% in the middle of the façade.
- The calculated WDR reduction coefficient can be used for mid-rise buildings with similar building geometry and climate condition as Vancouver and Fredericton. However, the possibility of applying WDR reduction coefficient for different climate conditions should be investigated.

**3) Improvement of accuracy of ISO model to assess the WDR loads on facade**

- The analysis on additional data available for three test buildings shows that over/under estimation of WDR on building façade based on ISO model is mainly due to ISO prescribed wall factor. There are only two wall factors prescribed in ISO model for multi-storey buildings with low-slopped roof and they are constant across the building façade.
- In general, applying calculated hourly wall factors in ISO model significantly improves the estimation of WDR; however the discrepancy between measured and estimated amount of WDR in not eliminated.
- The application of high resolution 5min data instead of hourly data in calculation of wall factor and WDR estimation significantly improves the results; the discrepancy between measured and estimated WDR is almost eliminated for Vancouver building and significantly reduced for Fredericton and Montreal building. The only exception is south-west façade of Fredericton building.
- The conversion of 5min data to hourly data eliminates or reduces the effect of critical data in calculation of airfield driven rain index and wall factor. For inclined wind directions, converting measured 5-min data to hourly data can highly affect the results; i.e. 34% for north façade of Vancouver. However, for almost normal wind direction its effect is less than 10% for other facades.
- The analysis shows that using arithmetic averaging instead of weighted averaging does not affect the analysis due to high resolution data measurement through field experiment.

- The differences on wind conditions (wind speed and wind direction) between airport and the site is the main contributor to the discrepancy that still exists.
    - The measured wind speed at the place of anemometer is generally lower than what it is expected based on weather station data with power law conversion for stable conditions. As the result applying proper correction factor based on onsite data will improve the estimations significantly.
    - Discrepancies regarding wind direction changes can be accounted by filtering the hourly wind direction and is mainly effective for inclined prevailing wind directions blowing towards the study façade.
- Field measurements have been conducted over a long period of time. Therefor snow precipitation does not have a significant impact on WDR analysis due to low percentage of snow precipitation in comparison with rain precipitation during study periods.

Overall, the accurate quantification of WDR on façade is essential for designing and modelling durable building envelopes. By neglecting building specific features a significant overestimation or underestimation may be encountered when using the ISO standard. However, the semi-empirical ISO model can provide accurate estimation of WDR on façade if more detailed wall factors are provided. High-resolution measurements at 5-min or 10-min intervals should be made available for the calculation of wall factors, which will help compensate the difference in wind conditions between airport weather station and the site, and consequently greatly improve the accuracy of ISO WDR model. Moreover, for mid-rise building facades that are protected by roof overhang applying proper WDR reduction coefficient with respect to wind speed and direction lead to more accurate estimation of WDR load received by the façade.

## 7.2. Recommendation for Future Work

In current study WDR reduction coefficient is introduced for mid-rise buildings located in regions with similar climate conditions. The high-resolution data provided through field measurements can be used to validate CFD simulation in study of overhang effectiveness for different building geometries with different façade detail design exposed to different climate

conditions. Also, WDR reduction coefficient can be provided for a wider range of wind speeds and wind directions.

WDR spatial distribution and overhang effectiveness can also be studied through simulation of WDR in boundary layer wind tunnels. The available data and analysis can be used to validate wind tunnel and nozzle setup and, consequently, study of WDR spatial distribution and quantify overhang effectiveness for different building geometries.

In current study the amount of WDR received by the façade and effect of overhang in reduction of WDR load is quantified by collecting all impinged WDR on façade. Under real life condition, depending on building façade's material, the impinged raindrops might be completely absorbed or partially absorbed and flow down after the façade is saturated, which is also known as rain water runoff. The effect of overhang on reduction of runoff rain water should be studied for commonly used materials and enclosure assemblies.

The effect of overhang with different configurations on WDR loads should be studied for different types of buildings and its effect on the hygrothermal performance of different building enclosures should be also investigated.

# References


Abuku, M., Blocken, B., & Roels, S. (2009a). Field measurement and numerical analysis of wind-driven rain absorption and evaporation on building facades. *5th European and African Conference on Wind Engineering, EACWE 5*.

Abuku, M., Blocken, B., & Roels, S. (2009b). Moisture response of building facades to wind-driven rain: Field measurements compared with numerical simulations. *Journal of Wind Engineering and Industrial Aerodynamics*, *97*(5–6), 197–207.

ASHRAE 160.PDF. (2009).

Baheru, T., Chowdhury, A. G., & Pinelli, J.-P. (2015). Estimation of Wind-Driven Rain Intrusion through Building Envelope Defects and Breaches during Tropical Cyclones. *Natural Hazards Review*, *16*(2), 04014023.

Baheru, T., Chowdhury, A. G., Pinelli, J. P., & Bitsuamlak, G. (2014). Distribution of wind-driven rain deposition on low-rise buildings: Direct impinging raindrops versus surface runoff. *Journal of Wind Engineering and Industrial Aerodynamics*, *133*, 27–38.

Blocken, B. (2004). Wind-driven Rain on builidngs; Measurments, numerical modeling and applications, PHD thesis, Department of Civil Engineering, Katholieke Univeritet Leuven

Blocken, B., Abuku, M., Nore, K., Briggen, P. M., Schellen, H. L., Thue, J. V., … Carmeliet, J. (2011). Intercomparison of wind-driven rain deposition models based on two case studies with full-scale measurements. *Journal of Wind Engineering and Industrial Aerodynamics*, *99*(4), 448–459.

Blocken, B., & Carmeliet, J. (2002). Spatial and temporal distribution of driving rain on a low-rise building. *Wind and Structures, An International Journal*, *5*(5), 441–462.

Blocken, B., & Carmeliet, J. (2004). A review of wind-driven rain research in building science. *Journal of Wind Engineering and Industrial Aerodynamics*, *92*(13), 1079–1130.

Blocken, B., & Carmeliet, J. (2006a). On the accuracy of wind-driven rain measurements on buildings. *Building and Environment*, *41*(12), 1798–1810.

Blocken, B., & Carmeliet, J. (2006b). On the validity of the cosine projection in wind-driven rain

calculations on buildings. *Building and Environment*, *41*(9), 1182–1189.

Blocken, B., & Carmeliet, J. (2006c). The influence of the wind-blocking effect by a building on its wind-driven rain exposure. *Journal of Wind Engineering and Industrial Aerodynamics*, *94*(2), 101–127.

Blocken, B., & Carmeliet, J. (2010). Overview of three state-of-the-art wind-driven rain assessment models and comparison based on model theory. *Building and Environment*, *45*(3), 691–703.

Blocken, B., Carmeliet, J., & Poesen, J. (2005). Numerical simulation of the wind-driven rainfall distribution over small-scale topography in space and time. *Journal of Hydrology*, *315*(1–4), 252–273.

Blocken, B., Dezsö, G., van Beeck, J., & Carmeliet, J. (2010). Comparison of calculation models for wind-driven rain deposition on building facades. *Atmospheric Environment*, *44*(14), 1714–1725.

Blocken, B., Ph, D., Carmeliet, J., & Ph, D. (2004). A Simplified Approach for Quantifying Driving Rain on Buildings.

Briggen, P. M., Blocken, B., & Schellen, H. L. (2009). Wind-driven rain on the facade of a monumental tower: Numerical simulation, full-scale validation and sensitivity analysis. *Building and Environment*, *44*(8), 1675–1690.

Bureau voor Normalisatie. (2009). *Geregistreerde Belgische norm norme belge enregistrée*.

Carbonez, K., Van Den Bossche, N., Ge, H., Lobelle, G., & Janssens, A. (2015). The spell definition in ISO-15927 and its impact on the rain deposition on the building facade. *Energy Procedia*, *78*(0), 2548–2553.

Chiu, V. (2016). The Effect of Overhang on Wind-Driven Rain Wetting for a Mid-Rise Building, *Depatrmetnt Building Civil and Environmental Enineering, Concrodia University*.

Choi, E. C. C. (1994). Determination of wind-driven-rain intensity on building faces. *Journal of Wind Engineering and Industrial Aerodynamics*, *51*(1), 55–69.

Choi, E. C. C. (1994). Parameters affecting the intensity of wind-driven rain on the front face of a building. *Journal of Wind Engineering and Industrial Aerodynamics*, *53*(1–2), 1–17.

Choi, E. C. C. (1999). Wind-driven rain on building faces and the driving-rain index. *Journal of Wind Engineering and Industrial Aerodynamics*, *79*(1–2), 105–122.

Domínguez-Hernández, J., Pérez-Bella, J. M., Alonso-Martínez, M., Cano-Suñén, E., & del Coz-Díaz, J. J. (2016). Assessment of water penetration risk in building facades throughout Brazil. *Building Research & Information*, *3218*(June), 1–16.

Ge, H. (2015). Influence of time resolution and averaging techniques of meteorological data on the estimation of wind-driven rain load on building facades for Canadian climates. *Journal of Wind Engineering and Industrial Aerodynamics*, *143*, 50–61.

Ge, H., Chiu, V., & Stathopoulos, T. (2017). Effect of overhang on wind-driven rain wetting of facades on a mid-rise building: Field measurements. *Building and Environment*, *118*, 234–250.

Ge, H., Chiu, V., Stathopoulos, T., & Souri, F. (2017). Effect of overhang on wind-driven rain wetting of facades on a mid-rise building: Field measurements. *Building and Environment*, *118*, 234–250.

Ge, H., Chiu, V., Stathopoulos, T., & Souri, F. (2018). Improved assessment of wind-driven rain on building façade based on ISO standard with high-resolution on-site weather data. *Journal of Wind Engineering and Industrial Aerodynamics*, *176*(December 2017), 183–196.

Ge, H., Deb Nath, U. K., & Chiu, V. (2017a). Field measurements of wind-driven rain on mid- and high-rise buildings in three Canadian regions. *Building and Environment*, *116*, 228–245.

Ge, H., & Krpan, R. (2007). Field measurement of wind-driven rain on a low-rise building in the coastal climate of British Columbia. *11th Canadian Conference on Building Science and Technology*.

Ge, H., & Krpan, R. (2009). Wind-driven Rain Study in the Coastal Climate of British Columbia. *Research Report Submitted to Canadian Mortgage and Housing Corporation*.

Gualtieri, G., & Secci, S. (2011). Comparing methods to calculate atmospheric stability-dependent wind speed profiles: A case study on coastal location. *Renewable Energy*, *36*(8), 2189–2204.

Hazleden, D., & Rousseau, J. (1996). Survey of building envelope failures in the coastal climate

Presented to : High-Rise and Multiples Submitted By : Morrison Hershfield Limited. *CMHC*.

Högberg, A., Kragh, M., & Van Mook, F. J. R. (1999). A comparison of driving rain measurements with different gauges. *Proceedings of the 5th Symposium on Building Physics in the Nordic Countries*, (August), 24–26.

Juras, P., & Jakubcik, M. (2016). Comparison of Driving Rain Index Calculated According to EN 15927-3 to the CFD Simulation and Experimental Measurement. *Applied Mechanics and Materials*, *861*, 239–246.

Khalilzadeh, A. (2017). Numerical Parametric Study of Wind-Driven Rain and Overhang Effectiveness on a Mid-Rise Building Depatrmetnt Building Civil and Environmental Enineering, Concrodia University.

Kontoleon, K. J., & Giarma, C. (2016). Dynamic thermal response of building material layers in aspect of their moisture content. *Applied Energy*, *170*, 76–91.

Kubilay, A., Carmeliet, J., & Derome, D. (2017). Computational fluid dynamics simulations of wind-driven rain on a mid-rise residential building with various types of facade details. *Journal of Building Performance Simulation*, *10*(2), 125–143.

Kubilay, A., Derome, D., Blocken, B., & Carmeliet, J. (2014). Numerical simulations of wind-driven rain on an array of low-rise cubic buildings and validation by field measurements. *Building and Environment*, *81*, 283–295.

Kubilay, A., Derome, D., Blocken, B., & Carmeliet, J. (2015). Wind-driven rain on two parallel wide buildings: Field measurements and CFD simulations. *Journal of Wind Engineering and Industrial Aerodynamics*, *146*, 11–28.

Mao, J., & Gao, N. (2015). The airborne transmission of infection between flats in high-rise residential buildings: A review. *Building and Environment*, *94*(September), 516–531.

Mohaddes Foroushani, S. S. (2013). A numerical study of the effects of overhangs on the wind-driven rain wetting of building facades.

Mohaddes Foroushani, S. S., Ge, H., & Naylor, D. (2014). Effects of roof overhangs on wind-driven rain wetting of a low-rise cubic building: A numerical study. *Journal of Wind*

*Engineering and Industrial Aerodynamics*, *125*, 38–51.

Nath, U. K. D. (2015). Field Measurements of Wind-Driven Rain on Mid - and High - Rise Buildings in Two Canadian Regions, *Depatrmetnt Building Civil and Environmental Enineering, Concrodia University*.

Nath, U. K. D., Chiu, V., & Ge, H. (2015). Measurements of wind-driven rain on mid- and high-rise buildings in three Canadian regions. *Energy Procedia*, *78*(c), 2512–2517.

Nore, K., Blocken, B., Jelle, B. P., Thue, J. V., & Carmeliet, J. (2007). A dataset of wind-driven rain measurements on a low-rise test building in Norway. *Building and Environment,* 42 (2007) 2150–2165

Osorio, M. (2013a). Error analysis of the wind-driven rain measurements taken on a six-storey building in Lower Mainland, British Columbia. Concordia University, Montreal, Canada.

Osorio, M. (2013b). Report on the errors associated with a wind-driven rain gauge. Concordia University, Montreal, Canada.

Stathopoulos, T. (1984). Design and fabrication of a wind tunnel for building aerodynamics. *Journal of Wind Engineering and Industrial Aerodynamics*, *16*(2–3), 361–376.

Straube, J. F., & Burnett, E. F. P. (2000). Simplified prediction of driving rain deposition. *Proceedings of the International Building Physiscs Conference*, (September 2000), 375–382.

Surry, D., Inculet, D. R., Skerlj, P. F., Lin, J.-X., & Davenport, a. G. (1994). Wind, rain and the building envelope: a status report of ongoing research at the University of Western Ontario. *Journal of Wind Engineering and Industrial Aerodynamics*, *53*(1–2), 19–36.

Zhou, X., Derome, D., & Carmeliet, J. (2016). Robust moisture reference year methodology for hygrothermal simulations. *Building and Environment*, *110*, 23–35.

# A. APPENDIX A

Model and specification of equipment used in three test buildings to measure air temperature, relative humidity, horizontal rainfall intensity, wind speed, wind direction and WDR received by building façade.

| Instrument | Model | Function | Photograph | Range/Accuracy |
|---|---|---|---|---|
| Wind Monitor | 05103 | Measures wind speed and wind direction. |  | Range: 0–50 m s–1<br>Accuracy: ±0.2 m s–1<br>1% of reading |
| Temperature & Relative Humidity Probe | HC2-S3-L | Measures temperature and relative humidity. |  | Temperature Sensor:<br>Range: -50°C to +50°C<br>Accuracy: ±0.1° C<br>RH Sensor:<br>Range: 0 to 100% non-condensing<br>Accuracy: 0.8% |
| Horizontal Rain Gauge | TE525M | Measures the horizontal rainfall intensity. |  | Collection Diameter: 24.5 cm<br>Rainfall per tip: 0.1 mm/tip<br>Accuracy: 1% up to 50 mm/hr |
| Wind-Driven Rain Gauges | BSC custom made | Measures the quantity of WDR on the facade. |  | Collection Area: 30.5 cm by 30.5 cm<br>Wind-driven rainfall per tip: 0.06 mm/tip |

Figure A.1- Instrumentation technical specifications that are used in field measurement for all three test buildings

Phisical characterisctics of atmospheric boundry layer wind tunnel, Concordia University

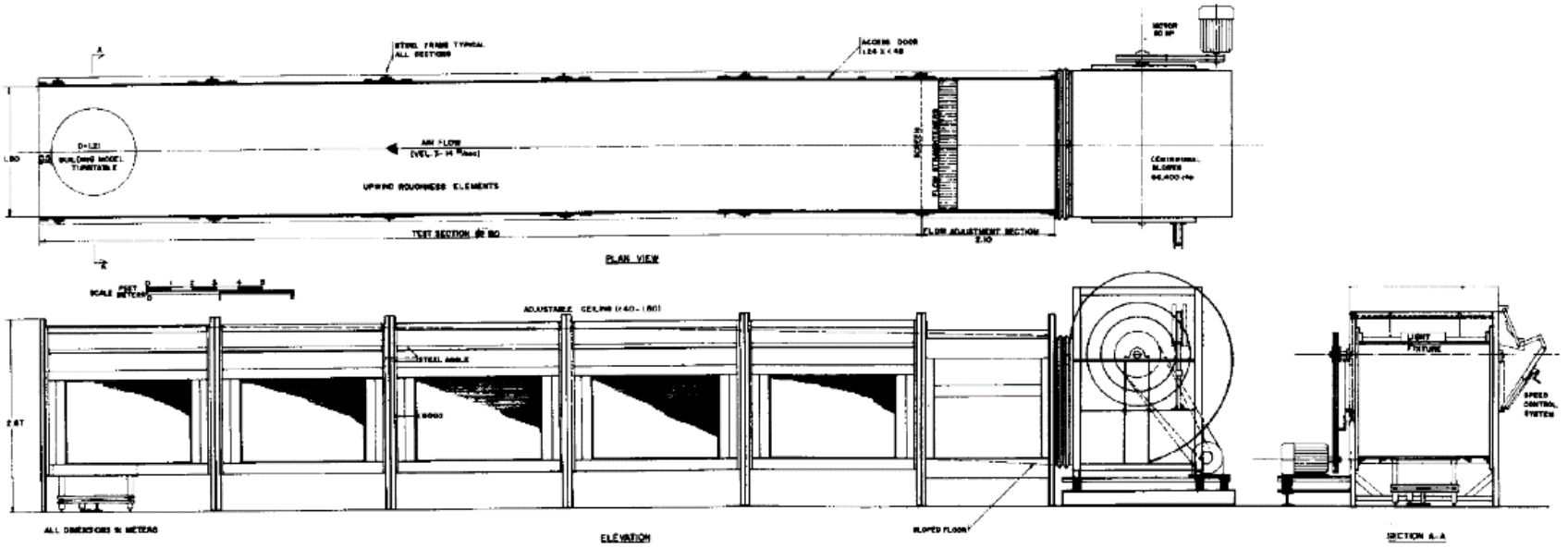


Figure A.2 - Concordia University's atmospheric boundary layer wind tunnel ((Stathopoulos, 1984)

Wind tunnel experiment 1:200 modles used in generalizing overhnag effectiveness results for mi-rise buildings

(a) (b)

Figure A.3 - Wind velocity measurement points on Fredericton south-west façade 1:200 stand-alone model; (a) with and (b) without 6 mm (1.2 m) overhang

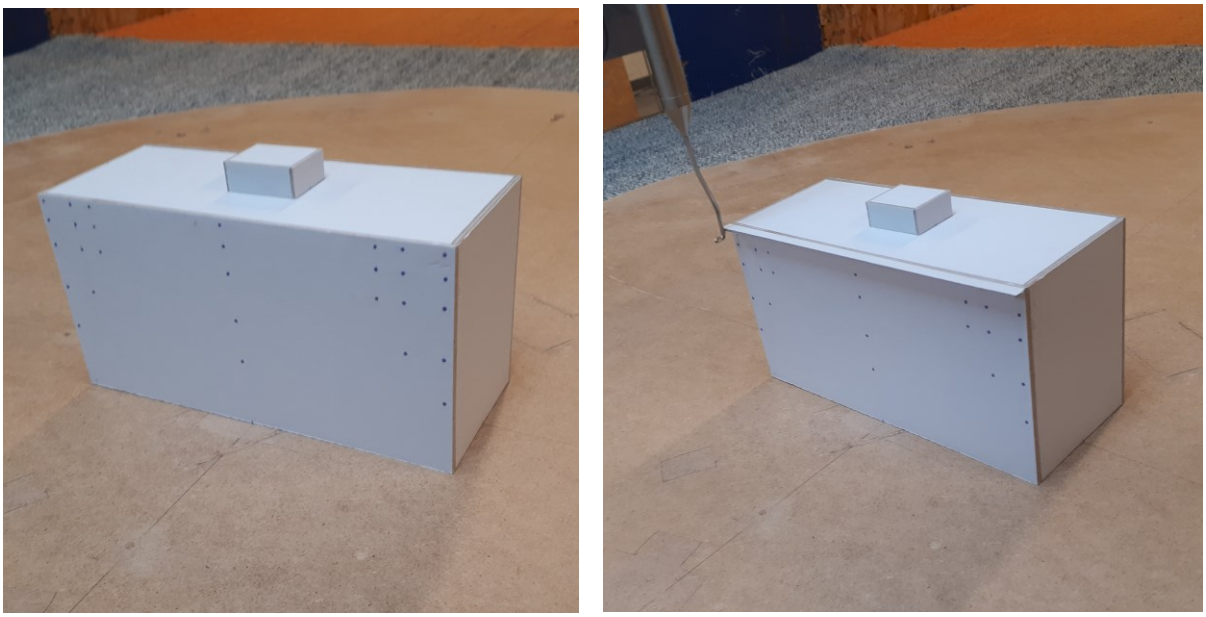

(a) (b)

Figure A.4 - Wind velocity measurement points on Vancouver east façade 1:200 stand-alone model; (a) with and (b) without 6 mm (1.2 m) overhang

Wind velocity measuring points near south-west façade of McLeod House 1:200 model.

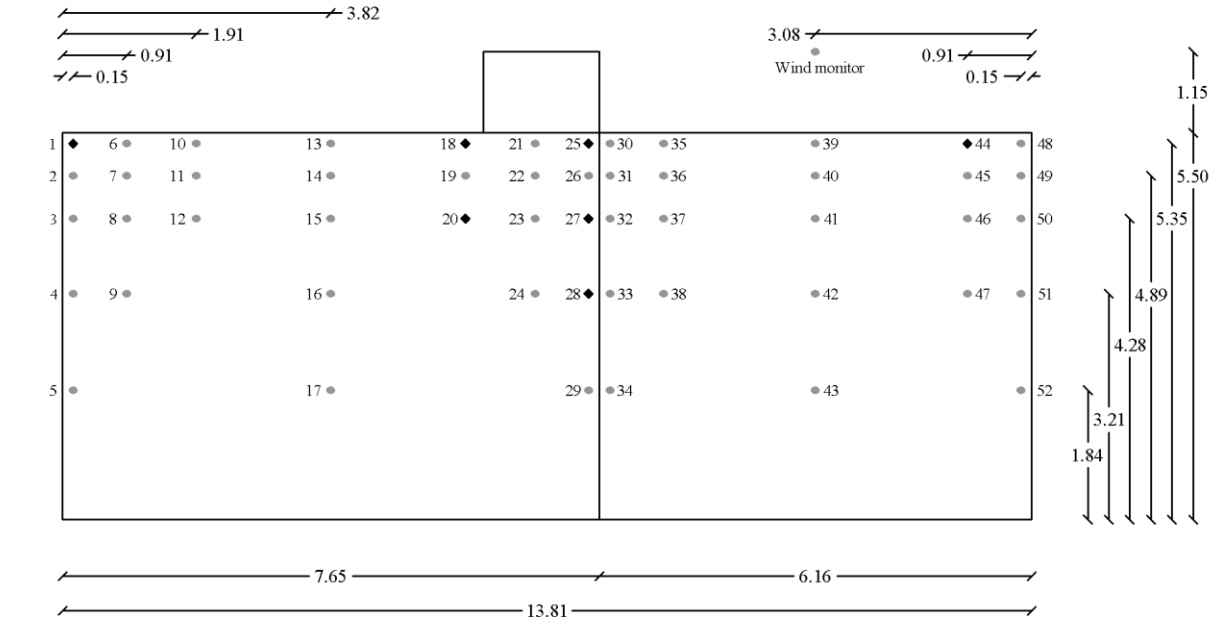


(a)

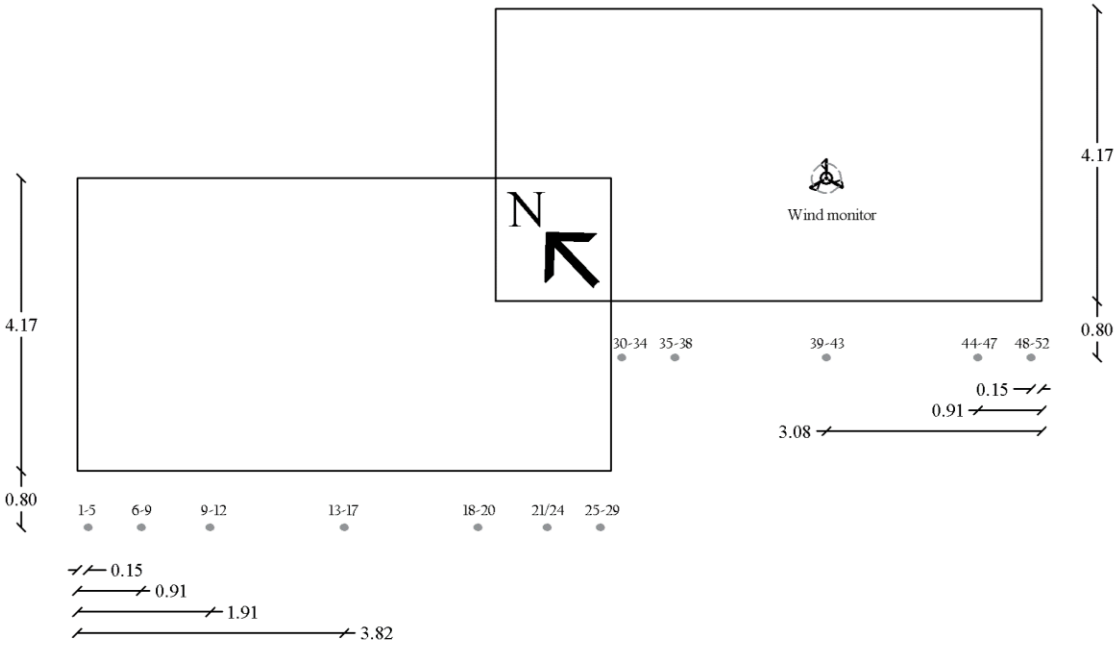


(b)

Figure A.5 - South-west elevation (a) and top view (b) of the McLeod House building model with 1.2 m overhang (SC:1/400). The measurement points near the south-west facade are shown in addition to the wind monitor location. All values aye in cm.

Comparison of meteorological data measured onsite with data reported by Environmental Canada during the same period of time for three test buildings.

## Cassiar building, Vancouver, BC

Table A.1- Exposure type, elevation, reference height, gradient height, and mean speed exponent for Vancouver Sea Island weather station and Cassiar building

| | ***Cassier Building, Vancouver, BC*** | ***Vancouver Sea Island weather station*** |
|---|---|---|
| *Exposure* | *Suburban* | *Open country* |
| *Elevation (m)* | *34* | *2.1* |
| *Reference Height, $Z_{ref}$ (m)* | *26.8* | *10* |
| *Gradient Height, $Z_g$ (m)* | *400* | *300* |
| *Mean Speed Exponent (α)* | *0.25* | *0.15* |

Wind Direction:

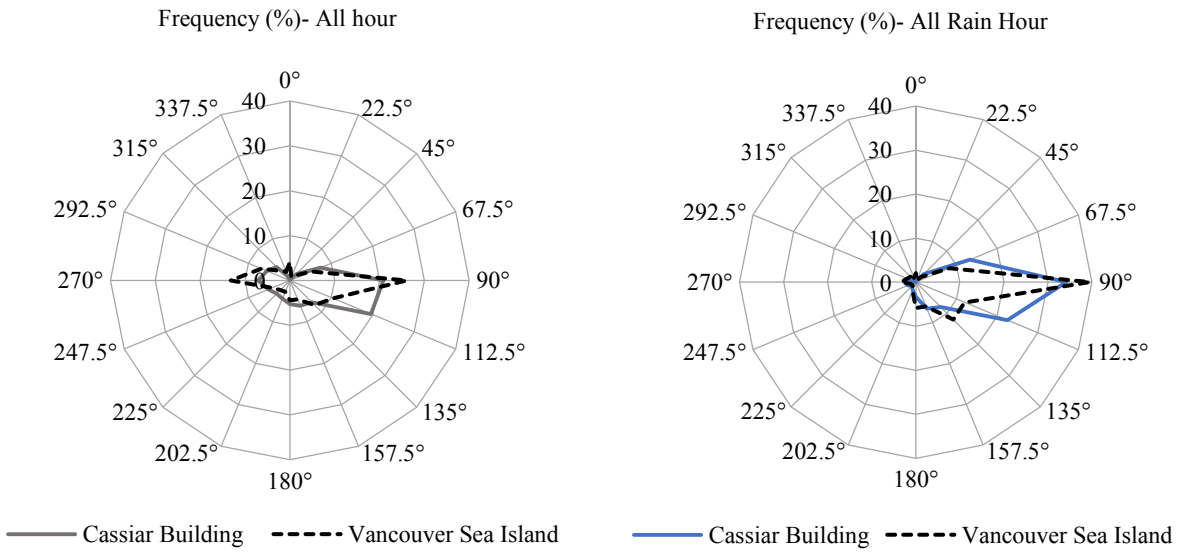


(a) (b)

Figure A.6 - Frequency of hourly wind direction (°) at the Cassier test building and Vancouver Sea (Period from August 16, 2013 to December 01, 2014)

Wind Speed:

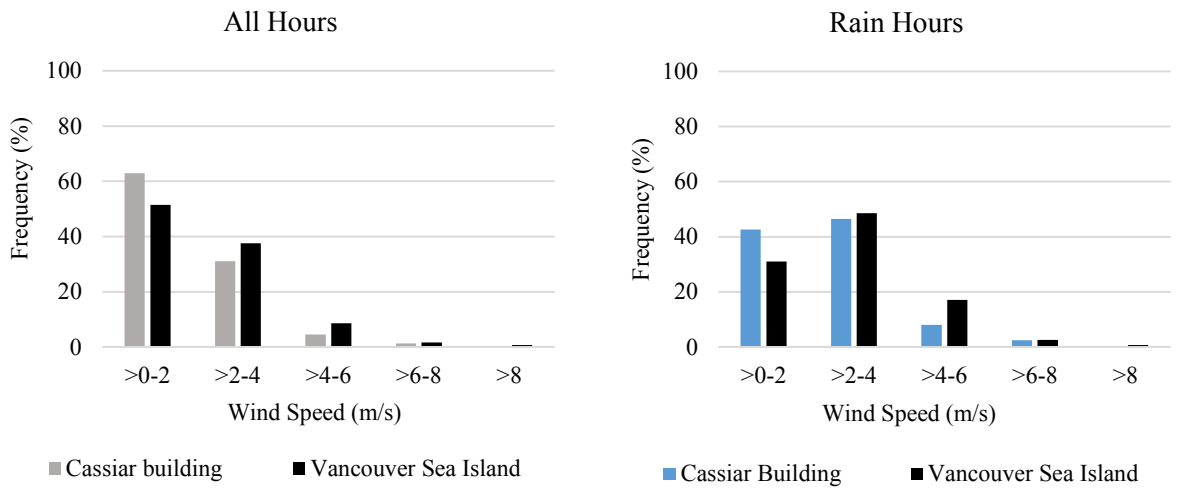


(a) (b)

Figure A.7 - Hourly wind speed (m/s) at the Cassier test building and Vancouver Sea (Period from August 16, 2013 to December 01, 2014)

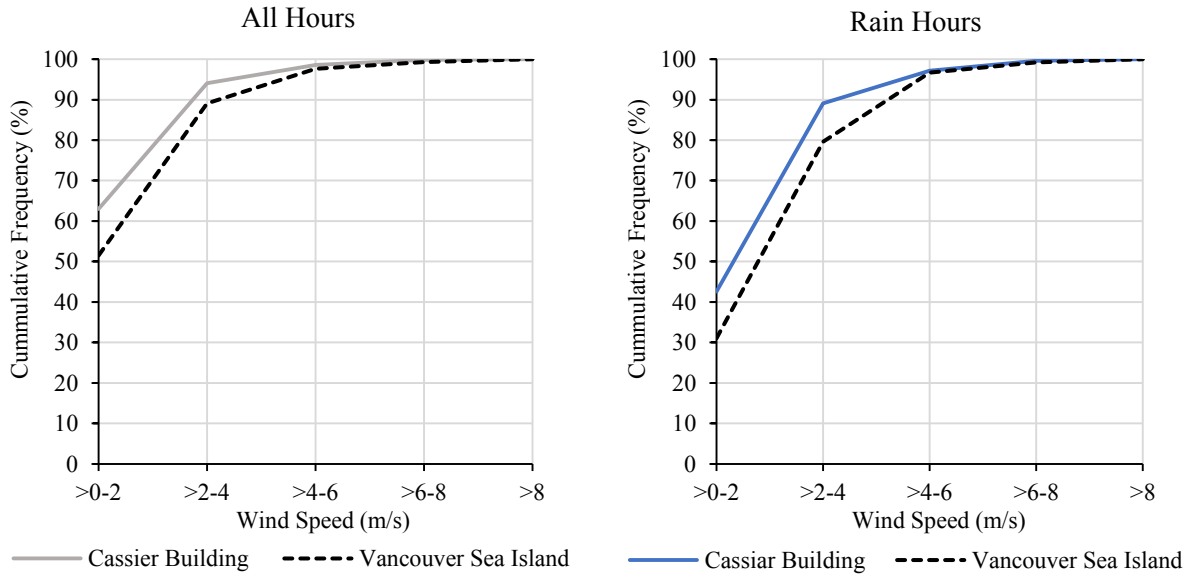


(a) (b)

Figure A.8 - Cumulative frequency of hourly wind speed (m/s) at the Cassier test building and Vancouver Sea (Period from August 16, 2013 to December 01, 2014)

**McLeod House, Fredericton, NW**

Table A.2 - Exposure type, elevation, reference height, gradient height, and mean speed exponent for Fredericton INTL Airport weather station and McLeod House

| | ***McLeod House, Fredericton, NB*** | ***Fredericton INTL Airport weather station*** |
|---|---|---|
| *Exposure* | *Suburban* | *Open country* |
| *Elevation (m)* | *97* | *20.7* |
| *Reference Height, $Z_{ref}$ (m)* | *26.8* | *10* |
| *Gradient Height, $Z_g$ (m)* | *400* | *300* |
| *Mean Speed Exponent ($\alpha$)* | *0.25* | *0.15* |

Wind Direction:

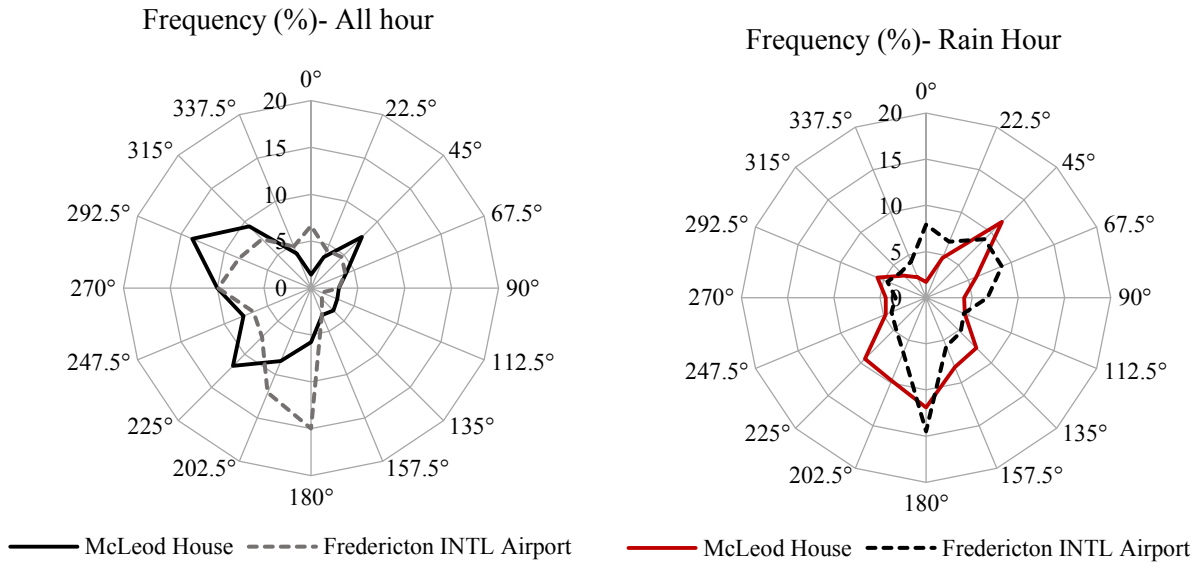


(a) (b)

Figure A.9 - Frequency of hourly wind direction (°) at the McLeod House test building and Fredericton INTL Airport (Period from June 21, 2015 to November 07, 2016)

Wind Speed:

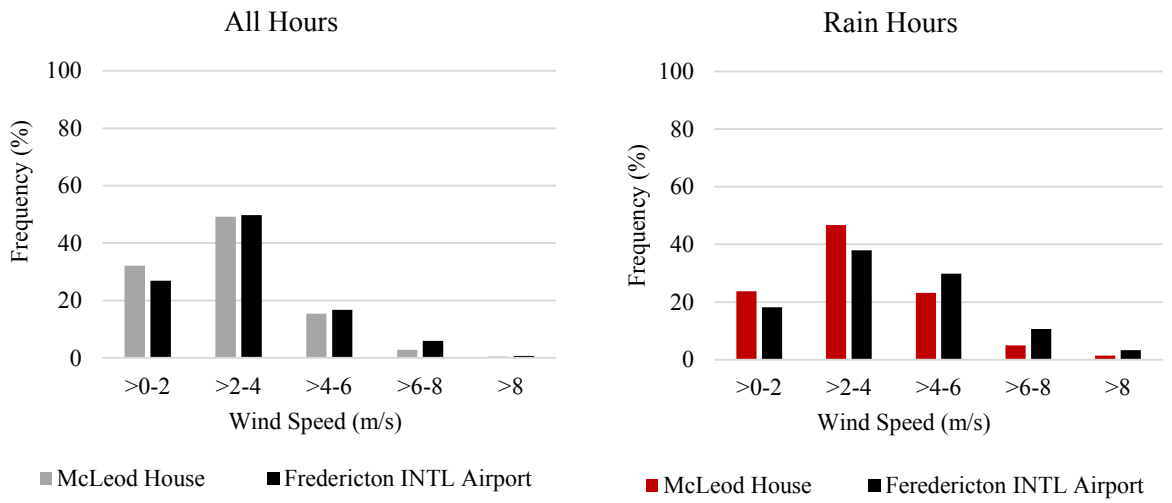


(a) (b)

Figure A.10 - Hourly wind speed (m/s) at the McLeod House test building and Fredericton INTL Airport (Period from June 21, 2015 to November 07, 2016)

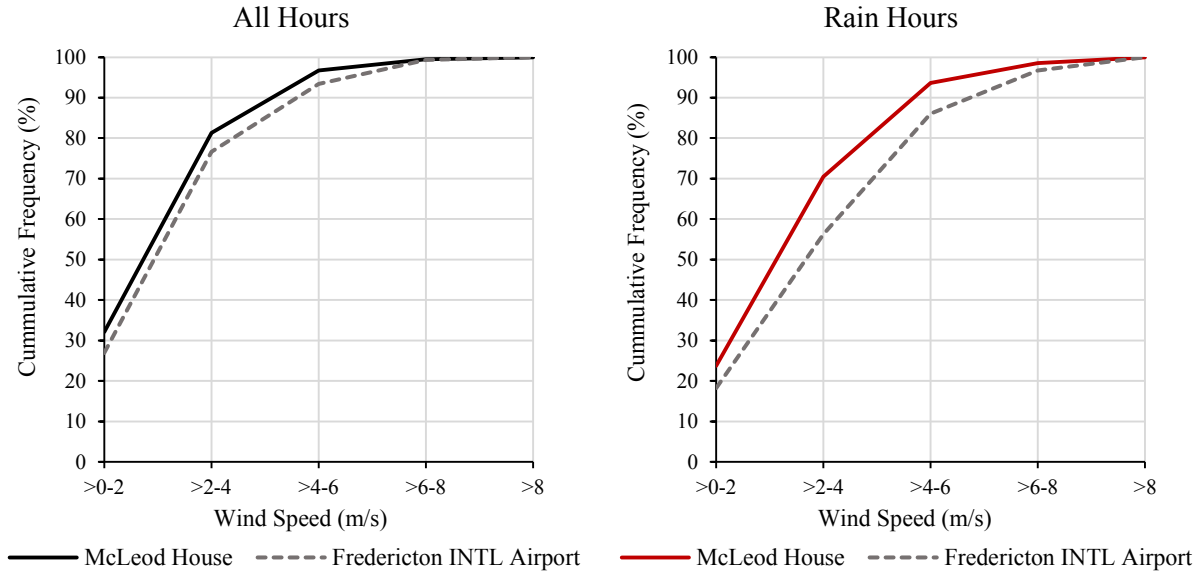


(a) (b)

Figure A.11 - Cumulative frequency of hourly wind speed (m/s) at the McLeod House test building and Fredericton INTL Airport (Period from June 21, 2015 to November 07, 2016)

**Concordia FB Building, Montreal, QC**

Table A.3- Exposure type, elevation, reference height, gradient height, and mean speed exponent for Montreal INTL Airport weather station and FB Building

| | ***FB Building, Montreal, QC*** | ***Montreal INTL Airport weather station*** |
|---|---|---|
| *Exposure* | *Urban* | *Open country* |
| *Elevation (m)* | *54.2* | *36* |
| *Reference Height, $Z_{ref}$ (m)* | *46* | *10* |
| *Gradient Height, $Z_g$ (m)* | *500* | *300* |
| *Mean Speed Exponent (α)* | *0.36* | *0.15* |

Wind Direction:

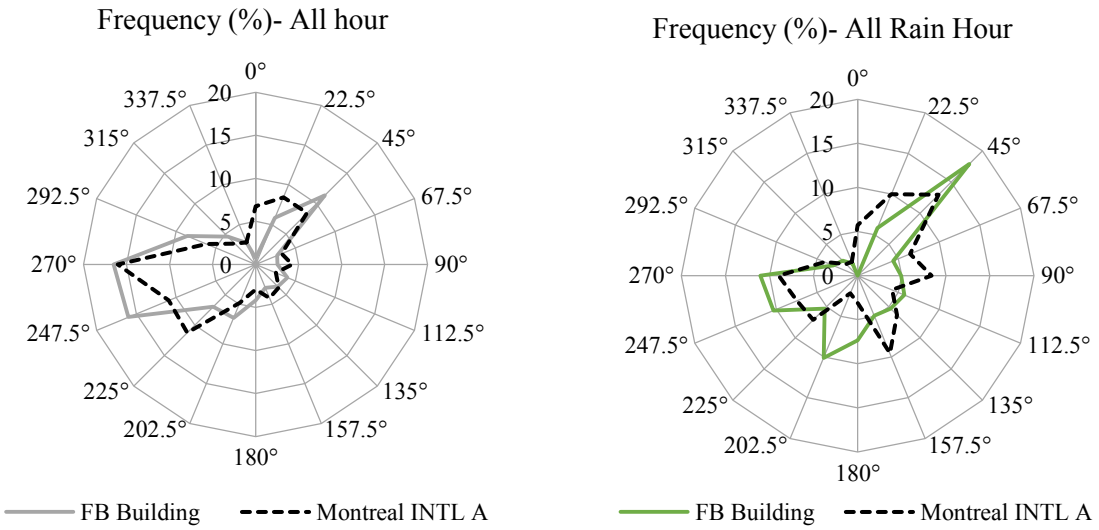


(a) (b)

Figure A.12- Frequency of hourly wind direction (°) at the FB Building test building and Montreal INTL Airport (Period from October 13, 2016 to July 13, 2017)

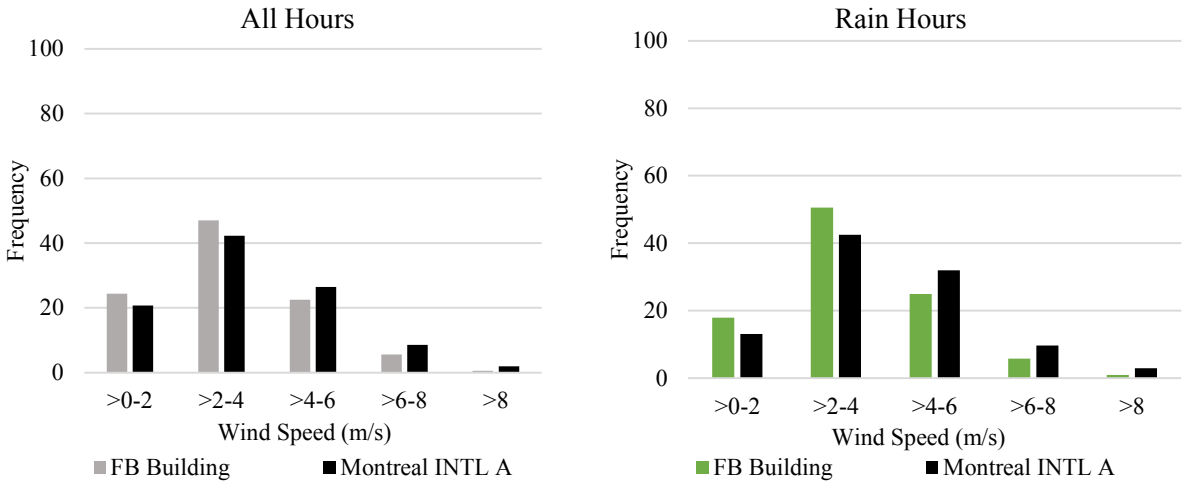


(a) (b)

Figure A.13 - Hourly wind speed (m/s) at the FB Building test building and Montreal INTL Airport (Period from October 13, 2016 to July 13, 2017)

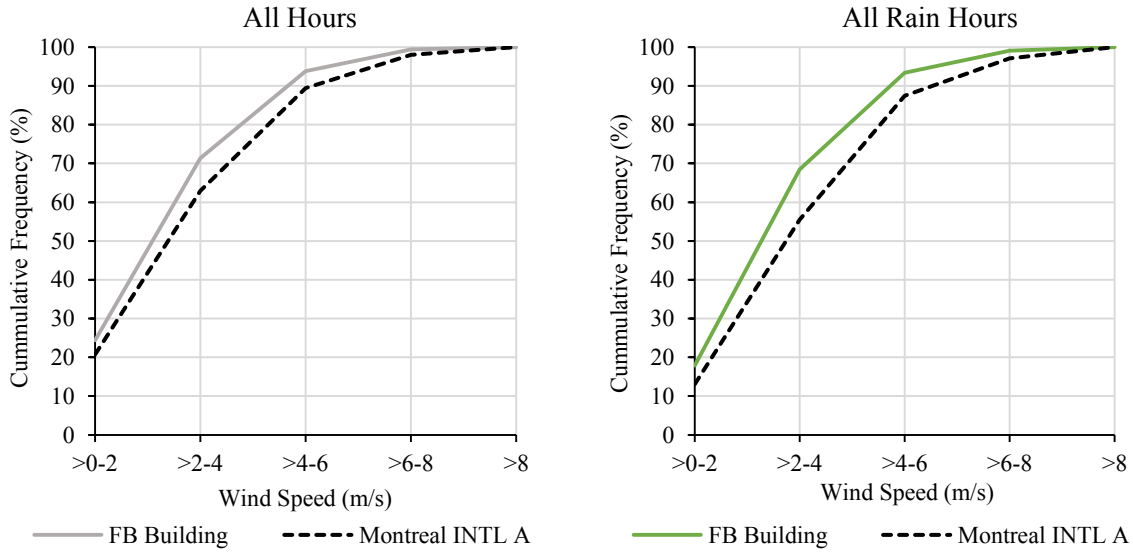


(a) (b)

Figure A.14 - Cumulative frequency of hourly wind speed (m/s) at the FB Building test building and Montreal INTL Airport (Period from October 13, 2016 to July 13, 2017)

Validity of power low and exposure type for wind speed conversion from weather station to the site for stable wind conditions

**McLeod House, Fredericton, NW**

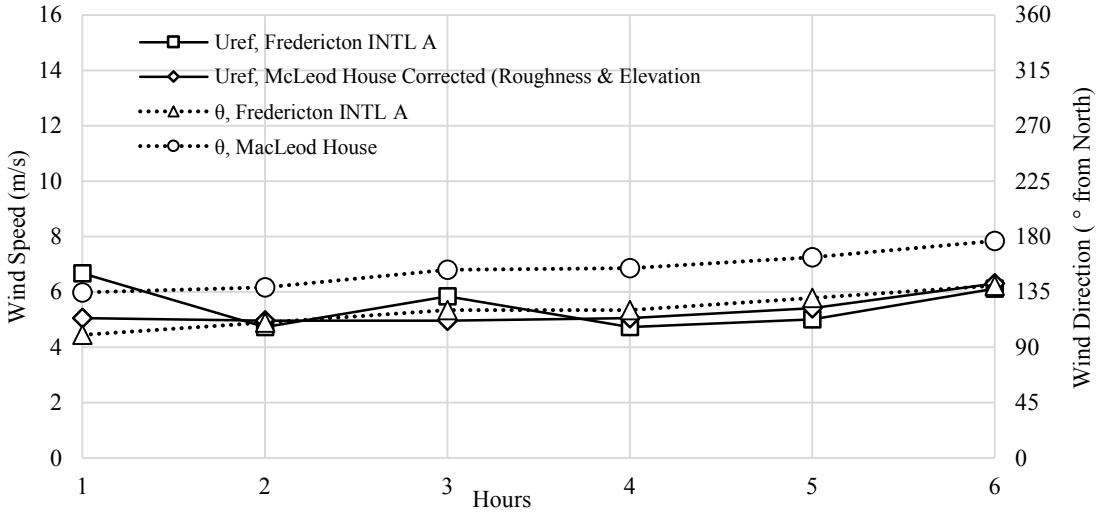


(a) South-west façade, October 29th ,2015 from 2:00 -8:00 AM

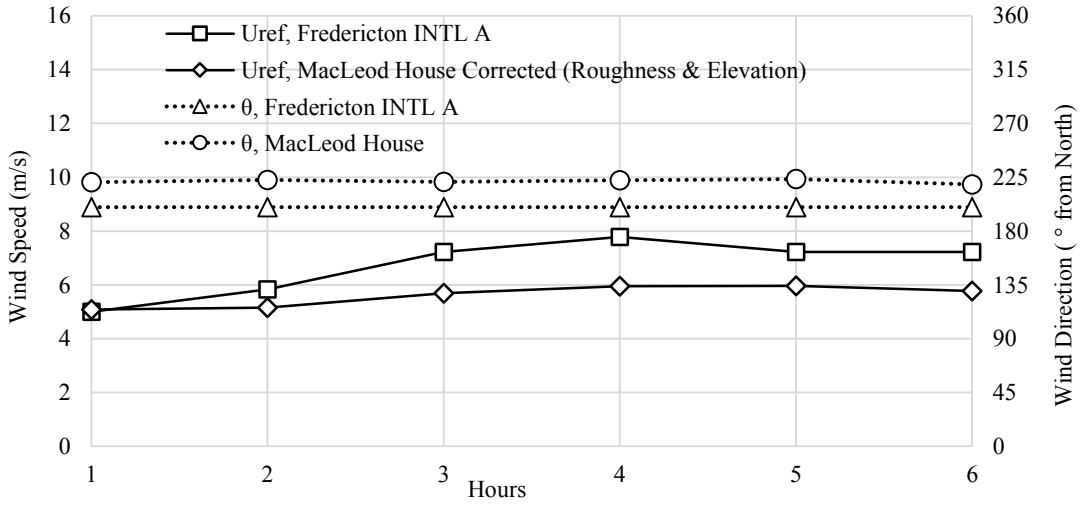


(b) South-east façade, November 26th and 27th, 2016 from 10:00 PM –1:00 AM

Figure A.15 - Wind speed at the McLeod House corrected to Fredericton INTL Airport, Average onsite WD (a) 150° and (b) 220° from the North

**Concordia FB Building, Montreal, QC**

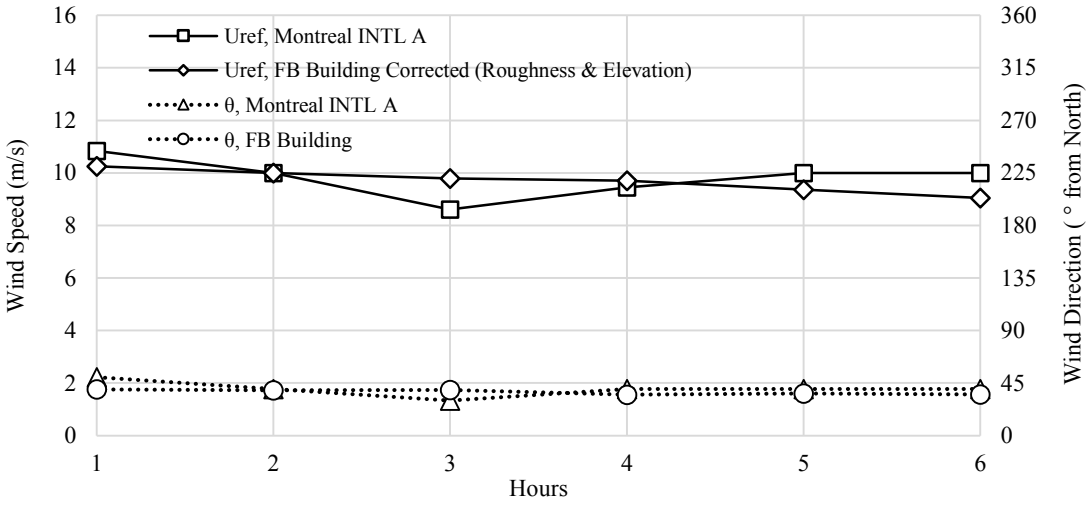


(a) North-east façade, October 23th ,2017 from 1:00 -6:00 AM

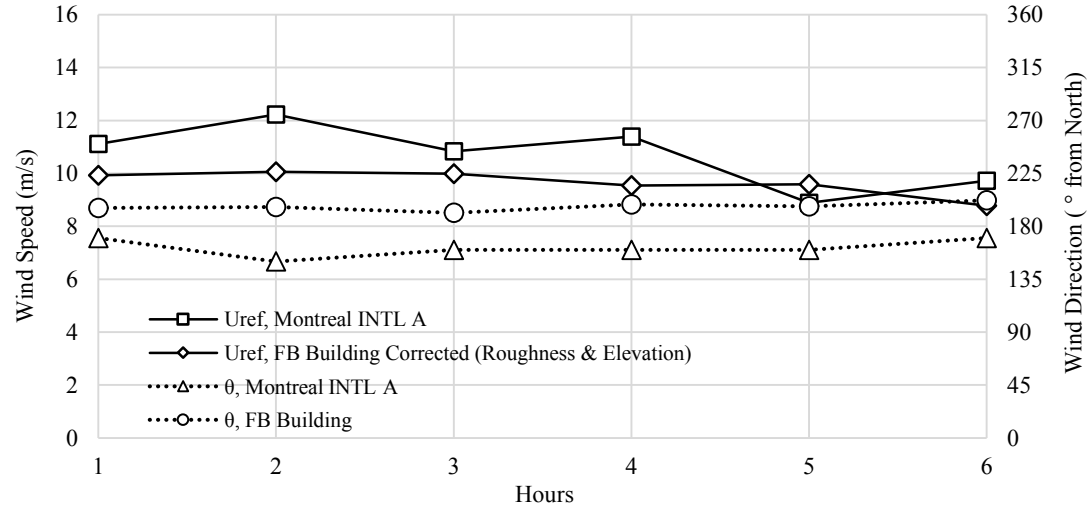


(b) South-east façade, January 11th ,2017 from 0:00 -5:00 AM

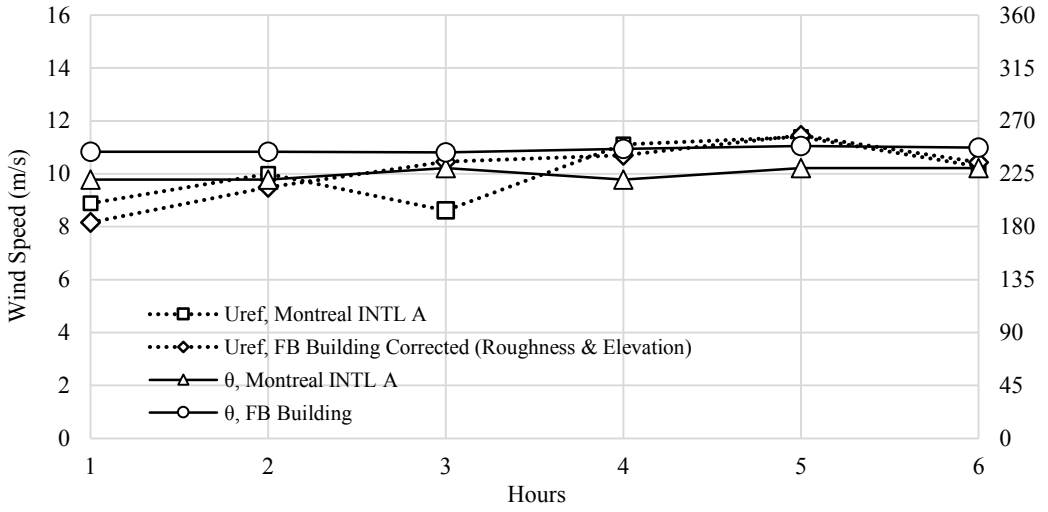


(c) South-west façade, May 18th ,2017 from 10:00 AM -3:00 PM

Figure A.16 - Wind speed at the FB Building corrected to Montreal INTL Airport, Average onsite WD (a) 40°, (b) 160° and (c) 225° from the North(Chiu, 2016)

**Cassiar building, Vancouver, BC**

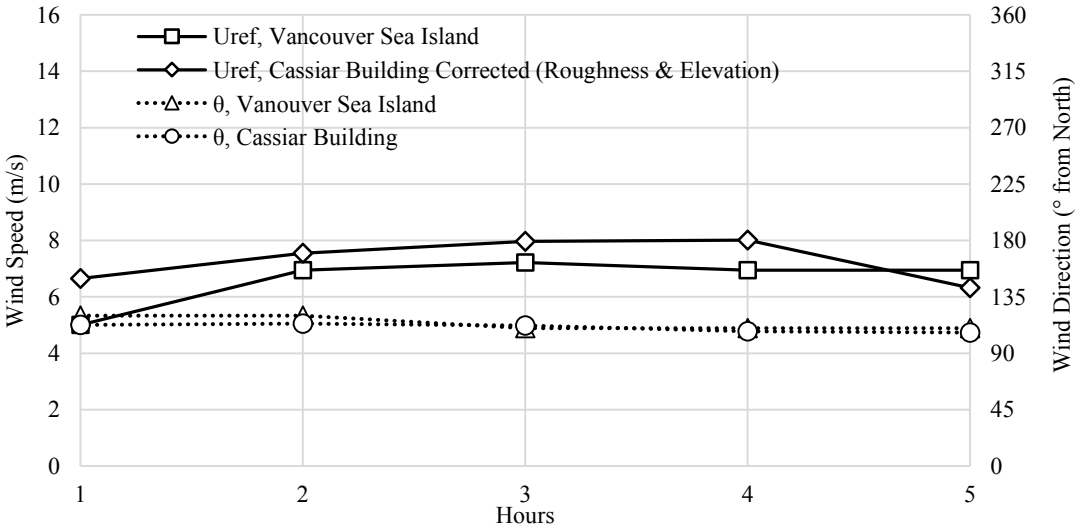


East façade, February 5th, 2014 from 14:00 to 18:00

Figure A.17- Wind speed at the Cassiar building corrected to Vancouver Sea Island, Average onsite WD 110° from the North(Chiu, 2016)

Validation of exposure type simulated in wind tunnel in comparison with onsite data

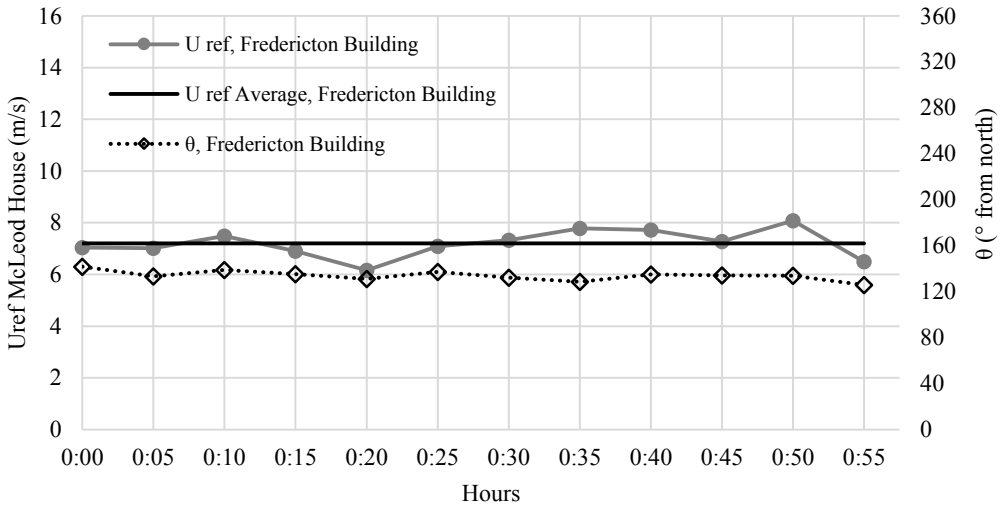


Figure A.18 - Five-minute data record for 1-hour, McLeod House Fredericton, November 1st 2016 12AM, WD south-east (135°)

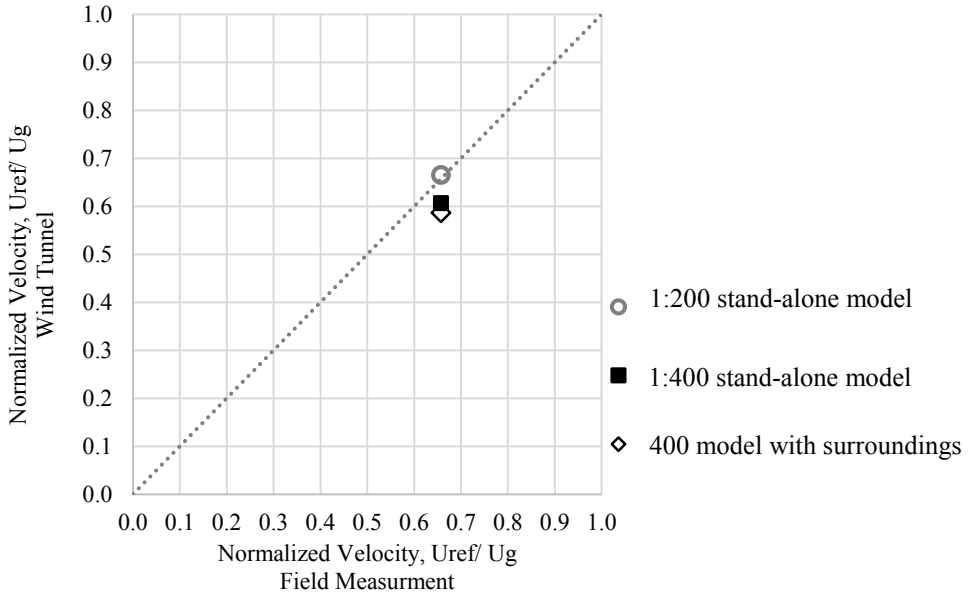


Figure A.19 - Comparison of the normalized velocity at the wind monitor location in the wind tunnel vs. in the field (Stand-alone test building, Scale 1:400 and 1:200, test building with surrounding, scale 1:400); for the direction θ=135° (South-east)

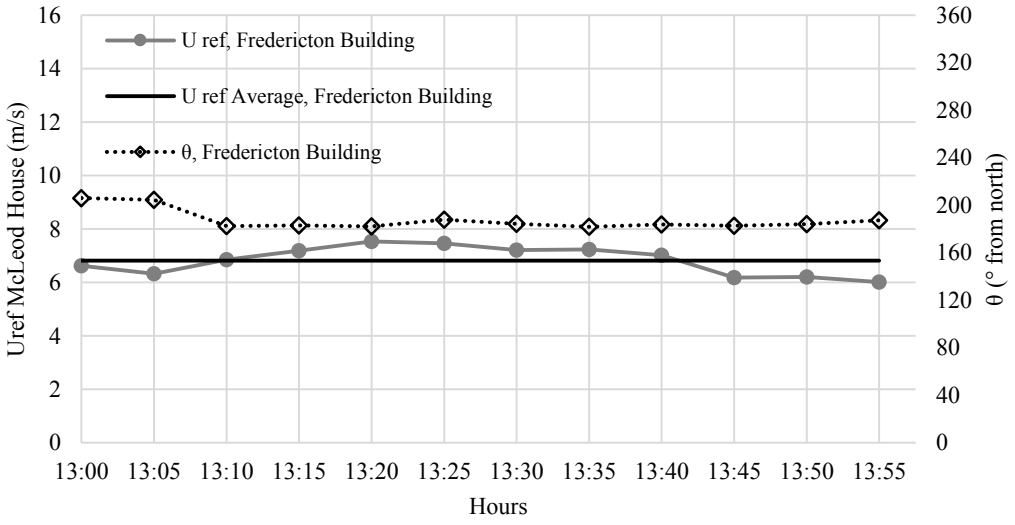


Figure A.20 - Five-minute data record for 1-hour, McLeod House Fredericton, February 25th t 2016 1 PM, WD south (180°)

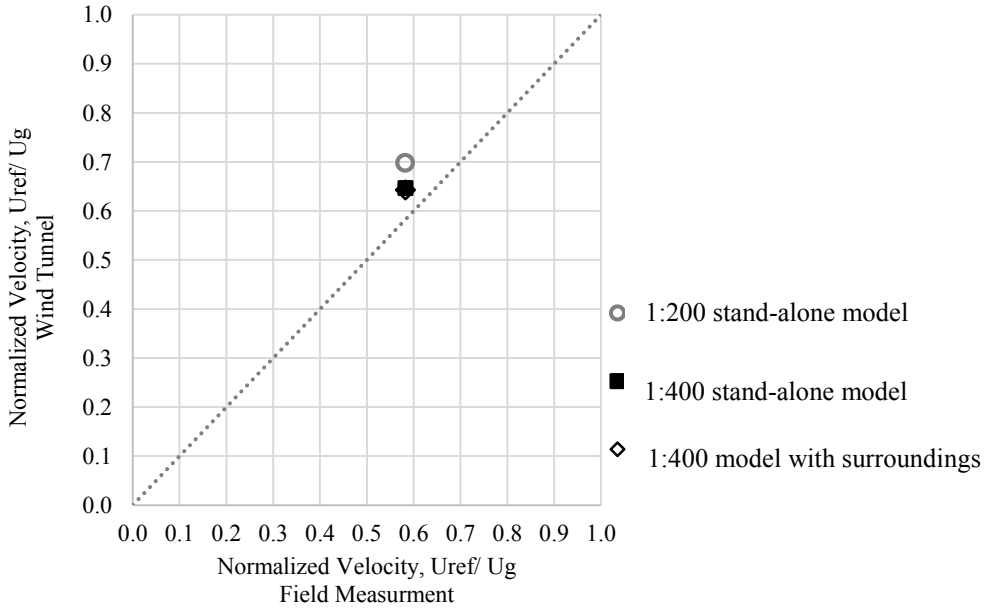


Figure A.21- Comparison of the normalized velocity at the wind monitor location in the wind tunnel vs. in the field (Stand-alone test building, Scale 1:400 and 1:200, test building with surrounding, scale 1:400); for the direction θ=180° (South)

**Example of similarity approach in calculation of overhang effectiveness:**

Table A.4shows the catch ratios on the east façade for two similar rain events, RE 6 during the period without overhang, and RE 54 during the period with the 0.9 m overhang. The comparison of onsite meteorological data indicates similar wind and rain characteristics between these two rain events that yield similar catch ratios on the gauges not sheltered by the overhang, which are the un-shaded values (EC1, EC2, ES1 to ES7). The wind and rain characteristics of these two rain events: (1) RE6: Oct. 12 2013 to Jan. 02 2014; total rainfall amount=111.5mm, no. of rain hours=161 hours, average wind speed =1.52m/s, average arithmetic wind direction=120$^{o}$ and average rain fall intensity=0.7mm/hr. (2) RE54: Oct. 19 2016 to Oct. 30 2016; Total rainfall amount=103.4mm, no. of rain hours=110 hours, average wind speed =1.64m/s, average arithmetic wind direction=115$^{o}$, average rain fall intensity=1mm/hr.

Table A.4 - Catch ratios and overhang effectiveness on the east façade for rain events 6 and 54.

| WDR Gauge | Catch Ratios | | Overhang Effectiveness (%) |
|---|---|---|---|
| | RE 6 (No OH) | RE 54 (0.9 m OH) | |
| EN1 | 0.108 | 0.022 | 80 |
| EN2 | 0.096 | 0.036 | 63 |
| EN3 | 0.049 | 0.042 | 15 |
| EN4 | 0.038 | 0.026 | 33 |
| EN5 | 0.093 | 0.003 | 97 |
| EN6 | 0.050 | 0.012 | 76 |
| EN7 | 0.034 | 0.012 | 63 |
| EN8 | 0.093 | 0.001 | 99 |
| EN9 | 0.045 | 0.010 | 78 |
| EC1 | 0.101 | 0.105 | |
| EC2 | 0.021 | 0.018 | |
| ES1 | 0.111 | 0.101 | |
| ES2 | 0.062 | 0.061 | |
| ES3 | n/a | 0.054 | |
| ES4 | 0.025 | 0.019 | |
| ES5 | 0.085 | 0.100 | |
| ES6 | 0.057 | 0.044 | |
| ES7 | 0.035 | 0.029 | |

** Shaded rows catch ratios for WDR gauges located under the retractable overhang. Data for gauge ES3 was not available during this period due to hardware malfunction.*

# B. APPENDIX B

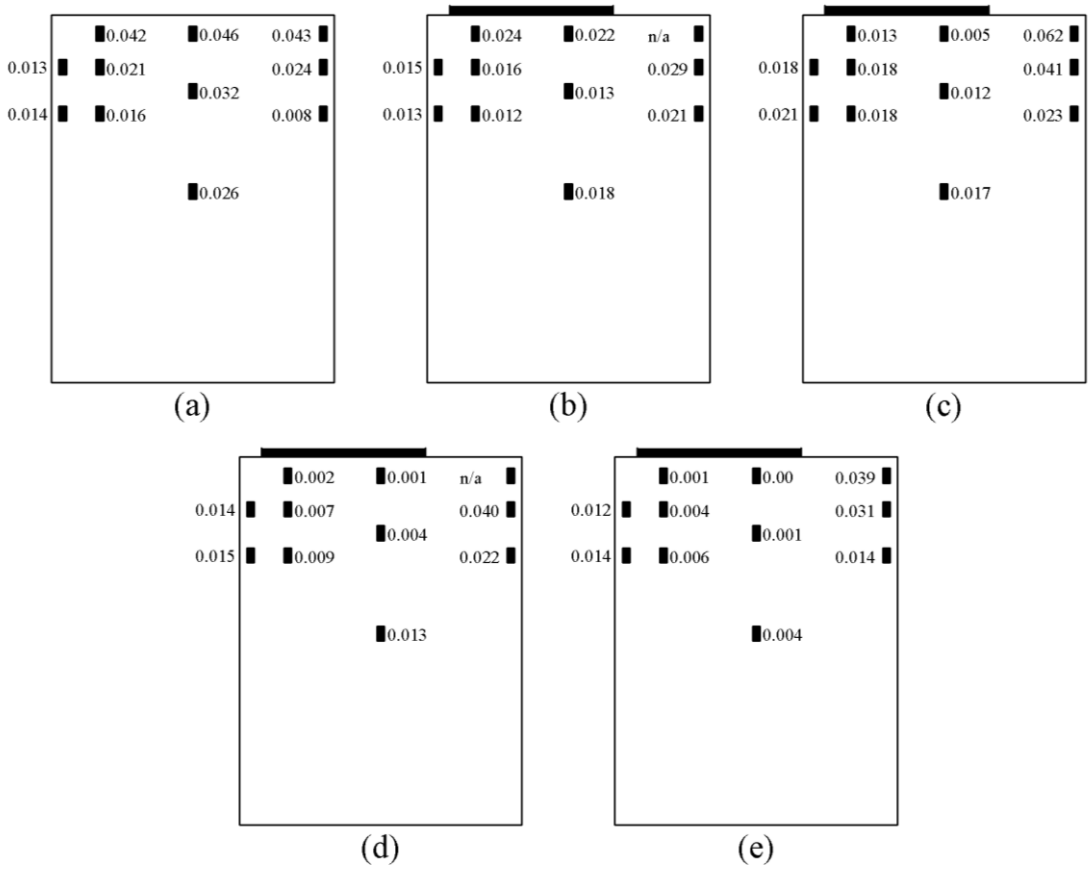


Figure B.1- Catch ratio on the north facade (a) no overhang; (b) 0.3 m overhang, (c) 0.6 m overhang, (d) 0.9 m overhang and (e) 1.2 m overhang, Cassier building, Vancouver

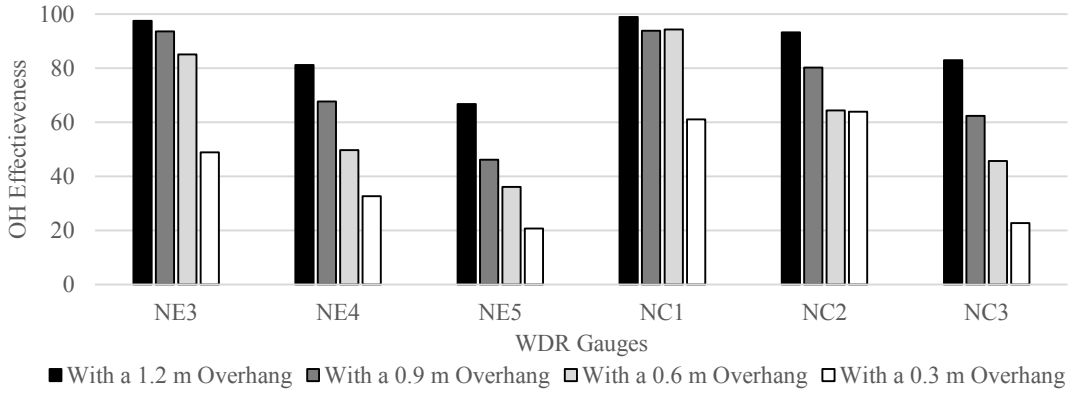


Figure B.2 - Effectiveness of overhangs on the North façade of Cassiar Building, Vancouver

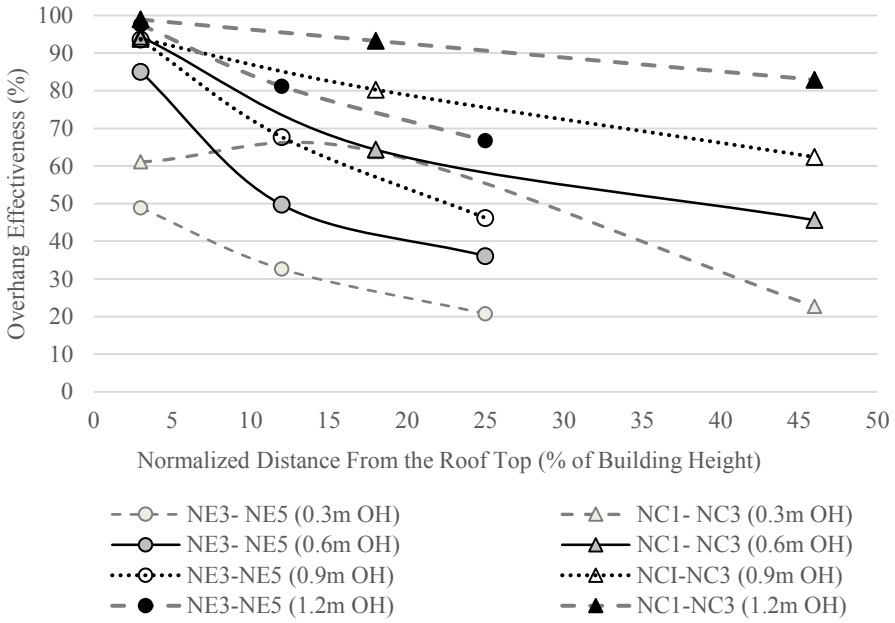


Figure B.3 - Overhang effectiveness on the north façade with respect to normalized distance from the roofline, Cassiar Building, Vancouver

The comparison of overhang effectiveness for different measurement points based on two different approach of symmetry and similarity.

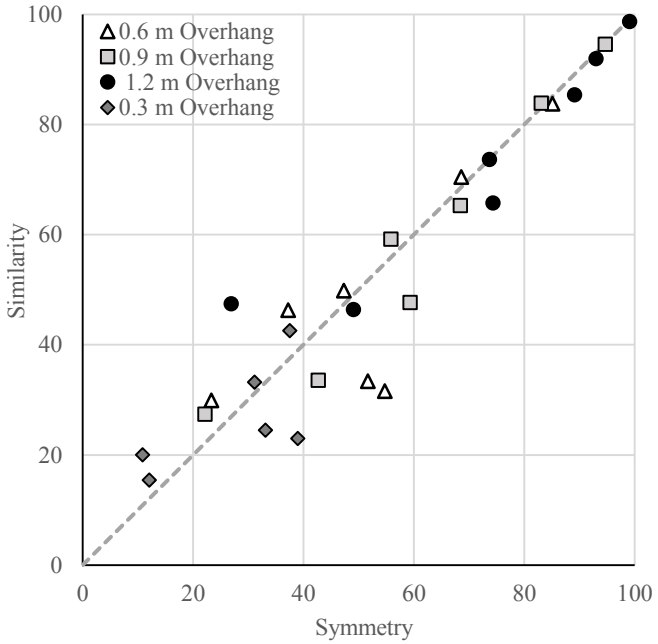


Figure B.4 - Comparison of overhang effectiveness calculated using similarity and symmetry approaches for gauges on the east façade

# C. Appendix C

Normalized Wind velocity near MacLeod House for inclined wind directions in compare with Vancouver experiment

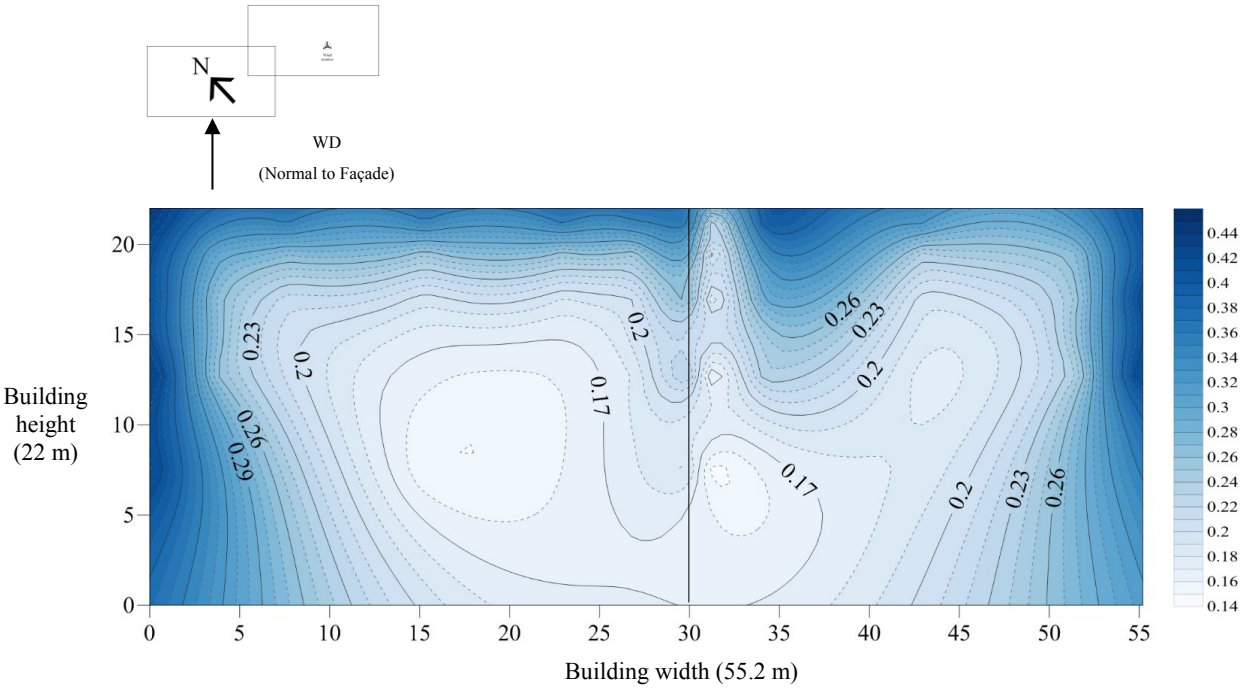


(a)

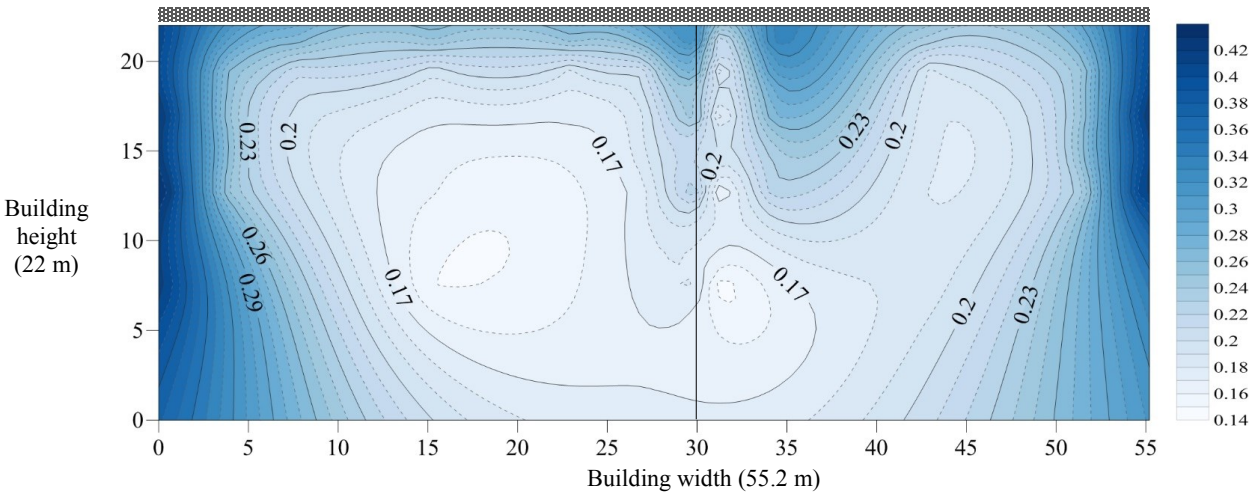


(b)

Figure C.1- Wind velocities on south-west façade of Fredericton model for normal wind direction, 1:200 stand-alone model; (a) without overhang and (b) with overhang

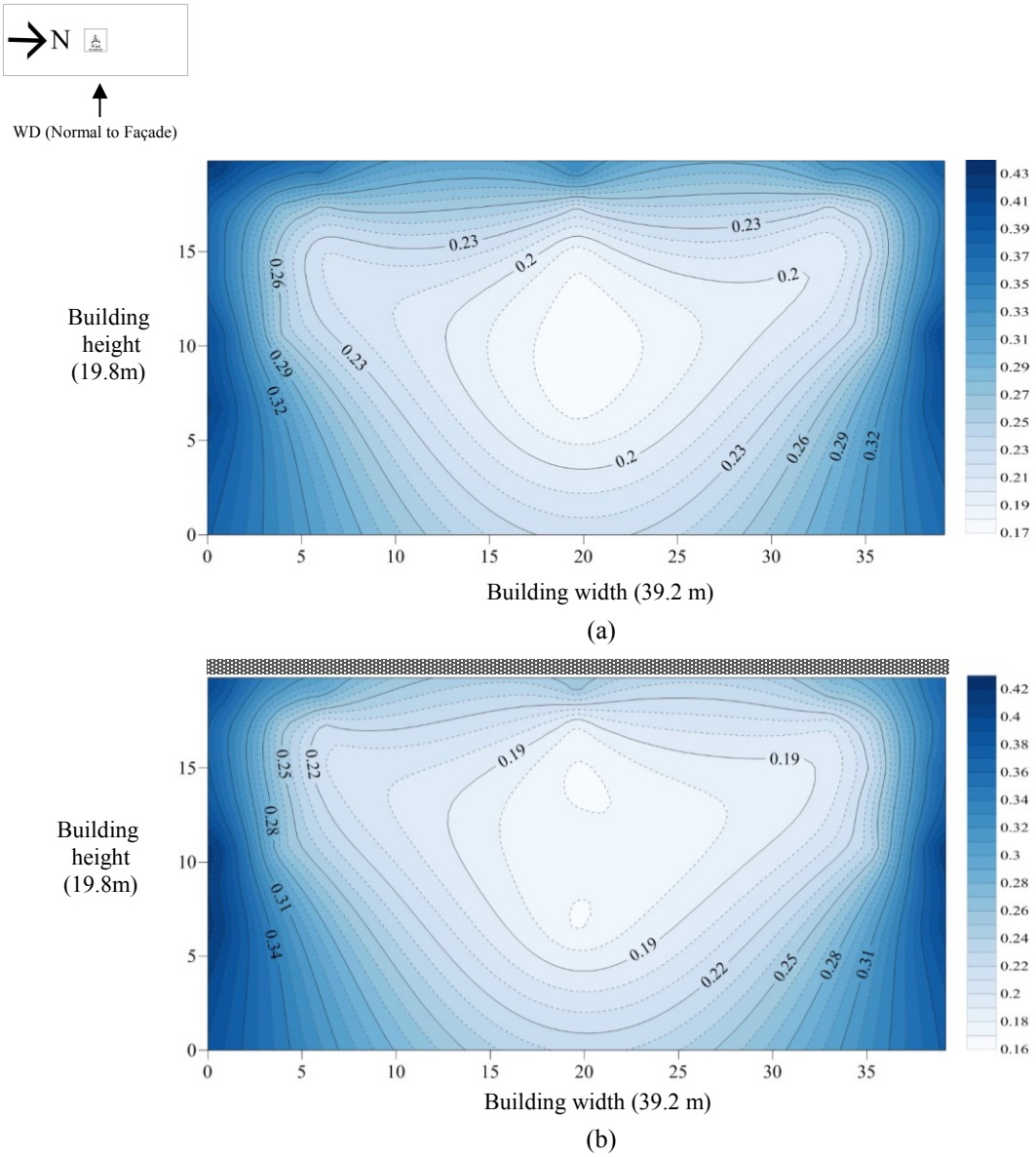


Figure C.2– Wind velocities on east of Vancouver model for normal wind direction, 1:200 stand-alone model; (a) without overhang and (b) with overhang

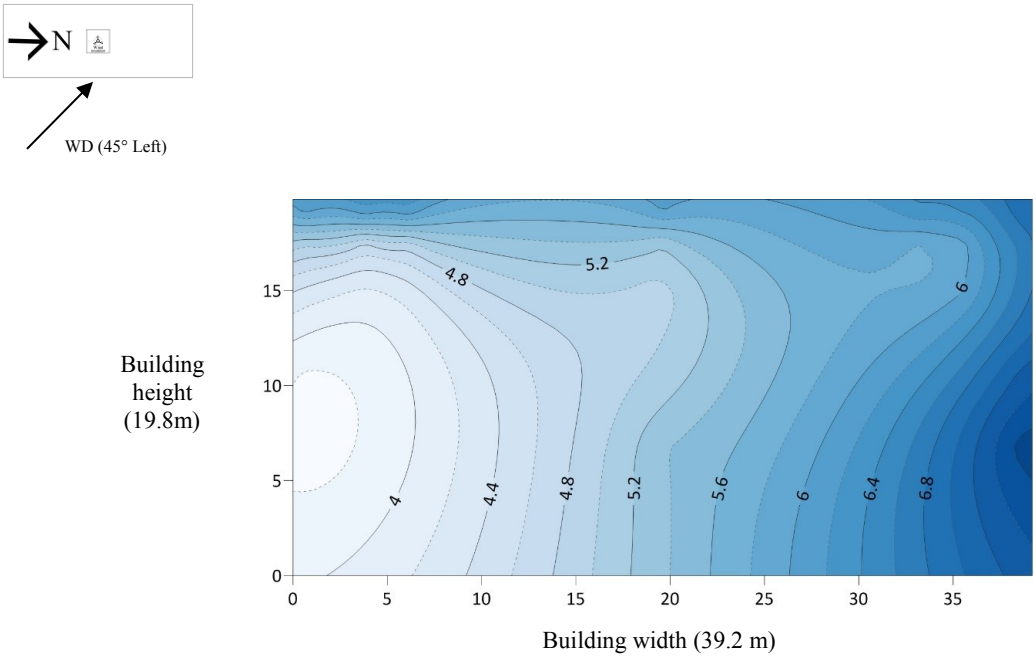


Figure C.3– Wind velocities on east façade of Cassiar Building, Model scale: 1/200, standalone building without overhang, θ = 45° (from south-east)

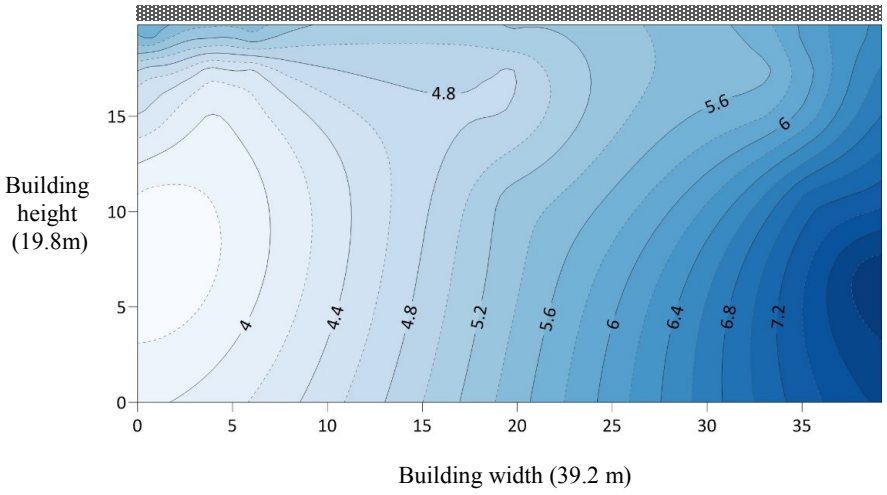


Figure C.4 - Wind velocities on east façade of Cassiar Building, 1:200 stand-alone standalone model for (a) without overhang and (b) with overhang, wind direction θ = 45° (from south-east)

# D. Appendix D

Calculated catch ratios at the place of WDR gauges on windward facades of study buildings.

Vancouver

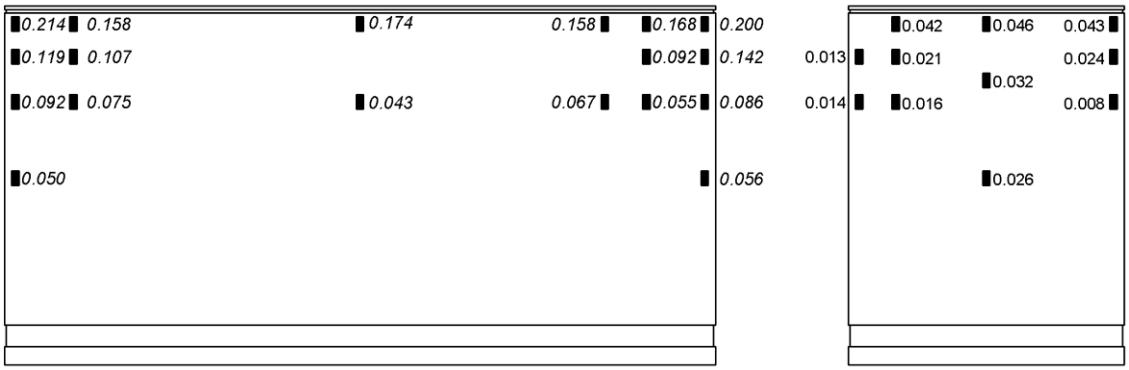


(a) (b)

Figure D.1- Catch ratio values at rain gauge locations on the (a) east and (b) north façade of Cassiar Building for the period of NO OH, Vancouver

Fredericton

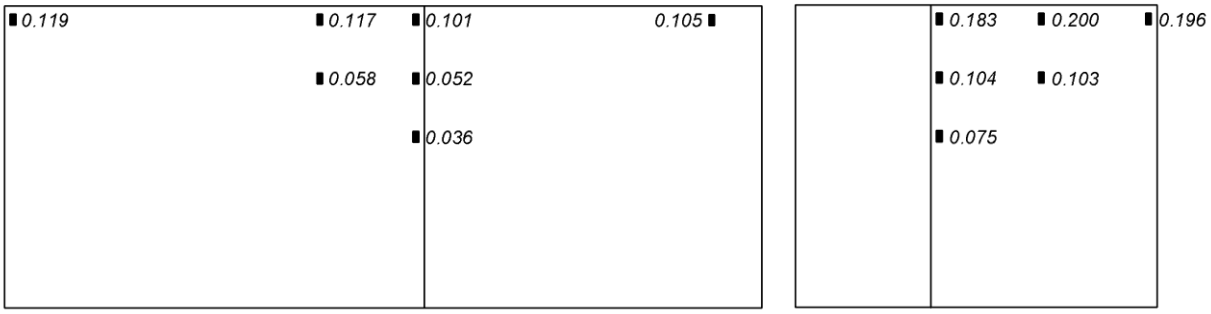


(a) (b)

Figure D.2- Catch ratio values at rain gauge locations on the (a) south-west and (b) south-east façade of McLeod House, Fredericton

Montreal

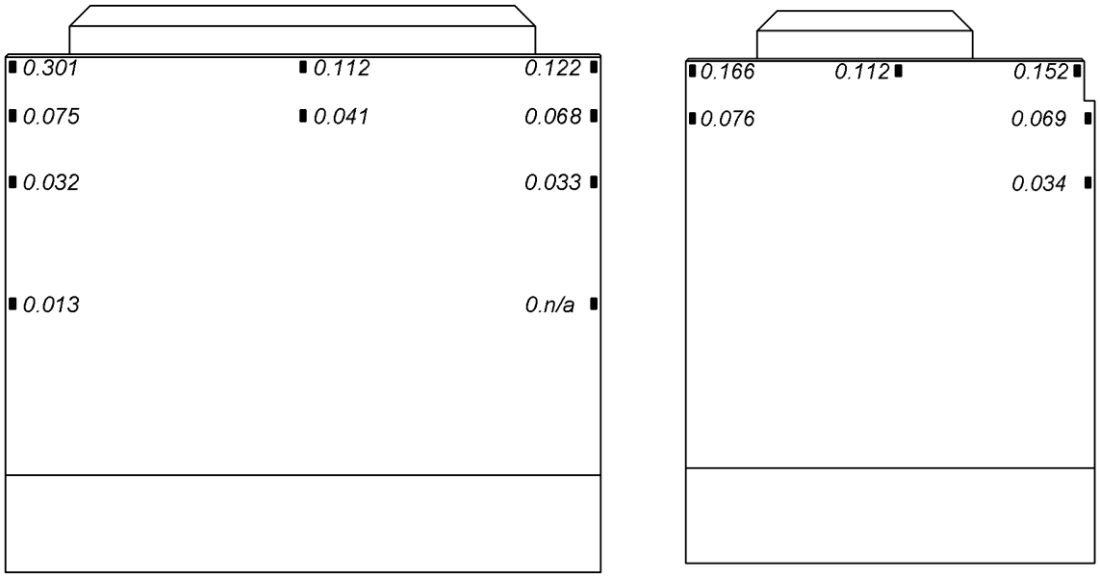


(a) (b)

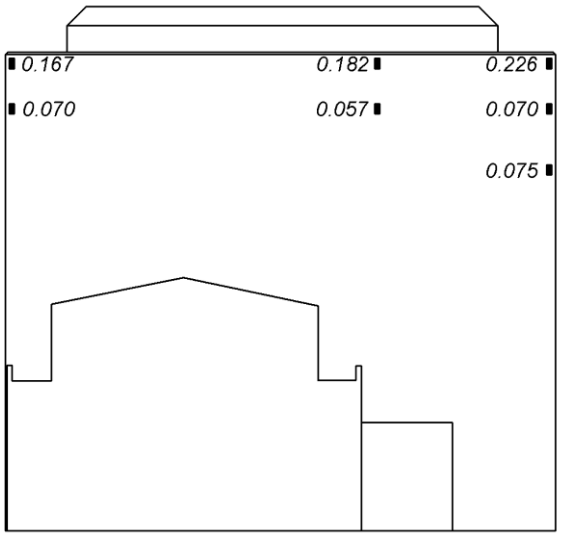


(c)

Figure D.3 - Catch ratio values at rain gauge locations on the (a) south-west, (b) south-east and (c) north-east façade of FB Building, Montreal

Estimation of wall indices at the place of WDR gauges calculated by applying ISO wall factor, calculated hourly and 5-min wall factor in compare with measured amount of WDR

Vancouver

Table D.1- Comparison of measured WDR, ISO wall indices and calculated wall indices considering wall factors calculated based on different time resolutuion, Cassiar Building, No OH period, Vancouver

| ***Cassiar Building, Vancouver, NO OH*** | | | | | | | | | |
|---|---|---|---|---|---|---|---|---|---|
| Distance from the Roof Top | WDR Gauges | ISO Standard | Measured WDR (mm) | Hourly Data | | | 5- min Data | | |
| | | | | Calculated Wall Indices | Wall Factor | | Calculated Wall Indices | Wall Factor | |
| 0.6 m | **EN1** | 494.42 | 405.00 | 486.31 | 0.49 | -20% | 399.23 | 0.40 | 1% |
| | **EN5** | 494.42 | 339.82 | 408.04 | 0.41 | -20% | 334.98 | 0.34 | 1% |
| | **EN8** | 494.42 | 319.03 | 383.08 | 0.39 | -20% | 314.49 | 0.32 | 1% |
| | **EC1** | 494.42 | 352.43 | 423.18 | 0.43 | -20% | 347.41 | 0.35 | 1% |
| | **ES5** | 494.42 | 320.57 | 384.93 | 0.39 | -20% | 316.01 | 0.32 | 1% |
| | **ES1** | 494.42 | 432.65 | 519.51 | 0.53 | -20% | 426.49 | 0.43 | 1% |
| 2.4 m | **EN2** | 482.51 | 287.44 | 345.37 | 0.36 | -20% | 283.53 | 0.29 | 1% |
| | **EN6** | 482.51 | 185.37 | 222.73 | 0.23 | -20% | 182.85 | 0.19 | 1% |
| | **ES6** | 482.51 | 216.82 | 260.52 | 0.27 | -20% | 213.87 | 0.22 | 1% |
| | **ES2** | 482.51 | 241.80 | 290.53 | 0.30 | -20% | 238.51 | 0.25 | 1% |
| 4.9 m | **EN3** | 185.84 | 173.68 | 208.68 | 0.22 | -20% | 171.31 | 0.18 | 1% |
| | **EN7** | 185.84 | 112.30 | 134.93 | 0.15 | -20% | 110.77 | 0.12 | 1% |
| | **EN9** | 185.84 | 135.49 | 162.79 | 0.18 | -20% | 133.64 | 0.14 | 1% |
| | **EC2** | 185.84 | 86.88 | 104.39 | 0.11 | -20% | 85.70 | 0.09 | 1% |
| | **ES7** | 185.84 | 150.92 | 181.33 | 0.20 | -20% | 148.86 | 0.16 | 1% |
| | **ES3** | 185.84 | 73.60 | 80.08 | 0.27 | -9% | 67.10 | 0.23 | 9% |
| 9.1 m | **EN4** | 169.83 | 112.45 | 135.72 | 0.17 | -21% | 111.54 | 0.14 | 1% |
| | **ES4** | 169.83 | 101.13 | 120.79 | 0.14 | -19% | 99.16 | 0.12 | 2% |
| | | | | | | | | | |
| 0.6 m | **NW1** | 74.96 | 53.18 | 102.64 | 0.68 | -93% | 53.87 | 0.36 | -1% |
| | **NC1** | 74.96 | 67.29 | 129.88 | 0.87 | -93% | 66.52 | 0.45 | 1% |
| | **NE3** | 74.96 | 62.16 | 119.98 | 0.80 | -93% | 60.30 | 0.42 | 3% |
| 2.4 m | **NW2** | 73.15 | 33.01 | 63.75 | 0.44 | -93% | 33.46 | 0.23 | -1% |
| | **NE4** | 73.15 | 31.60 | 61.03 | 0.42 | -93% | 32.03 | 0.22 | -1% |
| | **NE1** | 73.15 | 18.79 | 36.29 | 0.25 | -93% | 19.05 | 0.13 | -1% |
| 3.7 m | **NC2** | 28.71 | 46.48 | 89.78 | 0.63 | -93% | 47.12 | 0.33 | -1% |
| 4.9 m | **NW3** | 28.17 | 11.93 | 23.04 | 0.16 | -93% | 12.09 | 0.09 | -1% |
| | **NE5** | 28.17 | 23.33 | 45.06 | 0.32 | -93% | 23.65 | 0.17 | -1% |
| | **NE2** | 28.17 | 20.31 | 39.22 | 0.28 | -93% | 20.59 | 0.15 | -1% |
| 9.1 m | **NC3** | 25.75 | 36.64 | 70.34 | 0.55 | -92% | 36.92 | 0.29 | -1% |

Fredericton

Table D.2- Comparison of measured WDR, ISO wall indices and calculated wall indices considering wall factors calculated based on different time resolutuion, McLeod House, Fredericton

| ***McLeod House, Fredericton*** | | | | | | | | | |
|---|---|---|---|---|---|---|---|---|---|
| Distance from the Roof Top | WDR Gauges | ISO Standard | Measured WDR (mm) | Hourly Data | | | 5- min Data | | |
| | | | | Calculated Wall Indices | Wall Factor | | Calculated Wall Indices | Wall Factor | |
| 0.6 m | **SE1** | 170.68 | 169.34 | 118.74 | 0.35 | 30% | 96.68 | 0.28 | 43% |
| | **SW1** | 170.68 | 162.28 | 113.62 | 0.33 | 30% | 92.51 | 0.27 | 43% |
| | **SW4** | 170.68 | 188.85 | 132.23 | 0.39 | 30% | 107.66 | 0.32 | 43% |
| | **SW6** | 170.68 | 191.94 | 134.32 | 0.39 | 30% | 109.37 | 0.32 | 43% |
| 4.9 m | **SW2** | 64.71 | 83.80 | 58.93 | 0.18 | 30% | 47.98 | 0.15 | 43% |
| | **SW5** | 64.71 | 93.84 | 65.95 | 0.20 | 30% | 53.69 | 0.17 | 43% |
| 9.1 m | **SW3** | 60.12 | 58.22 | 40.93 | 0.14 | 30% | 33.33 | 0.11 | 43% |
| | | | | | | | | | |
| 0.6 m | **E1** | 255.62 | 295.32 | 331.90 | 0.65 | -12% | 275.60 | 0.54 | 7% |
| | **E4** | 255.62 | 321.88 | 361.67 | 0.71 | -12% | 300.32 | 0.59 | 7% |
| | **E6** | 255.62 | 316.45 | 355.24 | 0.69 | -12% | 294.98 | 0.58 | 7% |
| 4.9 m | **E2** | 96.92 | 166.72 | 187.77 | 0.39 | -13% | 155.92 | 0.32 | 6% |
| | **E5** | 96.92 | 165.85 | 186.90 | 0.39 | -13% | 155.20 | 0.32 | 6% |
| 9.1 m | **E3** | 90.05 | 120.50 | 135.45 | 0.30 | -12% | 112.48 | 0.25 | 7% |

Montreal

Table D.3 - Comparison of measured WDR, ISO wall indices and calculated wall indices considering wall factors calculated based on different time resolutuion, FB Building, Montreal

| *FB Building, Montreal* | | | | | | | | | |
|---|---|---|---|---|---|---|---|---|---|
| Distance from the Roof Top | WDR Gauges | ISO Standard | Measured WDR (mm) | Hourly Data | | | 5- min Data | | |
| | | | | Calculated Wall Indices | Wall Factor | | Calculated Wall Indices | Wall Factor | |
| 0.6 m | **NE1** | 305.17 | 180.41 | 317.37 | 0.52 | -76% | 245.41 | 0.40 | -36% |
| | **NE5** | 305.17 | 172.30 | 303.10 | 0.50 | -76% | 234.37 | 0.38 | -36% |
| | **NE7** | 305.17 | 186.87 | 328.73 | 0.54 | -76% | 254.19 | 0.42 | -36% |
| 4.9 m | **NE2** | 118.87 | 115.42 | 204.95 | 0.34 | -78% | 158.48 | 0.27 | -37% |
| | **NE6** | 118.87 | 62.51 | 111.00 | 0.19 | -78% | 85.83 | 0.14 | -37% |
| | **NE8** | 118.87 | 104.03 | 184.72 | 0.31 | -78% | 142.84 | 0.24 | -37% |
| 10.7 m | **NE3** | 113.95 | 49.12 | 88.36 | 0.16 | -80% | 68.32 | 0.12 | -39% |
| | **NE9** | 113.95 | 50.48 | 90.80 | 0.16 | -80% | 70.22 | 0.12 | -39% |
| 21.3 m | **NE4** | 102.26 | 19.35 | 35.62 | 0.07 | -84% | 27.54 | 0.05 | -42% |
| | NE10 | 102.26 | 3.61 | 6.64 | 0.01 | -84% | 5.14 | 0.01 | -42% |
| | | | | | | | | | |
| 0.6 m | **SE1** | 314.36 | 176.93 | 298.09 | 0.65 | -68% | 242.09 | 0.53 | -37% |
| | **SE3** | 314.36 | 131.84 | 263.43 | 0.53 | -100% | 227.79 | 0.46 | -73% |
| | **SE4** | 314.36 | 233.25 | 430.37 | 0.68 | -85% | 352.45 | 0.56 | -51% |
| 4.9 m | **SE2** | 122.45 | 117.29 | 218.44 | 0.36 | -86% | 178.89 | 0.29 | -53% |
| | **SE5** | 122.45 | 105.54 | 196.56 | 0.32 | -86% | 160.97 | 0.26 | -53% |
| 10.7 m | **SE6** | 117.38 | 52.99 | 99.98 | 0.17 | -89% | 81.88 | 0.14 | -55% |
| | | | | | | | | | |
| 0.6 m | **SW1** | 251.44 | 257.42 | 290.26 | 0.58 | -13% | 218.38 | 0.43 | 15% |
| | **SW3** | 251.44 | 279.74 | 315.43 | 0.63 | -13% | 239.35 | 0.48 | 14% |
| | **SW5** | 251.44 | 192.89 | 221.08 | 0.69 | -15% | 174.08 | 0.54 | 10% |
| 4.9 m | **SW2** | 97.94 | 108.21 | 123.16 | 0.25 | -14% | 92.36 | 0.19 | 15% |
| | **SW4** | 97.94 | 87.46 | 99.54 | 0.20 | -14% | 74.53 | 0.15 | 15% |
| | **SW6** | 97.94 | 106.95 | 121.73 | 0.25 | -14% | 90.84 | 0.19 | 15% |
| 10.7 m | **SW7** | 93.89 | 44.70 | 46.21 | 0.23 | -3% | 38.18 | 0.19 | 15% |

The comparison of wind speed and wind direction characteristics for Vancouver Building during the period without overhang considering hourly and 5-min data

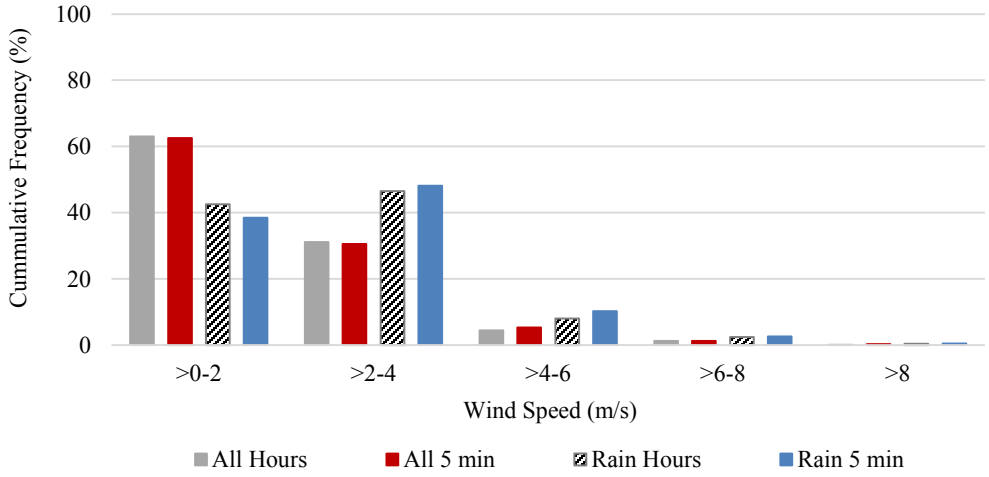


(a)

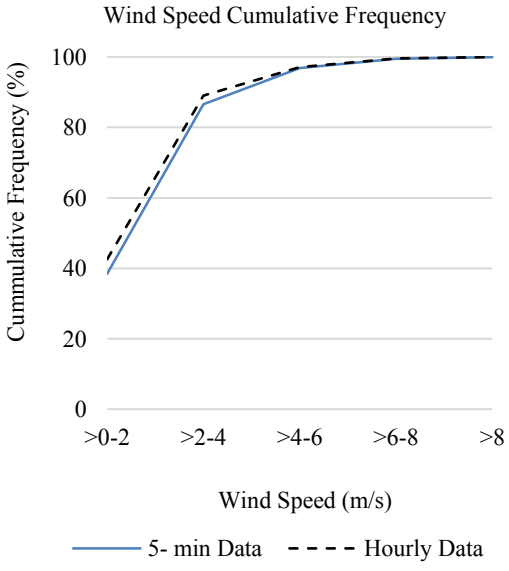


(a)

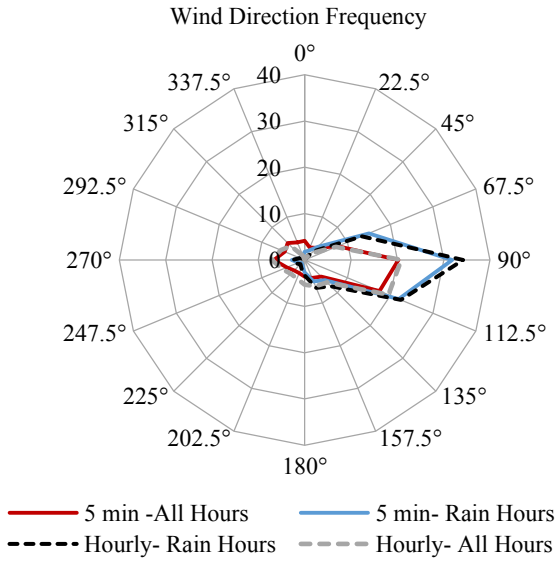


(c)

Figure D.4- Discrepancy of wind speed frequency (a), wind speed cumulative frequency (b) and wind direction for all and rain hours calculated based on different time intervals, Cassier Building, No OH period, Vancouver

Table D.4- Comparison of wind speed and wind direction considering 5-min registered data and hourly data for NO OH period, Cassiar Building, Vancouver

| | **Wind Speed** | | | |
|---|---|---|---|---|
| | 5-min Interval Data | | Hourly Data | |
| | All | Rain | All | Rain |
| Mean | 1.88 | 2.58 | 1.88 | 2.45 |
| Median | 1.61 | 2.35 | 1.62 | 2.21 |
| ST Devi | 1.33 | 1.44 | 1.24 | 1.35 |
| | **Wind Direction** | | | |
| | 5-min Interval Data | | Hourly Data | |
| | All | Rain | All | Rain |
| Mean | 158.32 | 114.93 | 158.33 | 116.65 |
| Median | 113.95 | 99.60 | 123.07 | 101.12 |
| ST Devi | 95.26 | 62.89 | 79.17 | 51.71 |

Comparison of onsite and weather station wind direction towards each study façade of test buildings

Fredericton, MacLeod House

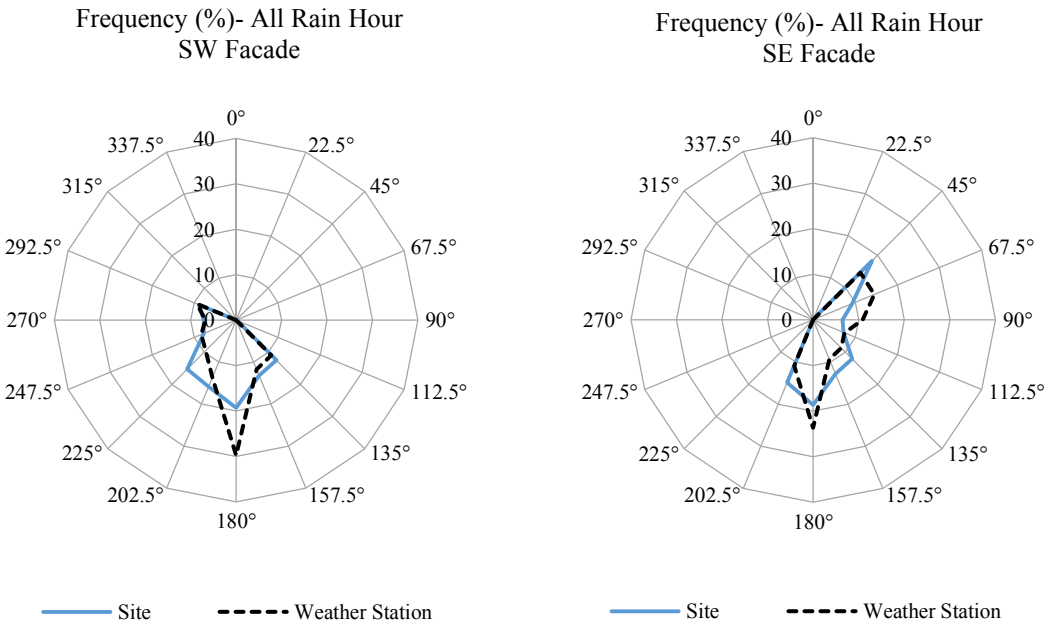


(a) (b)

Figure D.5– Comparison of wind direction frequency approaching towards (a) south-west and (b) south-east façade based on onsite and weather station data during rain hours, MacLeod house, Fredericton

Vancouver, Cassiar Building

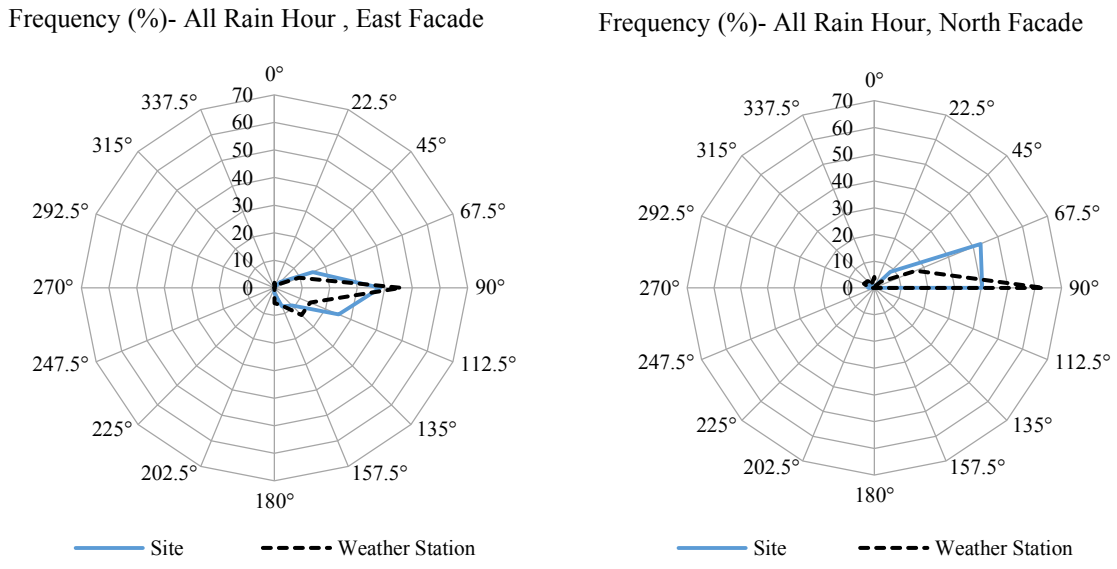


(a) (b)

Figure D.6– Comparison of wind direction frequency approaching towards (a) east and (b) north façade based on onsite and weather station data during rain hours, Cassiar Building, Vancouver

Montreal, FB Building

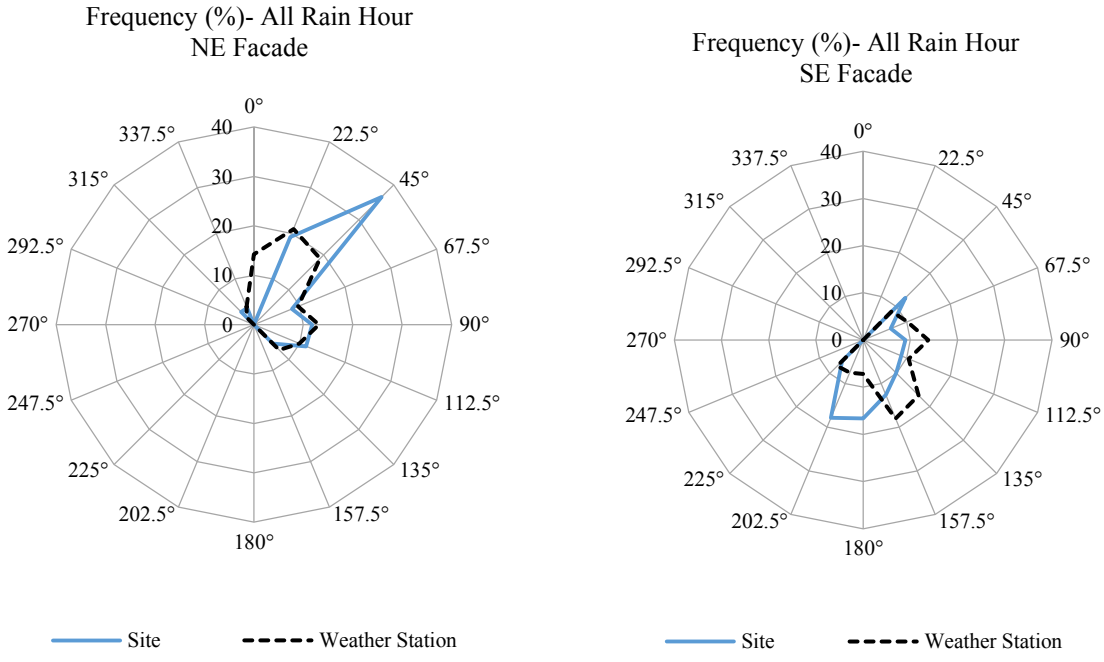


(a) (b)

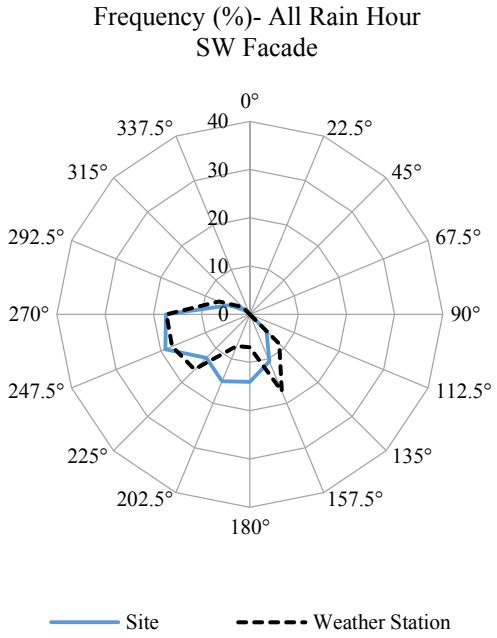


(c)

Figure D.7– Comparison of wind direction frequency approaching towards (a) north-east, (b) south-east and (c) south-west façade based on onsite and weather station data during rain hours, FB Building, Montreal

Vancouver

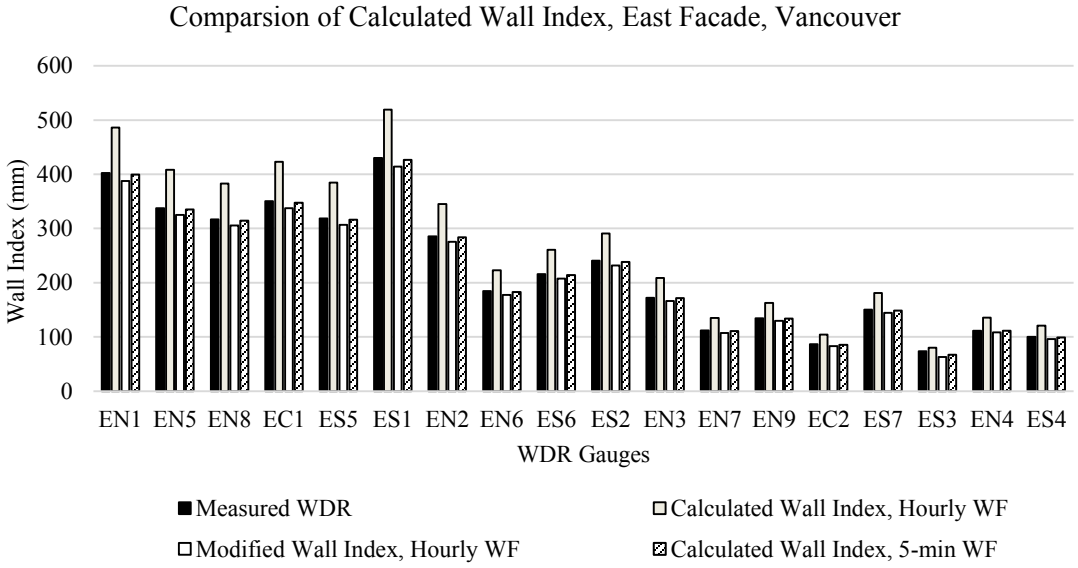


(a)

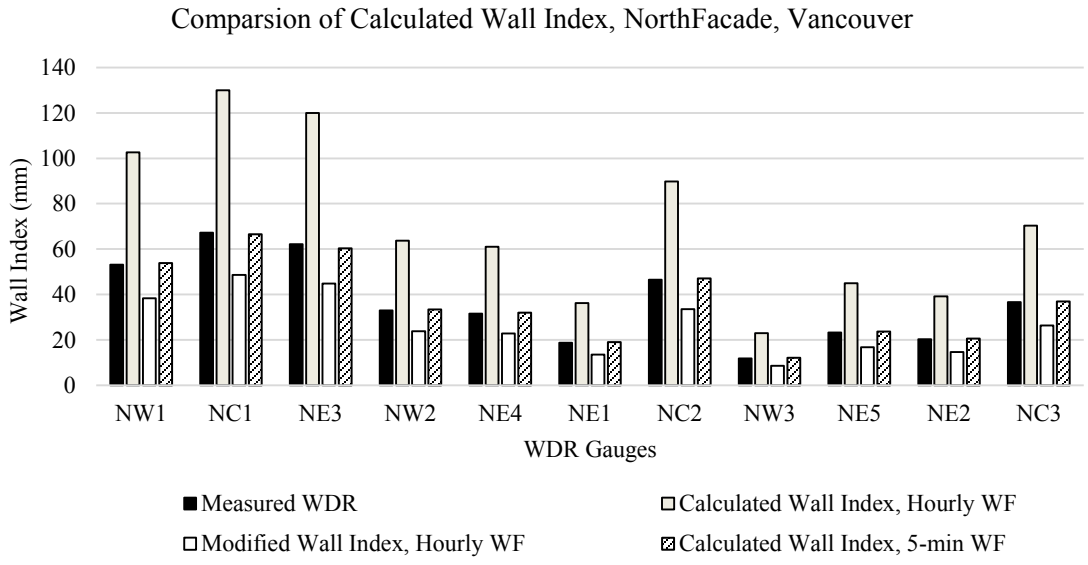


(b)

Figure D.8- Comparison between measured WDR and calculated WDR on the (a) East façade and (b) North façade with wind speed and wind direction corrections and wall factors calculated using 5-min measured data, Cassiar building, Vancouver

Fredericton

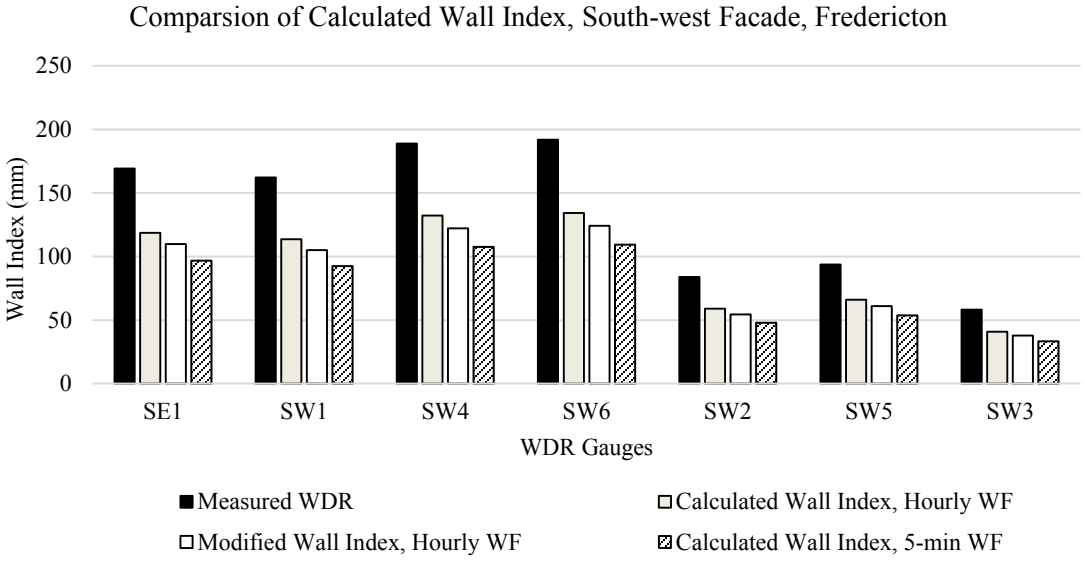


(a)

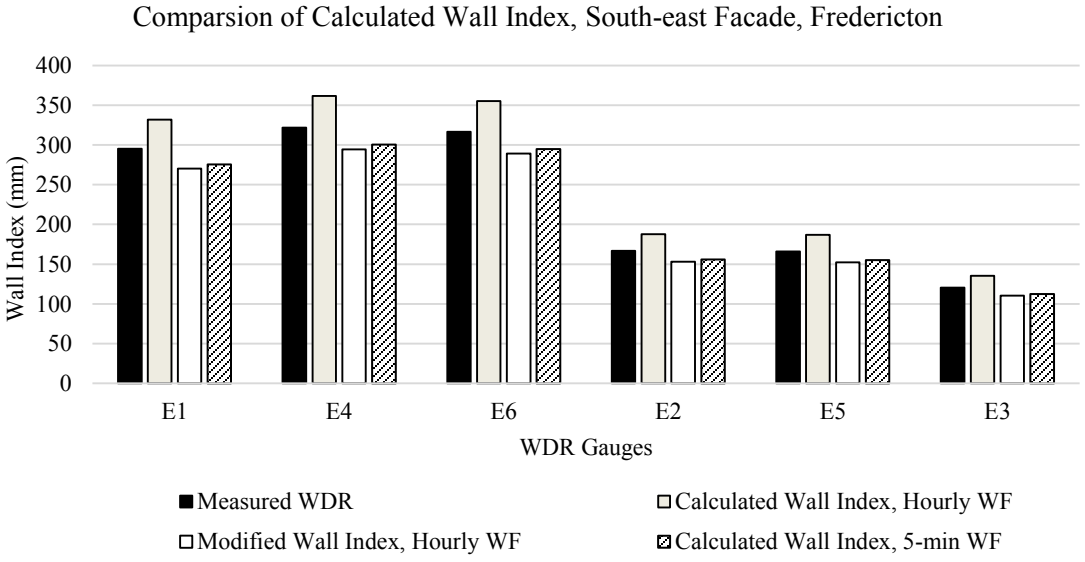


(b)

Figure D.9- Comparison between measured WDR and calculated WDR on the (a) South-west and (b) South-east façade with wind speed and wind direction corrections and wall factors calculated using 5-min measured data, McLeod house, Fredericton

Montreal

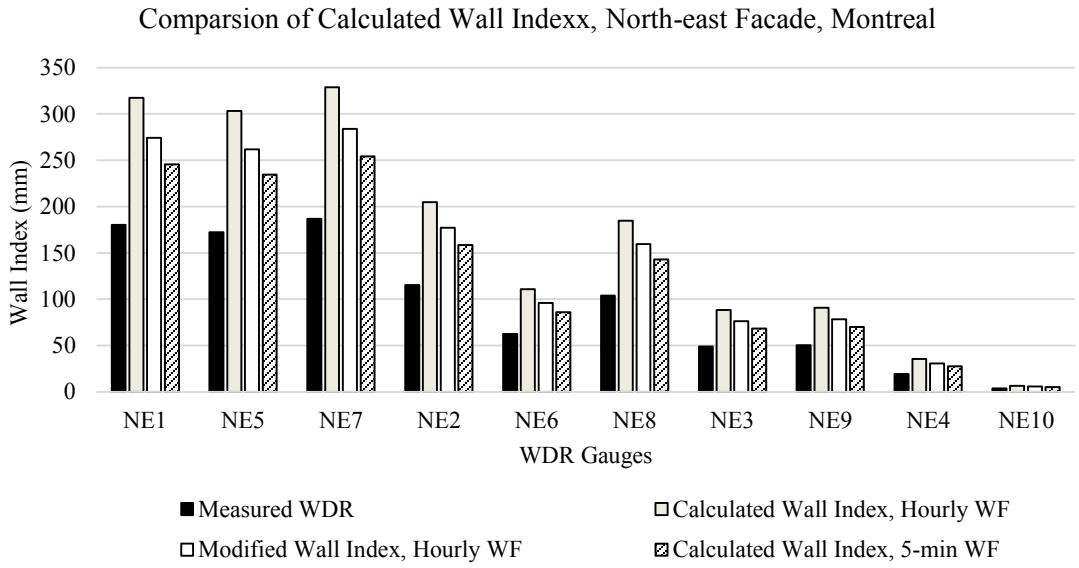
Comparsion of Calculated Wall Indexx, North-east Facade, Montreal
Wall Index (mm)
350
300
250
200
150
100
50
0
NE1
NE5
NE7
NE2
NE6
NE8
NE3
NE9
NE4
NE10
WDR Gauges
Measured WDR
Calculated Wall Index, Hourly WF
Modified Wall Index, Hourly WF
Calculated Wall Index, 5-min WF

(a)

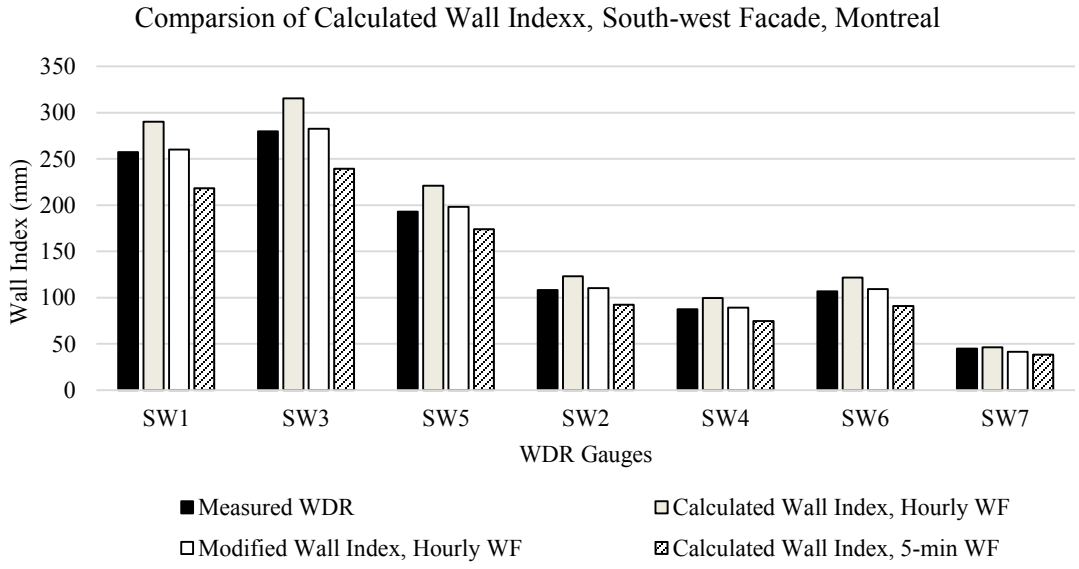
Comparsion of Calculated Wall Indexx, South-west Facade, Montreal
Wall Index (mm)
350
300
250
200
150
100
50
0
SW1
SW3
SW5
SW2
SW4
SW6
SW7
WDR Gauges
Measured WDR
Calculated Wall Index, Hourly WF
Modified Wall Index, Hourly WF
Calculated Wall Index, 5-min WF

(b)

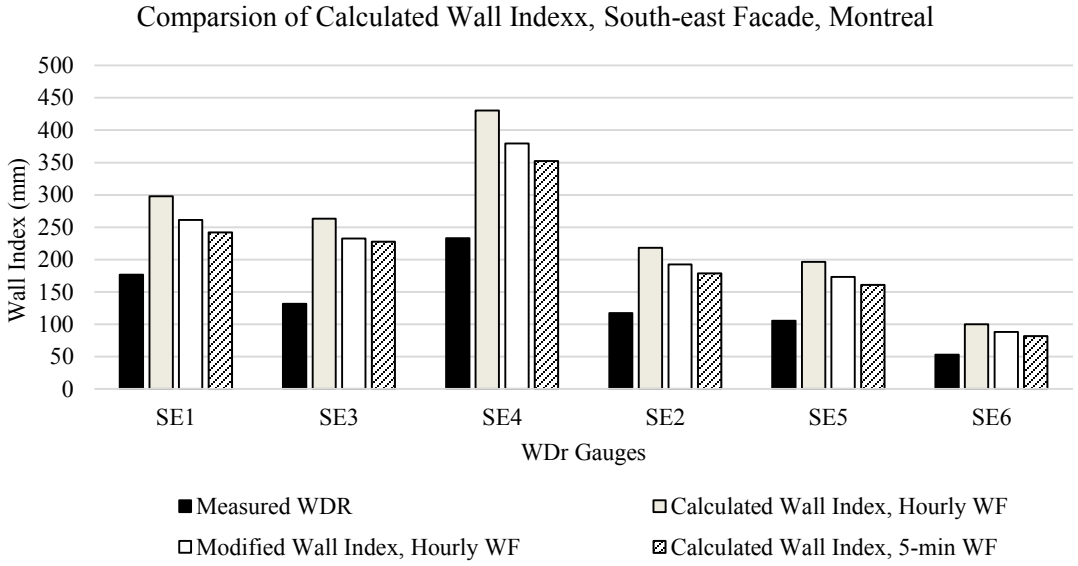


(c)

Figure D.10- Comparison between measured WDR and calculated WDR on the (a) North-east, (b) South-west and (c) South-east façade with wind speed and wind direction corrections and wall factors calculated using 5-min measured data, FB Building, Montreal

Table D.5- Comparison of primary and WS modified onsite airfield index and wall factor considering different time resolutions, McLeod House south-west façade and (b) south-east facade, Fredericton

(a) South-West Façade

**Onsite air filed index**

| | Modified | | | | Primary | | | |
|---|---|---|---|---|---|---|---|---|
| | DRI 5-min | | DRI Hourly | | DRI 5-min | | DRI Hourly | |
| | All Data | Filtered Data | All Data | Filtered Data | All Data | Filtered Data | All Data | Filtered Data |
| 0.61 m (2 ft) | 613.74 | 599.81 | 499.81 | 485.36 | 598.46 | 584.73 | 487.28 | 473.10 |
| 4.88 m (16 ft) | 580.52 | 567.35 | 472.76 | 459.10 | 566.07 | 553.09 | 460.91 | 447.50 |
| 9.15 m (30 ft) | 540.37 | 528.11 | 440.06 | 427.34 | 526.92 | 514.84 | 429.03 | 416.55 |

**Onsite calculated wall factor**

| | Modified | | | | Primary | | | |
|---|---|---|---|---|---|---|---|---|
| | WF 5-min | | WF Hourly | | DRI 5-min | | DRI Hourly | |
| | All Data | Filtered Data | All Data | Filtered Data | All Data | Filtered Data | All Data | Filtered Data |
| SE1 | 0.28 | 0.28 | 0.34 | 0.34 | 0.28 | 0.28 | 0.35 | 0.35 |
| SW1 | 0.26 | 0.26 | 0.32 | 0.32 | 0.27 | 0.27 | 0.33 | 0.33 |
| SW4 | 0.31 | 0.31 | 0.38 | 0.38 | 0.32 | 0.31 | 0.39 | 0.39 |
| SW6 | 0.31 | 0.31 | 0.38 | 0.39 | 0.32 | 0.32 | 0.39 | 0.40 |
| SW2 | 0.14 | 0.14 | 0.18 | 0.17 | 0.15 | 0.14 | 0.18 | 0.18 |
| SW5 | 0.16 | 0.16 | 0.20 | 0.20 | 0.17 | 0.16 | 0.20 | 0.20 |
| SW3 | 0.11 | 0.10 | 0.13 | 0.12 | 0.11 | 0.10 | 0.14 | 0.13 |

(b) South-East Façade

**Onsite air filed index**

| | Modified | | | | Primary | | | |
|---|---|---|---|---|---|---|---|---|
| | DRI 5-min | | DRI Hourly | | DRI 5-min | | DRI Hourly | |
| | All Data | Filtered Data | All Data | Filtered Data | All Data | Filtered Data | All Data | Filtered Data |
| 0.61 m (2 ft) | 548.91 | 534.01 | 456.05 | 442.03 | 548.29 | 533.26 | 455.28 | 441.18 |
| 4.88 m (16 ft) | 519.20 | 505.11 | 431.37 | 418.10 | 518.62 | 504.40 | 430.64 | 417.30 |
| 9.15 m (30 ft) | 483.29 | 470.17 | 401.53 | 389.19 | 482.75 | 469.52 | 400.86 | 388.44 |

**Onsite calculated wall factor**

| | Modified | | | | Primary | | | |
|---|---|---|---|---|---|---|---|---|
| | WF 5-min | | WF Hourly | | DRI 5-min | | DRI Hourly | |
| | All Data | Filtered Data | All Data | Filtered Data | All Data | Filtered Data | All Data | Filtered Data |
| E1 | 0.54 | 0.54 | 0.65 | 0.65 | 0.54 | 0.54 | 0.65 | 0.65 |
| E4 | 0.59 | 0.57 | 0.71 | 0.69 | 0.59 | 0.58 | 0.71 | 0.70 |
| E6 | 0.58 | 0.57 | 0.69 | 0.69 | 0.58 | 0.57 | 0.69 | 0.69 |
| E2 | 0.32 | 0.31 | 0.39 | 0.38 | 0.32 | 0.31 | 0.39 | 0.38 |
| E5 | 0.32 | 0.31 | 0.39 | 0.38 | 0.32 | 0.31 | 0.39 | 0.38 |
| E3 | 0.25 | 0.24 | 0.30 | 0.29 | 0.25 | 0.24 | 0.30 | 0.30 |

Table D.6- Comparison of primary and WD modified onsite airfield index and wall factor considering different time resolutions, McLeod House south-west façade and (b) south-east facade, Fredericton

Onsite air filed index

| | Modified | | | | Primary | | | |
|---|---|---|---|---|---|---|---|---|
| | DRI 5-min | | DRI Hourly | | DRI 5-min | | DRI Hourly | |
| | All Data | Filtered Data | All Data | Filtered Data | All Data | Filtered Data | All Data | Filtered Data |
| 0.61 m (2 ft) | 553.01 | 537.92 | 459.53 | 441.54 | 548.29 | 533.26 | 455.28 | 441.18 |
| 4.88 m (16 ft) | 523.08 | 508.81 | 434.66 | 417.64 | 518.62 | 504.40 | 430.64 | 417.30 |
| 9.15 m (30 ft) | 486.91 | 473.62 | 404.60 | 388.76 | 482.75 | 469.52 | 400.86 | 388.44 |

Onsite calculated wall factor

| | Modified | | | | Primary | | | |
|---|---|---|---|---|---|---|---|---|
| | WF 5-min | | WF Hourly | | DRI 5-min | | DRI Hourly | |
| | All Data | Filtered Data | All Data | Filtered Data | All Data | Filtered Data | All Data | Filtered Data |
| E1 | 0.53 | 0.54 | 0.64 | 0.65 | 0.54 | 0.54 | 0.65 | 0.65 |
| E4 | 0.58 | 0.57 | 0.70 | 0.70 | 0.59 | 0.58 | 0.71 | 0.70 |
| E6 | 0.57 | 0.56 | 0.69 | 0.69 | 0.58 | 0.57 | 0.69 | 0.69 |
| E2 | 0.32 | 0.31 | 0.38 | 0.38 | 0.32 | 0.31 | 0.39 | 0.38 |
| E5 | 0.32 | 0.31 | 0.38 | 0.38 | 0.32 | 0.31 | 0.39 | 0.38 |
| E3 | 0.25 | 0.24 | 0.30 | 0.29 | 0.25 | 0.24 | 0.30 | 0.30 |

Comparison of calculated wall factor based on filtered data with respect to precipitation type

Montreal

Table D.7- Comparison of measured WDR, ISO wall indices and calculated wall indices considering wall factors calculated based on filtered data and different time resolutuion, FB Building, Montreal

**FB Building, Montreal (Filtered Data)**

| Distance from the Roof Top | WDR Gauges | ISO Standard | Measured WDR (mm) | Hourly Data | | | 5- min Data | | |
|---|---|---|---|---|---|---|---|---|---|
| | | | | Calculated Wall Indices | Wall Factor | | Calculated Wall Indices | Wall Factor | |
| 0.6 m | **NE1** | 277.54 | 166.94 | 295.48 | 0.53 | -77% | 227.87 | 0.41 | -36% |
| | **NE5** | 277.54 | 160.49 | 284.07 | 0.51 | -77% | 219.06 | 0.39 | -36% |
| | **NE7** | 277.54 | 176.89 | 313.10 | 0.56 | -77% | 241.45 | 0.43 | -36% |
| 4.9 m | **NE2** | 108.11 | 107.45 | 191.97 | 0.36 | -79% | 148.04 | 0.27 | -38% |
| | **NE6** | 108.11 | 58.16 | 103.91 | 0.19 | -79% | 80.13 | 0.15 | -38% |
| | **NE8** | 108.11 | 98.03 | 175.14 | 0.32 | -79% | 135.06 | 0.25 | -38% |
| 10.7 m | **NE3** | 103.63 | 45.12 | 81.66 | 0.16 | -81% | 62.98 | 0.12 | -40% |
| | **NE9** | 103.63 | 46.47 | 84.11 | 0.16 | -81% | 64.86 | 0.13 | -40% |
| 21.3 m | **NE4** | 93.00 | 17.84 | 33.04 | 0.07 | -85% | 25.48 | 0.05 | -43% |
| | NE10 | 93.00 | 3.11 | 5.76 | 0.01 | -85% | 4.44 | 0.01 | -43% |
| 0.6 m | **SE1** | 293.94 | 174.28 | 271.76 | 0.65 | -56% | 219.87 | 0.52 | -26% |
| | **SE3** | 293.94 | 119.50 | 250.10 | 0.51 | -109% | 215.88 | 0.44 | -81% |
| | **SE4** | 293.94 | 214.87 | 387.78 | 0.66 | -80% | 316.42 | 0.54 | -47% |
| 4.9 m | **SE2** | 114.50 | 109.11 | 198.76 | 0.35 | -82% | 162.18 | 0.28 | -49% |
| | **SE5** | 114.50 | 101.20 | 184.35 | 0.32 | -82% | 150.43 | 0.26 | -49% |
| 10.7 m | **SE6** | 109.76 | 49.21 | 90.81 | 0.17 | -85% | 74.10 | 0.14 | -51% |
| 0.6 m | **SW1** | 214.44 | 257.42 | 279.73 | 0.65 | -9% | 222.89 | 0.52 | 13% |
| | **SW3** | 214.44 | 279.74 | 303.98 | 0.71 | -9% | 242.22 | 0.56 | 13% |
| | **SW5** | 214.44 | 192.89 | 207.18 | 0.78 | -7% | 171.93 | 0.65 | 11% |
| 4.9 m | **SW2** | 83.53 | 108.21 | 118.69 | 0.28 | -10% | 94.58 | 0.23 | 13% |
| | **SW4** | 83.53 | 87.46 | 95.93 | 0.23 | -10% | 76.44 | 0.18 | 13% |
| | **SW6** | 83.53 | 106.95 | 117.31 | 0.28 | -10% | 93.47 | 0.22 | 13% |
| 10.7 m | **SW7** | 80.07 | 44.70 | 41.97 | 0.26 | 6% | 34.90 | 0.21 | 22% |

Fredericton

Table D.8 - Comparison of measured WDR, ISO wall indices and calculated wall indices considering wall factors calculated based on filtered data and different time resolutuion, McLeod House, Fredericton

**McLeod House, Fredericton (Filtered Data)**

| Distance from the Roof Top | WDR Gauges | ISO Standard | Measured WDR (mm) | Hourly Data | | | 5- min Data | | |
|---|---|---|---|---|---|---|---|---|---|
| | | | | Calculated Wall Indices | Wall Factor | | Calculated Wall Indices | Wall Factor | |
| 0.6 m | **SE1** | 160.80 | 161.32 | 113.24 | 0.35 | 30% | 91.62 | 0.28 | 43% |
| | **SW1** | 160.80 | 145.38 | 106.55 | 0.33 | 27% | 86.21 | 0.27 | 41% |
| | **SW4** | 160.80 | 168.41 | 124.45 | 0.39 | 26% | 100.69 | 0.31 | 40% |
| | **SW6** | 160.80 | 174.41 | 127.56 | 0.40 | 27% | 103.21 | 0.32 | 41% |
| 4.9 m | **SW2** | 60.97 | 74.62 | 54.36 | 0.18 | 27% | 43.99 | 0.14 | 41% |
| | **SW5** | 60.97 | 84.08 | 61.56 | 0.20 | 27% | 49.81 | 0.16 | 41% |
| 9.1 m | **SW3** | 56.64 | 50.18 | 36.21 | 0.13 | 28% | 29.30 | 0.10 | 42% |
| 0.6 m | **E1** | 250.77 | 264.56 | 328.21 | 0.65 | -24% | 271.54 | 0.54 | -3% |
| | **E4** | 250.77 | 285.41 | 348.98 | 0.70 | -22% | 288.72 | 0.58 | -1% |
| | **E6** | 250.77 | 281.60 | 344.91 | 0.69 | -22% | 285.35 | 0.57 | -1% |
| 4.9 m | **E2** | 95.08 | 146.95 | 180.23 | 0.38 | -23% | 149.11 | 0.31 | -1% |
| | **E5** | 95.08 | 146.74 | 180.98 | 0.38 | -23% | 149.73 | 0.31 | -2% |
| 9.1 m | **E3** | 88.34 | 106.64 | 130.32 | 0.30 | -22% | 107.82 | 0.24 | -1% |